



***Towards Sustainable Handling of Waste***

Pyrolysis and Gasification of Biomass and Waste Tyre for Syngas

Production: Kinetics Study and Process Simulation

Fahima Ahmed Abdullah Al Balushi

Supervisors: Prof. Meihong Wang

Dr Abby Samson

A thesis submitted in partial fulfilment of the requirement for the degree of  
Doctor of Philosophy

Department of Chemical and Biological Engineering

Faculty of Engineering

The University of Sheffield

August 2023

## Acknowledgement

With the grace of Allah, I would like to express my deepest gratitude to my supervisor Prof. Meihong Wang for his continuous patience in guiding me on how to do research and develop my skills. Prof. Wang was supportive throughout my PhD study by sharing knowledge and providing valuable suggestions. I thank Prof. Wang for his motivation, encouragement and supervision throughout my research.

I would like to extend my grateful thanks to everyone in the Process and Energy Systems Engineering research group who provided their support, contributions and advice during my PhD. Many thanks to Dr Yue Chai for his effort, time and technical support especially in the first 18 months of my study. I had the pleasure of collaborating with Dr Kiran Gupta Burra from the Combustion Laboratory, Department of Mechanical Engineering, University of Maryland, USA. In addition, this endeavour would not have been possible without the financial support from the Ministry of Higher Education Research and Innovation, Oman.

I am deeply indebted to my family, especially my mother Fatma Al Balushi and sister Fahida Al Balushi for their moral support. Special thanks to my lovely husband Ali Al Bulushi for his love, patience, encouragement and emotional support. The belief of all my family members in me has kept my spirits and motivation high during this stage of my life. Despite the busy time I had while taking care of my son Redha Ali, I thank Allah for his mercy in having my son with me, especially after a long, busy and stressful day at the university.

Lastly, I am thankful to everyone who was part of my PhD journey; friends, colleagues and relatives and express my sincere apologies to those I could not personally mention.

## Abstract

The global demand for energy and chemical production is drastically increasing due to the rapid increase in the world population and industrialization. Intensive reliance on fossil fuels poses environmental challenges related to energy security, climate change and increased greenhouse gas emissions. The increase in world population and the improvement in living standards also lead to the increased demand for the automobile sector. This in turn results in excessive production of waste tyres leading to another environmental concern. Gasification of biomass and waste tyre provides a viable pathway with the potential to tackle the concerns of energy supply security and waste management. This thesis aims to kinetically analyse the thermal decomposition of biomass and waste tyre and to investigate the syngas production from gasification of biomass and waste tyre through process modelling and simulation.

Understanding the decomposition of biomass and waste tyre in terms of thermal behaviour and the underlying kinetics is important to evaluate the existence of synergetic interaction and optimise their uses. The experimental data acquired through thermogravimetric analysis (i.e. TGA) of pine bark, waste tyre and their blends are used to evaluate the behaviour of the samples during thermal decomposition and to calculate the kinetics data. The main findings are as follows: (i) The increase in the heating rate shifted the differential thermogravimetric (i.e. DTG) curves to higher temperatures and resulted in the variation in the difference in weight loss thus the extent of positive synergetic interaction, (ii) Based on various kinetic analysis approaches adopted in this thesis, the use of pine bark and waste tyre with a mass ratio of 1:3 showed maximum synergetic interaction in which the activation energy decreased by 13.95-17.21% compared to a single waste tyre, (iii) The reaction mechanisms describing the thermal decomposition of pine bark,

waste tyre and their blended samples are a combined effect of nucleation, growth and diffusion which are estimated using the Sestak Berggren model. The differences in the chemical structures and composition of the pine bark and waste tyre account for the different thermal and kinetic behaviours observed.

CO<sub>2</sub> gasification of biomass and waste tyre was conducted through process modelling and simulation using ASPEN Plus® to utilise CO<sub>2</sub>. After the successful validation of the developed model, the effect of gasification temperature, CO<sub>2</sub>-to-feed ratio and feed flow rate was analysed. Gasification temperature and feed flow rate had a positive effect on H<sub>2</sub> and CO production in which the temperature had a predominant effect on CO<sub>2</sub> conversion to CO. The maximum total concentration of H<sub>2</sub> and CO with the highest fraction of H<sub>2</sub> compared to CO was found to be 62.97 vol% at a temperature, CO<sub>2</sub>-to-feed ratio and feed flow rate of 1173 K, 0.20 and 0.045 kg/hr. Under the same conditions, the highest H<sub>2</sub>/CO ratio and LHV with values of 1.56 and 17.75 MJ/Nm<sup>3</sup> were obtained. Comparing the pine bark and waste tyre blended samples, pine bark and waste tyre with a mass ratio of 1:3 resulted in syngas with slightly better H<sub>2</sub>/CO ratio and LHV than other blended samples.

Since the use of steam has a positive effect on H<sub>2</sub> production, co-gasification of biomass and the waste tyre was analysed using steam and steam/CO<sub>2</sub> mixture as gasifying agents using ASPEN Plus®. The increase in temperature showed a positive effect on the H<sub>2</sub> content of the syngas in both steam and steam/CO<sub>2</sub> gasification. The maximum H<sub>2</sub> content was reported at a temperature of 1223 and 1273 K for steam and steam/CO<sub>2</sub> gasification respectively. The highest H<sub>2</sub>/CO ratio was reported at a temperature of 1173 and 1048 K with values of 4.76 and 3.79 for steam and steam/CO<sub>2</sub> gasification respectively. During steam gasification, a negligible effect on

syngas composition was reported at steam-to-feed ratio higher than 2.90 which was not the case in steam/CO<sub>2</sub> gasification. Therefore, the H<sub>2</sub>/CO ratio peaked at an average steam-to-feed ratio of 3.22 with values ranging between 2.32 and 4.80 for all the samples. Feed flow rate and gasification temperature of 0.20 kg/hr and 1173 K, respectively, resulted in syngas with LHV of 13.96-17.74 MJ/Nm<sup>3</sup> in steam gasification and 10.34-13.01 MJ/Nm<sup>3</sup> in steam/CO<sub>2</sub> gasification. In comparison to CO<sub>2</sub> gasification, steam/CO<sub>2</sub> gasification produced syngas with a total H<sub>2</sub> and CO content three times higher than CO<sub>2</sub> gasification whereas H<sub>2</sub>/CO ratio was higher by a minimum of 1.7 times in case of WT1PB0 at a temperature, feed flow rate and CO<sub>2</sub>-to-steam mass ratio of 1173 K, 0.045 kg/hr and 0.5:0.5.

The findings of the current research could provide a comprehensive understanding of the co-gasification of biomass and waste tyre under different operating conditions prior to considering experimental and/or large-scale implementation of such technology. In addition, they aid in diversifying waste disposal options with the potential to mitigate CO<sub>2</sub> emissions.

**Keywords:** Pyrolysis and Gasification; Biomass; Waste tyre; Process modelling and simulation; Syngas Production, CO<sub>2</sub> utilisation

## Peer-reviewed Publications and Presentations Related to the Current Research

Part of the current research work has been published in a peer-reviewed journal and delivered as a conference presentation.

- Journal Publication

**Al-Balushi, F.A.**, Burra, K.G., Chai, Y., Wang, M. (2023). Co-pyrolysis of waste tyre and pine bark: Study of reaction kinetics and mechanisms. *Biomass and Bioenergy*, 168, 106654.

- ✓ This paper covers the content included in Chapter 3 of the PhD thesis

- Conference Presentation

**Al-Balushi, F.A.**, Chai, Y., Wang, M. (2021), Chemical Reaction Kinetics of Pyrolysis/Gasification of Waste Tyre and Biomass for Syngas Production, *The 1st European Conference on Fuel and Energy Research and Its Application*, University of Nottingham, Nottingham, UK, 06-09 September 2021.

- ✓ Delivered as an oral presentation.

## Table of Contents

Acknowledgement .....	i
Abstract.....	ii
Peer-reviewed Publications and Presentations Related to the Current Research.....	v
Table of Contents.....	vi
List of Figures .....	xii
List of Tables .....	xviii
Nomenclatures.....	xxi
List of Abbreviations .....	xxiv
CHAPTER 1 Introduction .....	1
1.1 Research Background.....	1
1.1.1 Worldwide energy and chemical demand.....	1
1.1.2 Global warming and environmental issues .....	2
1.1.3 Solid waste disposal and management .....	3
1.2 Biomass and waste tyre as alternative feedstocks .....	4
1.2.1 Biomass.....	4
1.2.2 Waste tyre.....	7
1.2.3 A mixture of biomass and waste tyre .....	8
1.3 Pyrolysis and gasification of biomass and waste tyre.....	9
1.3.1 Pyrolysis .....	10
1.3.2 Gasification .....	10
1.3.3 Co-pyrolysis and co-gasification .....	12

1.4	Syngas potential from gasification of biomass and waste tyre .....	13
1.4.1	Global syngas market.....	13
1.4.2	Syngas quality and associated applications.....	13
1.5	Kinetics analysis for potential synergetic interaction during co-pyrolysis.....	14
1.6	Motivation of the current research .....	15
1.6.1	The first driver: to understand the potential synergy underlying the co-feeding of waste tyres with biomass. ....	16
1.6.2	The second driver: to utilise CO <sub>2</sub> through gasification for syngas production.....	16
1.7	Aim and objectives .....	17
1.8	Research methodology .....	18
1.8.1	Simulation tool for process modelling and simulation.....	20
1.9	Novel contributions.....	21
1.9.1	Estimation of reaction kinetics of co-pyrolysis of biomass and waste tyre through combined kinetic Analysis method.....	21
1.9.2	Insights from a comparison of co-gasification of biomass and waste tyre using different gasifying agents through process simulation.....	22
1.10	Outline of the thesis.....	22
CHAPTER 2	Literature review.....	24
2.1	Experimental studies of gasification of biomass and waste tyre.....	24
2.1.1	Experimental studies of gasification of biomass .....	24
2.1.2	Experimental studies of gasification of waste tyre.....	32
2.1.3	Experimental studies of gasification of waste tyre and biomass blend .....	37

2.2	Kinetics studies of pyrolysis of biomass and waste tyre .....	41
2.2.1	Kinetics studies of pyrolysis of biomass.....	41
2.2.2	Kinetics studies of pyrolysis of waste tyre .....	43
2.2.3	Kinetics studies of pyrolysis of biomass and waste tyre blend .....	45
2.3	Modelling and simulation studies of gasification of biomass and waste tyre .....	47
2.3.1	Modelling and simulation studies of gasification of biomass.....	47
2.3.2	Modelling and simulation studies of gasification of waste tyre.....	49
2.3.3	Modelling and simulation studies of gasification of biomass and waste tyre blend	
	50	
2.4	Summary .....	50
CHAPTER 3	Kinetics analysis of co-pyrolysis of pine bark and waste tyre.....	53
3.1	Methodology .....	53
3.1.1	Kinetics study .....	53
3.2	Experimental data .....	59
3.2.1	Materials .....	59
3.2.2	TGA.....	60
3.3	Results and discussion.....	61
3.3.1	TG and DTG analysis.....	61
3.3.2	Kinetics analysis .....	75
3.3.3	Kinetics of waste tyre, biomass and their blends: previous studies.....	101
3.4	Conclusion .....	104

CHAPTER 4	Co-gasification of pine bark and waste tyre using CO <sub>2</sub> through process modelling and simulation .....	105
4.1	Model development.....	105
4.1.1	Overview of experimental study.....	105
4.1.2	Assumptions.....	107
4.1.3	Model development in ASPEN Plus® .....	107
4.2	Model validation .....	113
4.3	Process analysis.....	115
4.3.1	Performance evaluation indices .....	115
4.3.2	Plan of process analysis .....	117
4.3.3	Effect of temperature .....	117
4.3.4	Effect of CO <sub>2</sub> flow rate (CO <sub>2</sub> -to-feed ratio) .....	123
4.3.5	Effect of feed flow rate .....	129
4.4	Synergetic interaction between waste tyre and pine bark in CO <sub>2</sub> environment.....	133
4.5	Conclusion .....	133
CHAPTER 5	Comparative evaluation of co-gasification of pine bark and waste tyre using steam and steam/CO <sub>2</sub> mixture through process modelling and simulation .....	135
5.1	Modification in the developed model.....	135
5.2	Process analysis of steam co-gasification of pine bark and waste tyre: Case 1 .....	136
5.2.1	Effect of temperature .....	137
5.2.2	Effect of steam-to-feed ratio (i.e. SFR) .....	142
5.2.3	Effect of feed flow rate .....	146

5.3	Process analysis of steam/CO <sub>2</sub> co-gasification of pine bark and waste tyre: Case 2...	150
5.3.1	Effect of temperature .....	151
5.3.2	Effect of steam-to-feed ratio (i.e. SFR) .....	156
5.3.3	Effect of CO <sub>2</sub> -to-steam ratio .....	160
5.3.4	Effect of feed flow rate .....	166
5.4	Comparative evaluation of syngas composition and process performance from CO <sub>2</sub> , steam and steam/CO <sub>2</sub> gasification .....	169
5.5	Conclusion .....	172
CHAPTER 6	Conclusions and recommendations for future work .....	174
6.1	Concluding remarks.....	174
6.1.1	Evaluation of the existence of synergetic interaction between pine bark and waste tyre	174
6.1.2	Estimation of the kinetics underlying the co-pyrolysis of waste tyre and pine bark at different blend ratios.....	174
6.1.3	CO <sub>2</sub> utilisation in the co-gasification of waste tyre and pine bark for syngas production through process modelling and simulation .....	175
6.1.4	Improve syngas composition while utilising CO <sub>2</sub> in the gasification process through process analysis .....	175
6.2	Future Recommendations.....	176
6.2.1	Using different type of biomass and waste tyre to evaluate the synergetic interaction and the kinetics analysis .....	176

6.2.2 Detailed process modelling and simulation of co-gasification of biomass and waste tyre	177
References .....	179
Appendix A .....	204

## List of Figures

<b>Figure 1.1</b> Total primary energy consumption in Quad Btu and percent share of primary energy consumption by source (Source: reproduced using data from (BP, 2022)) .....	2
<b>Figure 1.2</b> (a) Share of different sectors toward global CO <sub>2</sub> equivalent emissions as of 2010 (IPCC, 2014) and (b) global CO <sub>2</sub> emission and (c) the annual change in global CO <sub>2</sub> emission over 1900-2021 (IEA, 2022).....	3
<b>Figure 1.3</b> Flow diagram presenting a comparison between 1st, 2nd and 3rd generation biomass (Source: constructed according to the info in Lee and Lavoie, 2013) .....	6
<b>Figure 1.4</b> Percent Share of Primary Energy Production by Source in (a) 1960 and (b) 2020 (Source: constructed using data from (EIA, 2023)).....	7
<b>Figure 1.5</b> Van-Krevelen diagram of biomass and waste tyre materials (Source: author elaboration based on the literature) .....	9
<b>Figure 1.6</b> Flow diagram of the research methodology adopted in the current research project .....	20
<b>Figure 3.1</b> (a) TG and (b) DTG curves of pyrolysis of the waste tyre (i.e. WT1PB0) at 10, 20, 30 and 40 K/min.....	63
<b>Figure 3.2</b> (a) TG and (b) DTG curves of pyrolysis of pine bark (i.e. WT0PB1) at 10, 20, 30 and 40 K/min.....	64
<b>Figure 3.3</b> (a) TG and (b) DTG curves of co-pyrolysis of the waste tyre and pine bark at 10, 20, 30 and 40 K/min for WT3PB1 .....	67
<b>Figure 3.4</b> (a) TG and (b) DTG curves of co-pyrolysis of the waste tyre and pine bark at 10, 20, 30 and 40 K/min for WT1PB1 .....	68

<b>Figure 3.5</b> (a) TG and (b) DTG curves of co-pyrolysis of the waste tyre and pine bark at 10, 20, 30 and 40 K/min for WT1PB3 .....	69
<b>Figure 3.6</b> Variation in the difference of weight loss (i.e. $\Delta W$ ) for waste tyre and pine bark blends at (a) 10, (b) 20, (c) 30 and (d) 40 K/min.....	73
<b>Figure 3.7</b> Correlation coefficient (i.e. $R^2$ ) versus reaction order, $n$ , for different blend ratios at the heating rate (a) 10, (b) 20, (c) 30 and (d) 40 K/min based on Coats-Redfern method .....	76
<b>Figure 3.8</b> Curves of $\ln g(\alpha)/T^2$ versus $1/T$ of the waste tyre and pine bark pyrolysis at a different waste tyre to pine bark blend ratios at the heating rate (a) 10, (b) 20, (c) 30 and (d) 40 K/min using Coats-Redfern method .....	77
<b>Figure 3.9</b> Kinetics analysis curves of $\ln g(\alpha)/T^2$ versus $1/T$ of different blend samples; (a) WT1PB0, (b) WT3PB1, (c) WT1PB1, (d) WT1PB3 and (e) WT0PB1 at 20 K/min.....	78
<b>Figure 3.10</b> Comparison between experimental and theoretical average activation energy of the samples relative to waste tyre.....	83
<b>Figure 3.11</b> Kinetics analysis curves of different blend samples; (a) WT1PB0, (b) WT3PB1, (c) WT1PB1, (d) WT1PB3 and (e) WT0PB1 using FWO method .....	85
<b>Figure 3.12</b> Kinetics analysis curves of different blend samples; (a) WT1PB0, (b) WT3PB1, (c) WT1PB1, (d) WT1PB3 and (e) WT0PB1 using KAS method .....	86
<b>Figure 3.13</b> Kinetics analysis curves of different blend samples; (a) WT1PB0, (b) WT3PB1, (c) WT1PB1, (d) WT1PB3 and (e) WT0PB1 using Friedman method .....	87
<b>Figure 3.14</b> Variation in $E_\alpha$ values obtained using Iso-conversional methods with conversion (i.e. $\alpha$ ) for (a) WT1PB0, (b) WT3PB1, (c) WT1PB1, (d) WT1PB3 and (e) WT0PB1 .....	89

<b>Figure 3.15</b> Linear relationship of compensation effect between $\ln A$ and $E_a$ of different blend samples; (a) WT1PB0, (b) WT3PB1, (c) WT1PB1, (d) WT1PB3 and (e) WT0PB1 using kinetics obtained through FWO method .....	91
<b>Figure 3.16</b> Comparison of theoretical master plots and experimental data for (a) WT1PB0, (b) WT3PB1, (c) WT1PB1, (d) WT1PB3 and (e) WT0PB1 at different heating rates .....	94
<b>Figure 3.17</b> Fitting results of combined kinetics analysis of (a) WT1PB0, (b) WT3PB1, (c) WT1PB1, (d) WT1PB3 and (e) WT0PB1 .....	96
<b>Figure 3.18</b> Combined kinetics analysis for normalized reaction mechanism, $\gamma(\alpha)$ of (a) WT1PB0, (b) WT3PB1, (c) WT1PB1, (d) WT1PB3 and (e) WT0PB1 .....	99
<b>Figure 3.19</b> Graphical comparison of average $E_a$ values for different samples obtained using a model fitting (CR), integral model free (FWO and KAS), differential model free (FR) methods and combined kinetic analysis. ....	101
<b>Figure 4.1</b> Schematic diagram of CO <sub>2</sub> co-gasification experimental facility of pine bark and waste tyre (Wang et al., 2019b) .....	106
<b>Figure 4.2</b> Process flowsheet developed in Aspen Plus® .....	108
<b>Figure 4.3</b> Comparison of syngas composition between experimental and model prediction at different feedstock compositions.....	115
<b>Figure 4.4</b> Effect of gasification temperature on syngas composition (a) H <sub>2</sub> , (b) CO, (c) CO <sub>2</sub> , and yield (d) H <sub>2</sub> , (e) CO, (f) CO <sub>2</sub> during CO <sub>2</sub> gasification of pine bark and waste tyre at different blend ratios .....	120
<b>Figure 4.5</b> Influence of gasification temperature on (a) H <sub>2</sub> /CO and (b) CO/CO <sub>2</sub> ratios of the syngas for CO <sub>2</sub> gasification process of pine bark and waste tyre at different blend ratios .....	121

<b>Figure 4.6</b> Effect of gasification temperature on (a) LHV of the syngas and (b) CGE of the process during CO <sub>2</sub> gasification of pine bark and waste tyre at different blend ratios.....	123
<b>Figure 4.7</b> Effect of CO <sub>2</sub> -to-feed ratio (0.2-5.0) on syngas composition (a) H <sub>2</sub> , (b) CO, (c) CO <sub>2</sub> , and yield (d) H <sub>2</sub> , (e) CO, (f) CO <sub>2</sub> during CO <sub>2</sub> gasification of pine bark and waste tyre at different blend ratios .....	126
<b>Figure 4.8</b> Effect of CO <sub>2</sub> -to-feed ratio on the syngas characteristics; (a) H <sub>2</sub> /CO and (b) CO/CO <sub>2</sub> ratios during CO <sub>2</sub> gasification process of pine bark and waste tyre at different blend ratios ...	127
<b>Figure 4.9</b> Effect of CO <sub>2</sub> -to-feed ratio on syngas characteristic (a) LHV of the syngas and (b) CGE of the process during CO <sub>2</sub> gasification of pine bark and waste tyre at different blend ratios...	129
<b>Figure 4.10</b> Effect of feed flow rate (0.2-2.0 kg/hr) on syngas composition (a) H <sub>2</sub> , (b) CO, (c) CO <sub>2</sub> , and yield (d) H <sub>2</sub> , (e) CO, (f) CO <sub>2</sub> during CO <sub>2</sub> gasification process of pine bark and waste tyre at different blend ratios .....	131
<b>Figure 4.11</b> The variation in (a) H <sub>2</sub> /CO ratio and (b) CO/CO <sub>2</sub> ratio in response to the change in feed flow rate during CO <sub>2</sub> gasification of pine bark and waste tyre at different blend ratios...	132
<b>Figure 4.12</b> Effect of feed flow rate on the gasification performance (a) LHV of the syngas and (b) CGE of the CO <sub>2</sub> gasification process of pine bark and waste tyre at different blend ratios.....	133
<b>Figure 5.1</b> Process flowsheet for the improved model .....	136
<b>Figure 5.2</b> Effect of gasification temperature on syngas composition (a) H <sub>2</sub> , (b) CO, (c) CO <sub>2</sub> , and yield (d) H <sub>2</sub> , (e) CO, (f) CO <sub>2</sub> during steam gasification of pine bark and waste tyre at different blend ratios .....	139
<b>Figure 5.3</b> Effect of gasification temperature on (a) H <sub>2</sub> /CO ratio and (b) CO/CO <sub>2</sub> ratio of the syngas during steam gasification of pine bark and waste tyre at different blend ratios.....	141

<b>Figure 5.4</b> Effect of gasification temperature on (a) LHV of the syngas and (b) CGE of the process during steam gasification of pine bark and waste tyre at different blend ratios.....	141
<b>Figure 5.5</b> Effect of steam to feed ratio on syngas composition (a) H <sub>2</sub> , (b) CO, (c) CO <sub>2</sub> , and yield (d) H <sub>2</sub> , (e) CO, (f) CO <sub>2</sub> during steam gasification of pine bark, waste tyre and their blends .....	144
<b>Figure 5.6</b> Variation in syngas characteristics (a) H <sub>2</sub> /CO, and (b) CO/CO <sub>2</sub> ratio with the change in steam-to-feed ratio for different samples during steam gasification .....	145
<b>Figure 5.7</b> Effect of steam-to-feed ratio on (a) LHV of the syngas, and (b) CGE of the steam gasification process of different pine bark and waste tyre blended samples.....	146
<b>Figure 5.8</b> Variation in syngas composition (a) H <sub>2</sub> , (b) CO, (c) CO <sub>2</sub> , and yield (d) H <sub>2</sub> , (e) CO, (f) CO <sub>2</sub> with the change in feed flow rate during steam gasification of pine bark and waste tyre at different blend ratios .....	148
<b>Figure 5.9</b> Change in syngas characteristics (a) H <sub>2</sub> /CO, and (b) CO/CO <sub>2</sub> ratio with the change in the feed flow rate for different blend samples during steam gasification.....	149
<b>Figure 5.10</b> Effect of feed flow rate on the (a) LHV of the syngas, and (b) CGE of the steam gasification process of different pine bark and waste tyre blended samples.....	150
<b>Figure 5.11</b> Variation in syngas composition; (a) H <sub>2</sub> , (b) CO and (c) CO <sub>2</sub> , and yield; (d) H <sub>2</sub> , (e) CO and (f) CO <sub>2</sub> with gasification temperature for steam/CO <sub>2</sub> gasification of WT1PB0, WT3PB1 and WT0PB1.....	154
<b>Figure 5.12</b> Effect of gasification temperature on syngas characteristics; (a) H <sub>2</sub> /CO, and (b) CO/CO <sub>2</sub> ratios for steam/CO <sub>2</sub> gasification of WT1PB0, WT3PB1 and WT0PB1 .....	155
<b>Figure 5.13</b> Effect of gasification temperature on (a) LHV of syngas, and (b) CGE of the steam/CO <sub>2</sub> gasification process of WT1PB0, WT3PB1 and WT0PB1 .....	156

**Figure 5.14** Effect of steam-to-feed ratio on syngas composition; (a) H<sub>2</sub>, (b) CO and (c) CO<sub>2</sub>, and yield; (a) H<sub>2</sub>, (b) CO and (c) CO<sub>2</sub> during steam/CO<sub>2</sub> gasification of WT1PB0, WT3PB1 and WT0PB1 ..... 158

**Figure 5.15** Effect of steam-to-feed ratio on syngas characteristics; (a) H<sub>2</sub>/CO, and (b) CO/CO<sub>2</sub> ratios for WT1PB0, WT3PB1 and WT0PB1 during steam/CO<sub>2</sub> gasification ..... 159

**Figure 5.16** Effect of steam-to-feed ratio on (a) LHV of syngas, and (b) CGE of the steam/CO<sub>2</sub> gasification process of WT1PB0, WT3PB1 and WT0PB1 ..... 160

**Figure 5.17** Effect of CO<sub>2</sub>-to-steam ratio in the gasifying agent on syngas composition; (a) H<sub>2</sub>, (b) CO and (c) CO<sub>2</sub>, and yield; (a) H<sub>2</sub>, (b) CO and (c) CO<sub>2</sub> during steam/CO<sub>2</sub> gasification of WT1PB0, WT3PB1 and WT0PB1 ..... 162

**Figure 5.18** Variation in syngas characteristics; (a) H<sub>2</sub>/CO, and (b) CO/CO<sub>2</sub> ratios for WT1PB0, WT3PB1 and WT0PB1 with the change in CO<sub>2</sub>-to-steam ratio in the gasifying agent during steam/CO<sub>2</sub> gasification ..... 163

**Figure 5.19** Results of the effect of CO<sub>2</sub>-to-steam ratio in the gasifying agent on (a) LHV of syngas, and (b) CGE of the steam/CO<sub>2</sub> gasification process for WT1PB0, WT3PB1 and WT0PB1 ..... 165

**Figure 5.20** Effect of feed flow rate on syngas composition; (a) H<sub>2</sub>, (b) CO and (c) CO<sub>2</sub>, and yield; (a) H<sub>2</sub>, (b) CO and (c) CO<sub>2</sub> during steam/CO<sub>2</sub> gasification of WT1PB0, WT3PB1 and WT0PB1 .. 167

**Figure 5.21** Variation in syngas characteristics; (a) H<sub>2</sub>/CO, and (b) CO/CO<sub>2</sub> ratios for WT1PB0, WT3PB1 and WT0PB1 with the change in feed flow rate during steam/CO<sub>2</sub> gasification ..... 168

**Figure 5.22** Results of the effect of feed flow rate on (a) LHV of syngas, and (b) CGE of the steam/CO<sub>2</sub> gasification process for WT1PB0, WT3PB1 and WT0PB1 ..... 169

## List of Tables

<b>Table 1.1</b> Typical composition of passenger car tyre and truck tyre (Williams, 2013) .....	7
<b>Table 1.2</b> Types of gasifying agents used in the gasification process and their advantages and disadvantages .....	10
<b>Table 1.3</b> List of main reactions taking place during the gasification process based on the literature (Ramos et al., 2018; Sadhwani et al., 2016) .....	12
<b>Table 1.4</b> List of some syngas end-uses and their requirement in terms of H <sub>2</sub> :CO ratio (Ephraim et al., 2016) .....	14
<b>Table 1.5</b> Comparison between model fitting and iso-conversional methods for the analysis of solid-state reaction kinetics using TGA data (Slopiecka et al., 2012) .....	15
<b>Table 2.1</b> Summary of gasification studies of biomass according to the type of gasifying agent	27
<b>Table 2.2</b> Selection of Commercial, demonstration and pilot gasification plants (IEA Bioenergy, n.d.) .....	30
<b>Table 2.3</b> Summary of the gasification studies of waste tyre .....	36
<b>Table 2.4</b> Summary of the Waste tyre gasification pilot plants .....	37
<b>Table 2.5</b> Summary of biomass and waste tyre co-gasification studies available in the literature .....	40
<b>Table 2.6</b> Summary of previous kinetic studies on pyrolysis of biomass .....	42
<b>Table 2.7</b> Summary of studies related to kinetic analysis of the pyrolysis of waste tyre .....	44
<b>Table 2.8</b> Summary of Kinetics analysis studies of co-pyrolysis of biomass and waste tyre .....	46
<b>Table 2.9</b> A selection of steady-state modelling/simulation studies of gasification of biomass using various approaches .....	48

<b>Table 2.10</b> Summary of modelling/simulation studies on gasification of waste tyre .....	49
<b>Table 2.11</b> List of the references for the key papers with the benefit for the current research project.....	51
<b>Table 3.1</b> Mathematical expressions of solid-state reaction functions; $f(\alpha)$ and $g(\alpha)$ , of different reaction mechanisms (White et al., 2011; Yeo et al., 2019).....	54
<b>Table 3.2</b> Proximate and Ultimate analysis of pine bark (Wang et al., 2019b, 2020b).....	60
<b>Table 3.3</b> Proximate and ultimate analysis of waste tyre (Wang et al., 2019b, 2020b) .....	60
<b>Table 3.4</b> Waste tyre and pine bark content in wt% of the blended samples .....	60
<b>Table 3.5</b> Thermal decomposition characteristics of the waste tyre and pine bark in the <i>Zone I</i> at different heating rates .....	70
<b>Table 3.6</b> Thermal decomposition characteristics of the waste tyre and pine bark blends in the <i>Zone I</i> at different heating rates .....	71
<b>Table 3.7</b> Average values of reaction kinetics parameters of the pyrolysis of single and blended samples in <i>Zone I</i> at four different heating rates .....	79
<b>Table 3.8</b> Average $E_a$ values for the co-pyrolysis of the waste tyre and pine bark at different blend ratios obtained by Iso-conversional methods and KCE. ....	92
<b>Table 3.9</b> Values of optimum parameters, activation energy and pre-exponential factor for different blend samples obtained through combined kinetic analysis .....	100
<b>Table 3.10</b> A comparison of the activation energy values of the samples used in the current study and those available in the literature.....	102
<b>Table 4.1</b> Summary of the experimental study-related parameters used in the model development (Wang et al., 2019b).....	106

<b>Table 4.2</b> Empirical expressions for the calculation of biomass devolatilization products (Neves et al., 2011; Pauls et al., 2016) .....	109
<b>Table 4.3</b> Kinetic data for the simulation of waste tyre devolatilization (Ismail et al., 2017) ...	110
<b>Table 4.4</b> The reactions and their kinetics used to simulate the gasification stage. ....	111
<b>Table 4.5</b> Main model blocks and their corresponding use in the model development .....	112
<b>Table 4.6</b> Results of model validation at different feedstock composition .....	114
<b>Table 4.7</b> Plan of process analysis .....	117
<b>Table 5.1</b> List of additional blocks and their application in the existing model .....	135
<b>Table 5.2</b> Process analysis plan for case 1: steam co-gasification of pine bark and waste tyre	137
<b>Table 5.3</b> Process analysis plan for case 2: steam/CO <sub>2</sub> co-gasification of pine bark and waste tyre .....	151
<b>Table 5.4</b> A comparison of CO <sub>2</sub> , steam and steam/CO <sub>2</sub> gasification results of WT1PB0, WT3PB1 and WT0PB1 at a temperature of 1173 K.....	171

## Nomenclatures

$\frac{d\alpha}{dt}$	The reaction rate in terms of conversion (the rate of change in conversion with time)
$\frac{d\alpha}{dT}$	The reaction rate at a constant heating rate (i.e. $\beta = dT/dt$ ) (the rate of change in conversion with temperature)
$k(T)$	The temperature dependence of the reaction rate
$f(\alpha)$	Differential reaction model function
$f(\alpha)_{0.5}$	Differential reaction model function at conversion (i.e. $\alpha$ ) = 0.5
$g(\alpha)$	Integral reaction model function
$y(\alpha)_{theoretical}$	Function for the calculation of theoretical master plots
$y(\alpha)_{exp}$	Function for the calculation of experimental master plots
$A$	Pre-exponential factor, $\text{min}^{-1}$
$E_a$	The apparent activation energy (J/mol)
$E_\alpha$	The activation energy (J/mol) at specific reaction extent or conversion, $\alpha$
$R$	Gas constant (8.3145 J/mol K)
$T$	Temperature (K)
$\alpha$	Conversion or reaction extent
$w_0$	The sample weight at the start of analysis where time $t = 0$
$w_t$	The sample weight when the time equals $t$
$w_\infty$	The sample weight at the end of the analysis
$\beta$	Heating rate (K/min)
$n$	Reaction order
$m, n$ and $p$	Parameters in Sestak-Berggren expression

$T_i$	Initial temperature, K
$T_{max}$	The maximum temperature at which the DTG peak occurs, K
$T_f$	Final temperature, K
$\Delta W$	The difference in weight loss
$W_{exp}$	Experimentally measured weight loss
$W_{cal}$	Theoretically calculated weight loss
$x_{WT}$	The weight fraction of waste tyre in the blend
$x_{PB}$	The weight fraction of pine bark in the blend
$W_{WT}$	Weight loss when a single feed of waste tyre is used for pyrolysis, wt%
$W_{PB}$	Weight loss when a single feed of pine bark is used for pyrolysis, wt%
$\bar{E}_{a,exp}$	The experimental average activation energy, J/mol
$\bar{E}_{a,cal}$	The theoretically calculated average activation energy, J/mol
$m_{H_2}$	Mass fraction of H <sub>2</sub> in the gas stream produced from the devolatilization stage
$m_{CH_4}$	Mass fraction of CH <sub>4</sub> in the gas stream produced from the devolatilization stage
$m_{CO}$	Mass fraction of CO in the gas stream produced from the devolatilization stage
$m_{CO_2}$	Mass fraction of CO <sub>2</sub> in the gas stream produced from the devolatilization stage
$m_{C_2H_4}$	Mass fraction of C <sub>2</sub> H <sub>4</sub> in the gas stream produced from the devolatilization stage
$m_{C,TAR}$	Mass fraction of C in the tar produced from the devolatilization stage
$m_{H,TAR}$	Mass fraction of H in the tar produced from the devolatilization stage
$m_{O,TAR}$	Mass fraction of O in the tar produced from the devolatilization stage
$m_{C,CHAR}$	Mass fraction of C in the char produced from the devolatilization stage
$m_{H,CHAR}$	Mass fraction of H in the char produced from the devolatilization stage
$m_{O,CHAR}$	Mass fraction of O in the char produced from the devolatilization stage

$m_{C,feed}$	Mass fraction of C in the feed based on the ultimate analysis
$m_{H,feed}$	Mass fraction of H in the feed based on the ultimate analysis
$m_{O,feed}$	Mass fraction of O in the feed based on the ultimate analysis
$y_{H_2}$	Mole fraction of H <sub>2</sub> in the syngas
$y_{CO}$	Mole fraction of CO in the syngas
$y_{CH_4}$	Mole fraction of CH <sub>4</sub> in the syngas
$y_{C_2H_4}$	Mole fraction of C <sub>2</sub> H <sub>4</sub> in the syngas
$LHV_g$	Lower heating value of the syngas in MJ/Nm <sup>3</sup>
$LHV_{f1}, LHV_{f2}$	Lower heating value of feed 1 and feed 2, respectively, in MJ/Nm <sup>3</sup>
$w_{i1}, w_{i2}$	Weight fraction of feed 1 and feed 2, respectively, in the blended sample
$V_g$	Volumetric flow rate of the syngas in Nm <sup>3</sup> /hr
$m_f$	Mass flow rate of feed in kg/hr

## List of Abbreviations

NR	Natural rubber
SBR	Styrene-butadiene rubber
PBR	Polybutadiene rubber
ICTAC	International Confederation for Thermal Analysis and Calorimetry
O/C	Oxygen to carbon molar ratio
H/C	Hydrogen to carbon molar ratio
BD	Boudouard reaction
WG	Water-gas reaction
WGS	Water-gas shift reaction
MR	Methane steam reforming reaction
MDR	Methane dry reforming
DR	Dry reforming reaction
RWGS	Reverse Water-gas shift reaction
H <sub>2</sub> /CO	Hydrogen to carbon monoxide molar ratio
CO/CO <sub>2</sub>	Carbon monoxide to carbon dioxide molar ratio
PB	Pine Bark
WT	Waste Tyre
CR	Coats-Redfern
FWO	Flynn-Wall-Ozawa
KAS	Kissinger-Akahira-Sunose
FR	Friedman

KCE	Kinetic Compensation Effect
CK	Combined Kinetics
SB	Sestak-Berggren
LHV	Lower Heating Value
TGA	Thermogravimetry/ Thermogravimetric Analysis
DTG	Differential Thermogravimetry
$T_i$	Initial temperature, K
$T_{max}$	The maximum temperature at which the DTG peak occurs, K
$T_f$	Final temperature, K
CGE	Cold Gas Efficiency, %
ASPEN	Advanced System for Process Engineering
PR-BM	Peng Robinson's equation of state with the Boston-Mathias alpha function
RE	Relative error, %
FTS	Fischer Tropsch synthesis

## CHAPTER 1 Introduction

Energy security and environmental unsustainability are the two main concerns over the world. These issues are due to irrational utilisation of conventional energy sources (consequently, greenhouse gas emissions and climate change) and increased generation of solid waste. To simultaneously address these concerns, gasification of biomass and waste tyre while considering CO<sub>2</sub> as a gasifying medium is an auspicious solution. This chapter will provide the research background in *Section 1.1*. In *Section 1.2*, biomass and waste tyre as feedstocks of interest in the current research are briefly introduced. In *Section 1.3*, an overview of the underpinning principles of pyrolysis and gasification process as thermochemical conversion routes of biomass and waste tyre are introduced. In addition, co-pyrolysis and co-gasification as a trending research field are highlighted along with their possible benefits. *Section 1.4* provides an overview of syngas as a versatile product of the gasification process and its application. In *Section 1.5*, kinetics analysis, its importance and the analysis methods are defined. Research motivation and aim and objectives are introduced in *Sections 1.6* and *1.7*, respectively. *Section 1.8* introduces the research methodology. *Section 1.9* justifies the novel contribution of the current research work. *Section 1.10* provides an outline of this thesis.

### 1.1 Research Background

#### 1.1.1 Worldwide energy and chemical demand

Globally, there is continuing industrial development and economic growth. Consequently, the demand for chemical and energy production is increasing. According to bp Statistical Review of World Energy (BP, 2022), the annual demand for primary energy has arisen by 5.80% in 2021 which accounts for an increase of 1.30% compared to 2019. Despite the increase in the share of

renewables as the sources of primary energy consumption from 1980 to 2020 as shown in Figure 1.1, fossil fuels, including coal, natural gas, and petroleum, are continuing to serve as the main sources to cover these ever-growing demands with the highest share of coal and petroleum and other liquids.

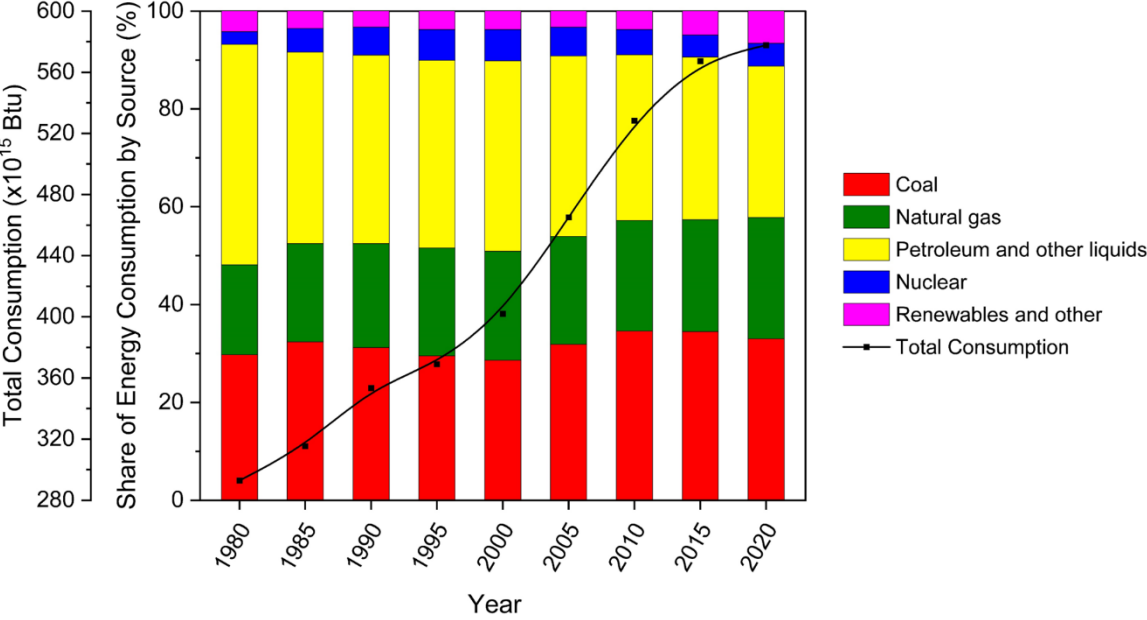


**Figure 1.1** Total primary energy consumption in Quad Btu and percent share of primary energy consumption by source (Source: reproduced using data from (BP, 2022))

1.1.2 Global warming and environmental issues

The extensive reliance on fossil fuels caused its depletion as well as various interrelated environmental issues. Consumption of fossil fuels by different industrial and transportation sectors releases carbon dioxide which is one of the greenhouse gases. The emission of carbon dioxide is contributing to the rise in average global temperature causing global warming and consequently climate change. Figure 1.2 (a) shows the percent share of different economic sectors in greenhouse gas emissions in the unit of Gt of CO<sub>2</sub> equivalent as of 2010 (IPCC, 2014).

Electricity and heat production, AFOLU (Agriculture, Forestry and Other Land Use), industry and transportation are the largest contributors to direct greenhouse gas emissions with a total share of 86.00%. According to International Energy Agency, IEA, (IEA, 2022), there is an increase in global CO<sub>2</sub> emission by 6.00% in 2021 compared to 2020, accounting for a total of 36.30 Gt as shown in Figure 1.2 (b) and (c).

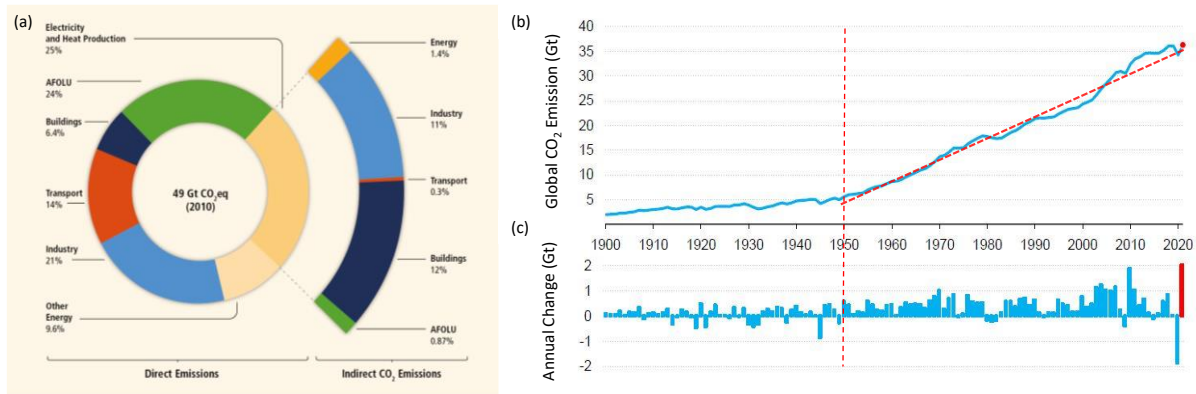


**Figure 1.2** (a) Share of different sectors toward global CO<sub>2</sub> equivalent emissions as of 2010 (IPCC, 2014) and (b) global CO<sub>2</sub> emission and (c) the annual change in global CO<sub>2</sub> emission over 1900-2021 (IEA, 2022)

To simultaneously mitigate these negative environmental impacts and minimize the dependence on fossil fuels, there is an urgent need to find new routes for chemical and energy production that are renewable and environmentally friendly, considering both the feedstock and the technologies involved.

### 1.1.3 Solid waste disposal and management

Parallel to the negative environmental impact driven by the overexploitation of fossil fuels, solid waste disposal and management is another emerging issue associated with the growing world population and its demand along with the increasing industrial activities. According to Kaza et al. (2018), it is projected that the global annual waste production will excessively increase to nearly 3.40 billion tonnes in 2050 compared to 2.01 billion tons in 2016. This resulted in an annual CO<sub>2</sub>

emission of an equivalent of 1.60 billion tonnes by 2016 and is expected to increase to 2.60 billion tonnes by 2050. Therefore, to minimize the negative environmental impacts induced by the current waste disposal and management routes, it is important to develop efficient treatment technologies involving material recycling and energy recovery.

## 1.2 Biomass and waste tyre as alternative feedstocks

In recent years, there has been a worldwide growing interest in the utilisation of renewable energy sources as well as waste materials as alternative energy sources. This is to maintain the issue of energy security associated with the gradual depletion of fossil fuels reserves as well as climate change and to ensure the disposal and utilisation of waste in a sustainable and environmental-friendly manner (Hita et al., 2016; Lahijani et al., 2013).

### 1.2.1 Biomass

In recent years, biomass has drawn great attention as an alternative energy source. This is because of its (1) abundance with total worldwide production of relatively 220 billion dry tons per year, making it the largest renewable energy source (Zhang et al., 2016a), (2) diversity in which it is available in different forms including agricultural residues, wood residues, dedicated energy crops and municipal solid waste (Abnisa and Daud, 2014) (3) carbon-neutrality contributing to natural CO<sub>2</sub> utilisation through photosynthesis (Hassan et al., 2016). In fact, biomass is complex biopolymers originated from living organisms. It is composed of mainly cellulose, hemicellulose and lignin with a mass fraction of nearly 40-50, 15-30 and 15-30 wt%, respectively, depending on the type of the species (Zhang et al., 2016a). Cellulose consists of  $\beta$ -1,4-glycoside linked polysaccharide polymer of glucose (Giudicianni et al., 2013). In addition, it

contains different hydroxyl groups which contribute to the formation of hydrogen bonds (Zhang et al., 2016a).

Unlike cellulose, hemicellulose consists of branched monosaccharides including pentose, hexose and uronic acid (Giudicianni et al., 2013). Lignin is a complex, aromatic and three-dimensional cross-linked polymer (Akubo et al., 2019) of propyl-phenol groups (Zhang et al., 2016a). Since lignin is composed of a high fraction of carbon, it stores nearly 40% of biomass energy (Zhang et al., 2016a).

Biomass as a reliable source of energy is converted to what is known as bio-fuel. The selection of the type of conversion route and its economic feasibility is driven by the complexity of the biomass itself in terms of chemical composition. Biomass is classified as 1<sup>st</sup>, 2<sup>nd</sup> and 3<sup>rd</sup> generation according to the type of biomass material used for biofuel production. A comparison between different types of biomasses is provided in Figure 1.3. The current research will focus on the use of 2<sup>nd</sup> generation biomass for syngas production through gasification.

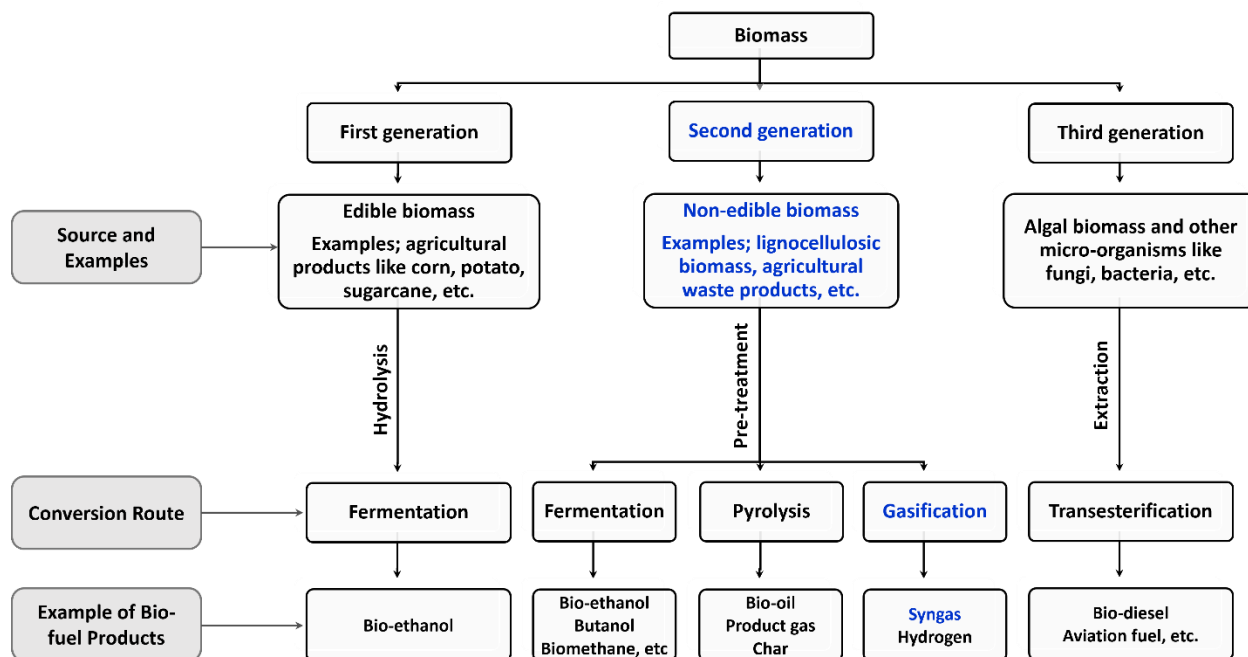


**Figure 1.3** Flow diagram presenting a comparison between 1st, 2nd and 3rd generation biomass (Source: constructed according to the info in Lee and Lavoie, 2013)

Biomass has a great potential to fulfil 25 to 30% of the world’s energy demand by 2050 (Alvarez et al., 2014; Farzad et al., 2016) therefore tackling the concerns related to energy security and increased resilience on fossil fuels. Figure 1.4 presents the biomass share in renewable energy production over the period from 1960 to 2020 accounting for 5.02% of the total primary energy production in 2020 compared to 3.08% in 1960 (EIA, 2023). This provides a good indication that the contribution of renewables in particular biomass to primary energy production will increase in the near future.

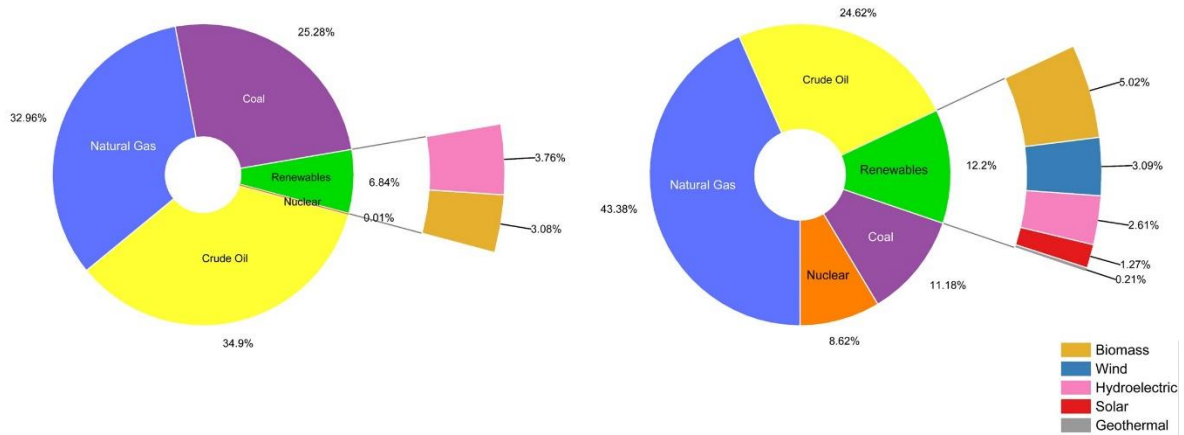


**Figure 1.4** Percent Share of Primary Energy Production by Source in (a) 1960 and (b) 2020 (Source: constructed using data from (EIA, 2023))

### 1.2.2 Waste tyre

Due to the rapid expansion in the automobile market as a result of economic growth and lifestyle standards, the disposal of waste tyres is another environmental issue worldwide. Tyre in fact is a polymeric material and varies in its composition due to intended application and end-use. Table 1.1 shows the typical composition of the passenger car and truck tyre in which the natural and synthetic rubbers make the highest fraction of around 45 wt%.

**Table 1.1** Typical composition of passenger car tyre and truck tyre (Williams, 2013)

Tyre component	Type of tyre	
	Passenger vehicle tyre, wt%	Truck tyre, wt%
1. Rubber	47	45
2. Carbon black	21.5	22
3. Metal	16.5	21.5
4. Textile	5.5	-
5. Zinc oxide	1	2
6. Sulphur	1	1
7. Additives	7.5	5

Worldwide, the annual tyre demand is expected to grow by 4.30% (Machin et al., 2017). In 2017, for instance, around 2.90 billion tons of tyres were produced to cover the demand of the automobile sector (Wang et al., 2019b) whereas 1 billion tons were disposed of in landfills.

The necessity towards the utilisation of waste tyres through material and chemical recycling is driven by several factors. First, the high energy content of waste tyres contained in the rubber fraction with an average of 32 MJ/kg (Choi et al., 2016) compared to 18 and 30 MJ/kg for biomass and coal, respectively (Ahmed and Gupta, 2011; Williams, 2005) makes it a viable source of fuel. Second, unsustainable disposal of waste tyres and low biodegradable nature cause environmental threats (Hita et al., 2016) including but not limited to land and water contamination and limitation in land capacity to sustain the increased waste production. Third, more than 90% of waste tyres composition is organic matter composing of carbon and hydrogen, making them a valuable resources (Zang et al., 2019). Therefore, it is likely to provide a potential source of hydrocarbon recycling. Finally, the formulation of waste-related regulations including the European Waste Landfill Directive 1999 prevented the landfilling of waste tyres (Williams, 2005). Therefore, waste tyres are likely to be promising feedstocks for thermochemical conversion routes, to simultaneously ensure effective management of waste tyres and sustain energy security.

### 1.2.3 A mixture of biomass and waste tyre

It has been recent research interest to use of a mixture of biomass and waste for the gasification processes. To assess the potential of solid feedstocks for chemical and/or energy production, however, the hydrogen-to-carbon molar ratio (i.e. H/C) and oxygen-to-carbon molar ratio (i.e. O/C) are important characteristics to consider (Škrbić et al., 2018). This is evaluated through the

Van-Krevelen diagram as shown in Figure 1.5. The waste tyre is characterized by a low O/C ratio compared to biomass, indicating its high heating value. However, both biomass and waste tyre are heterogeneous in their composition, therefore, the H/C ratio varies. In general, the potential of utilising certain feedstock for biofuel production is limited by its low H/C ratio. Therefore, blending two feedstocks with different H/C ratios through a thermochemical process would likely lead to positive synergetic interaction, improving the quality and quantity of the products.

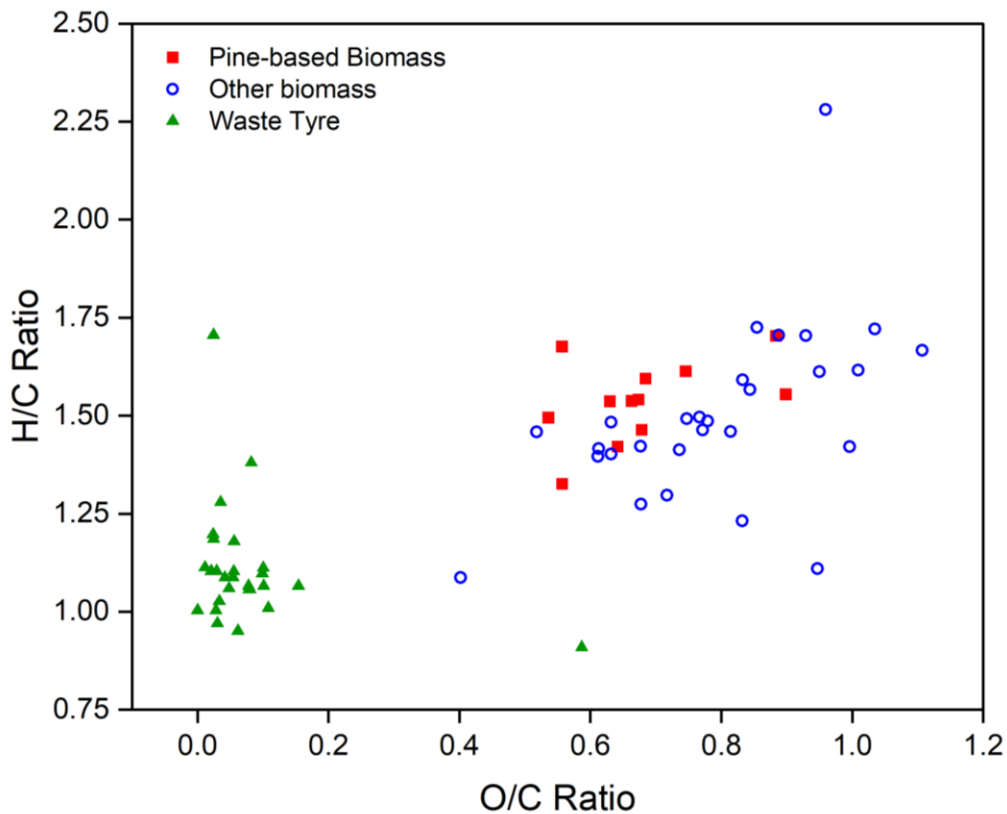


**Figure 1.5** Van-Krevelen diagram of biomass and waste tyre materials (Source: author elaboration based on the literature)

### 1.3 Pyrolysis and gasification of biomass and waste tyre

The most common thermochemical conversion pathways that contribute to waste management and biomass utilisation are pyrolysis and gasification. Since the improvements in these pathways are still feasible, they gain increasing research interest.

### 1.3.1 Pyrolysis

**Pyrolysis**, also known as de-volatilization, is the thermal-based degradation of the organic fraction of carbonaceous materials in the absence of gasifying agent like oxygen (Kandasamy and Gökalp, 2014). Oil, gas and char form the main products of the pyrolysis process. However, the quantity of these products is primarily affected by the operating conditions including temperature and heating rate (Williams, 2005).

### 1.3.2 Gasification

**Gasification** is a thermochemical conversion that involves the partial oxidation of the carbonaceous material into mainly gas (i.e. H<sub>2</sub>, CO, CH<sub>4</sub> and CO<sub>2</sub>) in the presence of a limited amount of gasifying agent, underlining the main difference between pyrolysis and gasification. In contrast to pyrolysis, gasification operates at higher temperatures (Farzad et al., 2016), varying between 800-1100 °C and 1000-1400 °C depending on the type of gasifying agent and the targeted end product compared to 400-800 °C in pyrolysis (Williams, 2005). Gasification is performed using different gasifying agents which include air, steam, oxygen, CO<sub>2</sub>, or a combination of them. Each type of gasifying agent has its advantages and disadvantages. These are summarised in Table 1.2. It should be emphasised that gasification inevitably involves pyrolysis.

**Table 1.2** Types of gasifying agents used in the gasification process and their advantages and disadvantages

Type of gasifying agent	Advantages	Disadvantages
1. Air	- Inexpensive (Zheng et al., 2018) and abundant (Islam, 2020) so economically feasible.	- Due to high N <sub>2</sub> content of the air, the produced gas will be diluted resulting in gas with low H <sub>2</sub> /CO ratio (Zheng et al., 2018) and energy content (<6

		MJ/m <sup>3</sup> ) (Aznar et al., 2006) thus limited application
<b>2. Steam</b>	<ul style="list-style-type: none"> <li>- Produces gas with high H<sub>2</sub> yield thus H<sub>2</sub>/CO ratio (Sharma and Sheth, 2016) and high heating value (Lee et al., 2014)</li> </ul>	<ul style="list-style-type: none"> <li>- Requires steam generator with reliable performance adding additional energy cost (Shen et al., 2019)</li> <li>- steam gasification processes are highly endothermic (Zheng et al., 2018).</li> <li>- High tar content (Aznar et al., 2006)</li> </ul>
<b>3. CO<sub>2</sub></b>	<ul style="list-style-type: none"> <li>- Produces CO-enriched gas.</li> <li>- Lower tar yield and improved cold gas efficiency (i.e. CGE) and carbon conversion (Shen et al., 2019)</li> </ul>	<ul style="list-style-type: none"> <li>- Highly endothermic thus requires an external heat source (Shen et al., 2019)</li> </ul>
<b>4. Oxygen</b>	<ul style="list-style-type: none"> <li>- High-quality product gas in terms of heating value (Aznar et al., 2006)</li> </ul>	<ul style="list-style-type: none"> <li>- Incur additional operating costs due to oxygen separation from air (Liu et al., 2018a)</li> </ul>

Throughout the gasification process, primary and secondary reactions take place. As part of primary reactions, the feeding solid materials will decompose into hydrocarbons and solid fractions known as char. The heavier hydrocarbons like tar, in turn, will crack into lighter ones through secondary reactions. Apart from hydrocarbon cracking, the presence of steam as gasifying agent aids in steam reforming and char gasification reactions (Oboirien and North, 2017). The gaseous fraction of the gasification product is known as product gas and contains mainly H<sub>2</sub>, CO, CO<sub>2</sub> and CH<sub>4</sub> (Elbaba and Williams, 2014) whereas syngas refers to the H<sub>2</sub> and CO content.

In the current work, the use of the word gasification refers to the use of both single stage and two stage reactors unless pyrolysis/reforming is mentioned which is specifically refers to two stage gasification process. In addition, the product gas of pyrolysis/ reforming or gasification process, containing H<sub>2</sub>, CO, CO<sub>2</sub> and CH<sub>4</sub> is referred to as syngas, unless otherwise stated.

Table 1.3 summarises a series of endothermic and exothermic reactions that occur in the presence of either air, steam or CO<sub>2</sub> as part of the gasification process.

**Table 1.3** List of main reactions taking place during the gasification process based on the literature (Ramos et al., 2018; Sadhwani et al., 2016)

Reaction name	Reaction equation	Heat of reaction (kJ/mol)
<b>Oxidation/ Combustion reactions</b>	$C + \frac{1}{2}O_2 \leftrightarrow CO_2$ (1.1)	-111
	$C + O_2 \leftrightarrow CO_2$ (1.2)	-394
	$CO + \frac{1}{2}O_2 \leftrightarrow CO_2$ (1.3)	-283
	$H_2 + \frac{1}{2}O_2 \leftrightarrow H_2O$ (1.4)	-242
<b>Boudouard (BD) reaction</b>	$C + CO_2 \leftrightarrow 2CO$ (1.5)	+172
<b>Water-gas (WG) reaction</b>	$C + H_2O \leftrightarrow CO + H_2$ (1.6)	+131
<b>Methanation reaction</b>	$C + 2H_2 \leftrightarrow CH_4$ (1.7)	-75
<b>Water-gas shift (WGS) reaction</b>	$CO + H_2O \leftrightarrow CO_2 + H_2$ (1.8)	-41
<b>Methane steam reforming (MR) reaction</b>	$CH_4 + H_2O \leftrightarrow 3H_2 + CO$ (1.9)	+206
<b>Methane dry reforming (MDR) or Dry reforming (DR) reaction</b>	$CH_4 + CO_2 \leftrightarrow 2H_2 + 2CO$ ( $C_nH_m + nCO_2 \leftrightarrow \frac{m}{2}H_2 + 2nCO$ ) (1.10)	+247

### 1.3.3 Co-pyrolysis and co-gasification

Co-pyrolysis and co-gasification involve using a mixture of feedstocks during the normal pyrolysis and gasification process (Hassan et al., 2016) while showing positive synergetic interaction. Nowadays, the research interest is towards the mixing of biomass and waste including waste tyres and plastics. This would help in overcoming the limitations of using biomass (like hydrogen deficiency and high oxygen content) in fuel production while effectively addressing the concern of waste disposal. In comparison to pyrolysis and gasification of a single feedstock, the use of a mixture of biomass and polymeric wastes showed positive results in terms of (1) higher yield of

volatiles thus better product quality (Burra and Gupta, 2018), (2) improved carbon conversion and carbon efficiency (Zhang et al., 2016a) and (3) lower activation energy (Chen et al., 2019c).

#### 1.4 Syngas potential from gasification of biomass and waste tyre

Due to the projected increase in world energy demand to be approximately  $7.15 \times 10^{20}$  J in 2030, accounting for a 44% increase since 2006, syngas will be of greater importance in the processes of power generation and liquid fuels production (Woolcock and Brown, 2013).

Syngas is a versatile product of the gasification process in which it can be used as either direct fuel in power generation or the synthesis of other valuable chemicals and fuels including diesel, hydrogen, ammonia and fertilizers (Farzad et al., 2016).

To date, steam reforming of fossil fuel resources like natural gas and coal forms the primary route of syngas production to meet the rising demand for the current economic growth (Chen et al., 2016). Therefore, syngas sourced from gasification of carbonaceous feedstock other than fossil fuels is inevitably important.

##### 1.4.1 Global syngas market

Worldwide, the syngas market had an economic value of 43.60 billion dollars in 2019. It is anticipated to rise at a compound annual growth rate (i.e. CAGR) of 6.10% from 2020 to 2027, reaching 66.50 billion dollars by 2027 (Research and Markets, 2021). This is due to increased demand for chemical synthesis and the production of synthetic natural gas.

##### 1.4.2 Syngas quality and associated applications

Typically, the raw syngas produced from different carbonaceous materials like coal, petroleum residues, etc., composes mainly of CO (30-60 vol%) followed by H<sub>2</sub> (25-30 vol%), CO<sub>2</sub> (5-15 vol%)

and H<sub>2</sub>O (Mondal et al., 2011). The difference in the composition and the quality of syngas is because of the variation in the composition of the feedstocks as well as the type of the gasifier thus temperature, feedstock particle size, etc. Table 1.4 provides examples of syngas applications and their requirement for syngas quality in terms of hydrogen to carbon monoxide molar ratio (i.e. H<sub>2</sub>/CO).

**Table 1.4** List of some syngas end-uses and their requirement in terms of H<sub>2</sub>:CO ratio (Ephraim et al., 2016)

Syngas Application	H <sub>2</sub> /CO Ratio
Solid oxide fuel cells	4.00–6.00
Combustion in gas turbine	2.50–4.00
Fischer-Tropsch for diesel fuels synthesis	1.50–3.00
Fischer-Tropsch (Fe and Co-based catalyst process)	0.50–1.50

### 1.5 Kinetics analysis for potential synergetic interaction during co-pyrolysis

From the designing, optimization and scaling up perspective of the pyrolysis and/or gasification process, it is crucial to understand the kinetics underpinning the pyrolysis and/or gasification of solid feedstocks, like biomass, waste tyre and their blends. Additionally, it provides fundamental knowledge of the mechanisms through which solid materials decompose (Ebrahimi-Kahrizsangi and Abbasi, 2008).

Various kinetic analysis methods have been developed to estimate the kinetics parameters including activation energy (i.e.  $E_a$ ) and pre-exponential factor (i.e.  $A$ ) of solid materials. These methods are grouped into model fitting and iso-conversional (also known as model-free). Due to the simplicity of model fitting methods, they are widely employed by researchers (Ganeshan et al., 2018; Hu et al., 2020; Singh et al., 2012). However, iso-conversional methods are more

accurate than model-fitting methods and do not require an estimation of the reaction model (Azizi et al., 2019; Menares et al., 2020; Slopiecka et al., 2012). A comparison, in brief, between the two methods is outlined in Table 1.5.

**Table 1.5** Comparison between model fitting and iso-conversional methods for the analysis of solid-state reaction kinetics using TGA data (Slopiecka et al., 2012)

Method	1. Model Fitting		2. Iso-conversional	
<b>Principle</b>	Based on the trial of different kinetics models where the kinetics parameters are calculated using the model with the best statistical fit (i.e. $R^2$ )		Uses TG data obtained at different heating rates to construct the kinetic curves and obtain the kinetic parameters for each reaction extent (i.e. $\alpha_i$ )	
<b>Advantages</b>	Uses single TGA measurement for the calculation of kinetics parameters		Demonstrates the dependence of the kinetics parameters on $\alpha_i$ and avoids the error associated with the selection of reaction model (i.e. $f(\alpha)$ or $g(\alpha)$ )	
<b>Disadvantages</b>	Difficulty in the selection of a suitable reaction model Kinetics parameters are likely to be overestimated, particularly in non-isothermal regime		Several experiments need to be conducted at multiple heating rates while maintaining the same experimental conditions (i.e. inert gas flow rate, sample mass, etc.).	
<b>Types</b>	Isothermal	Non-isothermal	Isothermal	Non-isothermal
<b>Examples</b>	Conventional	(1) Differential, (2) Freeman-Carroll and (3) Coats-Redfern (i.e. CR)	(1) Standard, (2) Friedman (i.e. FR) and (3) Advanced Iso-conversional (i.e. AIC)	(1) Kissinger, (2) Flynn-Wall and Ozawa (i.e. FWO), (3) Kissinger-Akahira-Sonuse (i.e. KAS) and (4) Vyazovkin and AIC

## 1.6 Motivation of the current research

The current research work is driven by two main motivations. First, to understand the synergy underlying the co-feeding of waste tyres with biomass in terms of weight loss and kinetics

analysis. Second, to simultaneously utilise CO<sub>2</sub> and increase syngas production from co-gasification of biomass and waste tyre.

1.6.1 The first driver: to understand the potential synergy underlying the co-feeding of waste tyres with biomass.

Understanding the synergy underlying the thermal decomposition of a blend of biomass and waste tyre is the main driver of the current research work. It is an important factor in the selection of the co-feeding materials and the appropriate mass blending ratios. Since waste tyre is high in C and H content which is relatively comparable if not higher than biomass so co-gasification is more likely to improve the products derived from biomass into better quality and yield. In addition, high amount of volatile matter contained in waste tyre contribute to the production of syngas which is highly suitable to be converted into high-value fuels and products (Fajimi et al., 2021). With clear understanding of the synergetic interaction between biomass and waste tyre, it would provide clear knowledge for the potential of improving the H<sub>2</sub>/CO ratio of the syngas derived from biomass only.

1.6.2 The second driver: to utilise CO<sub>2</sub> through gasification for syngas production.

Production of syngas through gasification of solid materials including biomass and waste is of great research interest. Syngas is a versatile product which can be used for various applications acting as an intermediate product for chemical and fuel synthesis as well as fuel for thermal energy generation (Wang et al., 2020b). Although the use of CO<sub>2</sub> as a gasifying agent involves endothermic reactions which require an external source of heat, it could contribute to the following advantages: (i) Replacing air with CO<sub>2</sub> as a gasifying agent could lower the undesirable

N<sub>2</sub> content in the product gas. At lower operating temperatures, CO<sub>2</sub> behaves as an inert medium whereas it could be converted to CO at higher temperatures (Shen et al., 2019), (ii) use of CO<sub>2</sub> during the gasification process could produce syngas with an energy content that is comparable to the one produced during air gasification (Shen et al., 2019), (iii) the use of CO<sub>2</sub> would improve the H<sub>2</sub> and CO content of the syngas due to enhanced hydrocarbons dry reforming reactions (Mauerhofer et al., 2019), (iv) since CO<sub>2</sub> is used as a gasifying agent and transferred through gasification process, this would provide a potential to be integrated to carbon capture technology for the utilisation of captured CO<sub>2</sub> (Lahijani et al., 2015).

On the other hand, the desire for syngas production is driven by the following benefits: (i) It is cleaner and more environmentally friendly to use syngas for heat and power generation, for example, than solid feedstocks (Molino et al., 2016). In addition, it has higher energy density than biomass (Cerone et al., 2020), (ii) it is a versatile product in which it can be widely utilised in either the synthesis of commercially valuable chemicals (Inayat et al., 2019), heat and power generation through CHP (Tezer et al., 2022) or biochemical production through fermentation. Furthermore, it can be easily converted to synthetic natural gas via catalytic methanation (Cerone et al., 2020), (iii) in addition to being conveniently stored and transported, it can also be fed into existing boilers and combustors with minimal modifications (Oboirien and North, 2017).

## 1.7 Aim and objectives

The current research work aims to investigate the existence of synergetic interaction during the thermal decomposition of pine bark and waste tyre and the production of syngas from co-gasification of pine bark and waste tyre using CO<sub>2</sub> as gasifying agent through process simulation.

Three main research objectives are outlined to address the research aim as shown below:

- 1) Examine the thermal decomposition behaviour of pine bark, waste tyre and their blends through manipulation of thermogravimetric analysis (i.e. TGA) data and to evaluate the existence of synergetic interaction between biomass and waste tyre in terms of weight loss and reaction kinetics. This is addressed in Chapter 3.
- 2) Develop a model for gasification of pine bark and waste tyre in the context of CO<sub>2</sub> utilisation as a gasifying agent using Aspen Plus® and to investigate the effect of process operating conditions on syngas production and quality as well as process performance. This research objective is addressed in Chapter 4.
- 3) Comparatively analyse the effect of using steam as a co-gasifying agent along with CO<sub>2</sub> for the potential to enhance syngas yield and quality during co-gasification of biomass and waste tyre through process simulation. This is addressed in Chapter 5.

## 1.8 Research methodology

The research methodology of the current research work is depicted as a flow diagram in Figure 1.6 and summarised as follows:

- 1) Review of the previous studies: It consists of a comprehensive literature review on the gasification process of the selected feedstocks (i.e. biomass and waste tyre) from a syngas production and kinetics analysis perspective. This helped in gaining knowledge of the recent research work, identifying the research gaps, and formulating the current research aim and objectives.
- 2) Experimental TGA data manipulation: Once the research gap is identified in the field of gasification of biomass and waste tyre, the experimental data on TGA was obtained in collaboration with The Combustion laboratory at the University of Maryland, USA. These

data were then manipulated to understand the thermal decomposition behaviour of the selected feedstocks and to assess the effect of different pine bark-to-waste tyre mass ratios on the kinetics and the existence of any synergetic interaction. This is achieved by the implementation of different analysis methods including model fitting, iso-conversional and combined kinetic analysis.

- 3) Steady-state modelling and simulation of co-gasification of biomass and waste tyre for syngas production using ASPEN Plus® software: After indicating the possible synergetic interaction between the two specified feedstocks in terms of kinetics analysis, they were modelled and simulated for the potential of higher syngas production using CO<sub>2</sub> and to comprehensively assess the potential of blending pine bark and waste tyre. In addition, it provides insight into the utilisation of CO<sub>2</sub> as gasifying medium and the effect of different operating parameters on the quantity and quality of the product, in particular syngas. The modelling/simulation works are based on the implementation of reaction kinetics, which more likely results in a model with better accuracy compared to an oversimplified non-stoichiometric approach. Since the H<sub>2</sub>/CO ratio of syngas is an important criterion for the intended use, insights are provided through a comparative evaluation of co-gasification of pine bark and waste tyre using steam and steam/CO<sub>2</sub> mixture.

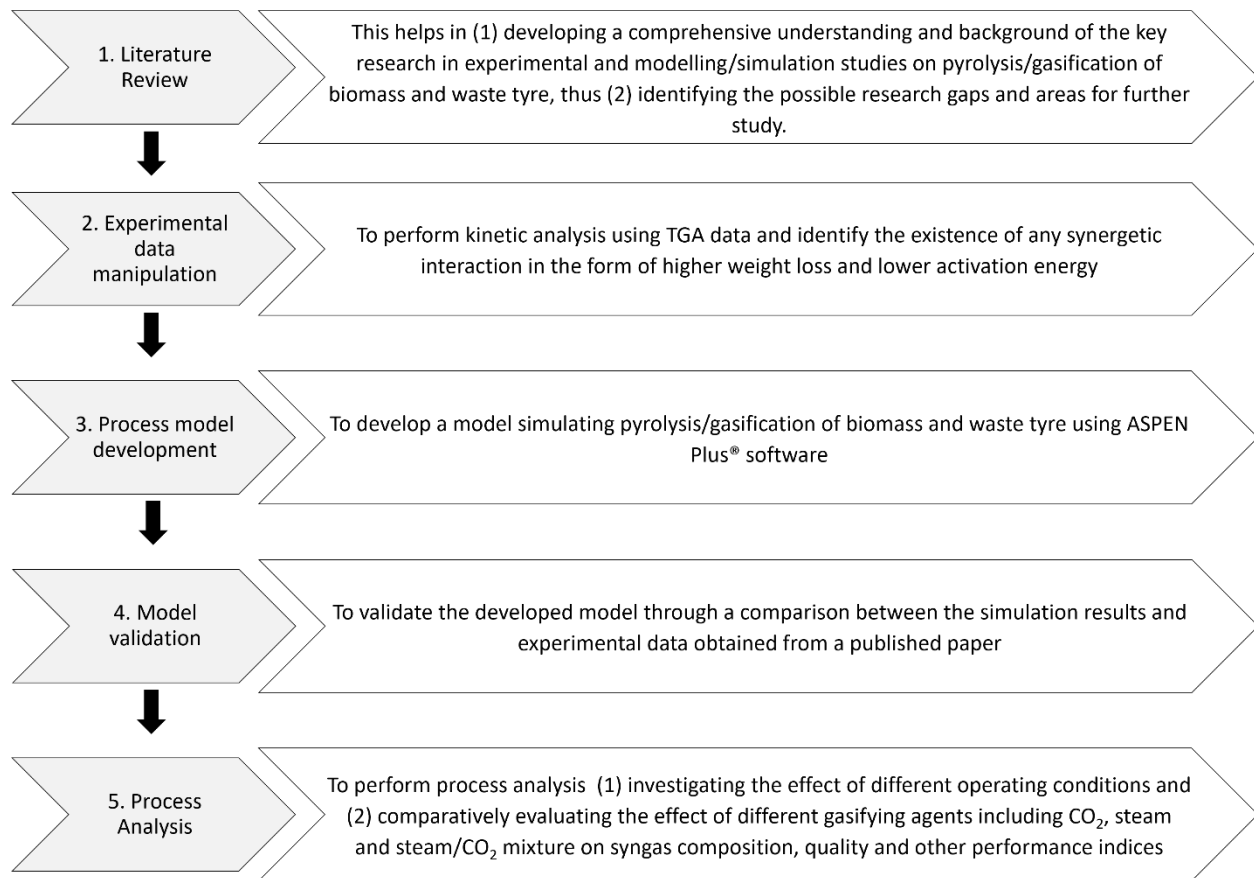


**Figure 1.6** Flow diagram of the research methodology adopted in the current research project

### 1.8.1 Simulation tool for process modelling and simulation

ASPEN Plus® software is used to model and simulate the co-gasification process of pine bark and waste tyre. Aspen Plus® is process modelling, simulation, and optimization software. ASPEN stands for Advanced System for Process ENgineering. It works on the principle of relating basic engineering principles including material and energy balances, thermodynamics, reaction stoichiometry and kinetics as well as heat and mass transfer (Al-Malah, 2017). Aspen Plus® was selected as process modelling/simulation software due to its superior database for the simulation of non-conventional solids (Abdelouahed et al., 2012).

## 1.9 Novel contributions

The novel contributions of the current research project are outlined as follows:

### 1.9.1 Estimation of reaction kinetics of co-pyrolysis of biomass and waste tyre through combined kinetic Analysis method

- No previous studies are available in the literature on the kinetics analysis of the thermal decomposition of a mixture of pine bark and waste tyre. This will advance the kinetics database that is currently available for the co-pyrolysis process and build fundamental knowledge about the possible synergetic in terms of weight loss and activation energy.
- Comprehensive experimental data manipulation was performed to investigate the existence of synergetic interaction. Most importantly, there is a lack of studies on the kinetics analysis of the thermal decomposition of a mixture of biomass and waste tyre through combined kinetics analysis. Therefore, the current study comparatively examines the kinetics obtained through different methods. Unlike previous studies which assumed the  $n^{\text{th}}$ -order reaction model, the current work offers important theoretical context for any possible reaction mechanisms that may underlie the co-pyrolysis of waste tyres and pine bark. In addition, the  $n^{\text{th}}$ -order reaction model is based on the estimation of the kinetics parameters at single heating rate. Therefore, this will result in less adaptability due to the tendency of the kinetics parameters to vary with the heating rate. In contrast, combined kinetics analysis utilises the data of different heating rate improving the adaptability of the estimated kinetics.

1.9.2 Insights from a comparison of co-gasification of biomass and waste tyre using different gasifying agents through process simulation.

- Neither experimental nor simulation comprehensive studies are available on the co-gasification of biomass and waste tyre using steam or steam/CO<sub>2</sub> mixture.
- Studies addressing the effect of CO<sub>2</sub> as an oxidizing agent on gasification behaviour are limited. Therefore, considering this would provide a mean to tackle the vast quantities of the released CO<sub>2</sub> from different sources like industrial and commercial.
- A comprehensive process analysis was performed to investigate the effect of changing operating conditions including gasification media on gas production, its characteristics and process performance.

1.10 Outline of the thesis

To accomplish the current research objectives, the thesis is organised as follows:

**Chapter 2** will review previous experimental and modelling/ simulation studies related to gasification of biomass and waste tyre in the context of waste tyre utilisation.

**Chapter 3** will present the results of experimental data manipulation to estimate the kinetic parameters underlying the thermal decomposition of biomass and waste tyre at different mass ratios.

**Chapter 4** will present modelling and simulation studies to utilise CO<sub>2</sub> as a gasifying medium in the co-gasification of biomass and waste tyre for syngas production.

**Chapter 5** will present simulation studies to provide insights on the effect of using steam and steam/CO<sub>2</sub> mixture as gasifying agents on syngas quality and yield as well as process performance.

**Chapter 6** will draw conclusions from the current research work and outline recommendations for further future work.

## CHAPTER 2 Literature review

In this chapter, previous studies on gasification of biomass and waste tyre for syngas production are reviewed. Both experimental and modelling/simulation studies are considered. In addition, the effect of various operating parameters including type of feedstock, temperature, and type of gasifying agent is analysed. At the end of the chapter, a summary of the main findings is provided and the research gaps are highlighted.

### 2.1 Experimental studies of gasification of biomass and waste tyre

Gasification of biomass and waste is a research topic of great importance to the world. Therefore, studies investigating the effect of operating parameters on syngas production are considerably available.

#### 2.1.1 Experimental studies of gasification of biomass

Syngas production through gasification of biomass is affected by the type of biomass used and the fraction of its constituents including cellulose, hemicellulose and lignin. According to Akubo et al. (2019), the presence of both steam and catalyst promotes the decomposition of lignin, resulting in an increase in syngas fraction and in particular the H<sub>2</sub> content. However, the high fraction of hemicellulose and cellulose positively contributes to syngas fraction in the absence of both the catalyst and steam.

In addition to the effect of the biomass material, the gasification temperature has a significant effect on syngas composition and yield and varies in response to the change in other operating parameters like the type of the gasifying agent, reactor and catalyst. For instance, Liu et al. (2018a), Waheed et al. (2016) and Xie et al. (2012) investigated the effect of gasification temperature on syngas yield and composition but under different operating conditions. Under

30% O<sub>2</sub>-enriched air in a bubbling fluidized bed, the H<sub>2</sub> and CO content in the syngas was positively affected in response to the increase in temperature from 600 to 800 °C (Liu et al., 2018a). Similarly, Waheed et al. (2016) found a positive significant effect of temperature on H<sub>2</sub> yield and content during pyrolysis/catalytic steam reforming in entrained flow gasifier. However, the use of steam in a two-stage fixed bed reactor, in the presence of a Ni-based catalyst, has a negative effect on syngas yield and H<sub>2</sub> and CO content as the temperature increased beyond 800 °C (Xie et al., 2012). Therefore, this indicates that the type of the gasifying agent as another factor has an impact as well on both the composition and yield of syngas.

Different gasifying agents, including air, steam, oxygen and carbon dioxide, have been examined in various studies of biomass gasification for the desired syngas composition. Despite the benefit of using air as a gasifying agent in providing heat for the gasification process as a result of partial combustion and being economically feasible, it produces syngas with low heating value and high tar yield (Puig-Gamero et al., 2018; Ramos et al., 2018; Sansaniwal et al., 2017; Yu et al., 2013). There is a large number of studies (e.g., Fu et al., 2023; Zhang et al., 2023; Zheng et al., 2018), that have reported the negative effect of the increase in equivalence ratio (i.e. ER) on CH<sub>4</sub>, CO and H<sub>2</sub> content of the syngas. However, the use of O<sub>2</sub>-enriched air and pure O<sub>2</sub> improves the syngas composition, particularly H<sub>2</sub> and CO content. This was demonstrated by Liu et al. (2018a), Wang et al. (2015) and Yu et al. (2013). Although pure oxygen results in improved syngas quality in terms of higher H<sub>2</sub> and CO content and lower tar content, it is more expensive to produce. According to Mauerhofer et al. (2019), CO<sub>2</sub> as a gasifying agent may have a catalytic activity that improves tar cracking. The unconverted CO<sub>2</sub> fraction in the syngas, however, will increase as a result of excessive CO<sub>2</sub> input (Antolini et al., 2019). Therefore, in the gasification process, it is

essential to take into account the type of gasifying agent to use and the selection of the proper gasifying agent to biomass ratio.

Use of different catalysts in the gasification process affected differently the syngas composition and yield. For instance, the effect of Ni- $\text{AlO}_x$  catalyst on syngas composition and yield was studied for various Ni-loading and the type of promoter. Dong et al. (2017) reported the highest syngas and  $\text{H}_2$  yield with a Ni loading of 35 mol% during pyrolysis/ steam reforming of wood sawdust. Using Zn as a promoter in Ni- $\text{AlO}_x$  catalyst showed a positive effect on  $\text{H}_2$  production and better performance against coke formation (Dong et al., 2017) whereas Ca reduced undesirable  $\text{CO}_2$  content in syngas with  $\text{H}_2$  and CO forming nearly 90% of its volume (Chen et al., 2016). This is due to enhanced dry reforming (i.e. DR) reactions induced by the presence of alkaline earth metal (i.e. Ca). However, the change in Zn to Al ratio in Fe-Zn/ $\text{Al}_2\text{O}_3$  showed minimal effect on the fractions of hydrocarbon in the syngas (Chen et al., 2015). A summary of some of the previous studies on gasification of biomass is provided in Table 2.1 according to the type of the gasifying agent.

**Table 2.1** Summary of gasification studies of biomass according to the type of gasifying agent

Gasifying agent	Feedstock	Temperature (°C)		Type of Reactor	Application	Ref.
		Pyrolysis	Reforming			
Steam	Pinewood sawdust	600-900	700-900	2-stage Tube furnace reactor	Syngas production	Xie et al. (2012)
	Wood sawdust	500	800	2-stage fixed bed reactor	H <sub>2</sub> -rich syngas production	Chen et al. (2015)
	Rice husk	950	850-1050	2-stage fixed bed reactor	Syngas production	Waheed et al. (2016)
	Pinewood sawdust	500	800	2-stage fixed bed reactor	H <sub>2</sub> -rich syngas production	Chen et al. (2016)
	Sawdust pellets	500	900	2-stage fixed bed reactor	H <sub>2</sub> -rich syngas production	Al-Rahbi and Williams (2017)
	Wood sawdust	550	800	2-Stage fixed bed reactor	H <sub>2</sub> production	Ye et al. (2018)
	Rice husk, coconut shell, sugarcane bagasse, palm kernel shell, cotton stalk and wheat straw	550	750	2-stage fixed bed reactor	H <sub>2</sub> / Syngas production	Akubo et al. (2019)
Air	Corn Stalk	< 578	≈ 900	3-air stage downdraft fixed bed	Syngas production	Guo et al. (2014)
	Black pine pellets	Max. of 943		Updraft fixed bed	Syngas production	Kihedu et al. (2016)
	Waste wood pellets	700/800		Lab scale fixed bed	Syngas Production	Shen et al. (2019)

	A mixture of wood chips/ corn cobs and sugarcane bagasse/ coconut shells	800		pilot-scale (24kW <sub>e</sub> ) downdraft fixed bed	Syngas Production	Awais et al. (2022)
<b>O<sub>2</sub>- enriched air or O<sub>2</sub></b>	Rice straw	1000		Entrained flow	Syngas Production	Yu et al. (2013)
	Rice straw	700		2-stage fluidized bed	Syngas production	(Liu et al., 2018a)
<b>CO<sub>2</sub></b>	Pine sawdust	700-935		bubbling fluidized bed	Syngas production	Sadhvani et al. (2016)
	Waste wood pellets	700/800		Lab scale fixed bed	Syngas Production	Shen et al. (2019)
	Pine bark	700-1000		Fixed bed semi-batch	Syngas Production	Wang et al. (2020)
<b>CO<sub>2</sub>/ steam</b>	Softwood pellets	817-828	934-938	100 kW <sub>th</sub> dual fluidized bed pilot plant	Syngas Production	Mauerhofer et al. (2019)
<b>CO<sub>2</sub>/air</b>	Waste wood pellets	561 <sup>1</sup> & 770 <sup>2</sup>		Autothermal downdraft fixed bed	Syngas Production	Shen et al. (2019)
<b>Steam/ air</b>	Black pine pellets	Max. of 943		Updraft fixed bed	Syngas Production	Kihedu et al. (2016)

<sup>1</sup> Combustion temperature

<sup>2</sup> Reduction temperature

In short, despite the available studies on the gasification of biomass, there are some challenges inherent to the use of biomass for syngas production. These challenges include but are not limited to; (1) Unlike fossil fuels, biomass is highly heterogeneous due to the existence of various biomass species, which shows variation in oxygen, moisture and energy content (Cherubini, 2010). Thus, this will affect the quality and the yield of final products as well as the process operation, (2) high inherent oxygen content of the biomass, relative to waste tyres and conventional fuels, (Likun and Zhang, 2020) affects the process performance and the quality of the product resulting in syngas with low heating value, (3) Due to (2), biomass is low in effective hydrogen content so producing syngas with  $H_2/CO$  ratio close to unity or lower (Alvarez et al., 2014; Chiodini et al., 2017), and (4) seasonal availability of the biomass affects the supply thus the process operation.

#### *2.1.1.1 Examples of commercial and pilot plants*

Table 2.2 provides a summary of some of the operational gasification plants around the world. Based on the global database available in IEA Bioenergy (no date), most of the commercial plants in operation are located in Europe with applications in power and heat production. Wood pellets and chips form the largest fraction of the biomass used through the gasification process at different scales.

**Table 2.2** Selection of Commercial, demonstration and pilot gasification plants (IEA Bioenergy, n.d.)

<b>A. Commercial, Pilot and Demonstration with Power/ CHP Technology</b>							
Scale	Location	Project Name/ Owner	In operation since	Type of feedstock	Type of Reactor	Output	
						Electricity (MW)	Heat (MW)
Commercial	Germany	Pritscher Landshut	1995	Wood chips	-	0.045	0.120
	Denmark	CHP B&W Harboore	1996	Wood chips	Updraft fixed bed	1.000	3.500
	Finland	District heating plant	2005	Wood chips	Fixed bed in co-current flow	0.030	0.080
	Italy	Comune Quingentole	2006	Wood chips	Downdraft fixed bed	0.070	0.140
	Germany	Kuntschar Wolfshagen	2006	Wood chips and pellets	Fixed bed	0.200	0.270
	Japan	CHP Updraft gasifier Yamagata	2007	Lignocellulosic (not specified)	Updraft fixed bed	2.000	8.000
	Switzerland	CHP Pyroforce Nidwalden	2007	demolition wood chips	2-zone downdraft Pyroforce gasifier	1.380	1.200
	Italy	Castel DAAiano	2008	Wood chips	Updraft fixed bed	0.035	0.140
	Denmark	Skive CHP plant	2008	Wood pellets	Bubbling fluidized bed	6.000	13.000
	Germany	Burkhardt Cham	2009	Wood chips and pellets	Fluidized bed in co-current flow	0.180	0.270
	Austria	CraftWerk Schwaz	2009	Wood chips	Floating fixed bed	0.100	0.500
	Germany	Burkhardt Neumarkt	2010	Wood chips and pellets	Fluidized bed in co-current flow	0.180	0.270
	Ireland	Carlow	2011	Wood chips	Updraft fixed bed	0.035	-
	Finland	Kymijaervi II	2012	Organic residues and waste streams	Circulating Fluidized Bed	50.000	90.000
	Germany	WUN Bioenergy	2012	Wood chips and pellets	Fluidized bed in co-current flow	0.36	0.54
	Switzerland	Steiner A. & Cie AG	2013	Wood chips	Downdraft Spanner gasifier	0.045	0.105
	Germany	HGKW Bad Wildungen	2014	Wood chips	Fixed bed	0.3	0.5
	Austria	CraftWerk Hatlerdorf	2014	Wood chips	Staged floating fixed bed	0.25	0.35
	Germany	Bioenergie Schnellingen	2015	Wood chips and pellets	Fluidized bed in co-current flow	0.4	0.518
Austria	CraftWerk Stadl	2017	Wood chips	Staged floating fixed bed	0.40	0.615	

	United Kingdom	Birmingham Bio-power	2018	Waste Wood	Nexterra (close-coupled)	10.3	-
	Thailand	Nongbua DFB gasifier	2018	Wood chips	Dual fluidized bed	1.0	1.25
	Belgium	Mont-Godinne Hospital (Xylowatt)	2018	Wood chips + Recycled wood	Downdraft gasifier	0.75	1.6
	Switzerland	Kombi Power System Charmey	2020	Wood chips	Updraft gasifier (ReGaWatt)	0.89	4.5
<b>Pilot</b>	Germany	CHP Agnion Biomasse Heizkraftwerk Pfaffenhofen	2001	Waste Wood	-	6.1	28
	Finland	Kempele Ecovillage	2009	Wood chips	-	0.03	0.08
<b>Demonstration</b>	Austria	CHP Demonstrationsanlagen URBAS	2001	Wood chips	-	0.15	0.30
	Italy	ICQ/SIAG/ERBA	2009	Wood chips	-	0.5	-
	Germany	Wegscheid Demo	2009	Wood chips and pellets	Fixed bed in co-current flow	0.125	0.23
	Sweden	VIPP Demonstration	2012	Biomass pellets	-	1.2	2.2
	Germany	Ecoloop GmbH	2020	Wood chips + Expanded polystyrene	Fixed bed counter flow	0.068	0.123

### ***B. Commercial, Pilot and Demonstration with Gasification/ Fuel Synthesis Technology***

<b>Scale</b>	<b>Location</b>	<b>Project Name/ Owner</b>	<b>In operation since</b>	<b>Type of feedstock</b>	<b>Type of Reactor</b>	<b>Output</b>
<b>Commercial</b>	United Kingdom	Sustainable Energy Centre	2021	Organic residues and waste streams	-	1.8 MWe
	United Kingdom	Swindon Advanced Biofuels Plant	2022	Refuse derived fuel and waste wood	ABSL RadGas and Wood VESTA technology	- 1500 t SNG/y - 500 t Hydrogen/y
<b>Pilot</b>	Denmark	Viking Gasifier	2002	Organic residue and waste stream	2 Stage Gasifier	- Clean syngas - 0.002 t FT Liquids/y - Mixed alcohols
	United States	technology development laboratory and pilot plant – thermochemical	2007	Cellulosics, Municipal wastes, syngas	-	-
<b>Demo.</b>	Austria	Waste2Value	2022	Biogenic residue and waste	-	- Clean syngas - 44 t FT Liquids/y

### 2.1.2 Experimental studies of gasification of waste tyre

Along with the biomass, studies related to the gasification of the waste tyre were reviewed, considering the effect of different operating conditions like tyre composition, gasification temperature, use of catalyst and its type, etc., on the syngas composition and yield.

There are different types of tyres according to their composition which are intended for various uses. Research on the effect of different waste tyres according to their type as well as the contained components including natural rubber (i.e. NR), styrene-butadiene rubber (i.e. SBR) and polybutadiene rubber (i.e. PBR) on the product quantity and quality is important. However, most of the studies do not provide details on the type of tyre used. This might be related to the lack of waste tyre categorization in most of the waste tyre collection points.

The effect of temperature on syngas composition and yield during gasification of waste tyres was investigated by several studies. Portofino et al. (2013) investigated the effect of gasification temperatures ranging from 850 to 1000 °C on product yield and composition during steam gasification of waste tyre in a rotary kiln reactor. Syngas yield as well as H<sub>2</sub> and CO content was significantly increased. Similar findings were reported by Ahmed and Gupta (2011) in response to the increase in gasification temperature during the steam gasification of rubber in semi-batch fixed bed reactor. However, the variation in the catalytic bed temperature in the absence of gasifying agent (i.e. steam) showed an insignificant effect on syngas yield whereas H<sub>2</sub> production and content in syngas improved (Zhang and Williams, 2016). Therefore, the presence of both gasifying agents, like steam, and catalyst is likely to result in syngas with better composition. According to Gašparovič et al. (2013), the high temperature of the catalytic bed is beneficial in terms of; (1) improved syngas quality and

quantity and (2) improved catalyst resistance to deactivation, coking, sintering, etc., resulting in a better operational lifetime as a result of promoted carbon conversion.

In addition to the influence of the operating temperature, various studies are conducted to understand the effect of the catalyst and its composition on the quality and quantity of the products during the gasification process (Elbaba et al., 2011; Elbaba and Williams, 2013; Kordoghli et al., 2017, 2019; Zhang et al., 2015, 2017). Among the catalysts, Ni-based catalyst with different supports such as alumina and dolomite, as well as different promoters is commonly used in the gasification process. The use of a Ni-based catalyst is supported by its activity in enhancing H<sub>2</sub> production while minimizing the tar content of the syngas (Elbaba and Williams, 2013), which is in turn a function of Ni-loading and the type of both support as well as the promoter. For example, Zhang et al. (2015) showed that the highest yield of syngas and H<sub>2</sub> is attainable with Ni-alumina catalyst having 10 wt% Ni-loading during pyrolysis/catalytic reforming of waste tyres. Similarly, Elbaba and Williams (2013) recommended Ni-loading of less than 20 wt% for higher H<sub>2</sub> production through pyrolysis/steam reforming. Although Ni-based catalysts with alumina support had a positive effect on syngas as well as H<sub>2</sub> production, Ni-dolomite was found to be superior. This is because of its increased catalytic activity, improved resistance to coke formation and sulphur poisoning, and better selectivity towards H<sub>2</sub> production (Elbaba and Williams, 2014; Gašparovič et al., 2013).

The effect of different gasifying agents like steam, O<sub>2</sub>, air, CO<sub>2</sub> and a mixture of them on syngas production, composition and its energy content during gasification of waste tyres has been widely investigated (Galvagno et al., 2009; Karatas et al., 2013; Karatas et al., 2012; Policella et al., 2019; Portofino et al., 2013; Zhang and Williams, 2016).

Karatas et al. (2013) studied the gasification of the waste tyre in a bubbling fluidized bed using air as a gasifying agent. The effect of ER on syngas composition was examined. The results indicated that the lower ER produces syngas with higher H<sub>2</sub> and CH<sub>4</sub> content and higher lower heating value (i.e. LHV). To improve syngas composition in terms of H<sub>2</sub> content as well as yield and to enhance the energy content, steam is used in most of the waste tyre gasification studies (Donatelli et al., 2010; Galvagno et al., 2009; Portofino et al., 2013; Serrano et al., 2022). The reported improvement in syngas quality and composition in steam gasification studies might be explained by enhanced water-gas shift (i.e. WGS) reaction as well as char and hydrocarbon reforming.

Serrano et al. (2022) studied waste tyre gasification in a bubbling fluidised bed reactor using different gasifying agents with a focus on complete gas analysis. A total of 25 different C<sub>3</sub>-C<sub>6</sub> and high molecular weight hydrocarbons (C<sub>6</sub>+) plus two light aromatics (benzene and toluene) were analysed and their effect on the syngas energy content is evaluated.

Karatas et al. (2012) examined the effect of air/CO<sub>2</sub> and air/steam mixture as gasifying agents on syngas composition. It has been reported that both mixtures of gasifying agents produce lower quality syngas in terms of CH<sub>4</sub> and H<sub>2</sub> content compared to steam gasification. However, syngas with better H<sub>2</sub>, CO, CO<sub>2</sub> and CH<sub>4</sub> content is produced through air/CO<sub>2</sub> gasification compared to air/steam gasification.

Due to the current global concern of increased emissions of greenhouse gases, therefore, finding routes to mitigate related climate change issues, CO<sub>2</sub> is utilised as a gasifying agent in limited waste tyre gasification studies. Policella et al. (2019) studied automobile waste tyre gasification in a fixed-bed reactor using CO<sub>2</sub> as a gasifying agent. The only operating parameter investigated is the temperature and a positive effect on syngas yield and CGE was

reported. However, the syngas was CO-rich due to the contribution of DR and Boudouard (i.e. BD) reactions. The highest CGE of 62.3% was achieved at 1273 K. Table 2.3 summarises the key references for the gasification studies of waste tyre.

A summary of additional gasification studies of waste tyres investigating different gasifying agents as well as operating conditions is also available in Oboirien and North (2017). Even though the current research is toward CO<sub>2</sub> utilisation through gasification, there is a lack of comprehensive study highlighting the effect of different operating parameters in CO<sub>2</sub> gasification of waste tyres on syngas composition and yield as well as process performance.

Indeed, the use of waste tyres through gasification is advantageous due to its (1) high volatile content which is higher than biomass and coal, (2) higher hydrogen fraction than coal but similar carbon, (3) higher heating value and lower moisture, resulting in products with high energy content (Labaki and Jeguirim, 2017) and (4) continuous supply which compensates for the seasonal availability of the biomass. Despite the benefits of waste tyre utilisation through gasification, it has some drawbacks. The waste tyre has higher sulphur content than biomass which will be transformed into undesirable contaminants including H<sub>2</sub>S, and SO<sub>x</sub> from technical as well as environmental perspectives (Muzenda, 2014). In addition, the waste tyre is petroleum-based material which can be melted, producing tarry material. This in turn will affect the process performance and result in a high tar fraction. Therefore, the selection of the proper process conditions is important.

**Table 2.3** Summary of the gasification studies of waste tyre

Ref.	Gasifying agent	Feedstock	Temperature (°C)		Type of Reactor	Application
			Pyrolysis	Reforming		
Galvagno et al. (2009)	Steam	Scrap tyre	850		Rotary kiln	Char and syngas production
Portofino et al. (2011)	Steam	Tyre sample	850		Rotary kiln	H <sub>2</sub> Production
Elbaba and Williams (2012)	Steam	Rubber tread of passenger car waste tyre	500	600-900	2-Stage fixed bed	H <sub>2</sub> Production
Karatas et al. (2012)	Air/CO <sub>2</sub> , air/steam and steam	Waste tyre	Bottom heater: 790 and 820 Top heater: 720 and 740		bubbling fluidized bed	Syngas composition and LHV
Portofino et al. (2013)	Steam	Granulated tyre sample	850–1000		Rotary kiln	Syngas and char composition
Karatas et al. (2013)	Air	Waste tyre	710–805		bubbling fluidized bed	Syngas composition and LHV
Zhang and Williams (2016)	Steam	Rubber of truck waste tyre	600	700-900	2-Stage fixed bed	Carbon nanotubes and hydrogen production
Policella et al. (2019)	CO <sub>2</sub>	passenger car waste tyre	700-1000		Fixed bed semi-batch	Syngas production

### 2.1.2.1 Examples of commercial and pilot plants

Most of the studies on the gasification of the waste tyre has been carried out at laboratory scale and few were conducted at a pilot scale. Table 2.4 provides a summary of the waste tyre gasification studies at the pilot scale.

**Table 2.4** Summary of the Waste tyre gasification pilot plants

Author	Location of the plant	Type of Reactor	Feeding rate (kg/hr)	gasifying agent	Purpose
Raman et al. (1981)	Department of Chemical Engineering, Kansas State University, U.S.A.	Bubbling fluidized bed	6.2-13.1	Steam (2.4-3.2 kg/hr)	Syngas production
Saito et al. (1987)	Central Research Laboratory, Onoda Cement Co. Ltd, Japan	Rotary kiln (REG gasifier)	300-400	Air	Energy recovery
Conesa et al. (2004)	Department of Chemical Engineering, University of Alicante, Spain	Fixed bed	-	Air (10% O <sub>2</sub> )	Analysis of the products
Donatelli et al. (2010)	Italian National Agency for New Technologies, Energy and Environment – Environment, Italy	Rotary kiln	5	Steam	Syngas production
Wieckert et al. (2013)	Solar Technology Laboratory, Paul Scherrer Institute, Switzerland	150 kW <sub>th</sub> Packed-Bed Solar Reactor	63.4	Steam (10.5 kg/hr)	Process performance and syngas production

### 2.1.3 Experimental studies of gasification of waste tyre and biomass blend

The use of biomass and other materials including plastic and coal as a mixture in the gasification process is evaluated by several studies (Arregi et al., 2017; Aznar et al., 2006; Chai et al., 2020; Kumabe et al., 2007; Li et al., 2010; Mastellone et al., 2010; Park et al., 2016).

This was performed to improve syngas yield and composition in terms of tar content and hydrogen concentration and to enhance its heating value. However, studies on co-gasification of biomass and waste tyre are limited. This could be contributed to the potential of catalyst deactivation by Sulphur-poisoning and carbon deposits. In general, the waste tyre has

comparable sulfur content as coal which varies between less than 1 wt% and up to 3 wt% depending on the type of coal (Mastellone et al., 2010; Straka and Bučko, 2009; Xu et al., 2014).

According to Muzenda (2015), however, during waste tyre pyrolysis the sulphur presented in waste tyres is mostly converted into sulfur-based polycyclic aromatic hydrocarbons and only a fraction of it is transferred in the product gas in the form of H<sub>2</sub>S and COS.

Research on co-gasification of biomass and waste tyre is still limited. The available few studies were conducted to either improve the reactivity of the tyre char in a CO<sub>2</sub> environment (Lahijani et al., 2013), lower the Methanol production cost (Brachi et al., 2014), control the emission of undesired N and S-containing compounds (Oboirien and North, 2017), to utilise waste tyre (Wu et al., 2017) or to produce better quality syngas (Wang et al., 2019b).

The effect of temperature during the co-gasification of pine bark and waste tyre using CO<sub>2</sub> as a gasifying agent was examined by (Wang et al., 2019b). The higher the gasification temperature is, the better the syngas yield due to increased production of CO. However, Yusup et al. (2013) found that the increase in gasification temperature produced H<sub>2</sub>-rich syngas during catalytic steam gasification of waste tyre and palm kernel shells in a pilot-scale fluidised bed reactor. This highlights the combined effect of the catalyst, the gasifying agent and temperature in obtaining syngas with different compositions.

Yang et al. (2019) studied the effect of waste tyre fraction in the waste tyre and pine sawdust blend on both syngas composition and its energy content using air at a fixed temperature of 850 °C. Increased fraction of waste tyre in the blend affected positively the H<sub>2</sub> and CH<sub>4</sub> content of the syngas and the heating value. A heating value of 7.87 MJ/Nm<sup>3</sup> was obtained with a waste tyre fraction of 44 wt%.

The effect of air and steam as gasifying agents during the co-gasification of pine sawdust and the waste tyre was investigated by Wu et al. (2017). Increasing ER during air gasification produced syngas composed mainly of CO and CO<sub>2</sub>. In addition, gasification efficiency was improved up to 56.5% at ER of 0.3. Considering the gasification efficiency and syngas heating value, the optimum ER and waste tyre content was 0.3 and 44%.

In addition to the use of waste tyre as co-feeding material with biomass during the gasification process, its derived pyrolysis char was used as a catalyst for the pyrolysis/reforming of biomass (Al-Rahbi et al., 2016; Al-Rahbi and Williams, 2017). This is to improve the production of H<sub>2</sub>-rich syngas.

To enhance tyre char reactivity in the presence of CO<sub>2</sub> as a gasifying agent, it was used in co-gasification with biomass-derived char in a thermogravimetric analyser at 900 °C (Lahijani et al., 2013). Higher carbon conversion was reported in the case of a high operating temperature of 900 °C and using a blended sample compared to a single one. Biomass char showed a catalytic effect due to the presence of naturally occurring alkali metals mainly K followed by Ca and Mg. An increased fraction of biomass char in the blended feedstock signified its catalytic effect.

Despite the availability of few studies on the co-gasification of biomass and waste tyre, there is a lack of comprehensive knowledge of the synergetic effect underlying the use of these feedstocks and the potential impact the various operating conditions would have on syngas yield as well as quality. In addition, a limited species of biomass was studied as co-feeding material with waste tyres. This includes pine bark, palm kernel shell, agro-wastes, olive husk and palm empty fruit bunch. Table 2.5 summarises the available studies on the co-gasification of biomass and waste tyre, highlighting the specific target of the co-gasification process.

**Table 2.5** Summary of biomass and waste tyre co-gasification studies available in the literature

Author	Type of Feedstock	Type of reactor	Operating conditions			Application
			Gasifying agent	Temperature	Catalyst	
Kaewluan and Pipatmanoma (2011)	Rubber woodchip and rubber waste (10-20 wt%)	Bubbling fluidized bed	Air	800 °C	None	To find an alternative to pre-drying of biomass
Yusup et al. (2013)	Waste tyre (WT) and Palm kernel shell (PKS)	fluidized bed followed by a fixed bed for tar cracking	Steam	600-800 °C	Ni-based <sup>3</sup>	Hydrogen production
Lahijani et al. (2013)	Tyre Char and biomass-derived char <sup>4</sup>	TGA	CO <sub>2</sub>	850, 900, 950 and 1000 °C	None	Improve tyre-char reactivity in the CO <sub>2</sub> environment
Brachi et al. (2014)	80% Olive husk and 20% automobile tyre	Pre-pilot fluidized bed	O <sub>2</sub> -enriched air and steam	749-848 °C	pure $\gamma$ -Al <sub>2</sub> O <sub>3</sub> and Ni/ $\gamma$ -Al <sub>2</sub> O <sub>3</sub>	Production of syngas suitable for Bio-methanol production (cost reduction)
Wu et al. (2017)	Whole tyre and Pine sawdust (branch & straw)	Reverse-burning fixed-bed gasifier	Air	650-700 °C	None	Co-firing feasibility of biomass and tires
Wang et al. (2019b)	Waste tyre (WT) and Pine bark (PB)	Fixed-bed reactor	CO <sub>2</sub>	800 and 900 °C	None	Syngas (H <sub>2</sub> +CO) Production

<sup>3</sup> Feedstock was impregnated with Ni- catalyst

<sup>4</sup> Almond shell and palm empty fruit bunch

### 2.1.3.1 *Examples of commercial and pilot plants*

The production of syngas through gasification of biomass and waste tyre blended feed is not yet been run at a commercial scale. It has been investigated at a pilot scale by Yusup et al. (2013) and Brachi et al. (2014). A summary of these two studies is provided in Table 2.5.

## 2.2 Kinetics studies of pyrolysis of biomass and waste tyre

Several studies have been conducted at a laboratory scale to understand the thermal decomposition behaviour of biomass, waste tyre and their blends using a TGA analyser. Various methods are being widely applied to estimate the underlying kinetics including activation energy, pre-exponential factor, reaction order and mechanism.

### 2.2.1 Kinetics studies of pyrolysis of biomass

Kinetics analysis of the thermal decomposition of various biomass materials and the main constituents including cellulose, hemicellulose and lignin is widely studied. Blasi and Branca (2001) studied the thermal decomposition of wood and its underlying kinetics at a heating rate of 1000 K/min using the Arrhenius method. A comparison between single and multiple steps analyses was conducted.

Poletto et al. (2012) examined the kinetics describing the thermal decomposition of four wood species using the FWO method. It has been identified that the composition of biomass in terms of cellulose, hemicellulose and lignin and their crystallinity affects the degradation rate in which a high fraction of extractives and low crystallinity of cellulose promote the decomposition. In contrast, Font et al. (2009) assumed that the decomposition of pine needles and cones consists of multiple independent reactions. The kinetic parameters for each reaction were obtained by integrating differential Arrhenius-based equations while minimizing the sum of the square difference. The estimated reaction order for each reaction

forming the decomposition behaviours of both materials was higher than 1 (unity).

Furthermore, several studies on kinetics analysis of biomass decomposition through various methods are reported in Table 2.6.

**Table 2.6** Summary of previous kinetic studies on pyrolysis of biomass

Author	Type of biomass	Heating rate (K/min)	Analysis method	Reaction mechanism
Saddawi et al. (2009)	Willow	25	Reaction rate equation	$n^{\text{th}}$ order reaction model with $n = 1$
			Temperature integral approximation by various methods <sup>5</sup>	
Mui et al. (2010)	Raw bamboo	1, 5, 10 and 20	Arrhenius method	-
Singh et al. (2012)	Pinewood waste	25	CR	$n^{\text{th}}$ order reaction model with $n = 1$
Poletto et al. (2012)	Woody species	5, 10, 20 and 40	FWO and master plots <sup>6</sup>	Combination of diffusion and random nucleation
Sánchez-Jiménez et al. (2013)	Cellulose	1, 2, 5 and 10	FR and master plots	Random scission kinetic model
Mishra et al. (2015)	Pinewood	5, 10, 15, 20, 30 and 40	FR, KAS, FWO, Vyazovkin and Vyazovkin AIC method along with master plots	two-dimensional diffusion followed by $n^{\text{th}}$ order reaction mechanism with $n = 1.5$
Wang et al. (2016)	Agricultural residue	10, 20 and 30	FR method and master plots	$n^{\text{th}}$ order reaction followed by a 3D diffusion model
			Combined kinetics (single and multi-step)	the combined effect of nucleation, diffusion and high-order reaction mechanism
Mishra and Mohanty (2018)	Pine sawdust, sal sawdust, and areca nut husk	5, 10, 15, 20 and 25	KAS, FWO, FR, CR and DAEM	-
Yeo et al. (2019)	Cellulose	10 to 100 with an increment of 10 K/min	FR and combined kinetics	Chain scission
	Hemicellulose			$n^{\text{th}}$ order reaction with $n=3$
	Lignin			the combined effect of nucleation,

<sup>5</sup> Murray and White, Doyle, and Senum and Yang

<sup>6</sup> Criado method

				diffusion and power law mechanism
--	--	--	--	-----------------------------------

### 2.2.2 Kinetics studies of pyrolysis of waste tyre

Kinetics analysis of the thermal degradation of waste tyres and its constituents of natural and synthetic rubbers have been extensively studied since the work of Williams and Besler (1995). The effect of particle size on the kinetics governing the thermal decomposition of the waste tyre and/or its constituents was examined in several studies (Leung and Wang, 1999; Arias et al., 2022). Leung and Wang (1999) examined the decomposition of waste tyre under non-isothermal conditions at four heating rates and different particle sizes. The analysis was based on the assumption that the tyre consists of three components and based on the  $n^{\text{th}}$ -order reaction model thus the kinetics parameters were calculated for each component.

González et al. (2001) investigated the thermal decomposition kinetics of shredded automobile tyres under both isothermal and non-isothermal regimes. It was emphasized that the waste tyre decomposition could be described as a single and three stages process under isothermal and non-isothermal regimes, respectively. Moreover, Miranda et al. (2013) investigated the thermal decomposition of the rubber fraction of automobile tyre waste, considering both reaction kinetics and mechanism through the linearized form of the Arrhenius equation. It was proven that the reaction temperature affects the reaction mechanism underlying the pyrolysis of the waste tyre. Arias et al. (2022) studied the effect of the particle size and the heating rate on the kinetics of waste tyre decomposition in the TGA analyser. The kinetics were predicted according to Friedman (i.e. FR), Coats-Redfern (i.e. CR) and Arrhenius linearization methods. The decomposition reaction was assumed to be first order. The overall decomposition of the waste tyre was assumed to occur over two stages. On the other hand, Danon et al. (2015) assumed that the devolatilization of the rubber

components consists of three independent reactions. Indeed, the previous studies reported a variation in the activation energy values obtained using different methods and this variation was attributed to the difference in the mathematical approximation considered for each method and the conditions (composition of the tyre, TGA heating regime, etc.) under which the experiments are conducted.

A summary of some of the previous studies on kinetics analysis of waste tyres is provided in Table 2.7.

**Table 2.7** Summary of studies related to kinetic analysis of the pyrolysis of waste tyre

Author	Type of tyre	Heating rate (K/min)	Analysis method	Reaction mechanism
Williams and Besler (1995)	3 samples of tyres and pure rubber	5,20,40 or 80	Arrhenius method	$n^{\text{th}}$ order reaction model with $n = 1$
Chen et al. (1997)	Styrene butadiene rubber	2, 5, 10 and 20	FR	$n^{\text{th}}$ order reaction model with $n = 0.6$
Chen et al. (2001)	Passenger car and truck scrap tyres	5, 10, 20 and 30	FR	$n^{\text{th}}$ order reaction model with $n = 1.98$ and $1.63^7$
Mui et al. (2010)	Tyre rubber	1, 5, 10 and 20	Arrhenius method	-
Singh et al. (2012)	Waste tyre rubber	25	CR	$n^{\text{th}}$ order reaction model with $n = 1$
Danon et al. (2015)	Four rubber samples	2, 5, 10, 15 and 20	FR and Kissinger	Power law
Menares et al. (2020)	Automobile waste tyre granules	5, 10, 20 and 30	Model-based with Peak differentiation Starink	-
Hu et al. (2020)	Vehicle waste tyre	10	Temperature integral approximation by Doyle and CR (single-step)	$n^{\text{th}}$ order reaction model with $n = 1$
Tang et al. (2021)	Waste rubber	10, 20 and 40	FWO, KAS, Starink and master plots	Three consecutive stages with 2-D diffusional followed by $n^{\text{th}}$ -order reaction models with $n = 2$

<sup>7</sup> For passenger and truck tyres, respectively

	waste bicycle tyre			Three consecutive stages n <sup>th</sup> order reaction models with n = 1, 1.5 and 2
Chen et al. (2022)	waste tyre powder and CaO as a catalyst with a mass ratio of 1:1	150, 300 and 600	FWO, KAS and FR	-
			Two stages CR	n <sup>th</sup> -order reaction models with n = 1 and 1.5
			Master plots	

### 2.2.3 Kinetics studies of pyrolysis of biomass and waste tyre blend

Although the pyrolysis of a mixture of biomass and waste tyre for the desired end-products is widely investigated (Duan et al., 2015; Farooq et al., 2018; Wang et al., 2019a, 2017, 2020b), few studies are available to understand the kinetics underlying the thermal decomposition of a mixture of these materials. There are a variety of methods available for the kinetics analysis, including CR (Chen et al., 2019c; Cherop et al., 2018; Gao et al., 2021; Likun and Zhang, 2020; Uzun and Yaman, 2014), Arrhenius (Uzun and Yaman, 2014), FWO (Azizi et al., 2019; Chen et al., 2019a; Cherop, Kiambi and Musonge, 2018), KAS (Azizi et al., 2019; Chen et al., 2019a) and DAEM (Wang et al., 2018). This is to assess the effect that the use of biomass and waste tyre blends will have on the activation energy. An overview of the previous studies investigating the kinetics of co-pyrolysis of biomass and waste tyre is presented in Table 2.8.

Uzun and Yaman (2014) studied the kinetics of thermal decomposition of *Juglans regia* (i.e. walnut) shell, scrap tyre and their blends based on the CR method, assuming first-order reaction. The existence of synergetic interaction was evaluated by comparing the average value of the activation energy between single and blend samples. Similarly, Chen et al. (2019b) and Chen et al. (2019c) estimated the kinetic parameters using the CR method, assuming 1<sup>st</sup> order reaction. However, the presence of several peaks and/or shoulders in the DTG curves, as stated by the International Confederation for Thermal Analysis and

Calorimetry (i.e. ICTAC), indicates that there might have been many reactions occurring throughout the decomposition process (Vyazovkin et al., 2011). Therefore, Chen et al. (2019b), Chen et al. (2019c) and Gao et al. (2021) assumed first-order, multi-step analysis according to the temperature interval. This is to provide insight into the variation in the activation energy of each step during co-pyrolysis. On the other hand, Chen et al. (2019a), Azizi et al. (2019) and Cherop et al. (2018) implemented iso-conversional methods to determine the kinetics underlying the co-pyrolysis of tyre and biomass materials.

Regardless of the variation in the kinetics obtained by various methods and the possible limitations associated with each of them, it's been noticed that the type of biomass, as well as the waste tyre, has an important role in affecting the reaction kinetics and decomposition mechanisms. For instance, Azizi et al. (2019) examined the influence of co-pyrolysis of two different biomass materials, separately, with the waste tyre on the kinetics. The use of micro-algae in the co-pyrolysis resulted in a 15.71% reduction in the activation energy as compared to single waste tyre whereas wood exhibited a 28.06% reduction with the blend (Azizi et al., 2019)

**Table 2.8** Summary of Kinetics analysis studies of co-pyrolysis of biomass and waste tyre

Author	Type of biomass blended	Heating rate (K/min)	Analysis method	Reaction mechanism
Gao et al. (2021)	Offshore oil sludge	15	CR (multi-steps)	n <sup>th</sup> order reaction model with n = 1
Likun and Zhang (2020)	Torrefied bagasse	20	CR (multi-steps)	D1 (at lower temperature) and O2 (at higher temperature)
Chen et al. (2019b)	Tobacco stalk	10, 20 and 30	CR (multi-steps)	n <sup>th</sup> order reaction model with n = 1
Chen et al. (2019c)	Tobacco stalk	10	CR (multi-steps)	n <sup>th</sup> order reaction model with n = 1
Chen et al. (2019a)	Kitchen waste	10, 20 and 30	FWO and KAS	N/A
	Wood	10, 20 and 40	FWO and KAS	

Azizi et al. (2019)	Micro-algae		FWO and KAS	Assumed $n^{\text{th}}$ order reaction model for pre-exponential factor
Cherop et al. (2018)	Eucalyptus sawdust	2, 5, and 10	FWO and FR	$n^{\text{th}}$ order reaction model with $n = 1$
Uzun and Yaman (2014)	J. regia shell	5, 10, 15 and 20	CR and Arrhenius method	$n^{\text{th}}$ order reaction model with $n = 1$

## 2.3 Modelling and simulation studies of gasification of biomass and waste tyre

Modelling and simulation have become crucial components for research aiming industrial applications. This is because most of the recent developments are computer-aided. Understanding the impact of different operational parameters on the process performance is made possible through modelling and simulation. This will provide a basic knowledge and understanding of the optimum conditions for specific process operations. This, in turn, would help to lower the cost and effort involved in purchasing materials and equipment as well as process maintenance.

### 2.3.1 Modelling and simulation studies of gasification of biomass

Studies on gasification of biomass through process modelling and simulation are highly available in the literature. Various approaches are adopted by the researchers to understand the process performance under various operating conditions. Nikoo and Mahinpey (2008) investigated the performance of biomass gasification in a fluidized bed reactor using ASPEN Plus<sup>®</sup>. The overall process was divided into three stages: biomass decomposition, gas-phase reaction and char gasification. Gas phase reactions were based on the Gibbs equilibrium, whereas char gasification was based on the reaction kinetics. In addition, the reactor bed hydrodynamics is considered. Similarly, Abdelouahed et al. (2012) developed a detailed model of biomass gasification in a dual fluidized bed gasifier using ASPEN Plus<sup>®</sup>. In contrast to Nikoo and Mahinpey (2008), reaction kinetics are considered to simulate gas phase reactions as well as tar cracking. Janajreh et al. (2013) examined the process performance and syngas

production of plasma gasification and conventional air gasification for different types of feedstocks including biomass. The developed model was based on Gibbs energy minimization approach.

Table 2.9 presents a summary of other previous studies of gasification of biomass through process modelling and simulation.

**Table 2.9** A selection of steady-state modelling/simulation studies of gasification of biomass using various approaches

Author	Feedstock type	Gasifying agent	Type of reactor	Modelling/Simulation approach
Renganathan et al. (2012)	Model biomass (46C, 6H and 48O)	CO <sub>2</sub> , CO <sub>2</sub> /steam, CO <sub>2</sub> /O <sub>2</sub>	Not mentioned	Gibbs equilibrium
Begum et al. (2013)	MSW, wood wastes, green wastes and coffee bean husks	Air	Fixed-bed	Gibbs equilibrium
Banerjee et al. (2015)	Seed corn, maple-oak mixture and pine	A mixture of O <sub>2</sub> -enriched air and steam	100-kW <sub>th</sub> Pilot-scale fluidized-bed	Reaction kinetics
Pauls et al. (2016)	Pine sawdust	Air/steam	Bubbling fluidized bed	Empirical Correlations and reaction kinetics <sup>8</sup>
Kaushal and Tyagi (2017)	Wood	Steam	Fluidized bed	Gibbs equilibrium and reaction kinetics <sup>9</sup>
Haydary (2018)	A mixture of lignocellulosic-waste biomass	Oxygen-enriched air	2-stage fixed-bed	Gibbs equilibrium
Huang and Jin (2019)	Pine woodchip	Steam	Downdraft Fixed-Bed	Restricted Gibbs equilibrium
Antolini et al. (2019)	Wood pellets	CO <sub>2</sub> /Air	Fixed-bed reverse downdraft gasifier	Gibbs equilibrium
Chatrattanawet et al. (2019)	Sugarcane leftover	Steam, air and steam/air	Circulating fluidized bed	Gibbs equilibrium
Aghaalkhani et al. (2019)	Softwood pellets	Steam	100-kW dual fluidized bed	Empirical correlations and Restricted equilibrium <sup>10</sup>

<sup>8</sup> Pyrolysis stage product yields and volatile composition are defined using empirical equations. For both gas phase and tar-related reactions, reaction kinetics were considered.

<sup>9</sup> Gibbs equilibrium and reaction rate kinetics are implemented for gas phase and char gasification reactions, respectively.

<sup>10</sup> Semi-detailed kinetic approach was considered for the water-gas shift reaction

Islam (2020)	Pine woodchips	steam, H <sub>2</sub> O <sub>2</sub> , pure oxygen, CO <sub>2</sub> and air	Bubbling fluidized bed	Gibbs equilibrium
--------------	----------------	---	------------------------	-------------------

### 2.3.2 Modelling and simulation studies of gasification of waste tyre

Limited studies are reported in the literature on the gasification of waste tyres through process modelling and simulation (Donatelli et al., 2010; Fajimi et al., 2021; Janajreh and Raza, 2015; Lerner et al., 2012; Mitta et al., 2006; Mozafari et al., 2017; Zang et al., 2019).

Martínez et al. (2014) studied gasification of the waste tyre using a stoichiometric equilibrium model as well as material and energy balance calculations in an air-steam environment. Process analysis was carried out to investigate the effect of steam-to-feed ratio and equivalence ratio on syngas composition and process performance.

Fajimi et al. (2021) developed a model for the comparative evaluation of the co-production of syngas and activated carbon from gasification of waste tyre considering three different reactor configurations. Each reactor configuration was modelled on a different basis. A comparison in the technical and economic performance of two types of reactor; fixed bed and fluidized bed for syngas production from waste tyre gasification was conducted by Zang et al. (2019) through process simulation using ASPEN Plus<sup>®</sup>. Syngas with higher energy content and carbon conversion was achieved with the use of a fluidized bed reactor.

Other studies on gasification of waste tyres are summarised in Table 2.10.

**Table 2.10** Summary of modelling/simulation studies on gasification of waste tyre

Author	Feedstock type	Gasifying agent	Type of reactor	Modelling/Simulation Approach
Donatelli et al. (2010)	Rubber grain derived from waste tyres	Steam	Rotary kiln	Numerical simulation/ Gibbs equilibrium
Lerner et al. (2012)	Used tyre	Steam	Plasma gasification	Numerical / Thermodynamic equilibrium model

Janajreh et al. (2013)	Different feed including waste tyre	Air	Plasma gasification	Gibbs free energy minimization approach
Sánchez et al. (2013)	Waste tyre rubber	Air-steam	Fixed bed	Gibbs free energy minimization approach
Zang et al. (2019)	Wood, tyre or mixture	Air-steam	Fluidized bed	Semi-empirical model
			Fixed bed	Kinetics model
Nie et al. (2022)	Natural rubber	Sub- and supercritical water	N/A	Reactive force field molecular dynamics

### 2.3.3 Modelling and simulation studies of gasification of biomass and waste tyre blend

The research on the gasification of a mixture of biomass and waste tyre through process modelling and simulation is limited. Kartal and Özveren (2023) developed an Aspen HYSYS® steady-state model for an Integrated Gasification Combined Cycle (i.e. IGCC) system to evaluate CO<sub>2</sub>/air co-gasification of biochar and waste tyre. The model was based on the Gibbs free energy minimization approach to analyse the effect of different operating parameters including gasification temperature, CO<sub>2</sub> to gasifying agent ratio, etc. on process performance in terms of syngas composition as well as energy and exergy efficiency.

## 2.4 Summary

To summarise, the following are the ***key findings*** from the literature review

- (1) Co-gasification of biomass and waste tyre could enhance syngas production due to the composition of both materials thus the possible synergetic interaction.
- (2) Due to the difference in the composition of different types of waste tyres as well as the existence of various biomass materials, it is important to understand the thermal decomposition behaviour of different feeding materials.
- (3) It is important to evaluate the process performance of gasification of biomass and waste tyre due to the variations in the contributing effect of both process conditions and feedstock composition. This in turn affects product yields and composition.

However, further research needs to be conducted to address the existing **research gaps** which are as follows:

- (1) The gasification technology of waste tyres and their blend with biomass for syngas production is not mature enough for large-scale commercialisation. As a result, it is essential to understand the thermal decomposition behaviour of waste tyre and its blend with biomass and the underlying decomposition kinetics and reaction mechanisms.
- (2) There is a lack of studies on the gasification of biomass and waste tyre through modelling/simulation. No papers can be found with a detailed analysis of the effect of various process conditions on product yield and composition.

Table 2.11 lists the key papers which provide insights into the current research.

**Table 2.11** List of the references for the key papers with the benefit for the current research project

Reference	Utilisation in the current research
Ahmed and Gupta (2011)	Insights into co-gasification of biomass and rubber waste (waste tyres)
Brachi et al. (2014)	
Oboirien and North (2017)	Insight into co-gasification of biomass and waste tyre through modelling/simulation
Policella et al. (2019)	Insight into the utilisation of CO <sub>2</sub> as a gasifying agent during co-gasification of biomass and waste tyre for the possibility to simultaneously obtain better quality syngas and mitigate climate change issues.
Shen et al. (2019)	
Renganathan et al. (2012)	Insight into the process simulation of gasification using CO <sub>2</sub> as gasifying agent
Kaushal and Tyagi (2017)	Insight into the simulation of biomass gasification using ASPEN Plus®
Pauls et al. (2016)	
Mishra and Mohanty (2018)	Insight into the kinetic analysis of biomass and waste tyre using Coats-Redfern and iso-conversional kinetic analysis methods

Sánchez-Jiménez et al. (2013)	Insight into the prediction of the reaction mechanism of biomass and waste tyre using the master plot method
Yeo et al. (2019)	Insight into the kinetic analysis of biomass and waste tyre using a combined kinetic analysis method
Mui et al. (2010)	Guide for the application of kinetic compensation effect for the calculation of pre-exponential factor

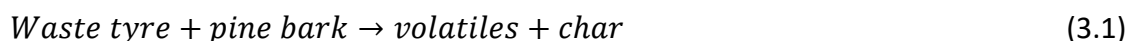
## CHAPTER 3 Kinetics analysis of co-pyrolysis of pine bark and waste tyre

In this chapter, the existence of synergetic interaction during co-pyrolysis of pine bark and waste tyre is investigated using different blend ratios on the mass basis at different heating rates. In *Section 3.1*, the methods of kinetics analysis used to predict the kinetics parameters are presented. In *Section 3.2*, the characterization of pine bark and waste tyre is provided in terms of proximate and ultimate analysis. In addition, the thermal characterization method is introduced. In *Section 3.3.1*, the results of thermal characteristics of co-pyrolysis of pine bark and waste tyre using different blend ratios are discussed. The difference in weight loss is used as a criterion to evaluate the existence of synergetic interaction between pine bark and waste tyre. In *Section 3.3.2*, the kinetics parameters including activation energy of co-pyrolysis of pine bark and waste tyre are estimated using different methods and the effect of co-pyrolysis on activation energy relative to single feedstock is discussed.

### 3.1 Methodology

#### 3.1.1 Kinetics study

The decomposition reaction that occurs during the co-pyrolysis of pine bark and waste tyre could be summarised as Equations (3.1) and (3.2) (Mui et al., 2010; Wang et al., 2019b).



The reaction rate of the co-pyrolysis process assuming single step process (i.e.  $d\alpha/dt$ ) can be described by Arrhenius law which is expressed as (Ebrahimi-Kahrizsangi and Abbasi, 2008)

$$\frac{d\alpha}{dt} = k(T) \cdot f(\alpha), \quad (3.3)$$

where  $k(T)$  refers to the temperature dependence of the reaction rate and it is represented by the Arrhenius equation as follows;

$$k(T) = A \exp^{-E_a/RT}, \quad (3.4)$$

where  $A$ ,  $E_a$ ,  $R$  and  $T$  are a pre-exponential factor ( $\text{min}^{-1}$ ), activation energy (J/mol), gas constant (8.3145 J/mol K) and temperature (K), respectively (Singh et al., 2012).

$f(\alpha)$  represents the process rate dependence on the conversion. It also refers to the differential reaction model function (Vyazovkin et al., 2011). The extent of reaction or known as conversion ( $\alpha$ ) is expressed as (Sánchez-Jiménez et al., 2013; Singh et al., 2012):

$$\alpha = \frac{w_o - w_t}{w_o - w_\infty}, \quad (3.5)$$

where  $w_o$ ,  $w_t$  and  $w_\infty$  are the sample weight at the start time, time equals to  $t$  and the end of the measurements, respectively.

By combining Equations (3.3) and (3.4), the reaction rate equation based on the differential kinetic methods is obtained as follows;

$$\frac{d\alpha}{dt} = A \exp^{-E/RT} \cdot f(\alpha) \quad (3.6)$$

For non-isothermal conditions with a constant heating rate (i.e.  $\beta = \frac{dT}{dt}$ ), then the reaction rate equation (i.e. Equation (3.3)) will become;

$$\beta \frac{d\alpha}{dT} = A \exp^{-E_a/RT} \cdot f(\alpha) \quad (3.7)$$

Differential reaction model (i.e.  $f(\alpha)$ ) can be expressed in the integral form  $g(\alpha)$  by integrating Equation (3.7) with respect to temperature at a constant heating rate, then

$$g(\alpha) = \frac{A}{\beta} \int_0^T \exp\left(\frac{-E_a}{RT}\right) \cdot dT \quad (3.8)$$

The mathematical expressions of  $f(\alpha)$  and  $g(\alpha)$  for different reaction mechanisms are summarised in Table 3.1.

**Table 3.1** Mathematical expressions of solid-state reaction functions;  $f(\alpha)$  and  $g(\alpha)$ , of different reaction mechanisms (White et al., 2011; Yeo et al., 2019)

Reaction Mechanism	Symbol	$f(\alpha)$	$g(\alpha)$
<b>Reaction Order</b>			
First	O1	$(1 - \alpha)^n$	$-\ln(1 - \alpha)$

<b>Second</b>	O2	$(1 - \alpha)^n$	$(n - 1)^{-1}(1 - \alpha)^{(1-n)}$
<b>nth order</b>	O3	$(1 - \alpha)^n$	$(n - 1)^{-1}(1 - \alpha)^{(1-n)}$
<b><i>Nucleation and Growth</i></b>			
<b>Power law</b>	P1-P4	$n(\alpha)^{1-1/n}$	$\alpha^n; n = 3/2, 1/2, 1/3, 1/4$
<b>Exponential law</b>	E1	$\ln(\alpha)$	$\alpha$
<b>Avrami-Erofeev</b>	N1-N4	$n((1 - \alpha)[-\ln(1 - \alpha)]^{1-1/n})$	$[-\ln(1 - \alpha)]^{1/n}; n = 1, 2, 3, 4$
<b><i>Diffusional</i></b>			
<b>1-D</b>	D1	$(1/2)\alpha$	$\alpha^2$
<b>2-D</b>	D2	$[-\ln(1 - \alpha)]^{-1}$	$(1 - \alpha)\ln(1 - \alpha) + \alpha$
<b>3-D (Jander)</b>	D3	$[3(1 - \alpha)^{2/3}]/[2(1 - (1 - \alpha)^{1/3})]$	$[1 - (1 - \alpha)^{1/3}]^2$
<b>3-D (Ginstling-Brounshtein)</b>	D4	$3/[2((1 - \alpha)^{-1/3} - 1)]$	$1 - (2/3)\alpha - (1 - \alpha)^{2/3}$
<b><i>Contracting Geometry</i></b>			
<b>Contracting area (<math>n = 2</math>)</b>	C1	$2(1 - \alpha)^{1/n}$	$1 - (1 - \alpha)^{1/n}$
<b>Contracting volume (<math>n = 3</math>)</b>	C2	$3(1 - \alpha)^{2/n}$	$1 - (1 - \alpha)^{1/n}$
<b>Šesták-Berggren function</b>	SB	$\alpha^m(1 - \alpha)^n[-\ln(1 - \alpha)]^p$	-

Various calculation methods of kinetics parameters,  $E_a$  and  $A$ , for solid-state reactions, exist in the literature. These methods are categorised into model fitting and iso-conversional (i.e. model-free) methods. Model fitting methods are based on the evaluation of various reaction models in which the model with the best statistical fit is used for the calculation of the kinetics. In contrast, iso-conversional methods are independent of the reaction model and require multiple TGA measurements at different heating rates. In addition, the kinetics parameters are estimated at different reaction extents (i.e. conversion). Therefore, the operating conditions of the TGA analysis determine the applicability of the kinetics analysis method. An overview of the model fitting and iso-conversional methods considered in the current study is provided in sections 3.1.1.1 and 3.1.1.2. Coats-Redfern was used as the model fitting method whereas FWO, KAS and FR are used as iso-conversional methods.

### 3.1.1.1 Single-step reaction: model fitting

#### 3.1.1.1.1 Coats-Redfern (CR)

Coats-Redfern method is based on an integral form of the reaction model as expressed in Equation (3.9). An assumption of the reaction order (i.e.  $n$ ) value is required to use such a method (Uzun and Yaman, 2014; White et al., 2011).

$$\ln \left[ \frac{g(\alpha)}{T^2} \right] = \ln \left( \frac{AR}{\beta E_a} \left[ 1 - \frac{2RT}{E_a} \right] \right) - \frac{E_a}{RT} \quad (3.9)$$

For the estimation of kinetics parameters using the Coats-Redfern method, the following steps were followed. First, the proper reaction order for the calculation of the reaction kinetics was evaluated. To do so, reaction order values ranging between 0 to 3 with an increment of 0.5 was substituted in the relevant expression of the reaction order mechanism as shown in Table 3.1. According to the literature (Chen et al., 2019c; Singh et al., 2012), the  $n$  value with the best fitting (i.e. the highest correlation coefficient,  $R^2$ ) was selected, indicating its ability to fit well with the experimental data. The results are provided in section 3.3.2.1. Then, conversion,  $\alpha$ , was calculated for each blended sample at different heating rates based on the corresponding TGA data using Equation (3.5). The value for the left-hand side of Equation (3.9) at a single heating rate was plotted against  $1/T$  where  $T$  is in K. Finally, the activation energy,  $E_a$ , and pre-exponential factor,  $A$ , were derived from the slope and intercept (i.e.  $-\frac{E_a}{R}$  and  $\ln \left[ \frac{AR}{\beta E_a} \right]$ , respectively) of the plot with best linear correlation coefficient for each blend sample.

### 3.1.1.2 Single-step reaction: iso-conversional methods

Iso-conversional methods are based on the estimation of kinetics parameters underlying solid state decomposition reaction without prior knowledge of the reaction mechanism (i.e.  $g(\alpha)$  or  $f(\alpha)$ ) and assuming that the reaction temperature is mainly affecting the reaction rate

(Anca-Couce, 2016). Since the temperature integral term in Equation (3.8) have no analytical solution, various approximation was provided in the literature, resulting in the existence of various iso-conversional methods (Vyazovkin et al., 2011).

#### 3.1.1.2.1 Flynn-Wall-Ozawa (FWO)

FWO method is based on Doyle's approximation (Lahijani et al., 2019) as expressed in Equation (3.10). It allows the estimation of the apparent  $E_\alpha$  for a given value of  $\alpha$  (Lahijani et al., 2019; Słopiecka et al., 2012). This is obtained from the slope of  $\ln(\beta)$  versus  $1/T_\alpha$ , where  $T_\alpha$  refers to the temperature at specific conversion.

$$\ln\beta = \ln\left(\frac{AE_\alpha}{Rg(\alpha)}\right) - 5.3305 - 1.052\left(\frac{E_\alpha}{RT_\alpha}\right) \quad (3.10)$$

#### 3.1.1.2.2 Kissinger-Akahira-Sunose (KAS)

KAS method is based on Marry and White approximation of the temperature integral (Vyazovkin et al., 2011) and presented in Equation (3.11). The apparent  $E_\alpha$  is estimated from the slope of linear plots of  $\ln\left(\frac{\beta}{T_\alpha^2}\right)$  against  $1/T_\alpha$  for different conversion value ( $\alpha$ ) (Słopiecka et al., 2012).

$$\ln\left(\frac{\beta}{T_\alpha^2}\right) = \ln\left(\frac{A_\alpha R}{E_\alpha g(\alpha)}\right) - \left(\frac{E_\alpha}{RT_\alpha}\right) \quad (3.11)$$

#### 3.1.1.2.3 Friedman method (FR)

Friedman method is the differential form of the iso-conversional method and is presented in Equation (3.12). Since the FR method is independent of any mathematical approximation for temperature integral term, It is widely used and considered more accurate than other iso-conversional methods (Yeo et al., 2019). An estimation for the value of  $E_\alpha$  was obtained from the slope of linear regression of  $\ln\left(\beta \frac{d\alpha}{dT}\right)$  against  $1/T_\alpha$ .

$$\ln\left(\beta \frac{d\alpha}{dT}\right) = \ln[A \cdot f(\alpha)] - \frac{E_\alpha}{RT_\alpha} \quad (3.12)$$

#### 3.1.1.2.4 Kinetic Compensation Effect (KCE)

The kinetic compensation effect (i.e. KCE) assumes that a linear variation exists between the  $E_\alpha$  and the  $A$ . It is explained by equation (3.13) (Mui et al., 2010).

$$\ln A = a E_\alpha + b \quad (3.13)$$

Where  $a$  and  $b$  are constants and known as compensation parameters

#### 3.1.1.2.5 Generalized master plot method

Criado et al. (1989) suggested a procedure to identify a possible reaction mechanism that describes a solid-state decomposition reaction. It is based on the comparison between experimental and theoretical master plots. Theoretical master plots are a unique set of plots which are specific to a particular reaction mechanism listed in Table 3.1. They are independent of reaction kinetics. Using  $y(\alpha)_{theoretical}$  function provided in Equation (3.14) and the expressions of reaction mechanism, theoretical master plots are constructed.

$$y(\alpha)_{theoretical} = f(\alpha)/f(\alpha)_{0.5} \quad (3.14)$$

Experimental curves are constructed using experimental  $y(\alpha)$  function as expressed in Equation (3.15) (Sánchez-Jiménez et al., 2013). The  $y(\alpha)_{exp}$  function is calculated considering the  $E_\alpha$  from FR method.

$$y(\alpha)_{exp} = \frac{(d\alpha/dt)}{(d\alpha/dt)_{0.5}} \cdot \frac{\exp(E/RT_\alpha)}{\exp(E/RT)_{0.5}} \quad (3.15)$$

#### 3.1.1.3 Single-step reaction: combined kinetic analysis

Combined kinetic analysis is based on the calculation of kinetic parameters including  $E_\alpha$  and  $A$  while accounting for the  $f(\alpha)$ . Similar to iso-conversional methods, this can be achieved by plotting the left-hand side of Equation (3.16) against the reciprocal of the temperature at a specific reaction extent (Vyazovkin et al., 2011; Wang et al., 2016). The slope and intercept of the resultant straight line are used to obtain the  $E_\alpha$  and  $A$ , respectively.

$$\ln\left(\beta \frac{\frac{d\alpha}{dT}}{f(\alpha)}\right) = \ln[A] - \frac{E_\alpha}{RT_\alpha} \quad (3.16)$$

However, the use of the combined kinetic analysis method as shown in Equation (3.15) requires the knowledge of proper reaction mechanism. Therefore, the Sestak-Berggren expression is used which is presented in Equation (3.17) (Cai and Liu, 2009; Vyazovkin et al., 2011) to estimate the possible reaction mechanism.

$$f(\alpha) = \alpha^m(1 - \alpha)^n[-\ln(1 - \alpha)]^p \quad (3.17)$$

Combining equations (3.16) and (3.17) will lead to the reaction rate equation in the form of;

$$\ln\left(\beta \frac{\frac{d\alpha}{dT}}{\{\alpha^m(1-\alpha)^n[-\ln(1-\alpha)]^p\}}\right) = \ln[A] - \frac{E_\alpha}{RT_\alpha} \quad (3.18)$$

The unknown parameters:  $m$ ,  $n$  and  $p$ , in Equation (3.17) are estimated using optimization functions '*lsqcurvefit*' and '*lsqnonlin*' in MATLAB R2021b software with minimization of least square difference as an objective function.

## 3.2 Experimental data

### 3.2.1 Materials

The biomass material used in the present study is pine bark (i.e. PB) and it is obtained from a local nursery in the USA. Pine bark sample was dried at temperature of 105 °C for 24 hr. Goodyear winter radial passenger car used tyre (i.e. WT) was used as tyre feedstock. The tyre sample was steel wire-free and composed of tread and sidewall parts. Both pine bark and waste tyre samples were grounded to a particle size of 140 mesh and dry mixed for the use as blended sample. The proximate and ultimate analyses of pine bark and waste tyre are presented in Tables 3.2 and 3.3, respectively, along with lower heating values (i.e. LHV).

**Table 3.2** Proximate and Ultimate analysis of pine bark (Wang et al., 2019b, 2020b)

Proximate Analysis	wt%	Ultimate Analysis	wt%
Volatile matter	63.86	C	50.37
Fixed carbon	26.19	H	4.20
Ash	4.77	N	1.61
Moisture	5.18	S	0.03
<b>LHV (MJ/kg)</b>	18.8	O	43.81

**Table 3.3** Proximate and ultimate analysis of waste tyre (Wang et al., 2019b, 2020b)

Proximate Analysis	wt%	Ultimate Analysis	wt%
Volatile matter	62.51	C	81.85
Fixed carbon	27.88	H	6.66
Ash	8.92	N	1.70
Moisture	0.69	S	1.37
<b>LHV (MJ/kg)</b>	33.3	O	9.80

Waste tyre and pine bark blend samples were defined as WT $\times$ PB $_y$ , where WT and PB refer to waste tyre and pine bark, respectively.  $x$  and  $y$  represent the weight ratio of the waste tyre and pine bark, respectively. Five samples including WT1PB0, WT3PB1, WT1PB1, WT1PB3 and WT0PB1 were examined. The waste tyre and pine bark content in each sample is given in Table 3.4.

**Table 3.4** Waste tyre and pine bark content in wt% of the blended samples

Blend Samples ID	Weight Percentage (wt%)	
	Waste tyre	Pine bark
WT1PB0	100	0
WT3PB1	75	25
WT1PB1	50	50
WT1PB3	25	75
WT0PB1	0	100

### 3.2.2 TGA

The thermal decomposition behaviour of PB, WT and their blends were investigated using a thermogravimetric STD-Q600 analyser. The analysis was conducted in the Combustion

Laboratory located in the department of Mechanical Engineering, University of Maryland. The TG analysis was carried out under an inert atmosphere of Ar with a purity and flow rate of 99.998% and 100 ml/min, respectively. The analysis was conducted at four different heating rates (i.e. 10, 20, 30 and 40 K/min). In each experimental run, a sample with a weight of 2.0 mg was subjected to a temperature increase from room temperature to 1173 K. Further details of the experimental procedure are provided by Wang et al. (2019b).

### 3.3 Results and discussion

The results of the current chapter are presented and discussed as follows. First, the results of TGA of waste tyre, pine bark and their blends are provided and discussed. Then, the difference in weight loss between single and blended samples was calculated and used as an index to evaluate the existence of synergetic interaction between pine bark and waste tyre. Furthermore, the kinetics of co-pyrolysis of pine bark and waste tyre derived using different methods are reported and analysed. From a reactor design and reaction engineering standpoint, it is crucial to determine the appropriate pine bark and waste tyre blend ratio. To do so, the effect of co-pyrolysis on the  $E_a$  was discussed.

#### 3.3.1 TG and DTG analysis

##### 3.3.1.1 *Thermal decomposition of single feedstock*

Thermogravimetric (TG) and differential thermogravimetric (DTG) curves of thermal degradation of a single feedstock of waste tyre (i.e. WT1PB0) and pine bark (i.e. WTOPB1) at the heating rates of 10, 20, 30 and 40 K/min are illustrated in Figures 3.1 and 3.2, respectively. As seen in Figures 3.1 and 3.2, the decomposition of the WT1PB0 and WTOPB1 could be divided into two stages where the moisture removal stage at a temperature below 423 K is excluded. These stages are referred to as *Zone I* and *Zone II*.

The degradation of WT1PB0 showed three major peaks in *Zone I* at temperatures of 538, 657 and 729 K. The type of rubber material and other contents in the tyre has a significant impact on the thermal degradation behaviour of the waste tyre (Cherop et al., 2018). During the degradation of the waste tyre, the additives used in its manufacturing including oils, plasticisers and others release volatiles which coincides with the appearance of the first peak (Kan et al., 2017; Zhang et al., 2016b). However, the latter two peaks are associated with the decomposition of rubber components including NR and SBR/PBR, respectively (Kan et al., 2017). Since constant weight loss is recorded starting at a temperature of 801 K, pyrolysis of the waste tyre was nearly completed.

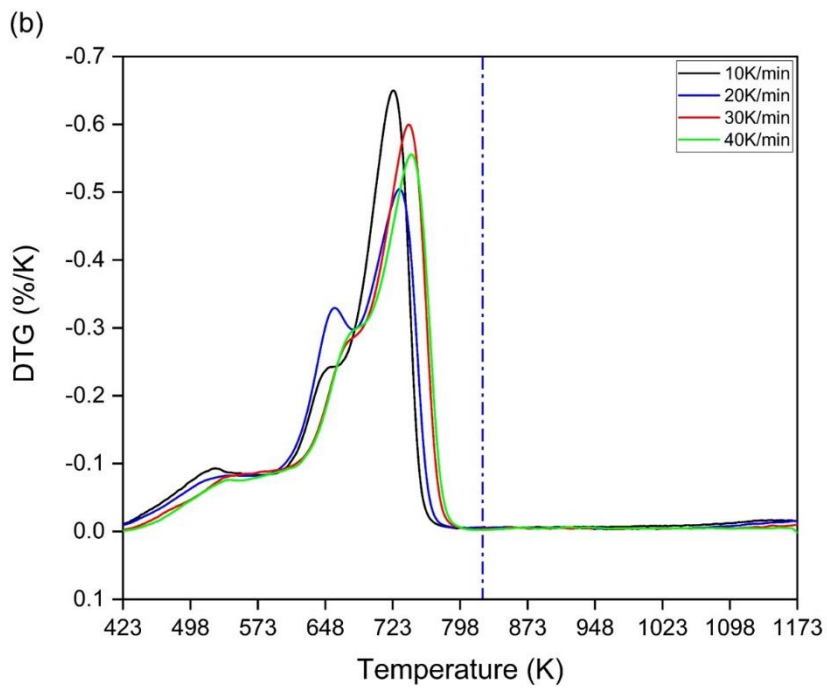
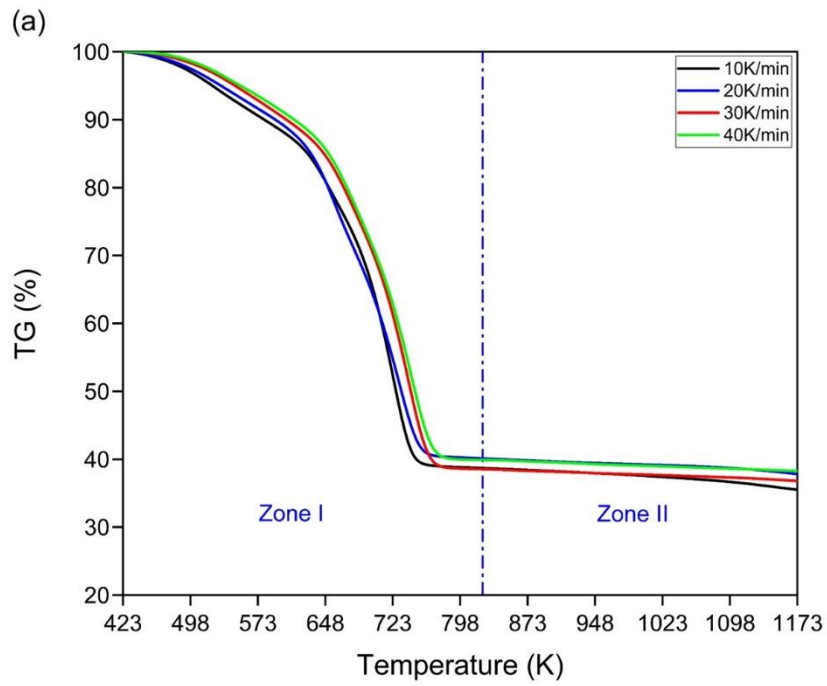


**Figure 3.1** (a) TG and (b) DTG curves of pyrolysis of the waste tyre (i.e. WT1PB0) at 10, 20, 30 and 40 K/min.

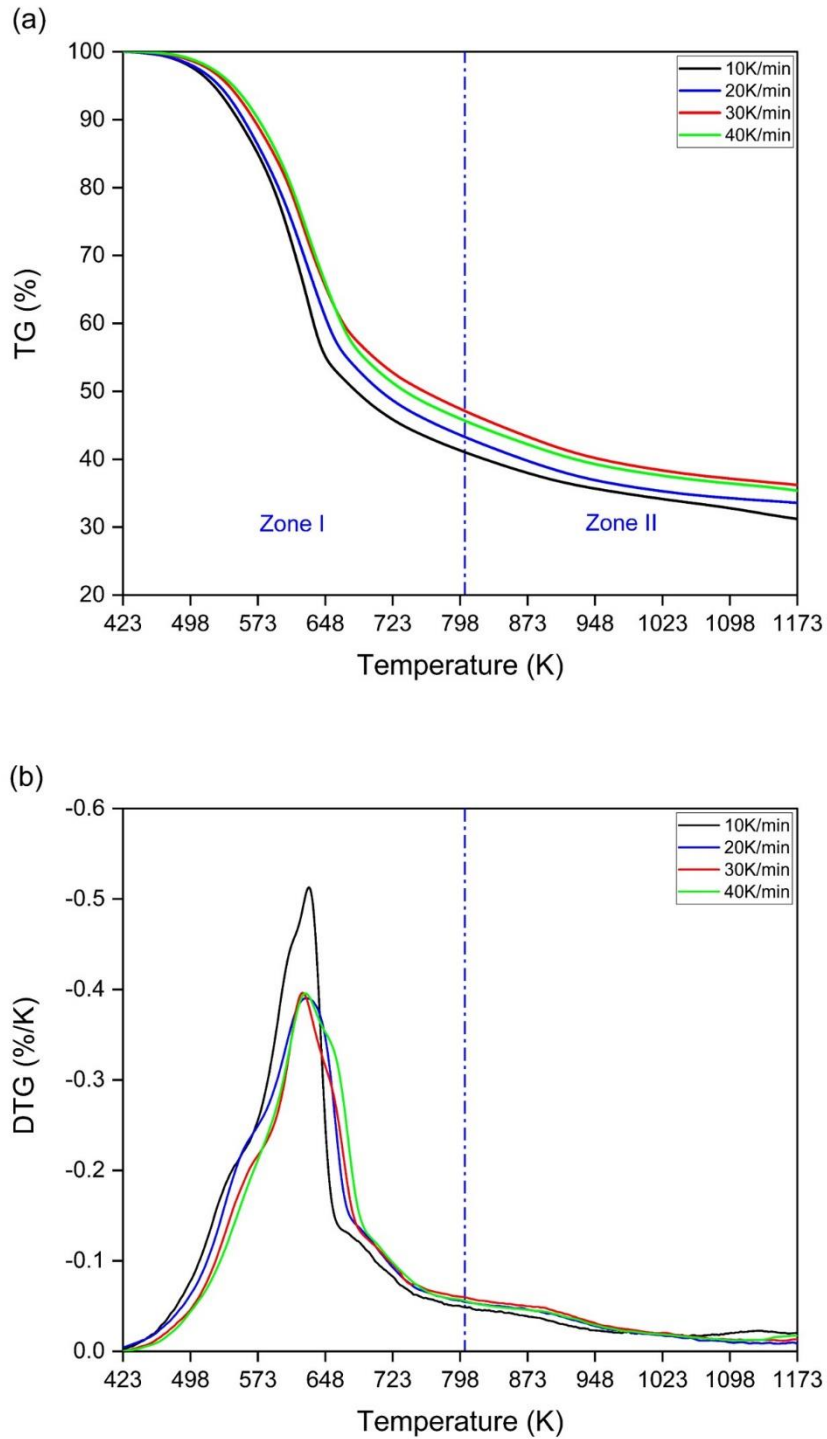


**Figure 3.2** (a) TG and (b) DTG curves of pyrolysis of pine bark (i.e. WT0PB1) at 10, 20, 30 and 40 K/min

The decomposition of WT0PB1, on the other hand, occurred throughout a wider temperature range, with *Zone I* exhibiting a single shoulder and peak as shown in Figure 3.2. The decomposition of hemicellulose would be the reason for the presence of the shoulder at a

lower temperature of about 553 K (Blasi, 2008). According to Azizi et al. (2019), the decomposition of hemicellulose appeared as a shoulder at a lower temperature rather than as a distinct peak. At a temperature of around 626 K, a maximum decomposition rate (%/ K) is reported. This result is in agreement with the literature (Singh et al., 2012). The peak decomposition would be due to the breakdown of cellulose (Akubo et al., 2019; Hassan et al., 2016). Since the decomposition of lignin as a constituent of biomass occurs throughout a wider temperature range (473-823 K) (Akubo et al., 2019; Blasi, 2008), it may occur at the same time as hemicellulose and cellulose decompose. The weight loss of WT0PB1 continued to increase throughout the chosen temperature range while no significant change in the weight of the WT1PB0 is recorded at around 791 K. On average, a total solid residue of 37.10 and 34.09 wt% is reported for WT1PB0 and WT0PB1, respectively, at a final temperature of 1173 K. According to the proximate analysis of WT0PB1 and WT1PB0 reported in Tables 3.2 and 3.3, high content of fixed carbon and ash contribute to a high fraction of solid residue (Menaes et al., 2020; Wang et al., 2018). Additionally, the usage of carbon black in the production of tyres results in a higher yield of char (Williams and Besler, 1995).

Thermal degradation characteristics of WT1PB0 differ from WT0PB1. Waste tyre started to decompose at a temperature higher than that of biomass. In addition, it shows more than one decomposition peak. Wang et al. (2018) reported similar observations during standalone pyrolysis of rice straw, poplar wood and waste tyre. They found that the decomposition of waste tyre started at nearly 653 K compared to 473 K for biomass materials. Based on the current findings, the decomposition of the WT0PB1 and WT1PB0 was at its maximum at the temperature range of 724-744 K and 623-630 K with average values of 0.58 and 0.42 wt%/K, respectively.

### 3.3.1.2 Thermal decomposition of waste tyre and pine bark blends

TG and DTG curves of the waste tyre and pine bark blends as shown in Figures 3.3 to 3.5 were divided into two zones where *Zone I* indicate the main pyrolysis zone. Following the addition of PB to the WT, it can be seen that the pyrolysis of the waste tyre was promoted to some extent. In comparison to the DTG curve of a single waste tyre, the increase in the pine bark fraction in the blend resulted in an increase in the mass loss rate associated with the first peak while the second peak decreased. Due to the difference in the composition of biomass in general and waste tyres and the complexity of their structure, the mechanism underlying the interaction between these two materials is still not clear. However, radical interaction is the most accepted and considered by many researchers (Abnisa and Daud, 2014; Wang et al., 2018). As the temperature of the TG analyser increases, waste tyre and pine bark will pack together initiating radical interaction. Because biomass contains unstable o-containing bonds (Liu et al., 2020; Wang et al., 2018), it will start to decompose at a lower temperature than the waste tyre. Consequently, it releases free radicals including O-radical, OH-radical and other O-containing radicals (Liu et al., 2020), enhancing the decomposition of waste tyre via chain scission of rubber components (Perejón et al., 2021). On the other hand, the chain scission of rubber components (Duan et al., 2015) is accompanied by the release of hydrocarbon- and H-radicals (Han et al., 2018; Liu et al., 2020) which could enhance the conversion of oxygenated compounds. Therefore, a higher degradation rate is reported at lower temperatures (as given in Table 3.6), referring to *stage b*, for blended samples (highest for WT1PB3) compared to WT1PB0.

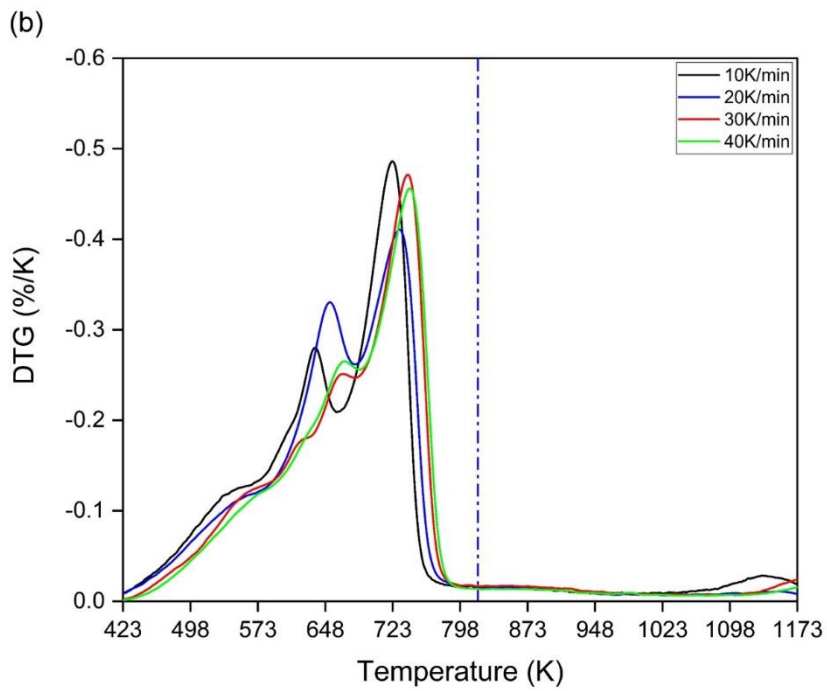
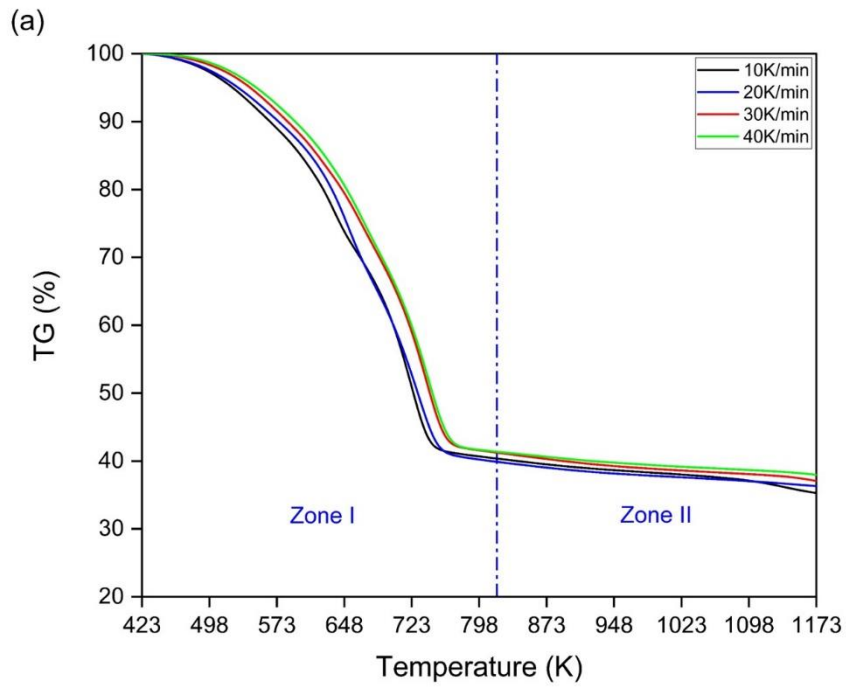


**Figure 3.3** (a) TG and (b) DTG curves of co-pyrolysis of the waste tyre and pine bark at 10, 20, 30 and 40 K/min for WT3PB1

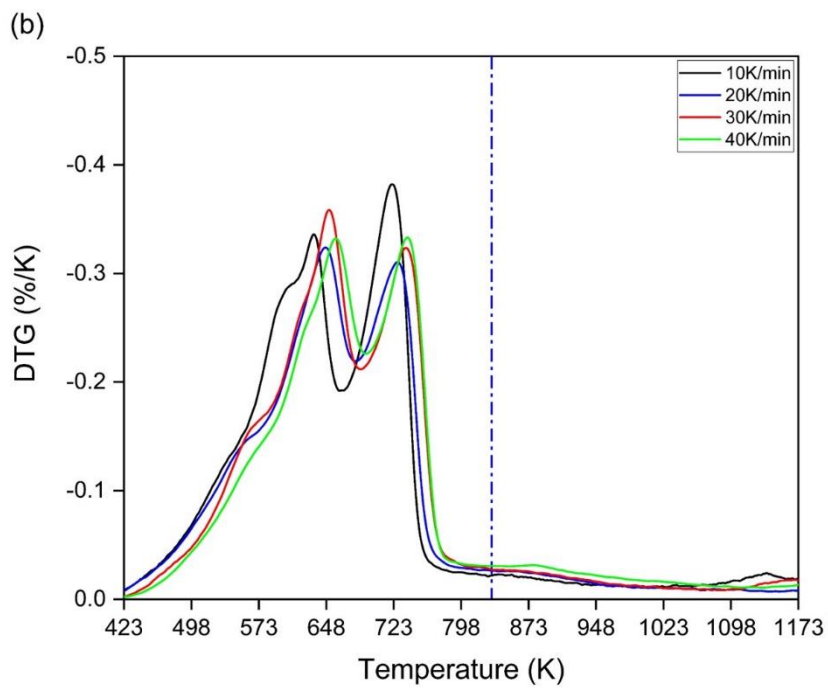
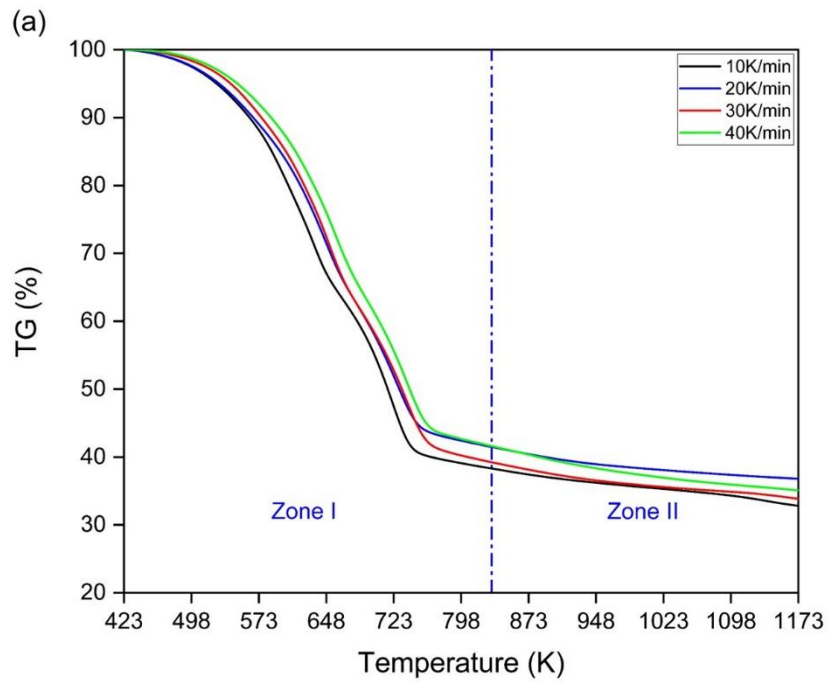


**Figure 3.4** (a) TG and (b) DTG curves of co-pyrolysis of the waste tyre and pine bark at 10, 20, 30 and 40 K/min for WT1PB1

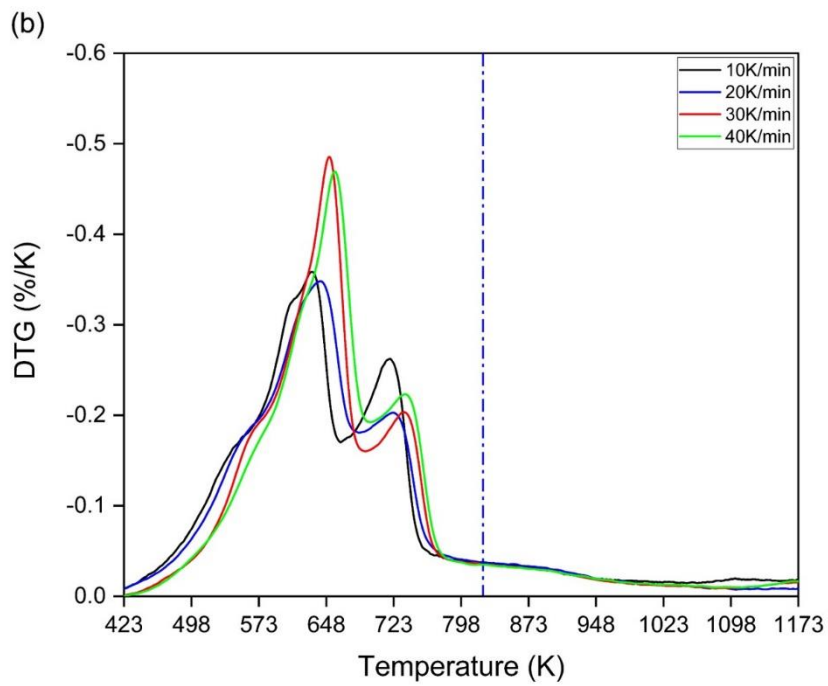
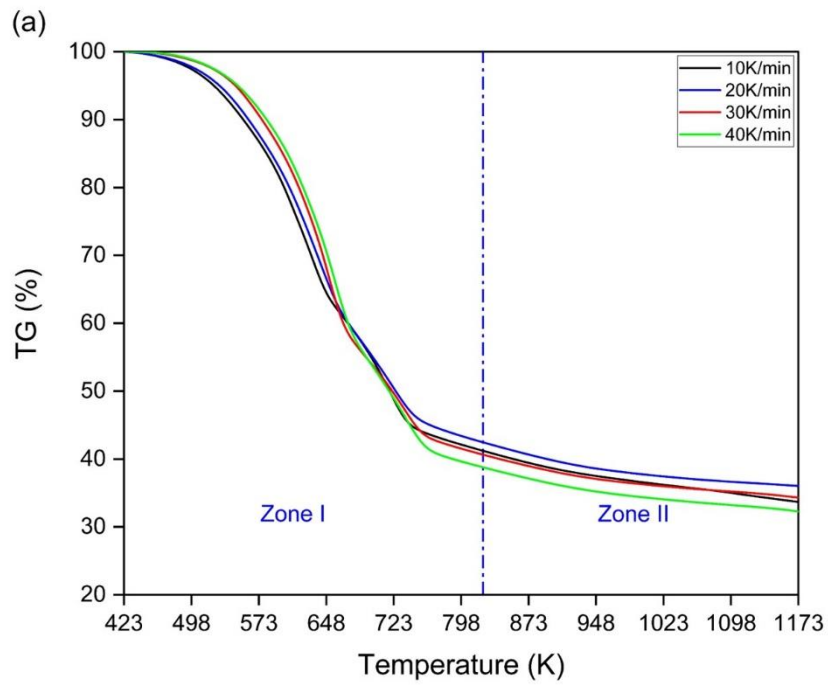


**Figure 3.5** (a) TG and (b) DTG curves of co-pyrolysis of the waste tyre and pine bark at 10, 20, 30 and 40 K/min for WT1PB3

### 3.3.1.3 Effect of heating rate on the decomposition of waste tyre, pine bark and their blends

The effect of the heating rate on the decomposition characteristics of WT1PB0, WTOPB1 and their blends can be figured out from Tables 3.5 and 3.6.  $T_i$ ,  $T_{max}$  and  $T_f$  refer to the initial temperature, the maximum temperature at which the DTG peaks occur and the final temperature, respectively. *Zone I* is represented by sub-stages (i.e. *stage a*, *stage b* and *stage c*) in accordance with the peaks and shoulders contained in the DTG curve of each sample. Since more the 50% of all the samples weight lost in *Zone I*, it is regarded as the main pyrolysis zone and used for the kinetics analysis.

**Table 3.5** Thermal decomposition characteristics of the waste tyre and pine bark in the *Zone I* at different heating rates

Sample ID	$\beta$ (K/min)	Sub-zones	Temperature (K)			Weight loss (%)
			$T_i$	$T_{max}$	$T_f$	
WT1PB0	10	Stage a	423.00	524.80	577.90	9.81
		Stage b	577.90	651.70	664.70	13.27
		Stage c	664.70	723.70	775.20	37.95
	20	Stage a	423.00	533.20	582.60	9.15
		Stage b	582.60	658.20	679.30	19.71
		Stage c	679.30	730.60	795.00	30.87
	30	Stage a	423.00	539.50	596.90	9.27
		Stage b	596.90	674.10	690.70	17.08
		Stage c	690.70	740.90	806.20	35.07
	40	Stage a	423.00	542.20	615.60	10.21
		Stage b	615.60	675.40	696.10	16.99
		Stage c	696.10	743.90	811.20	32.88
WTOPB1	10	Stage a	423.00	-	566.70	13.47
		Stage b	566.70	629.70	661.50	33.78
		Stage c	661.50	-	745.30	8.51
	20	Stage a	423.00	-	578.30	15.07
		Stage b	578.30	627.00	674.20	30.30

	<i>Stage c</i>	674.20	-	752.80	8.30
30	<i>Stage a</i>	423.00	-	583.10	13.21
	<i>Stage b</i>	583.10	622.80	682.90	29.35
	<i>Stage c</i>	682.90	-	763.30	7.81
40	<i>Stage a</i>	423.00	-	590.60	13.95
	<i>Stage b</i>	590.60	625.90	694.30	31.50
	<i>Stage c</i>	694.30	-	774.30	7.19

**Table 3.6** Thermal decomposition characteristics of the waste tyre and pine bark blends in the *Zone I* at different heating rates

Sample ID	$\beta$ (K/min)	Sub-zones	Temperature (K)			Weight loss (%)
			$T_i$	$T_{max}$	$T_f$	
WT3PB1	10.0	<i>Stage a</i>	423.00	534.60	566.30	10.53
		<i>Stage b</i>	566.30	636.70	663.50	19.05
		<i>Stage c</i>	663.50	722.50	777.10	29.39
	20.0	<i>Stage a</i>	423.00	545.60	582.10	10.88
		<i>Stage b</i>	582.10	653.20	681.00	23.05
		<i>Stage c</i>	681.00	730.50	805.50	25.98
	30.0	<i>Stage a</i>	423.00	557.90	590.10	10.67
		<i>Stage b</i>	590.10	667.50	681.10	17.88
		<i>Stage c</i>	681.10	739.70	817.10	30.22
	40.0	<i>Stage a</i>	423.00	-	594.60	10.16
		<i>Stage b</i>	594.60	669.20	685.90	18.85
		<i>Stage c</i>	685.90	743.60	823.90	29.71
WT1PB1	10.0	<i>Stage a</i>	423.00	-	559.50	9.49
		<i>Stage b</i>	559.50	634.10	662.80	26.59
		<i>Stage c</i>	662.80	721.20	788.10	24.59
	20.0	<i>Stage a</i>	423.00	557.60	576.50	11.51
		<i>Stage b</i>	576.50	647.30	680.30	25.60
		<i>Stage c</i>	680.30	727.30	819.50	21.07
	30.0	<i>Stage a</i>	423.00	566.30	583.90	11.36
		<i>Stage b</i>	583.90	651.30	686.30	27.01
		<i>Stage c</i>	686.30	736.80	811.90	21.82
	40.0	<i>Stage a</i>	423.00	568.30	592.10	10.89
		<i>Stage b</i>	592.10	658.70	692.10	25.74

		<i>Stage c</i>	692.10	738.30	818.10	21.34
<b>WT1PB3</b>	10.0	<i>Stage a</i>	423.00	548.40	560.60	10.88
		<i>Stage b</i>	560.60	632.20	663.80	27.71
		<i>Stage c</i>	663.80	718.80	807.90	19.65
	20.0	<i>Stage a</i>	423.00	559.70	575.70	12.71
		<i>Stage b</i>	575.70	641.50	684.60	29.49
		<i>Stage c</i>	684.60	721.90	815.40	15.07
	30.0	<i>Stage a</i>	423.00	568.00	581.20	10.95
		<i>Stage b</i>	581.20	651.40	691.30	33.91
		<i>Stage c</i>	691.30	734.30	809.80	14.04
	40.0	<i>Stage a</i>	423.00	-	585.30	10.69
		<i>Stage b</i>	585.30	657.50	697.40	35.24
		<i>Stage c</i>	697.40	735.70	814.10	15.00

An increase in the heating rate from 10 to 40 K/min resulted in a shift in the TGA curves and the peak temperature of all the samples to higher values. According to Williams and Besler (1995) and others (Azizi et al., 2019; Uzun and Yaman, 2014; Wang et al., 2022), this could be as a result of limited heat diffusion at the higher heating rate which in turn causes an increase in thermal lag (i.e. *the time delay for heat to be conducted through a material causing a temperature difference between the particle and its surrounding* (Czajka, 2021)) and change in the decomposition kinetics of the feedstocks.

#### 3.3.1.4 Synergetic interaction analysis

The improvement in the quality and quantity of the products obtained during co-pyrolysis is highly dependent on the synergetic interaction between the feedstocks used. Using the difference in weight loss (i.e.  $\Delta W$ ) as an index, the existence of synergetic interaction between waste tyre and pine bark during co-pyrolysis was evaluated (Likun and Zhang, 2020). This is assessed in response to the variation in operating conditions including heating rate as

well as the WT to PB blend ratio. According Likun and Zhang (2020), the difference in weight loss is defined as Equation (3.19);

$$\Delta W = W_{exp} - W_{cal} \quad (3.19)$$

Where  $W_{exp}$  and  $W_{cal}$  stand for the experimentally measured and theoretically calculated weight loss, respectively. Theoretically calculated weight loss,  $W_{cal}$ , is obtained using Equation (3.20);

$$W_{cal} = (x_{WT} \times W_{WT}) + (x_{PB} \times W_{PB}) \quad (3.20)$$

Where,  $x_{WT}$  = weight fraction of waste tyre in the blend,

$x_{PB}$  = weight fraction of pine bark in the blend,

$W_{WT}$  = weight loss when a single feed of waste tyre is used for pyrolysis (wt%),

$W_{PB}$  = weight loss when a single feed of pine bark is used for pyrolysis (wt%).

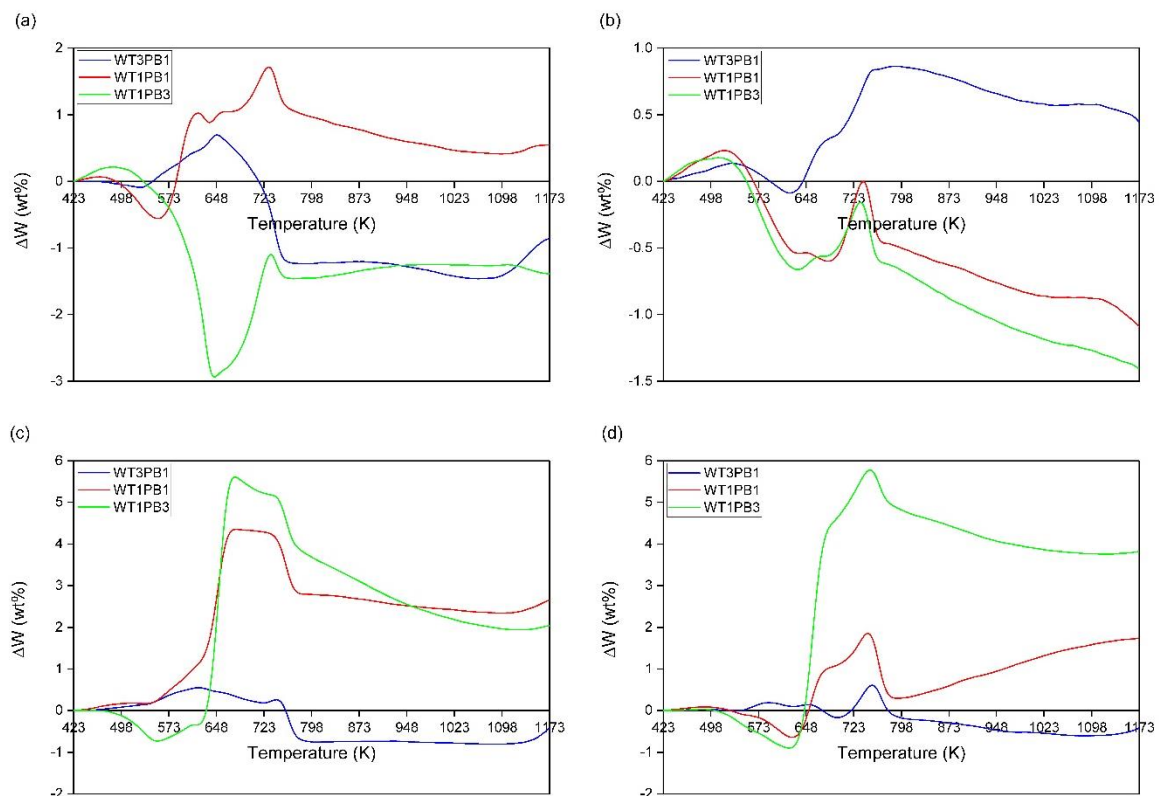


**Figure 3.6** Variation in the difference of weight loss (i.e.  $\Delta W$ ) for waste tyre and pine bark blends at (a) 10, (b) 20, (c) 30 and (d) 40 K/min.

Positive values of  $\Delta W$  reflect the existence of promoting effect, whereas the negative values imply the presence of the inhibitory effect. As illustrated in Figure 3.6, the effect of the change in heating rate on the  $\Delta W$  varied for each blended sample.

The decomposition of the WT3PB1 sample at a heating rate of 10, 30 and 40 K/min showed negative values of  $\Delta W$  at temperatures higher than 723 K. Use of a low heating rate of 10 K/min resulted in the most inhibitive interaction. This indicates lower experimental weight loss reported. In contrast, the use of a heating rate of 20 K/min was found to have promoting effect. Apart from the positive and negative change in the values of  $\Delta W$ , less variation in  $\Delta W$  in response to the increase in temperature is noticed for the WT3PB1 sample. This result may be explained by the fact that waste tyres have high thermal stability and are composed of a high fraction of fixed carbon. Therefore, the addition of 25 wt% of PB has no significant impact on its decomposition.

Interestingly, a blended sample of pine bark and waste tyre with a mass ratio of 1:1 showed almost contradictory results to WT3PB1. A promoting interaction was observed at all heating rates except at 20 K/min and it was limited to a temperature of 573 K.

Unlike WT3PB1 and WT1PB1 samples, the use of the high heating rate of 30 and 40 K/min in the thermal decomposition of WT1PB3 resulted in the most positive interaction as indicated by  $\Delta W$  values which reached the highest point of 5.61 and 5.78%, respectively. The results show that the largest synergetic effect appeared between 648 to 748 K which is the temperature range for the decomposition of synthetic rubber, cellulose and lignin (Akubo et al., 2019; Kan et al., 2017). This is supported by the highest degradation peaks at heating rates of 30 and 40K/min as shown in Figure 3.5. An inhibitive turning temperature of 520 and 571 K is observed at the heating rates of 10 and 20 K/min, respectively.

In summary, the effect of heating on the synergetic interaction between WT and PB in terms of weight loss varied with different blend ratios. The presence of positive synergetic interaction at a low heating rate might be a result of the longer heating time required to achieve the desired final temperature in TG analysis. This in turn will allow better heat diffusion, enhancing the decomposition reactions. On the other hand, the rapid increase in the temperature of the sample and the high gradient of temperature within the sample could be the causes of the promoting interaction at the higher heating rate (Lah et al.,2013).

### 3.3.2 Kinetics analysis

In this section, the results of the kinetics study of pyrolysis of individual and blended feedstocks using model fitting, iso-conversional and combined kinetic analysis methods are presented and discussed. To assess the occurrence of synergetic interaction during co-pyrolysis, the effect of different blend ratios on the kinetics parameter;  $E_a$  is discussed.

#### 3.3.2.1 *Kinetics analysis of pyrolysis and co-pyrolysis of waste tyre and pine bark using model-fitting methods*

Since the decomposition of the WT and PB blends presented a variation in the synergetic interactions at different heating rates, the results of TGA of the waste tyre, pine bark and their blends at all heating rates were used to predict the kinetics parameters using the CR method. First, the best reaction order describing the pyrolysis process of all the samples was evaluated in response to the highest  $R^2$ . This is achieved by plotting  $\ln \left[ \frac{g(\alpha)}{T^2} \right]$  against  $1/T$  for different blend ratios, where  $g(\alpha)$  replaced with various expressions of reaction orders given in Table 3.1. The results are provided in Figure 3.7.

As shown in Figure 3.7, the best  $n$  value with the highest  $R^2$  for all the samples varied between 1 and 1.5 at different heating rates. This finding is in agreement with others in the

literature (Chen et al., 2019c; Singh et al., 2012) who suggested the first reaction order to best describe the pyrolysis process. Therefore, the kinetics were predicted through the CR method using  $n$  value of 1 for all the samples.

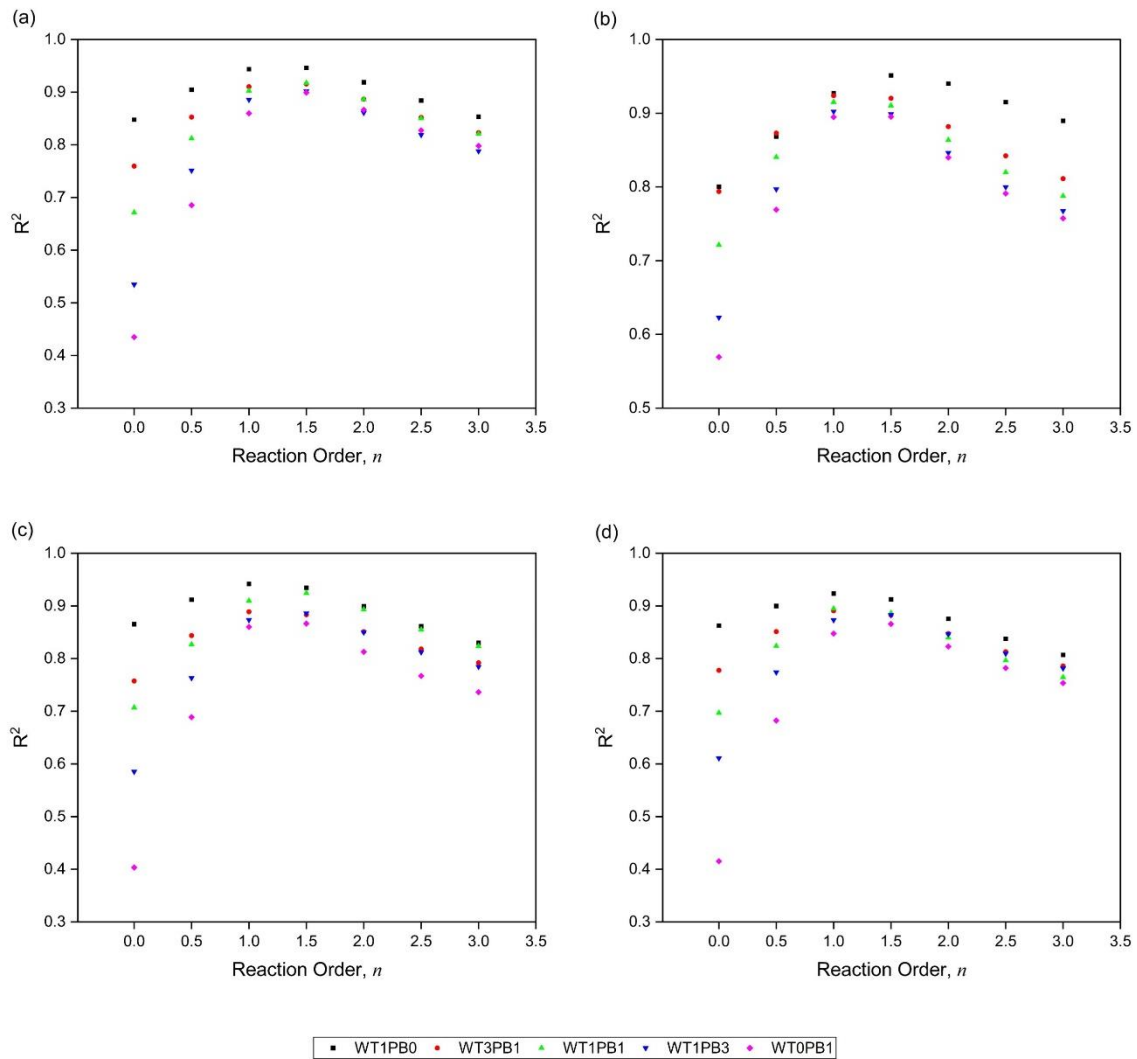


**Figure 3.7** Correlation coefficient (i.e.  $R^2$ ) versus reaction order,  $n$ , for different blend ratios at the heating rate (a) 10, (b) 20, (c) 30 and (d) 40 K/min based on Coats-Redfern method

As previously stated in section 3.3.1 that more than 50 wt% of the samples were decomposed in *Zone I*, the main decomposition zone, so it is considered for the calculation of the kinetics parameters of each sample. Because a non-linear trend was observed for the kinetic curves (i.e.  $\ln \left[ \frac{g(\alpha)}{T^2} \right]$  against  $1/T$ ) of the single-step pyrolysis process of the waste tyre, pine bark and

their blends as shown in Figure 3.8, the kinetic curves were divided into segments corresponding to different temperature ranges. These segments present the shoulders and peaks contained in *Zone I*, assuming multiple first-order reaction steps. The results for the heating rate of 20 K/min are presented in Figure 3.9, whereas for the heating rate of 10, 30 and 40 K/min are provided in Appendix A, Figures A.1-A.3.

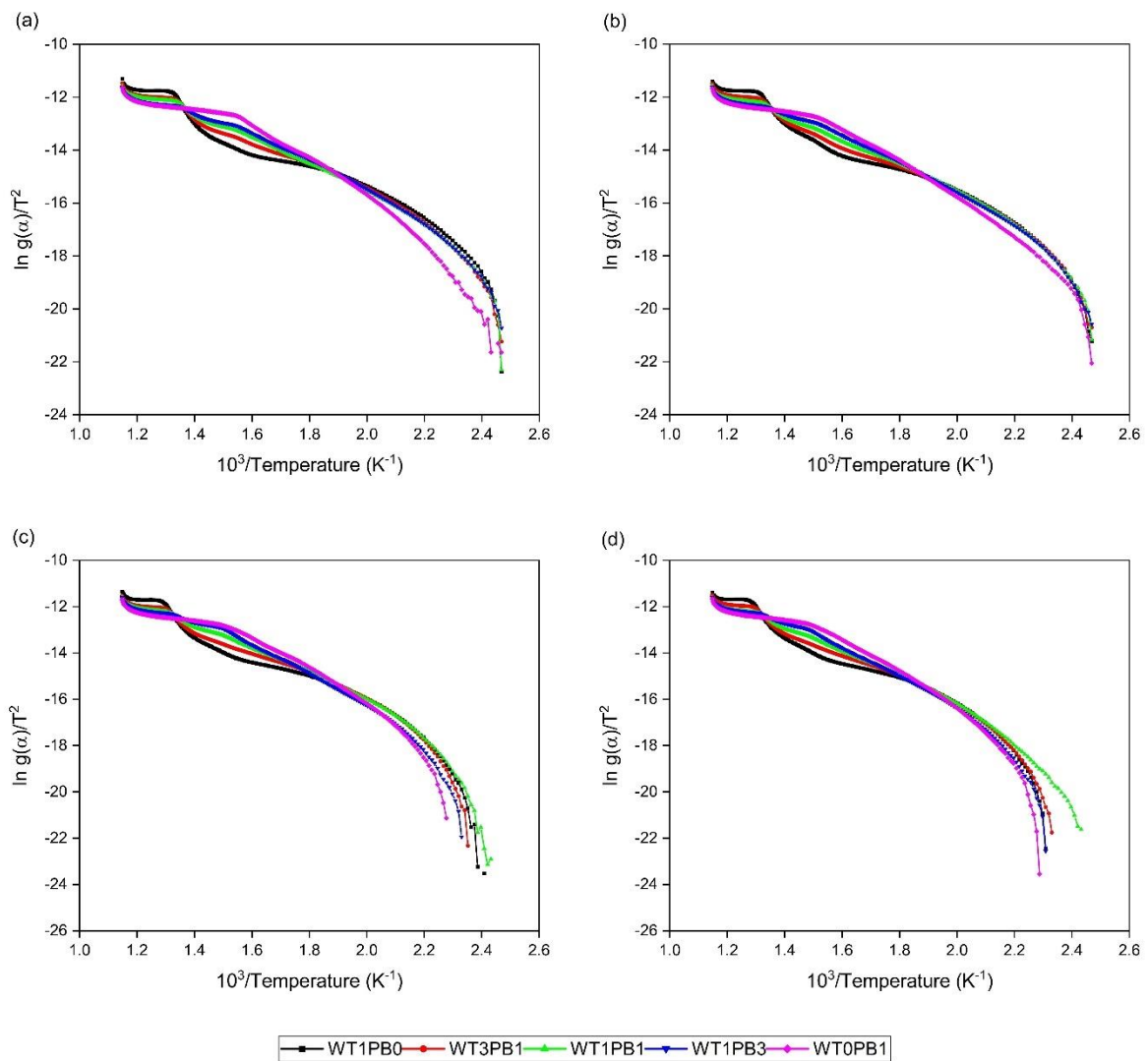


**Figure 3.8** Curves of  $\ln g(\alpha)/T^2$  versus  $1/T$  of the waste tyre and pine bark pyrolysis at a different waste tyre to pine bark blend ratios at the heating rate (a) 10, (b) 20, (c) 30 and (d) 40 K/min using Coats-Redfern method

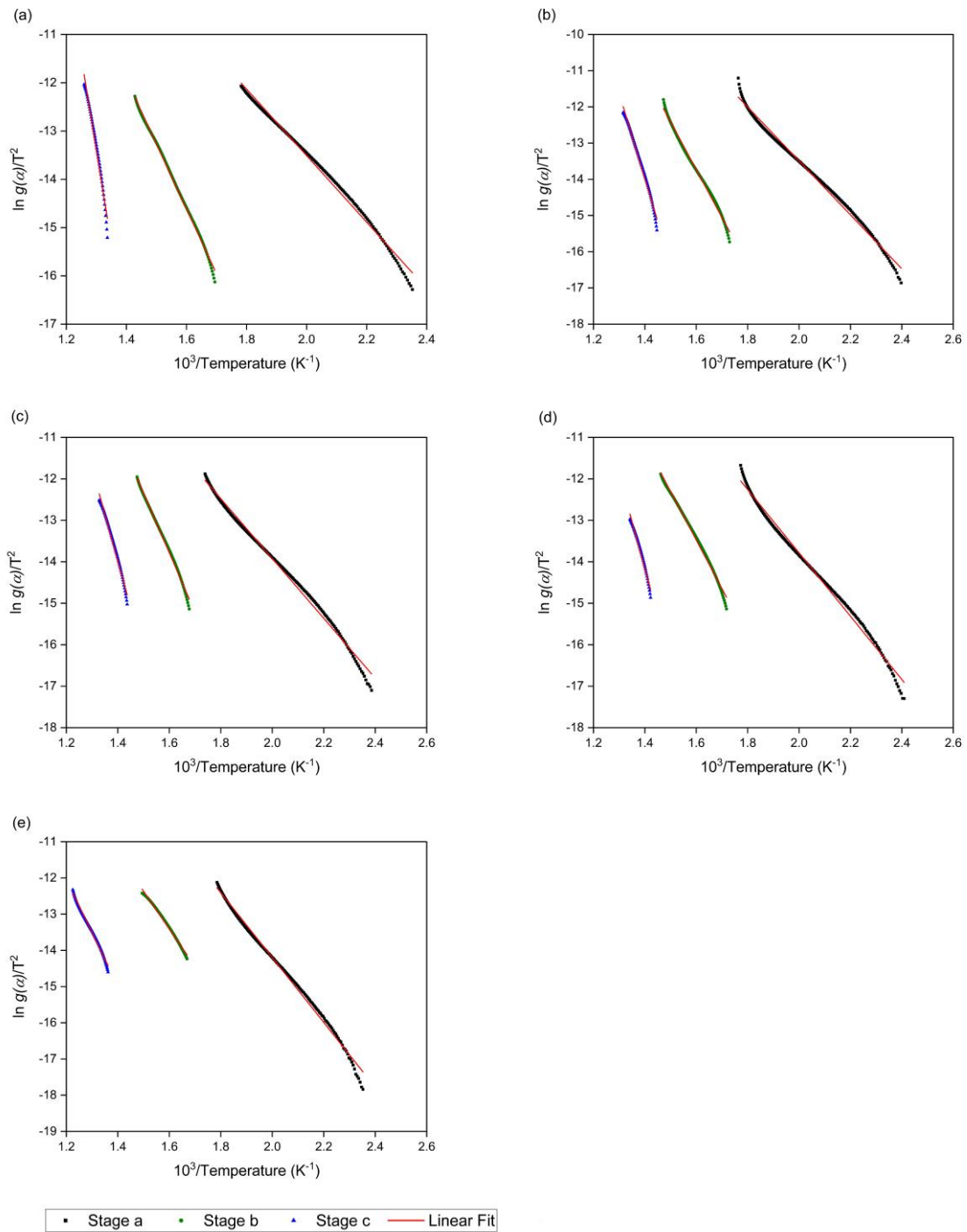


**Figure 3.9** Kinetics analysis curves of  $\ln g(\alpha)/T^2$  versus  $1/T$  of different blend samples; (a) WT1PB0, (b) WT3PB1, (c) WT1PB1, (d) WT1PB3 and (e) WT0PB1 at 20 K/min

Using the slope and intercept of the regression lines, the apparent  $E_a$  and  $A$  were calculated, respectively. The average values of four heating rates for all the samples are calculated and the results are summarised in Table 3.7.

**Table 3.7** Average values of reaction kinetics parameters of the pyrolysis of single and blended samples in Zone I at four different heating rates

Sample ID	Stage	Temperature (K)	$\alpha$ range	$E_a$ (kJ/mol)	$A$ (min <sup>-1</sup> )	$R^2$
WT1PB0	<i>a</i>	423-596	0.01-0.14	58.89	2.36E+05	0.992
	<i>b</i>	589-700	0.18-0.44	138.84	1.45E+13	0.996
	<i>c</i>	678-785	0.51-0.96	224.09	1.58E+20	0.991
WT3PB1	<i>a</i>	417-588	0.03-0.17	65.62	1.42E+06	0.993
	<i>b</i>	576-680	0.21-0.47	119.16	8.73E+09	0.993
	<i>c</i>	677-775	0.53-0.92	185.68	3.10E+13	0.994
WT1PB1	<i>a</i>	419-587	0.05-0.19	66.66	2.14E+06	0.993
	<i>b</i>	576-688	0.24-0.58	118.93	5.53E+09	0.995
	<i>c</i>	675-770	0.63-0.88	180.93	3.82E+13	0.992
WT1PB3	<i>a</i>	415-572	0.07-0.20	71.64	9.79E+06	0.993
	<i>b</i>	573-694	0.26-0.67	113.80	3.73E+09	0.995
	<i>c</i>	677-760	0.71-0.86	177.95	1.41E+13	0.988
WTOPB1	<i>a</i>	425-582	0.09-0.25	81.11	4.38E+07	0.994
	<i>b</i>	581-690	0.35-0.71	110.83	8.88E+09	0.994
	<i>c</i>	678-816	0.76-0.83	138.28	1.96E+10	0.993

According to Table 3.6, the values of apparent  $E_a$  vary among the samples as well as over different temperature ranges. This could be due to the heterogeneity in the composition of single feedstock and the compositional differences between different feedstocks.

It can be seen from the data in Table 3.7 that WT1PB0 showed the lowest  $E_a$  of 58.89 kJ/mol at *stage a*. This is contributed to the decomposition of additives used in the tyre manufacturing process which are known to be volatile and decompose more readily (Lah et al., 2013) at a temperature lower than 573 K. This is in agreement with that of Lah et al. (2013) who reported low  $E_a$  value of 33.50 kJ/mol for the volatiles. At the *stages b* and *c*, WT1PB0 had higher  $E_a$  with the values of 138.84 and 224.09 kJ/mol, respectively, which are mainly ascribed to the decomposition of waste tyre constituents including natural rubber and synthetic rubbers (Chen et al., 2019c). At lower temperatures, natural rubber decomposes

showing a peak at around 658 K compared to synthetic rubber decomposing at high temperatures. In accordance with the present results, Williams and Besler (1995) reported that NR has higher  $E_a$  than SBR which was 199.90 kJ/mol compared to 195.20 kJ/mol but lower than PBR (i.e. 223.80-244.40 kJ/mol) at a heating rate of 20 K/min. Therefore, the higher  $E_a$  of WT1PB0 at *stage c* compared to *b* could be explained by the presence of a higher fraction of PBR than SBR in its composition. In general, high values of  $E_a$  in the case of WT1PB0 might be explained by the fact that its constituents have higher thermal stability due to polymerization compared to WT0PB1 (Chen et al., 2019c).

On the other hand, WT0PB1 showed the lowest  $E_a$  in *stage a* followed by *stage b* then *c*. The high  $E_a$  in *stage b* compared to *stage a* could be explained by the decomposition of cellulose mainly, having higher thermal stability than hemicellulose. The high thermal stability of cellulose is due to the fact that it consists of  $\beta$  (1 $\rightarrow$ 4) linked D-glucose units (Akubo et al., 2019) whereas the branched polysaccharides that form hemicellulose structure contribute to its easy degradation at lower temperatures (Akubo et al., 2019; Yeo et al., 2019). For this reason, a lower  $E_a$  value is reported in *stage a*. In addition to the decomposition of hemicellulose in *stage a*, the decomposition of extractives contained in the WT0PB1 might take place. The current results of  $E_a$  per stage are consistent with the findings of other studies in which a lower  $E_a$  value is reported for hemicellulose than cellulose. According to Mui et al. (2010), Yeo et al. (2019), Ferreiro et al. (2016) and Font et al. (2009), the  $E_a$  of hemicellulose and cellulose decomposition varies in the range of 77.93-137.9 kJ/mol and 132.20-354.40 kJ/mol, respectively. Due to the presence of a three-dimensional alkyl-benzene structure in the lignin structure (Yeo et al., 2019), it is known to be thermally more stable than other biomass constituents. Therefore, this could be responsible for the highest  $E_a$  value (i.e. 138.28 kJ/mol) at higher temperatures. However, lignin decomposition might

overlap with the decomposition of other biomass constituents because its decomposition occurs over wider temperature range.

Indeed, the compositional differences between the WT and PB as well as the structural variation among their constituents contribute to the variation in their decomposition kinetics including  $E_a$  values.

As can be seen from Table 3.7, there is an increase in the  $E_a$  values of *stage a* from 65.62 to 71.64 kJ/mol as the fraction of the PB increased from 25 to 75% in the blends, respectively. This might be explained by the high  $E_a$  value of WT0PB1 compared to WT1PB0 in the same stage which is associated with the devolatilization of extractives as well as a fraction of hemicellulose. In contrast to *stage a*, the  $E_a$  is declining from 138.84 and 224.09 kJ/mol to 113.80 and 177.98 kJ/mol for *stages b* and *c*, respectively, as the PB mass fraction is increased to 75% in comparison to WT1PB0. This is associated with a maximum reduction of around 18.04% at *stage b* with a temperature range of 573-700 K and 20.58% at *stage c* with a temperature higher than 700 K compared to WT1PB0. These results reflect those of Uzun and Yaman (2014) who also found that using biomass and scrap tyre blended sample with a 1:1 mass ratio, showed a decrease in the activation energy to 63.80 kJ/mol in comparison to 78.70 kJ/mol for scrap tyre only.

Since PB has lower thermal stability than polymeric wastes like WT as supported by lower activation energy, it could tend to initiate the decomposition reaction more effectively thus lowering the activation energy of the blended samples (Gao et al., 2021; Wang et al., 2018). In addition, the formation of free radicals during biomass decomposition plays roles in activating the decomposition process of WT (Menares et al., 2020). This reflects the occurrence of positive synergetic interaction during the co-pyrolysis process. In comparison

to the WT1PB0, the blended sample of WT1PB3 was shown to have the lowest  $E_a$  and thus highest synergetic interaction. It is likely therefore that the energy required for the decomposition of fixed carbon fraction and synthetic rubber component of tyre could be lowered due to the addition of biomass.

To evaluate the occurrence of the synergetic interaction during co-pyrolysis based on the average  $E_a$ , a comparison between experimentally measured and theoretically calculated average  $E_a$  values was conducted. The experimental average activation energy (i.e.  $\bar{E}_{a,exp}$ ) is obtained using Equation (3.21) (Chen et al., 2019b).

$$\bar{E}_{a,exp} = (\sum_{i=1}^N \alpha_i E_{a,i}) / \sum_{i=1}^N \alpha_i \quad (3.21)$$

where,  $\alpha_i$  and  $E_{a,i}$  refer to the conversion and activation energy values in kJ/mol at each temperature range, respectively. The theoretical average activation energy (i.e.  $\bar{E}_{a,cal}$ ) is calculated using Equation (3.22) (Chen et al., 2019b).

$$\bar{E}_{a,cal} = (x_{WT} \times \bar{E}_{WT}) + (x_{PB} \times \bar{E}_{PB}) \quad (3.22)$$

Where,  $x_{WT}$  = the weight fraction of waste tyre in the blend,

$x_{PB}$  = the weight fraction of pine bark in the blend,

$\bar{E}_{WT}$  = the experimental average activation energy for a single waste tyre in kJ/mol,

$\bar{E}_{PB}$  = the experimental average activation energy for single pine bark in kJ/mol.

The results for the  $\bar{E}_{a,exp}$  and  $\bar{E}_{a,cal}$  values are depicted in Figure 3.10. The vertical bars show the percent change in the activation energy of the samples relative to the waste tyre while the horizontal ones represent the percent difference between the experimental and theoretical activation energy of each sample. Interestingly, the  $\bar{E}_{a,exp}$  of all the blend samples were lower than the  $\bar{E}_{a,cal}$ , showing that positive interaction occurred. Although WT1PB3

showed the lowest  $\bar{E}_{a,exp}$  value compared to other blend samples with a percent decrease of 30.53% relative to sole waste tyre, the highest percentage difference between  $\bar{E}_{a,exp}$  and  $\bar{E}_{a,cal}$  of 9.12% was reported for WT3PB1.

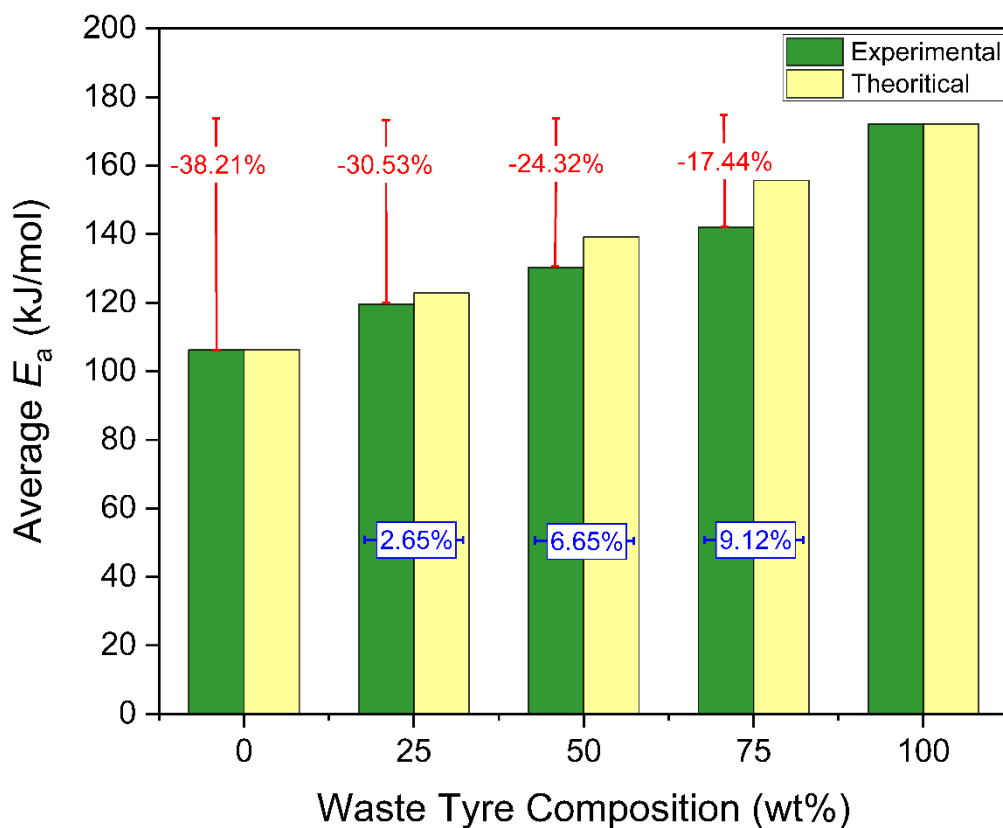


**Figure 3.10** Comparison between experimental and theoretical average activation energy of the samples relative to waste tyre

Indeed, using the CR method in the calculation of kinetics parameters of the decomposition of different blend samples with the assumption of first reaction order demonstrated high  $R^2$  (>0.98) as shown in Table 3.7. However, using the first-order reaction model might not necessarily provide an accurate representation of the reaction mechanism. Therefore, the reaction mechanism underlying the pyrolysis of the WT, PB and their blends is identified and will be discussed in sections 3.3.2.3 and 3.3.2.4.

### 3.3.2.2 *Determination of overall kinetics parameters using iso-conversional methods*

The apparent  $E_{\alpha}$  of all the blended samples was determined using iso-conversional methods. This was accomplished through the linear fitting of the left-hand side of the equations describing iso-conversional methods against the reciprocal of  $T_{\alpha}$ . The  $\alpha$  ranges from 0.10 to 0.90 with a step size of 0.05 was considered. To follow the recommendation made by ICTAC (Vyazovkin et al., 2011) for the kinetics analysis, the experimental data for three heating rates of 10, 30 and 40 K/min were assessed. This is because the fitting of four heating rates showed a low correlation coefficient,  $R^2$ . The kinetic plots of the iso-conversional methods are shown in Figures 3.11-3.13. The  $R^2$  values for all the samples were higher than 0.90 for each method which signifies that they were better fitted with experimental data except for WT1PB3 and WTOPB1 with  $\alpha$  values higher than 0.55.

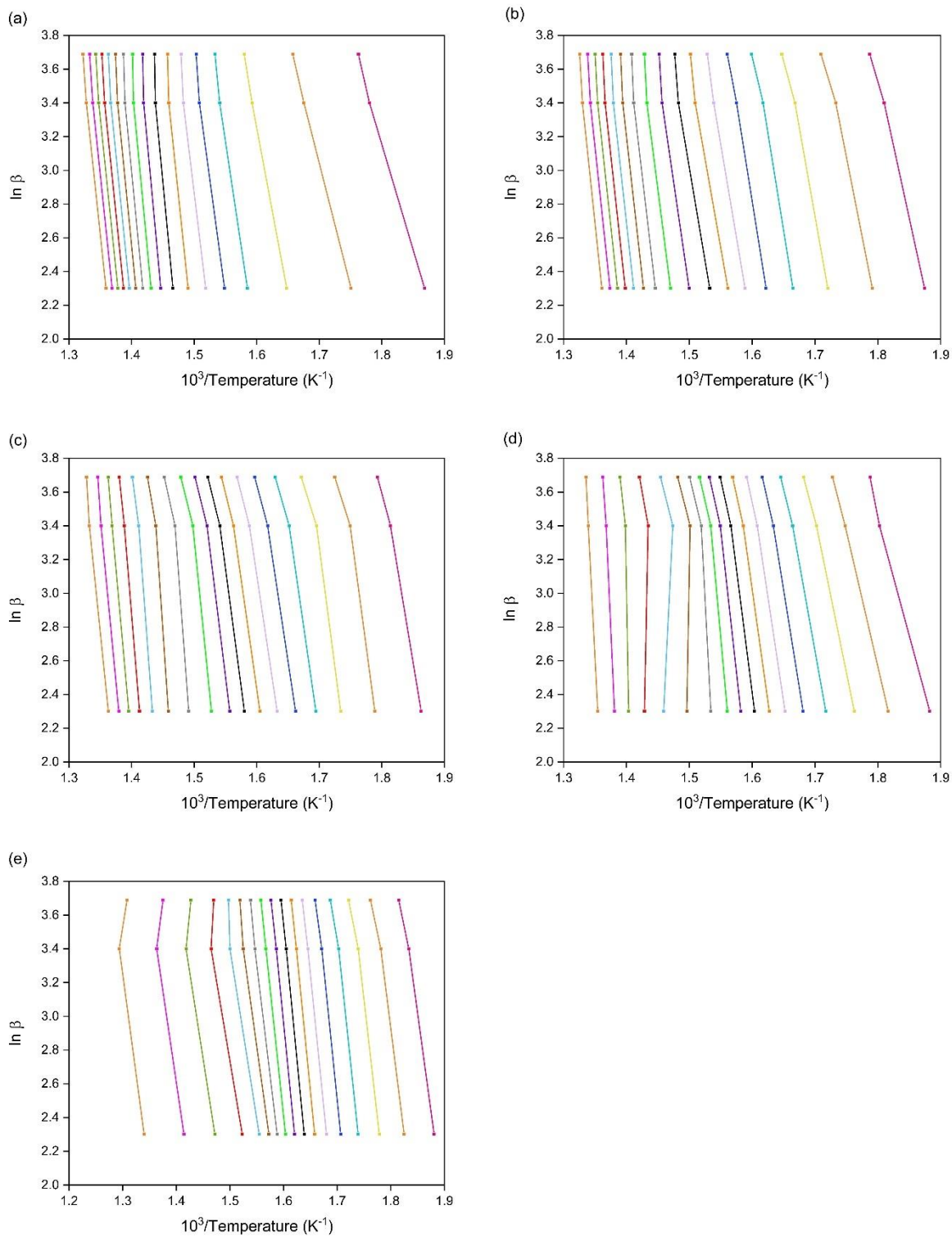


**Figure 3.11** Kinetics analysis curves of different blend samples; (a) WT1PB0, (b) WT3PB1, (c) WT1PB1, (d) WT1PB3 and (e) WT0PB1 using FWO method

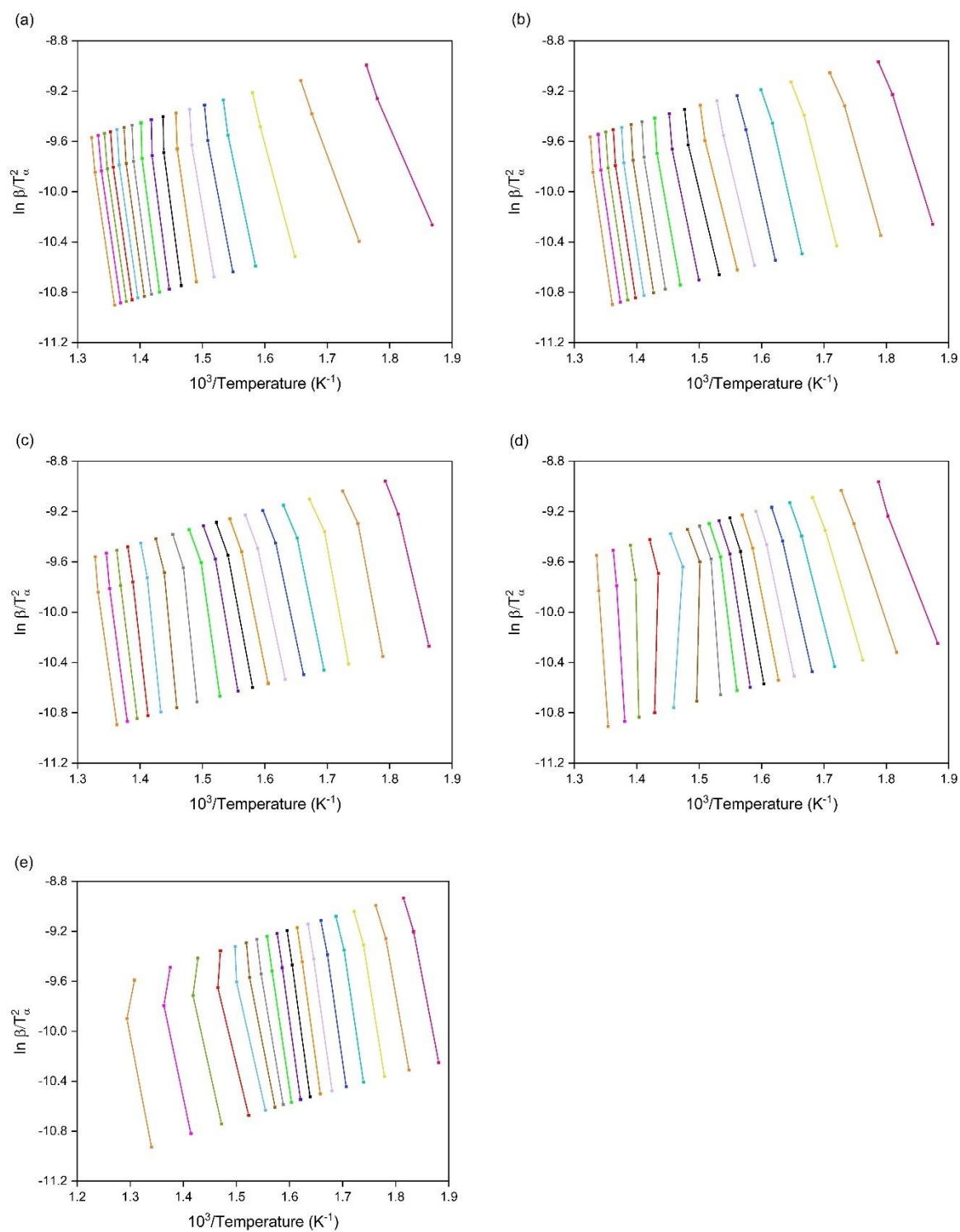


**Figure 3.12** Kinetics analysis curves of different blend samples; (a) WT1PB0, (b) WT3PB1, (c) WT1PB1, (d) WT1PB3 and (e) WTOPB1 using KAS method

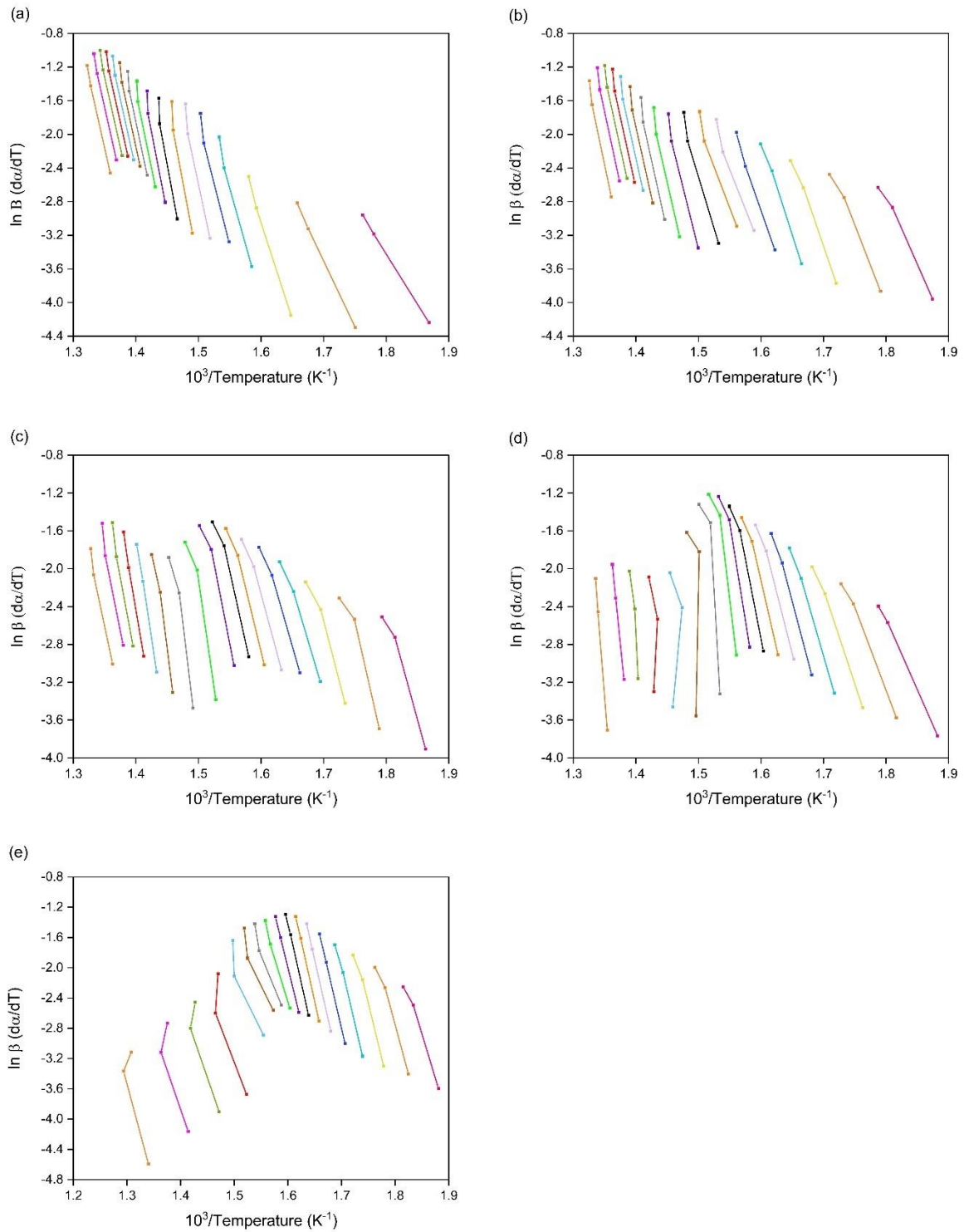


**Figure 3.13** Kinetics analysis curves of different blend samples; (a) WT1PB0, (b) WT3PB1, (c) WT1PB1, (d) WT1PB3 and (e) WTOPB1 using Friedman method

The results for the variation in  $E_\alpha$  values with  $\alpha$  for single and blended samples are presented in Figure 3.14. Differences in the change of  $E_\alpha$  with  $\alpha$  among the samples are observed. These

differences can be explained by the differences between the composition and molecular structure of WT and PB.

As seen in Figure 3.14 a and e, both WT0PB1 and WT1PB0 showed the lowest  $E_\alpha$  value at  $\alpha$  equal to 0.1 whereas it was lower for WT1PB0 compared to WT0PB1. For WT1PB0 and WT0PB1, the  $E_\alpha$  continued to increase with the  $\alpha$ , reaching a maximum value of higher than 350.00 and 250.00 kJ/mol for the  $\alpha$  values of 0.50 and 0.45, respectively. At conversions higher than 0.50, the  $E_\alpha$  of WT1PB0 decreased, however, a fluctuation in  $E_\alpha$  of WT0PB1 was reported at  $\alpha$  values higher than 0.45. The observed fluctuation in  $E_\alpha$  might indicate the presence of multiple decomposition reactions. Similarly, Yeo et al. (2019) observed high variation in the  $E_\alpha$  values as a function of  $\alpha$  for the decomposition of hemicellulose and lignin. According to Wang et al. (2016), there are two likely causes for the decrease in  $E_\alpha$ ; 1) the in-situ catalytic effect induced by the metals contained in the ash of either biomass, waste tyre or both, and 2) the enhanced diffusion of volatiles into porous char material making the reaction easier.

Waste tyre and pine bark blended samples showed large variations in  $E_\alpha$  values as a function of  $\alpha$  similar to WT0PB1. The reason for this is not clear but it may have something to do with the compositional differences between PB, WT and their blends (Kandasamy and Gökcalp, 2014; Zhang et al., 2016a). This in turn causes an overlapping in the decomposition temperature of WT and PB constituents including cellulose, hemicellulose, NR, etc. (Likun and Zhang, 2020) and the interactions that might take place between the reactive free radicals released throughout the devolatilization process. There are similarities between the variation expressed by the  $E_\alpha$  in response to conversion in this study and those described by Lah et al.

(2013), Wang et al. (2016), Williams and Besler (1995) and Yeo et al. (2019) for waste tyre and biomass constituents.

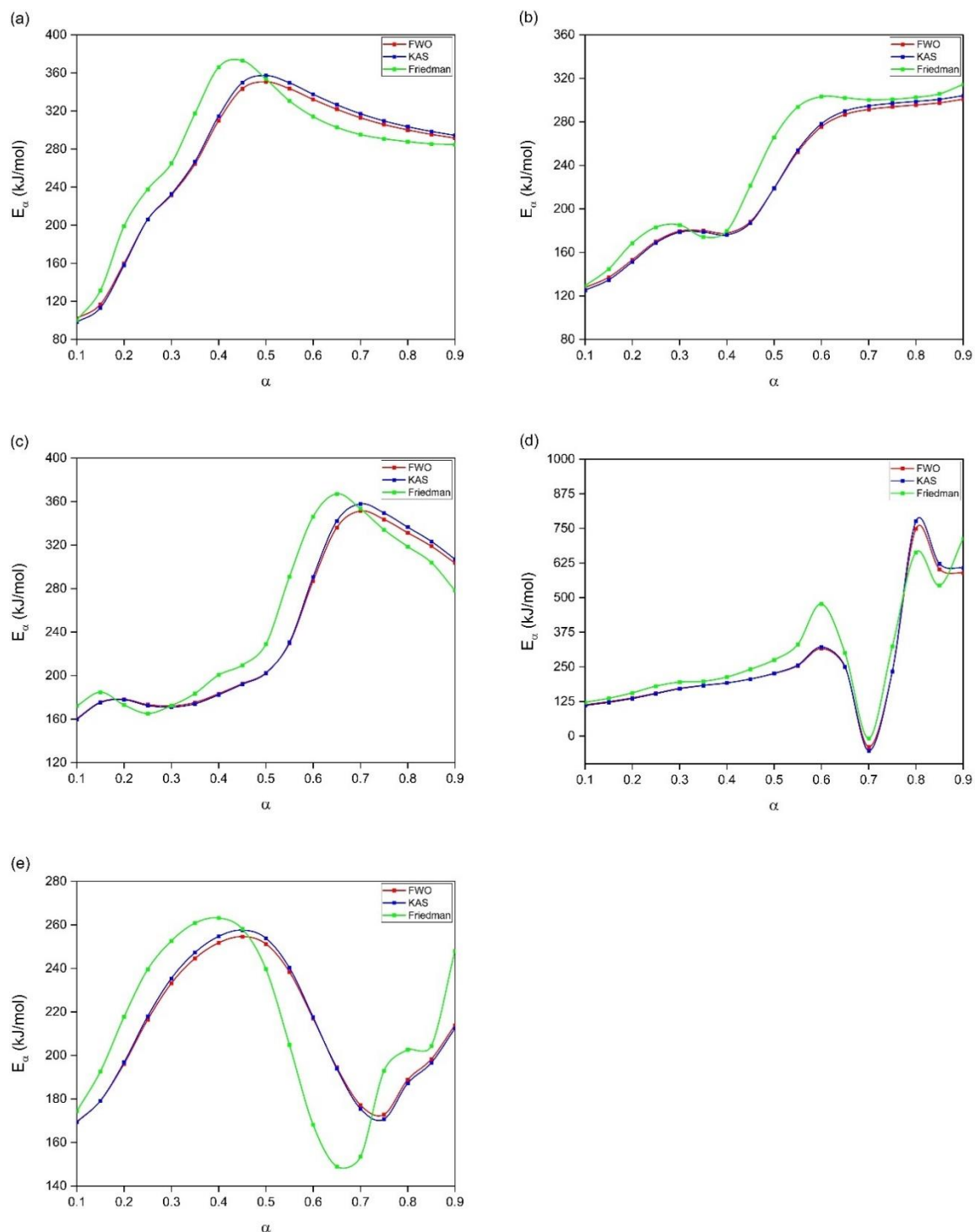


**Figure 3.14** Variation in  $E_{\alpha}$  values obtained using Iso-conversional methods with conversion (i.e.  $\alpha$ ) for (a) WT1PB0, (b) WT3PB1, (c) WT1PB1, (d) WT1PB3 and (e) WT0PB1

Since iso-conversional methods do not provide the values of the  $A$ , the Kinetic Compensation Effect (i.e. KCE) is introduced in section 3.1.1.2.4. The linear relationship between  $\ln A$  and  $E_\alpha$  based on the kinetic data obtained using the FWO method is plotted in Figure 3.15, whereas for KAS and FR methods are presented in Appendix A, Figures A.4 and A.5. The results are reported in Table 3.8.

Table 3.8 summarises the average values of kinetics parameters (i.e.  $E_\alpha$  and  $A$ ) obtained through the iso-conversional methods for different blended samples at the heating rates of 10, 30 and 40 K/min.

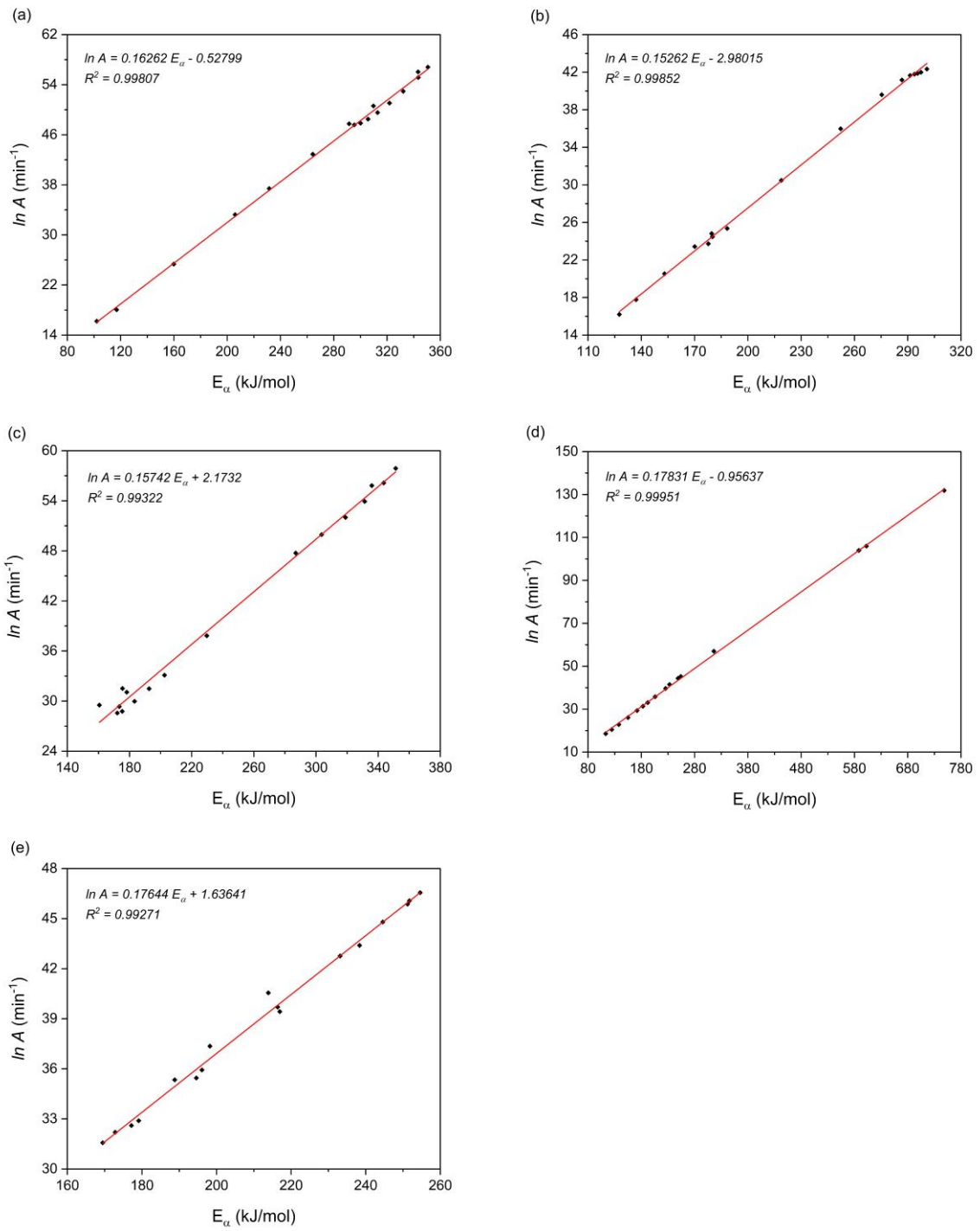


**Figure 3.15** Linear relationship of compensation effect between  $\ln A$  and  $E_{\alpha}$  of different blend samples; (a) WT1PB0, (b) WT3PB1, (c) WT1PB1, (d) WT1PB3 and (e) WTOPB1 using kinetics obtained through FWO method

**Table 3.8** Average  $E_{\alpha}$  values for the co-pyrolysis of the waste tyre and pine bark at different blend ratios obtained by Iso-conversional methods and KCE.

Sample ID	Kinetics Method	$E_{\alpha}$ (kJ/mol)	$R^2$	$A$ ( $min^{-1}$ )	$f(\alpha)$ or $g(\alpha)$	$R^2$
<b>WT1PB0</b>	FWO	269.87	0.979	6.76E+18	O4	0.998
	KAS	272.57	0.977	1.87E+21	O4	0.998
	Friedman	278.53	0.980	2.46E+19	D3	0.994
<b>WT3PB1</b>	FWO	225.04	0.983	4.19E+13	D3	0.999
	KAS	225.65	0.981	8.67E+15	D3	0.998
	Friedman	239.68	0.981	5.22E+16	D3	0.998
<b>WT1PB1</b>	FWO	242.06	0.958	3.11E+17	O4	0.993
	KAS	243.76	0.954	7.72E+19	O4	0.994
	Friedman	251.89	0.956	1.17E+18	D3	0.988
<b>WT1PB3</b>	FWO	262.40	0.626	8.03E+19	O7	1.000
	KAS	265.33	0.621	3.78E+21	O4	0.999
	Friedman	297.54	0.624	1.11E+23	O3	0.998
<b>WT0PB1</b>	FWO	211.60	0.921	8.43E+16	O7	0.993
	KAS	212.13	0.912	1.84E+19	O7	0.993
	Friedman	213.05	0.885	3.09E+17	O3	0.957

According to Table 3.8, it is interesting that the average  $E_{\alpha}$  values of the blend samples were lower than those of the WT1PB0 sample. The blended sample with a WT to PB mass ratio of 3:1 showed the lowest values of average  $E_{\alpha}$  with a reduction of 13.95-17.21% relative to WT1PB0. Despite the discrepancy between the average  $E_{\alpha}$  values obtained using iso-conversional methods and those estimated using the CR method, the visual comparison shows that the results agree that blended samples require lower energy input than WT1PB0.

### 3.3.2.3 Master plot method for $f(\alpha)$

The possible reaction mechanisms underlying the decomposition of the WT and PB blended samples were initially evaluated using the master plot method.

To construct theoretical master plots, the kinetic model expressions provided in Table 3.1 were used to calculate the  $y(\alpha)$  function using Equation (3.14) in which each theoretical master plot is unique for a specific kinetic model. For each sample, a master plot of the experimental data is constructed separately at different heating rates. This was achieved by calculating the  $y(\alpha)$  function for each sample using Equation (3.15) while taking into account the average  $E_\alpha$  value determined by the iso-conversional FR method. Experimental  $y(\alpha)$  plots of the samples along with the theoretical plots of the possible reaction mechanisms are presented in Figure 3.16. Although it was difficult to identify the possible reaction mechanisms based on the comparison between the theoretical and experimental master plots, it can be seen that the decomposition reactions of the WT, PB and their blends either following power law, diffusional, high order reaction mechanism, or combination of them. As illustrated in Figure 3.16, it is apparent that pyrolysis of the WT, PB and their blends follow different reaction mechanisms over the  $\alpha$  range of 0.05 to 0.95. For the  $\alpha$  value between 0.05 and 0.45, all the samples could resemble the diffusional reaction model (i.e. D2, D3 and D4). However, the high-order reaction mechanism (i.e. O4) is the most possible to describe the decomposition of all the samples for the range  $0.45 \leq \alpha < 0.95$ . To better identify the underlying reaction mechanism, a combined kinetic analysis was performed and discussed.

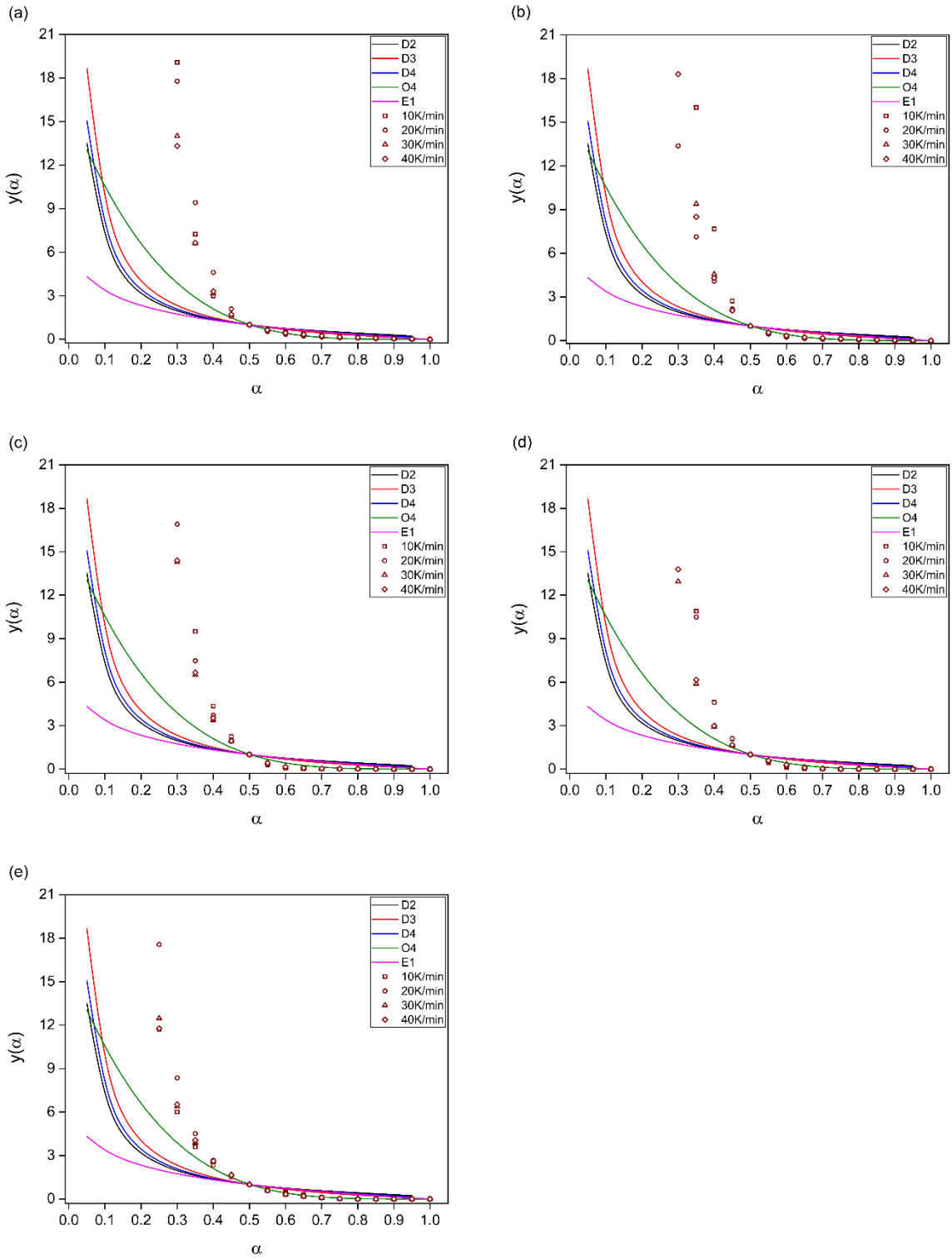


**Figure 3.16** Comparison of theoretical master plots and experimental data for (a) WT1PB0, (b) WT3PB1, (c) WT1PB1, (d) WT1PB3 and (e) WTOPB1 at different heating rates

#### 3.3.2.4 *Kinetic triplets through combined kinetic analysis*

To determine the kinetic triplets (i.e.  $E_a$ ,  $A$  and  $f(\alpha)$ ) through combined kinetic analysis, the experimental data of the main pyrolysis zone under different heating rates was fitted with  $SB$  empirical function shown in Equation (3.17) and the unknown parameters (i.e.  $m$ ,  $n$  and  $p$ ) were determined. The fitting results are displayed in Figure 3.17. The  $E_a$  and  $A$  of all the samples were calculated using the slope and the intercept of the linear fitting.

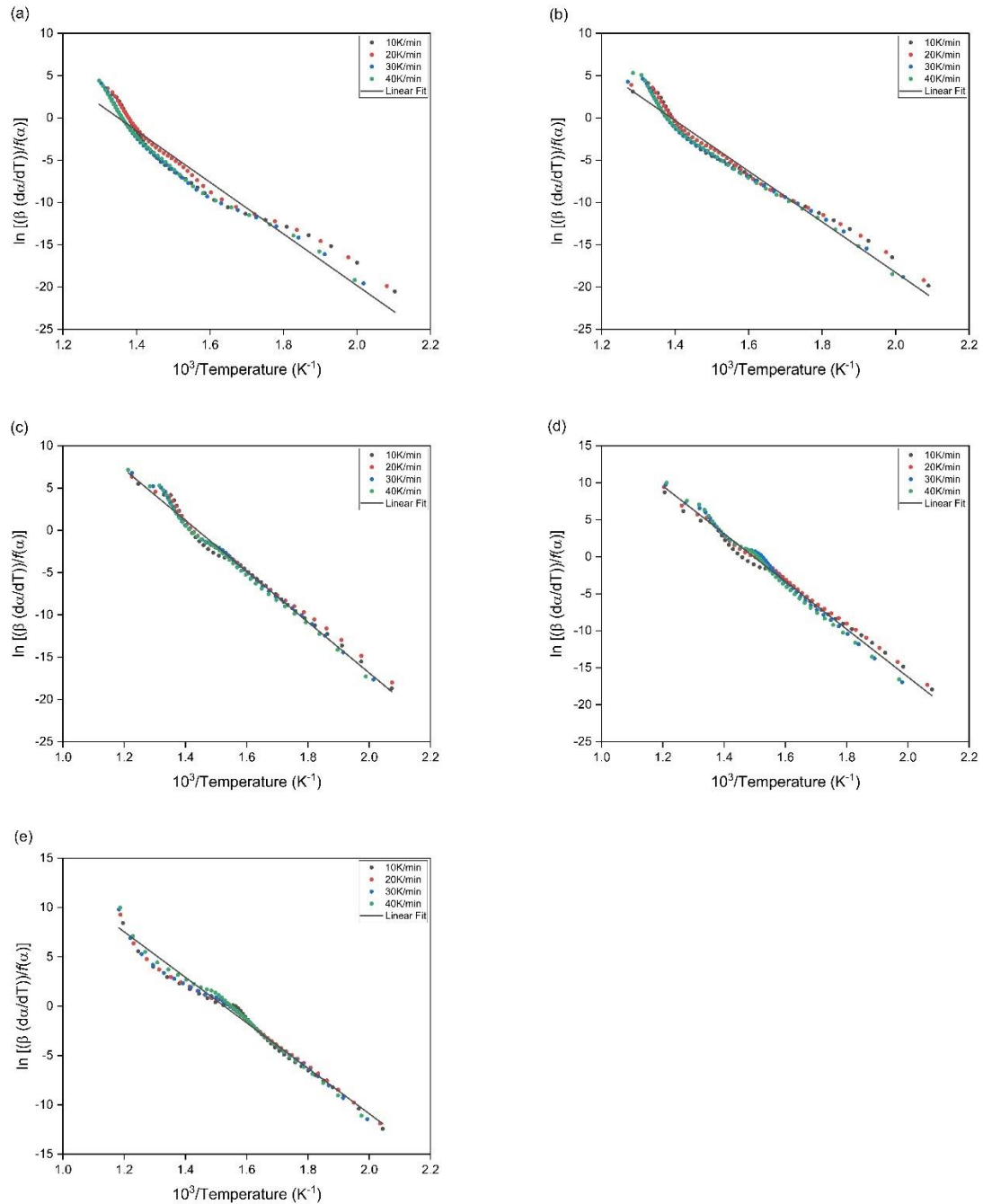


**Figure 3.17** Fitting results of combined kinetics analysis of (a) WT1PB0, (b) WT3PB1, (c) WT1PB1, (d) WT1PB3 and (e) WT0PB1

Figure 3.18 shows the experimental data and the fitted function of the *SB* model. The results of the kinetics parameter obtained by combined kinetic analysis are summarised in Table 3.9.

The co-pyrolysis process of the PB and WT at different blend ratios can be characterised by the *SB* model, as shown by a high  $R^2$  value (i.e. > 0.94) of the linear fitting. The parameters

$m$ ,  $n$  and  $p$  of the  $SB$  model are related to a power law, reaction order and nucleation reaction mechanism, respectively (Hidayat et al., 2021; Wang et al., 2016). It can be seen from Figure 3.18 and the results reported in Table 3.9 that the decomposition of the WT, PB and their blends comprise a combination of several reaction mechanisms including nucleation, diffusion, and power law in addition to reaction order. The decomposition of the waste tyre, pine bark and their blends follow 1-dimensional diffusion and power law reaction mechanisms as indicated by the negative as well as high values of the parameter  $m$  (Hidayat et al., 2021; Wang et al., 2016). Furthermore, the high values of parameter  $p$  suggest that the nucleation mechanism may have contributed to the decomposition of these samples. Based on previous studies, it has been suggested that waste tyre decomposes through a random bond scission model that involves free radicals formation, hydrogenation and recombination (Martínez et al., 2013; Perejón et al., 2021). This does not appear to be the case with combined kinetic analysis. According to Perejón et al. (2021), polymer degradation is significantly influenced by the diffusion of primary species released at lower operating temperatures.

Despite the combined kinetic analysis findings indicating that WT1PB0, WT3PB1 and WT1PB1 follow a first-order reaction model, the  $y(\alpha)$  profiles of the waste tyre, pine bark and their blends shown in Figure 3.18 look similar to the theoretical plot of high-order reaction model with  $n = 9$  for all the samples except WT0PB1 ( $n = 7$ ). This demonstrates the complexity of the decomposition reaction mechanism followed by these materials. There is a similarity between the shape of the normalized  $y(\alpha)$  of WT0PB1 in the current study and those reported by Wang et al. (2016) and Yeo et al. (2019) for lignin. This may be explained by lignin's heterogeneous composition and complex structure that is associated with the existence of aromatic benzene ring compounds (Wang et al., 2016). According to Díez et al.

(2020) and Phyllis database for biomass and waste (Phyllis2, 2023), PB is composed of 40 to 50 wt% of lignin. It is important to highlight that, several authors (Chen et al., 2019c; Gao et al., 2021; Likun and Zhang, 2020; Uzun and Yaman, 2014) assumed 1st order reaction model for the kinetics analysis. However, such an assumption may not be appropriate to describe the pyrolysis of the WT, PB and their blends.

In summary, the composition of the single feedstocks of the WT and PB has an impact on their thermal decomposition behaviour as well as their blends (Cherop et al., 2018). Because of the heterogeneity in the composition and the complexity of the structure of the WT and PB, the thermal degradation of these feedstocks and their blends follow a combined degradation mechanism.

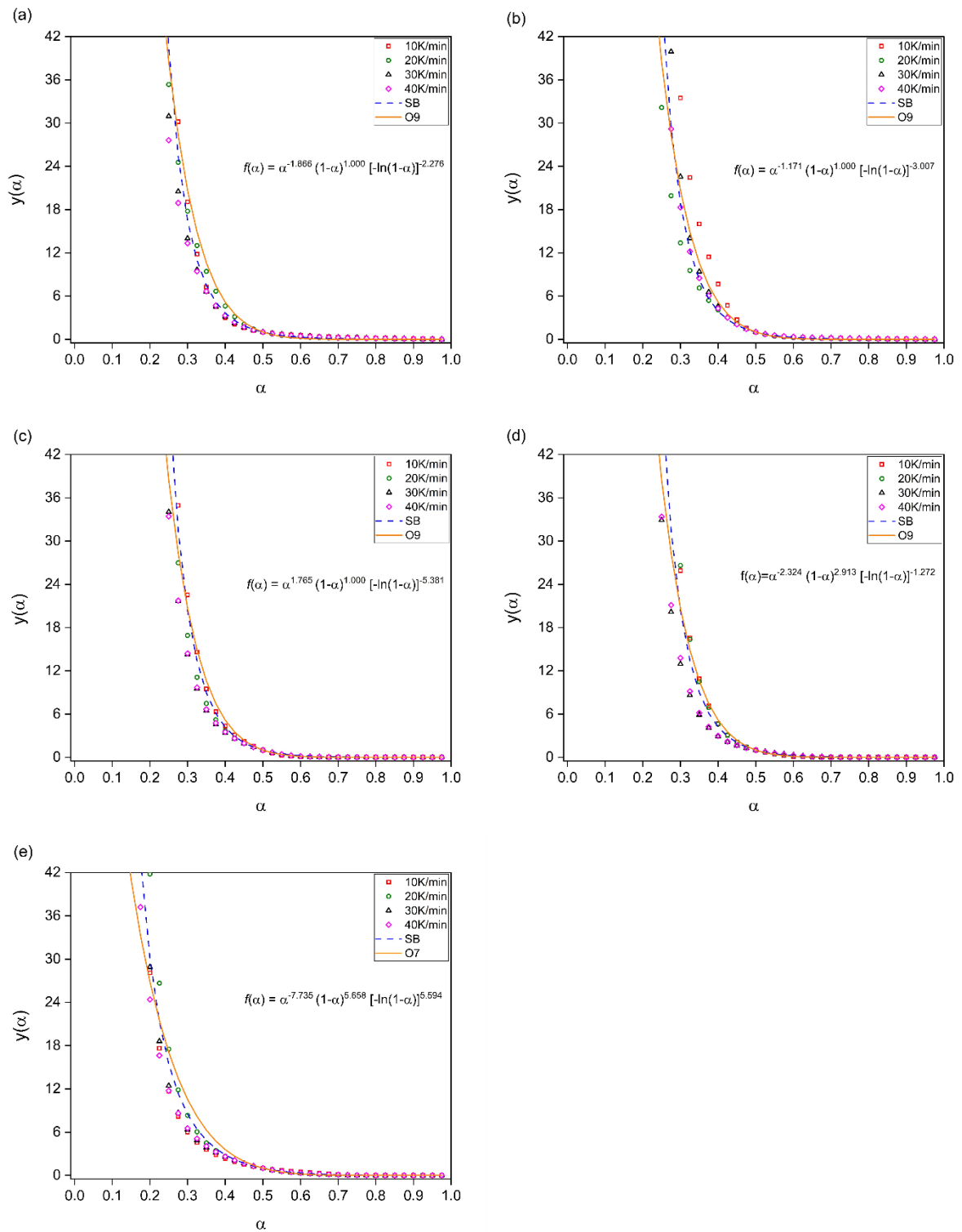


**Figure 3.18** Combined kinetics analysis for normalized reaction mechanism,  $y(\alpha)$  of (a) WT1PB0, (b) WT3PB1, (c) WT1PB1, (d) WT1PB3 and (e) WT0PB1

**Table 3.9** Values of optimum parameters, activation energy and pre-exponential factor for different blend samples obtained through combined kinetic analysis

Sample ID	$m$	$n$	$P$	$E_a$ (kJ/mol)	$A$ (min <sup>-1</sup> )	$R^2$
WT1PB0	-1.8660	1.0000	-2.2755	241.40	8.36E+17	0.942
WT3PB1	-1.1314	1.0000	-3.0069	232.62	4.59E+17	0.978
WT1PB1	1.7654	1.0000	-5.3813	236.45	7.68E+18	0.990
WT1PB3	-2.3241	2.9130	-1.2720	254.97	9.27E+20	0.990
WT0PB1	-7.7352	5.6576	5.5944	182.12	1.91E+15	0.985

### 3.3.2.5 Comparative evaluation of kinetics from different methods

A graphical comparison of the average  $E_a$  obtained using various kinetics analysis methods is shown in Figure 3.19. Since each of these methods used in the kinetic analysis is based on certain mathematical approximations (Das and Tiwari, 2017), the values of  $E_a$  predicted by these methods vary. Comparing the variation in  $E_a$  between the examined samples, it is worth noting that FWO and KAS revealed the least variation in  $E_a$  because they do not need an assumption of the reaction mechanism,  $f(\alpha)$ . However, the FR method contributes to the highest value of  $E_a$  among all the methods for all the samples. According to the literature (Wang et al., 2016), the FR method predicts the values of the  $E_a$  with better accuracy. Although the predicted  $E_a$  values showed a variation between different methods, the change in response to the difference in the WT to PB mass blend ratio looks similar, excluding the CR method. The  $E_a$  values acquired through a combined kinetics analysis approach are likely to be the most reliable ones. This is because this analysis approach takes into account both suitable reaction mechanisms and the utilisation of weight loss data from different heating rates (Hidayat et al., 2021; Wang et al., 2016; Yeo et al., 2019).

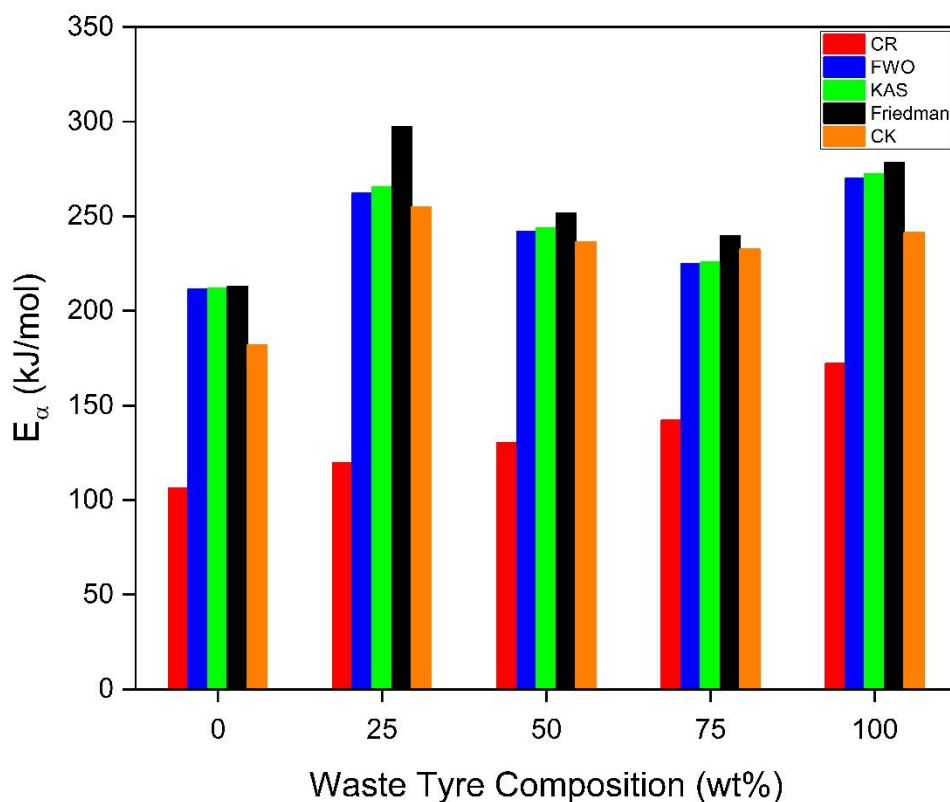


**Figure 3.19** Graphical comparison of average  $E_a$  values for different samples obtained using a model fitting (CR), integral model free (FWO and KAS), differential model free (FR) methods and combined kinetic analysis.

### 3.3.3 Kinetics of waste tyre, biomass and their blends: previous studies

A comparison of the average values of  $E_a$  of PB, WT and their blends with those of the other biomass, waste tyre and the blended samples reported in the literature is shown in Table 3.10. it can be figured out that the values of the  $E_a$  vary according to the type of biomass and waste tyre (i.e. composition and structure) as well as the kinetic analysis approach implemented. The  $E_a$  of biomass and waste tyre varies between 31.10 and 278.80 and 70.66 and 278.53 kJ/mol, respectively. Similarly, the mean  $E_a$  of PB, WT and their blends which were considered in the current study varied between 106.35 and 297.54 kJ/mol for different kinetics analysis methods.

**Table 3.10** A comparison of the activation energy values of the samples used in the current study and those available in the literature

Reference	Type of Material	Heating rate K/min	Average value of activation energy, $E_a$ , (kJ/mol)				
			Model-fitting	Iso-conversional			CK
			CR ( $n=1$ )	FWO	KAS	FR	
<b>(A) Biomss</b>							
Current study	Pine Bark	10, 30 and 40	106.35	211.60	212.13	212.88	182.12
Azizi et al. (2019)	Wood	10, 20 and 40	-	87.51	120.96	-	-
Azizi et al. (2019)	Microalgae	10, 20 and 40	-	153.09	219.04	-	-
Mishra and Mohanty (2018)	Pine sawdust	5, 10, 15, 20 and 25	-	179.29	171.66	168.58	-
Chen et al. (2019a)	Kitchen waste	10, 20 and 30	-	278.80	283.60	-	-
Uzun and Yaman (2014)	J. regia shell	20	89.78	-	-	-	-
Biagini et al. (2017)	Corn cobs	5, 10, 20 and 40	64.40	235.50	-	259.10	-
Biagini et al. (2017)	Rice husks	5, 10, 20 and 40	78.40	202.10	-	200.50	-
Biagini et al. (2017)	Vine prunings	5, 10, 20 and 40	73.40	228.70	-	250.20	-
Biagini et al. (2017)	Palm kernel shell	5, 10, 20 and 40	108.40	228.30	-	226.90	-
Chen et al. (2019b)	Tobacco stalk	20	31.10	-	-	-	-
Ding et al. (2016)	Beech wood	20, 40 and 60	-	165.18	163.25	-	-
Hidayat et al. (2021)	Hemicellulose	2.5, 5, 10, 17.5	-	-	-	198.12	194.71
Hidayat et al. (2021)	Cellulose	2.5, 5, 10, 17.5	-	-	-	181.14	179.97
Hidayat et al. (2021)	Lignin	2.5, 5, 10, 17.5	-	-	-	190.77	219.23
Slopiecka et al. (2012)	Poplar wood	2, 5, 10 and 15	-	158.58	157.27	-	-
Chandrasekaran et al. (2017)	Prosopis juliflora	2, 5, 10, 15, 20 and 25	-	203.20	204.00	219.30	-
Gao (2021)	off-shore oil sludge	15 (120-350 °C)	-	28.49	-	-	-
		15 (350-500 °C)	-	60.09	-	-	-
<b>(B) Waste Tyre</b>							

Current Study	Goodyear winter radial passenger car used tyre	10, 30 and 40	172.12	269.87	272.57	278.53	241.40
Azizi et al. (2019)	Scrap tyre	10, 20 and 40	-	189.68	273.64	-	-
Chen et al. (2019b)	Scrap tyre	20	70.66	-	-	-	-
Uzun and Yaman. (2014)	Scrap tyre	20	75.63	-	-	-	-
Chen et al. (2019a)	Waste tyre	10, 20 and 30	-	199.93	199.48	-	-
Tang et al. (2021)	Waste bicycle tyre rubber	10, 20 and 40	-	259.90	261.76	-	-
Chen et al. (2022)	Waste tyre	150, 300 and 600	-	90.82	88.42	97.29	-
Gao (2021)	side wall waste tire	15 (260-520 °C)	88.22	-	-	-	-
<b>(C) A blend of biomass and waste tyre</b>							
Current Study	Pine bark and waste tyre	10, 30 and 40	130.27	242.06	243.76	251.69	236.45
Chen et al. (2019b)	Tobacco stalk and waste tyre	20	36.21	-	-	-	-
Azizi, et al. (2019)	Microalgae and scrap tyre	10, 20 and 40	-	160.85	230.64	-	-
Azizi, et al. (2019)	Wood and scrap tyre	10, 20 and 40	-	136.72	196.86	-	-
Chen et al. (2019a)	Kitchen waste and waste tyre	10, 20 and 30	-	198.78	198.76	-	-
Gao (2021)	off-shore oil sludge and side wall waste tyre	15 (200-340 °C)	20.32	-	-	-	-
		15 (340-500 °C)	47.45	-	-	-	-
Cherop et al. (2018)	Eucalyptus sawdust and tyre crumb	2, 5, and 10	-	150.29	-	147.84	-

### 3.4 Conclusion

The thermal degradation behaviour and the kinetics underlying the co-pyrolysis of pine bark and waste tyre at different mass ratio were examined. This is to understand the existence of any synergetic interaction by comparing the mass loss rate and the kinetics between single feed and blended samples. According to the calculation of the difference in weight loss, positive synergetic interaction was observed between pine bark and waste tyre.

In general, comparing the predicted activation energy values of pine bark and waste tyre for various mass ratios, the blended samples showed lower values than that of a single waste tyre. For all kinetic analysis methods excluding CR, the lowest  $E_a$  was reported for the blended sample with a waste tyre to pine bark mass ratio of 3:1. This emphasizes the positive synergetic interaction that might occur between pine bark and waste tyre. Despite its limitations, the Coats-Redfern approach could be utilised as a visual evaluation tool to predict the potential variation in activation energy.

Pine bark, waste tyre and their blended samples exhibited complex degradation behaviour which was most likely the result of a reaction mechanism involving a combination effect of nucleation, growth, and diffusion. According to Sestak Berggren model the reaction mechanisms of WT1PB0, WT3PB1, WT1PB1, WT1PB3 and WT0PB1 are as follows:  $\alpha^{-1.866}(1 - \alpha)^{1.000}[-\ln(1 - \alpha)]^{-2.276}$ ,  $\alpha^{-1.171}(1 - \alpha)^{1.000}[-\ln(1 - \alpha)]^{-3.007}$ ,  $\alpha^{1.765}(1 - \alpha)^{1.000}[-\ln(1 - \alpha)]^{-5.381}$ ,  $\alpha^{-2.324}(1 - \alpha)^{2.913}[-\ln(1 - \alpha)]^{-1.272}$  and  $\alpha^{-7.735}(1 - \alpha)^{5.658}[-\ln(1 - \alpha)]^{5.594}$ , respectively.

Although waste tyre had higher activation energy than pine bark, both the waste tyre and pine bark demonstrated comparable reaction mechanisms. Therefore, they may be used in a blended form to develop a feed-flexible thermal processing unit with a lower requirement of energy input than a sole waste tyre.

## CHAPTER 4      Co-gasification of pine bark and waste tyre using CO<sub>2</sub> through process modelling and simulation

In this chapter, a model for the co-gasification process was developed using Aspen Plus® to simulate the gasification of biomass and waste tyre. The performance of the developed model is investigated through process analysis. *Section 4.1* provided detailed model development procedures. In *Section 4.2*, the validation of the developed model is introduced and the results are presented. In *Section 4.3*, the indices used to evaluate the performance of the developed model are defined. In addition, the process analysis is carried out with a focus on the effect of changing operating conditions, namely; gasification temperature, CO<sub>2</sub>-to-feed ratio, and feed flow rate.

### 4.1      Model development

#### 4.1.1      Overview of experimental study

In this study, a co-gasification process of biomass and waste tyre was simulated using Aspen Plus® according to the experimental study conducted by Wang et al. (2019b). This is to evaluate the presence of synergetic interaction and its effect on syngas composition and process performance. Wang et al. (2019b) studied the co-gasification process of the pine bark and waste tyre blends using CO<sub>2</sub> only as a gasifying medium. Pine bark sourced locally and dried at 105 °C for 24 hr. Waste tyre sample was steel free and composed of tread and sidewall parts. It was cut into particles with a size of nearly 1.5 × 1.5 cm.

The experimental facility that is used in their study consists of a pre-heating section, a semi-batch fixed-bed reactor and a gas analyser as presented in Figure 4.1. Pine bark and waste tyre with different mass ratios and a total weight of 35 g per batch were loaded in the reactor once the reactor reached the specified operating temperature. Each experimental run is

operated for 47 min. The product gas was analysed using micro-gas chromatography to obtain the fractions of different gas components. The char sample was extracted from the reactor bed and its weight is determined at the end of each experimental run. Table 4.1 summarises the experimental operating conditions that will be used for the development of the current model in Aspen Plus®.

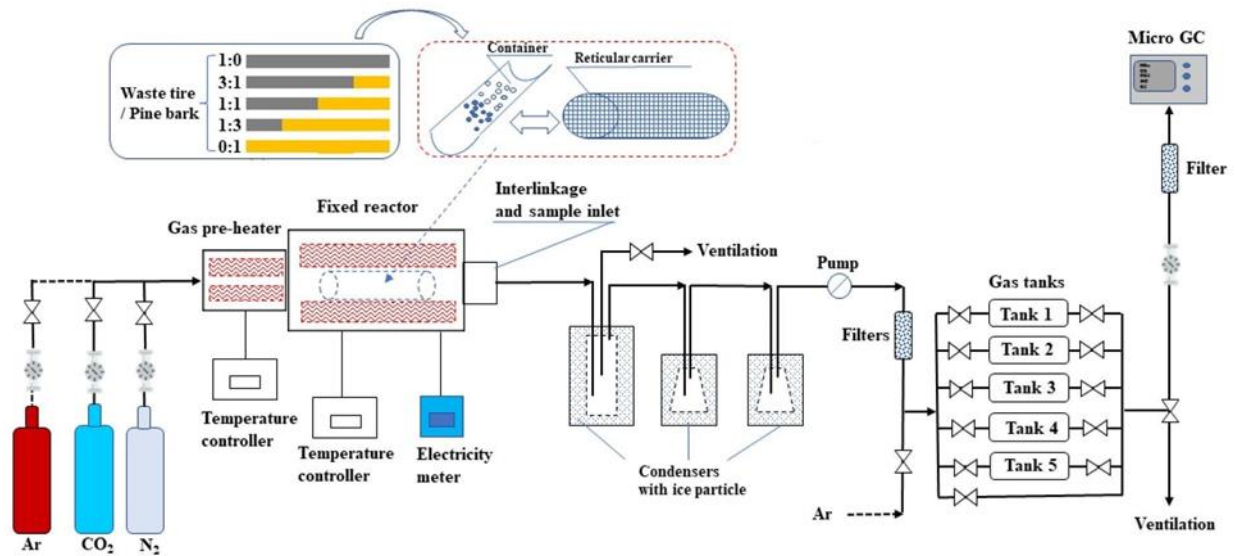


**Figure 4.1** Schematic diagram of CO<sub>2</sub> co-gasification experimental facility of pine bark and waste tyre (Wang et al., 2019b)

**Table 4.1** Summary of the experimental study-related parameters used in the model development (Wang et al., 2019b)

Parameters		Values
Reactor dimension	Length	45.70 cm
	Inner Diameter	5.00 cm
Bed material		Silica sand
Catalyst		None
Feedstock feeding rate		0.045 kg/hr
Reactor operating temperature and pressure ( $\pm 0.2\%$ )		1173 $\pm$ 2.346 K and 1 atm
N <sub>2</sub> flow rate ( $\pm 2.3\%$ )		0.525 $\pm$ 0.012 slpm (293 K and 1 atm)
CO <sub>2</sub> flow rate ( $\pm 2.8\%$ )		1.575 $\pm$ 0.044 slpm (293 K and 1 atm)

#### 4.1.2 Assumptions

The following assumptions are made for the development of the co-gasification model of biomass (i.e. pine bark) and waste tyre;

- a. The process operates at steady-state and the reactors operate under isothermal conditions (Kaushal and Tyagi, 2017)
- b. The process is operated under atmospheric pressure.
- c. Feedstocks are composed of uniformly-sized particles (Kaushal and Tyagi, 2017), so the effect of heat transfer is neglected.
- d. Char is assumed to compose of carbon.
- e. Ash is assumed to be inert. So, its catalytic effect on feedstock degradation is neglected.
- f. Main products are  $H_2$ ,  $CO$ ,  $CO_2$ ,  $CH_4$ ,  $C_2H_4$ ,  $C_6H_6$ ,  $C_7H_8$ ,  $C_6H_6O$ ,  $C_{10}H_8$  and  $H_2O$
- g. Tar formation and cracking kinetics are implemented. Tar is assumed to be mainly benzene, naphthalene, toluene and phenol, representing different classes and following the temperature at which they form (Aghaalikhani et al., 2019).
- h. Both devolatilization and gasification occur simultaneously.

#### 4.1.3 Model development in ASPEN Plus®

Process simulation of co-gasification can provide qualitative guidance on the performance of the process when the operating conditions are changed (Banerjee et al., 2015). ASPEN Plus® is a problem-oriented approach to process simulation which is based on mass and energy balance calculations and a phase equilibrium database to model various processes involving solid, liquid and gaseous streams under specified conditions (Kaushal and Tyagi, 2017).

The developed semi-detailed kinetic model of the WT and PB co-gasification consists of three major units: (i) devolatilization of the feedstocks into gas, char and tar species; (ii) secondary gas phase reactions of the released gas and tar species and (iii) char gasification and combustion. The process flowsheet is shown in Figure 4.2. Kinetic model parameters were

obtained from the literature and adjusted to find the best values that fit the experimental data with the simulation results.

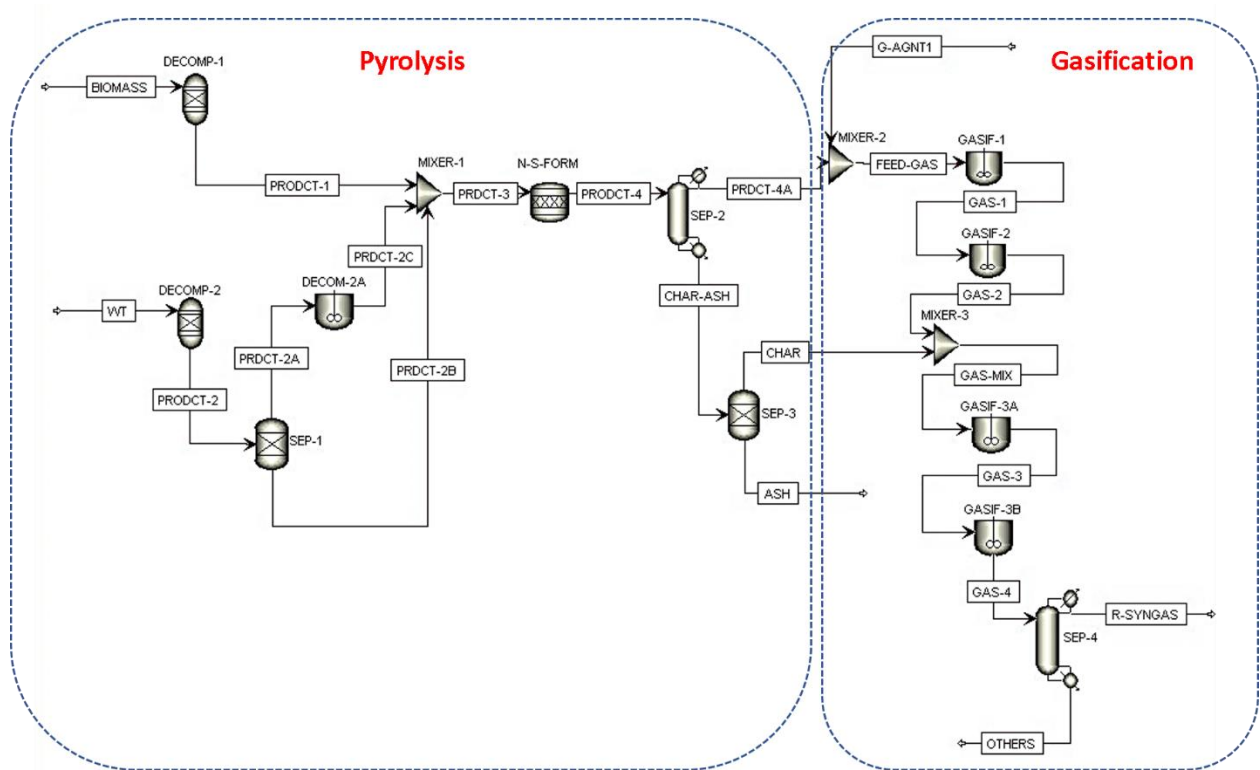


**Figure 4.2** Process flowsheet developed in Aspen Plus®

#### 4.1.3.1 Input components and physical property method

The input streams of pine bark and waste tyre are introduced in the Aspen Plus® model as non-conventional solids. They were specified with their proximate and ultimate analysis as given in Tables 3.2 and 3.3 in Chapter 3. The thermodynamics and other properties of the non-conventional solids including lower heating value, density, the enthalpy of formation, etc. are calculated using **HCOALGEN** and **DCOALIGT** models which in turn use the proximate analysis, ultimate analysis and Sulphur analysis (Gagliano et al., 2017).

For the physical property calculation, Peng Robinson equation of state with the Boston-Mathias alpha function (PR-BM) method is chosen. This is because the PR-BM method is one of the widely used and recommended for the estimation of the thermodynamic properties

related to the processes of gas processing, oil refining, and petrochemical industry (Pala et al., 2017). In addition, it is capable of providing reliable results over wider temperature and pressure ranges. This makes it suitable for the gasification process at high temperatures (Puig-Gamero et al., 2018).

#### 4.1.3.2 Pyrolysis stage

The devolatilization step of PB and the WT was modelled separately for each sample. For the devolatilization of biomass, empirical correlations available in the literature (Neves et al., 2011; Pauls et al., 2016) are written in FORTRAN code to calculate the yield of gas components, char and tar as provided in Table 4.2. The ' $T$ ' in the expressions refer to the temperature in °C. Based on the calculation of C, H and O content of char (on mass basis) from PB devolatilization, it was found that more than 90% of its composition is C. Therefore, it is assumed to compose of C. In contrast, the waste tyre is converted first to its elemental components including carbon, O<sub>2</sub>, N<sub>2</sub>, H<sub>2</sub>, Sulphur and ash according to its ultimate analysis in RYIELD (i.e. **DECOMP-2**) reactor. Then, a fraction of char in the form of carbon is separated from the other components through the SEP-1 block. The formation of the main devolatilization products of the waste tyre including CO, CO<sub>2</sub>, CH<sub>4</sub>, C<sub>2</sub>H<sub>4</sub>, C<sub>6</sub>H<sub>6</sub>, C<sub>7</sub>H<sub>8</sub>, C<sub>6</sub>H<sub>6</sub>O and C<sub>10</sub>H<sub>8</sub> is simulated in RCSTR (i.e. **DECOM-2A**) block through the implementation of reaction kinetics obtained from Ismail et al. (2017) and are summarised in Table 4.3.

**Table 4.2** Empirical expressions for the calculation of biomass devolatilization products (Neves et al., 2011; Pauls et al., 2016)

Empirical expression	Product stream
$m_{H_2} = (8.72 \times 10^{-8}) * T^2 - (0.00007 * T) + 0.0135$	Fraction of H <sub>2</sub> in the gas stream
$m_{CH_4} = (3.75 \times 10^{-7}) * T^2 - (0.0004 * T) + 0.1414$	Fraction of CH <sub>4</sub> in the gas stream
$m_{CO} = (2.55 \times 10^{-6}) * T^2 - (0.0025 * T) + 0.8247$	Fraction of CO in the gas stream
$m_{CO_2} = (-1.84 \times 10^{-6}) * T^2 + (0.0013 * T) + 0.5284$	Fraction of CO <sub>2</sub> in the gas stream

$m_{C_2H_4} = (-1.17 \times 10^{-6}) * T^2 - (0.0016 * T) - 0.4512$	Fraction of C <sub>2</sub> H <sub>4</sub> in the gas stream
$m_{C,TAR} = (1.05 + (1.9 \times 10^{-4} * T)) * m_{C,feed}$	Mass fraction of C in the tar
$m_{H,TAR} = (0.93 + (3.8 \times 10^{-4} * T)) * m_{H,feed}$	Mass fraction of H in the tar
$m_{O,TAR} = (0.92 - (2.2 \times 10^{-4} * T)) * m_{O,feed}$	Mass fraction of O in the tar
$m_{C,CHAR} = 0.93 - (0.92 * \exp(-(0.42 \times 10^{-2} * T)))$	Mass fraction of C in the char
$m_{H,CHAR} = (-0.41 \times 10^{-2}) + (0.1 * \exp(-(0.24 \times 10^{-2} * T)))$	Mass fraction of H in the char
$m_{O,CHAR} = 0.07 + (0.85 * \exp(-(0.48 \times 10^{-2} * T)))$	Mass fraction of O in the char

**Table 4.3** Kinetic data for the simulation of waste tyre devolatilization (Ismail et al., 2017)

Sl. No	Reaction	Pre-exponential Factor, $sec^{-1}$	Activation Energy, $kJ/mol$	Driving Force
1	$C + 2H_2 \rightarrow CH_4$	4.877	23.01	$C_C^n, n = 1$ $C_{H_2}^n, n = 1$
2	$2C + 2H_2 \rightarrow C_2H_4$	2.386	23.01	$C_C^n, n = 1$ $C_{H_2}^n, n = 1$
3	$C + O_2 \rightarrow CO_2$	0.226	23.01	$C_C^n, n = 1$ $C_{O_2}^n, n = 1$
4	$C + \frac{1}{2}O_2 \rightarrow CO$	0.096	23.01	$C_C^n, n = 1$ $C_{O_2}^n, n = 1$
5	$6C + 3H_2 \rightarrow C_6H_6$	1.654	33.89	$C_C^n, n = 1$ $C_{H_2}^n, n = 1$
6	$7C + 4H_2 \rightarrow C_7H_8$	7.305	33.89	$C_C^n, n = 1$ $C_{H_2}^n, n = 1$
7	$6C + 3H_2 + \frac{1}{2}O_2 \rightarrow C_6H_6O$	0.497	33.89	$C_C^n, n = 1$ $C_{H_2}^n, n = 1$
8	$10C + 4H_2 \rightarrow C_{10}H_8$	0.979	33.89	$C_C^n, n = 1$ $C_{H_2}^n, n = 1$
9	$7C + 2.5H_2 + \frac{1}{2}N_2 + 2S \rightarrow C_7H_5NS_2$	1.2	33.89	$C_C^n, n = 1$ $C_{H_2}^n, n = 1$

#### 4.1.3.3 Gasification stage

The gasification stage is simulated using four model blocks of RCSTR reactors. The first block (i.e. **GASIF-1**) is used to simulate the tar and hydrocarbon cracking reactions (i.e. **R1-R4**) in which the required reaction kinetics are obtained from (Abu El-Rub et al., 2008; Gerun et al.,

2008; Umeki et al., 2010). The second block of the RCSTR reactor (i.e. **GASIF-2**) is used to simulate tar and hydrocarbon reforming reactions. The last two RCSTR reactors (i.e. **GASIF-3A** and **GASIF-3B**) are used to simulate homogeneous gas phase reactions and char gasification reactions, respectively. The WGS, steam and dry reforming, and RWGS reactions are considered to represent homogeneous gas phase reactions. Reactions and the related kinetics are presented in Table 4.4.

**Table 4.4** The reactions and their kinetics used to simulate the gasification stage.

Sl. No	Reaction Expression	Kinetic Expression	Reference
<b>A. Tar and hydrocarbon cracking reactions</b>			
<b>R1</b>	$C_3H_6O_2 \rightarrow \frac{1}{2}C_6H_6O + 1.5H_2O$	$r_1 = 1.0 \times 10^4 \exp\left(-\frac{136}{RT}\right) [C_3H_6O_2]^{1.0}$	Umeki et al. (2010)
<b>R2</b>	$C_6H_6O \rightarrow CO + 0.4C_{10}H_8 + 0.15C_6H_6 + 0.1CH_4 + 0.75H_2$	$r_2 = 1.0 \times 10^7 \exp\left(-\frac{100}{RT}\right) [C_6H_6O]^{1.0}$	Gerun et al. (2008)
<b>R3</b>	$C_{10}H_8 \rightarrow 7.38C + 0.275C_6H_6 + 0.97CH_4 + 1.235H_2$	$r_3 = 1.10 \times 10^4 \exp\left(-\frac{61}{RT}\right) [C_{10}H_8]^{1.0}$	Abu El-Rub et al. (2008)
<b>R4</b>	$C_2H_4 \rightarrow \frac{1}{3}C_6H_6 + H_2$	$r_4 = 2.0 \times 10^6 \exp\left(-\frac{283}{RT}\right) [C_2H_4]^{1.0}$	Umeki et al. (2010)
<b>B. Tar and hydrocarbon reforming reactions</b>			
<b>R5</b>	$C_2H_4 + 2H_2O \rightarrow 2CO + 4H_2$	$r_5 = 3100.5 \exp\left(-\frac{124.7}{RT}\right) [C_2H_4]^{1.0} [H_2O]^{2.0}$	Umeki et al. (2010)
<b>R6</b>	$C_6H_6 + H_2O \rightarrow 3C + 2CH_4 + CO$	$r_6 = 4.00 \times 10^{16} \exp\left(-\frac{443}{RT}\right) [C_6H_6]^{1.3} [H_2O]^{0.2}$	Jess (1996)
<b>R7</b>	$C_6H_6O + 3H_2O \rightarrow \frac{1}{2}C + 2.95CH_4 + 2CO + CO_2 + 0.1H_2$	$r_7 = 1.0 \times 10^7 \exp\left(-\frac{100}{RT}\right) [C_6H_6O]^{1.0}$	Rafati et al. (2015)
<b>R8</b>	$C_7H_8 + H_2 \rightarrow C_6H_6 + CH_4$	$r_8 = 1.04 \times 10^{12} \exp\left(-\frac{247}{RT}\right) [C_7H_8]^{1.0} [H_2]^{0.5}$	Jess (1996)
<b>C. Homogeneous gas-phase reactions</b>			
<b>R9</b>	$CH_4 + 1.5O_2 \rightarrow CO + 2H_2O$	$r_9 = 4.4 \times 10^{11} \exp\left(-\frac{125.52}{RT}\right) [CH_4]^{0.5} [O_2]^{1.25}$	Gerun et al. (2008)
<b>R10</b>	$CO + H_2O \leftrightarrow CO_2 + H_2$	$r_{10} = 1389 \exp\left(-\frac{12.56}{RT}\right) [CO]^{1.0} [H_2O]^{1.0}$	Gerun et al. (2008)

<b>R11</b>	$CH_4 + H_2O \leftrightarrow 3H_2 + CO$	$r_{11} = 1.65 \times 10^{11} \exp\left(-\frac{329}{RT}\right) [CH_4]^{1.7} [H_2O]^{-0.8}$	Gerun et al. (2008)
<b>R12</b>	$CH_4 + CO_2 \rightarrow 2H_2 + 2CO$	$r_{12} = 0.66 \exp\left(-\frac{91.5}{RT}\right) P_{CH_4}^{0.5} P_{CO_2}^{0.2}$	Pinto et al. (2002)
<b>R13</b>	$CO_2 + H_2 \leftrightarrow CO + H_2O$	$r_{13} = 7.55 \times 10^{12} \exp\left(-\frac{192}{RT}\right) [CO_2]^{1.0} [H_2]^{1.0}$	Rafati et al. (2015)
<b>D. Char gasification reactions</b>			
<b>R14</b>	$C + CO_2 \rightarrow 2CO$	$r_{14} = 1.12 \times 10^8 \exp\left(-\frac{245}{RT}\right) P_{CO_2}^{0.31}$	Umeki et al. (2010)
<b>R15</b>	$C + H_2O \leftrightarrow CO + H_2$	$r_{15} = 2.07 \times 10^7 \exp\left(-\frac{220}{RT}\right) P_{H_2O}^{0.73}$	Umeki et al. (2010)
<b>R16</b>	$C + H_2 \leftrightarrow CH_4$	$r_{16} = 16.4 \exp\left(-\frac{94.8}{RT}\right) P_{H_2}^{0.93}$	Hejazi et al. (2017)

Specifications of the main blocks used to model the devolatilization and gasification stages are summarised in Table 4.5.

**Table 4.5** Main model blocks and their corresponding use in the model development

Name of the unit	Type of the block	Utilisation in model development
<b>DECOMP-1</b>	RYield block	for the conversion of non-conventional biomass ( <b>BIOMASS</b> ) into main pyrolysis products ( <b>PRODCT-1</b> ) using empirical correlations
<b>DECOMP-2</b>	RYield block	for the conversion of the non-conventional waste tyre ( <b>WT</b> ) into its constituent elements ( <b>PRODCT-2</b> ) based on ultimate analysis.
<b>DECOM-2A</b>	RCSTR block	to simulate the conversion of elements composing the waste tyre ( <b>PRODCT-2</b> ) into main pyrolysis products ( <b>PRDCT-2C</b> ) using reaction kinetics
<b>SEP-1</b>	A separator block	for the separation of a fraction of carbon ( <b>PRDCT-2B</b> ) assuming not all carbons are converted into volatiles ( <b>PRDCT-2A</b> ).
<b>MIXER-1</b>	A mixer block	for mixing volatiles (i.e. gas and tar) and char from the devolatilization stage of both biomass ( <b>PRODCT-1</b> ) and waste tyre ( <b>PRDCT-2B</b> and <b>PRDCT-2C</b> )
<b>N-S-FORM</b>	Rstoic block	to simulate the formation of nitrogen and sulfur-based compounds ( <b>PRODCT-4</b> ) using reactions stoichiometry
<b>SEP-2</b>	A separator block	for the separation of volatiles ( <b>PRDCT-4A</b> ) from the solid products ( <b>CHAR-ASH</b> )
<b>SEP-3</b>	A separator block	for the separation of char ( <b>CHAR</b> ) from ash ( <b>ASH</b> )
<b>MIXER-2</b>	A mixer block	for mixing volatiles from the complete devolatilization stage ( <b>PRDCT-4A</b> ) with the gasifying agent ( <b>G-AGNT1</b> )

<b>GASIF-1</b>	RCSTR block	used to simulate tar and hydrocarbon cracking reactions
<b>GASIF-2</b>	RCSTR block	used to simulate Tar and hydrocarbon reforming and combustion reactions
<b>GASIF-3A</b>	RCSTR block	used to simulate gas-phase homogeneous reactions
<b>GASIF-3B</b>	RCSTR block	used to simulate char gasification reactions
<b>SEP-4</b>	A separator block	to separate the syngas ( <b>R-SYNGAS</b> ) from the remaining components ( <b>OTHERS</b> ) including remaining tar, char, H <sub>2</sub> O, etc.

## 4.2 Model validation

Experimental data from Wang et al. (2019b) was used to validate the performance of the developed model. Model validation was performed by comparing the model predictions for syngas composition in terms of H<sub>2</sub>, CO and CO<sub>2</sub> against the experimental data for the different waste tyre to pine bark weight ratios at a fixed temperature of 1173 K. The accuracy of the model is evaluated in terms of the percentage of relative errors (i.e. *RE*), which are calculated as follows:

$$RE (\%) = \frac{\text{Experimental value} - \text{Predicted value}}{\text{Experimental value}} \times 100 \quad (4.1)$$

As shown in Table 4.6 and Figure 4.3, the *RE* values for all the syngas components at different feedstock compositions are less than 10.00%. This will confirm that the model is reliable for further process analysis and predictions of co-gasification process performance as well as product yields.

Comparing the *RE* values of different gas components for different feedstocks, the lowest value was reported for CO<sub>2</sub> followed by H<sub>2</sub> for all the samples except the single WT, where the lowest value was for CO<sub>2</sub> followed by CO. This could be contributed to the implementation of literature-based reaction kinetics in developing the model. However, the accuracy of the model is validated.

**Table 4.6** Results of model validation at different feedstock composition

Waste Tyre Content in Blend (wt%)	Syngas Composition (vol%)			RE (%)
	Component	Experimental <sup>11</sup> ( $\pm 0.1\%$ )	Model Prediction <sup>12</sup>	
100	H <sub>2</sub>	5.53	5.45	1.41
	CO	8.14	8.13	0.13
	CO <sub>2</sub>	86.33	86.42	-0.10
75	H <sub>2</sub>	5.42	5.65	-4.31
	CO	12.59	13.30	-5.71
	CO <sub>2</sub>	82.00	81.05	1.16
50	H <sub>2</sub>	5.83	5.86	-0.56
	CO	17.04	17.34	-1.81
	CO <sub>2</sub>	77.14	76.80	0.44
25	H <sub>2</sub>	5.72	5.98	-4.51
	CO	21.74	22.76	-4.71
	CO <sub>2</sub>	72.54	71.26	1.77
0	H <sub>2</sub>	5.77	6.20	-7.46
	CO	25.82	27.95	-8.26
	CO <sub>2</sub>	68.41	65.84	3.75

<sup>11</sup> Sourced from Wang et al. (2019b)<sup>12</sup> Results obtained from the current model.

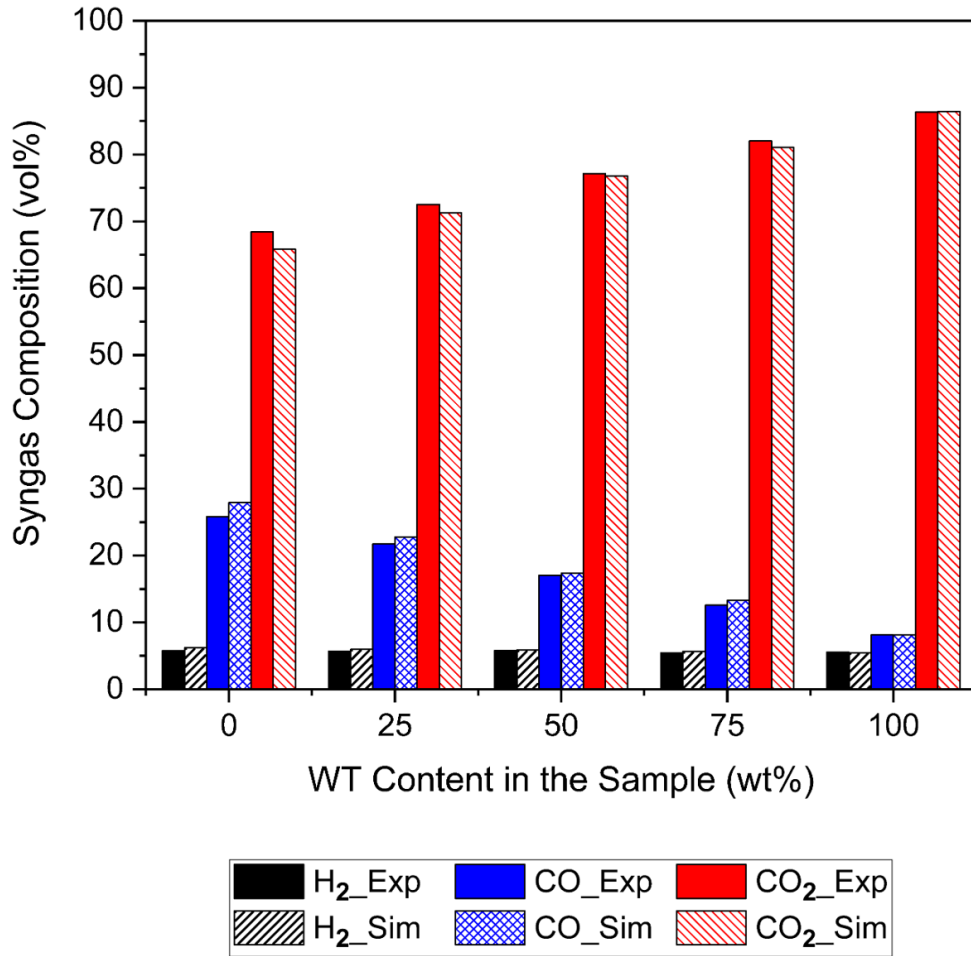


**Figure 4.3** Comparison of syngas composition between experimental and model prediction at different feedstock compositions

#### 4.3 Process analysis

##### 4.3.1 Performance evaluation indices

The performance of the co-gasification model of pine bark and waste tyre is evaluated based on the following indices:

##### a. Syngas composition and yield

Syngas composition and yield are the model predicted syngas (i.e. **R-SYNGAS**) content in terms of vol% and molar flow rate (mol/hr) of H<sub>2</sub>, CO and CO<sub>2</sub>.

##### b. H<sub>2</sub>/CO and CO/CO<sub>2</sub> ratios

The hydrogen to carbon monoxide (i.e. H<sub>2</sub>/CO) and carbon monoxide to carbon dioxide (i.e. CO/CO<sub>2</sub>) molar ratios are important parameters to identify the suitability of the syngas for

further applications including fuels and chemical synthesis (Ephraim et al., 2016). Both ratios are defined as Equations (4.2) and (4.3), respectively.

$$H_2/CO \text{ molar ratio} = \frac{\% \text{ mol of hydrogen}}{\% \text{ mol of carbon monoxide}} \quad (4.2)$$

$$CO/CO_2 \text{ molar ratio} = \frac{\% \text{ mol of carbon monoxide}}{\% \text{ mol of carbon dioxide}} \quad (4.3)$$

c. Lower heating value (i.e. LHV) of the syngas

The lower heating value (LHV) is a measure of the heat released through the combustion of a specified quantity of any fuel without considering the latent heat of vaporization of the moisture. The LHV of the syngas is a crucial parameter that must be taken into consideration to understand how efficient the gasification process is. It can be obtained using Equation (4.4) (Fajimi et al., 2021).

$$LHV_g \text{ (MJ/Nm}^3\text{)} = 10.789y_{H_2} + 12.625y_{CO} + 35.818y_{CH_4} \quad (4.4)$$

Where the numeric values and  $y_i$  represent the LHV<sub>s</sub> and the mole fraction of the corresponding syngas components,  $i$ . In our case, only H<sub>2</sub>, CO and CH<sub>4</sub> are considered in the calculation.

d. Cold gas efficiency (i.e. CGE) in terms of LHV

It is defined as the ratio between energy output from the process associated with the syngas and energy input as part of the feedstocks (Chatrattanawet et al., 2019), which are WT and PB in our case. The energy output and energy input are defined as LHV<sub>s</sub> of syngas and feedstock, respectively. It is expressed as Equation (4.5) (Fajimi et al., 2021; Zheng et al., 2018)

$$CGE \text{ (\%)} = \left[ \text{Syngas yield (Nm}^3\text{/kg feed)} \times \frac{LHV_g \text{ (MJ/Nm}^3\text{)}}{(w_{i1} \times LHV_{f1}) + (w_{i2} \times LHV_{f2})} \right] \times 100 \quad (4.5)$$

where;

$LHV_{f1}$  and  $LHV_{f2}$  are LHVs of feed 1 and 2, respectively, in MJ/kg,

$w_{i1}$  and  $w_{i2}$  are weight fractions of feed 1 and 2, respectively, in the sample.

Syngas yield is defined as the volumetric flow rate of syngas (i.e. **R-SYNGAS**) produced through the co-gasification process per feed flow rate and expressed as in Equation (4.6).

$$\text{Syngas yield (Nm}^3\text{/kg of feed)} = \frac{V_g}{m_f} \quad (4.6)$$

where  $V_g$  is the volumetric flow rate of syngas in Nm<sup>3</sup>/hr and  $m_f$  is the mass flow rate of feed in kg/hr.

#### 4.3.2 Plan of process analysis

Using the validated model, detailed analysis in terms of the effect of gasification temperature, CO<sub>2</sub>-to-feed ratio and feed flow rate on the syngas composition and quality as well as process performance is carried out. The plan for the process analysis is provided in Table 4.7.

**Table 4.7** Plan of process analysis

Case ID	Variables		
	Gasification temperature (K)	CO <sub>2</sub> -to-feed-ratio (Mass basis)	Feed flow rate (kg/hr)
Section 4.3.3	973-1273	3.90	0.045
Section 4.3.4	1173	0.20-5.00	0.045
Section 4.3.5	1173	3.90	0.02-2.00

#### 4.3.3 Effect of temperature

*Justification for case study:* Syngas quantity and quality are highly influenced by the operating temperature due to its effect on the reactions involved including tar cracking reactions as well as homogeneous and heterogeneous gasification reactions. In addition, CO<sub>2</sub>-induced reactions are endothermic. Therefore, it is important to understand how the change in the

gasification temperature will affect both syngas yield and composition as well as the process performance during CO<sub>2</sub> gasification.

*Setup of the case study:* To do this, the gasification temperature of the four RCSTR blocks (**GASIF-1**, **GASIF-2**, **GASIF-3A** and **GASIF-3B**) was varied simultaneously from 973 to 1273 K with an increment of 25 K using the *case study* option in model analysis tools. This temperature range was selected to cover the temperature at which the model was validated and considering the endothermicity of CO<sub>2</sub>-based reactions. Other operating parameters were kept the same as shown in Tables 4.1 and 4.7.

*Results and discussion:* Syngas composition and yield

The effect of gasification temperature on syngas composition and yield for different blend samples is shown in Figure 4.4. As the temperature increases, the H<sub>2</sub> content and yield increase at low temperatures (< 1173 K) and then start to slightly decrease for all the samples except WTOPB1. This could be contributed to the net effect of the reactions responsible for H<sub>2</sub> production and consumption including, WG (i.e. **R15**), RWGS (i.e. **R13**) and DR (i.e. **R12**) reactions (Renganathan et al., 2012). Both high gasification temperature and the presence of CO<sub>2</sub> enhance the RWGS reaction causing a decrease in H<sub>2</sub> content (Shen et al., 2019). However, the continuous increase in the H<sub>2</sub> composition and yield for WTOPB1 could be due to enhanced cracking and dry reforming reactions of the hydrocarbons at higher temperature (Liu et al., 2018b) which offset the decrease in H<sub>2</sub> due to RWGS reaction. This was observed by Sieradzka et al. (2022) during CO<sub>2</sub> gasification of pine sawdust. Meanwhile, there was a positive effect from the increase in temperature on CO content and yield, showing a sharper increase at higher temperatures than the lower ones (< 1173 K). The continuous increase in CO production is governed by the CO<sub>2</sub> DR reactions (Shen et al., 2019), BD and RWGS reactions

which consequently cause a decrease in CO<sub>2</sub> content and yield as shown in Figures 4.4 (c) and (f). Increased yield of H<sub>2</sub> and CO and the decrease in CO<sub>2</sub> with temperature is also been reported in the experimental study of CO<sub>2</sub> gasification of pine wood chips in a fluidized bed reactor by Sadhwani et al. (2016) and as part of numerical modelling of CO<sub>2</sub> gasification by Renganathan et al. (2012).

Comparing the results shown in Figure 4.4 (a) to (f) and regardless of the type of the blended samples, it can be concluded that the gasification temperature had a predominant effect on CO production compared to other syngas constituents. The CO content and yield rose from 3.06-10.73 vol% and 0.13-0.51 mol/hr at 973 K to 28.91-53.64 vol% and 1.45-3.46 mol/hr at 1273 K, respectively. Therefore, high gasification temperature is suggested to produce CO-rich syngas.

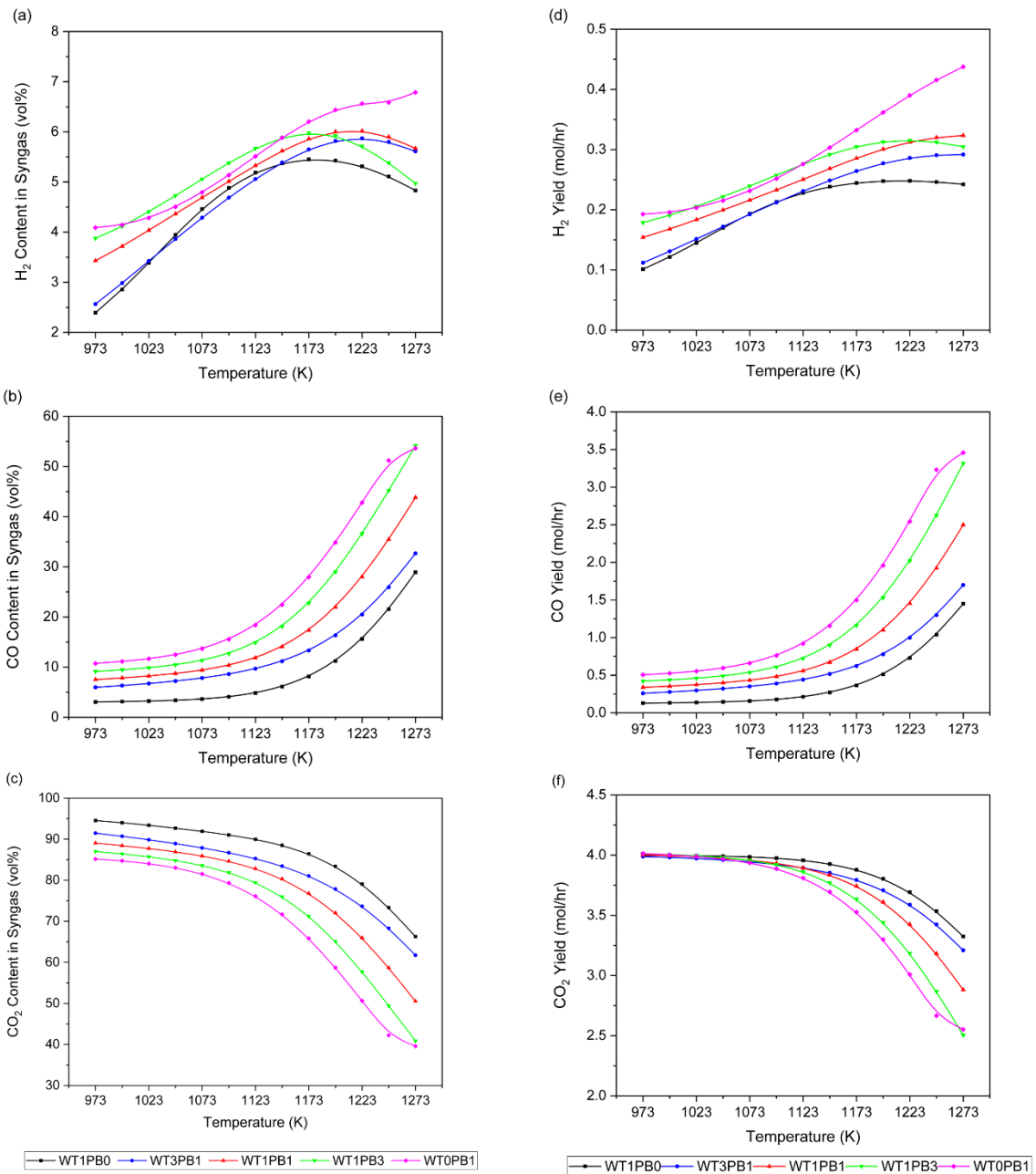


**Figure 4.4** Effect of gasification temperature on syngas composition (a) H<sub>2</sub>, (b) CO, (c) CO<sub>2</sub>, and yield (d) H<sub>2</sub>, (e) CO, (f) CO<sub>2</sub> during CO<sub>2</sub> gasification of pine bark and waste tyre at different blend ratios

*Results and discussion: H<sub>2</sub>/CO and CO/CO<sub>2</sub> Ratio*

Due to the pattern of the change in H<sub>2</sub> and CO content of the syngas, H<sub>2</sub>/CO molar ratio changes accordingly with temperature showing an increase and then decreasing with a turning point at temperatures of 1073 and 1123 K depending on the sample. This is given in Figure 4.5 (a). Comparing different samples in terms of H<sub>2</sub>/CO ratio, the highest value of 1.23

was reported for WT1PB0 at 1073 K. This is because the content of CO in the syngas is much higher than H<sub>2</sub> for all other samples compared to WT1PB0, resulting in lower values of H<sub>2</sub>/CO ratios. According to Butterman and Castaldi (2009), syngas with H<sub>2</sub>/CO ratio ranging between 0.80 to 1.40 would be suitable to be used for hydrocarbon synthesis through catalysed Fischer-Tropsch synthesis (i.e. FTS).

Although WT1PB0 resulted in syngas with the highest H<sub>2</sub>/CO ratio, CO<sub>2</sub> form the highest fraction of the syngas even at the highest operating temperature (i.e. 66.26 vol% at 1273 K). Figure 4.5 (b) reveals that there has been a steep increase in the CO/CO<sub>2</sub> ratio of all the samples at temperatures higher than 1173 K. This is due to the high production of CO with an in-parallel decrease of CO<sub>2</sub> in the syngas. The explanation for this might be due to the highly endothermic BD reaction (i.e. **R14**) which enhances at higher temperatures of greater than 973 K (Chan et al., 2021; Shen et al., 2019). The highest CO/CO<sub>2</sub> ratio is reported for WT0PB1 at 1273 K with a value of 1.36.

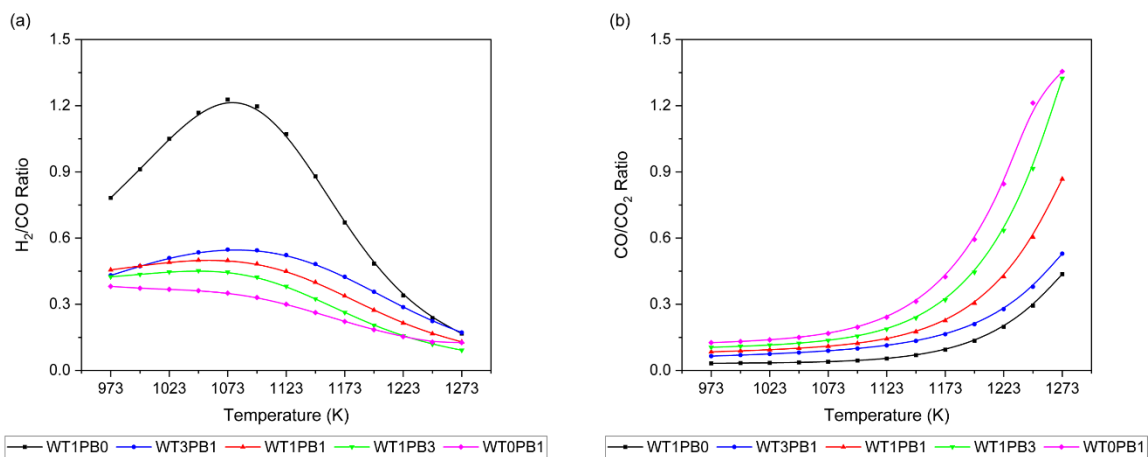


**Figure 4.5** Influence of gasification temperature on (a) H<sub>2</sub>/CO and (b) CO/CO<sub>2</sub> ratios of the syngas for CO<sub>2</sub> gasification process of pine bark and waste tyre at different blend ratios

#### Results and discussion: LHV and CGE

The increase in temperature had a positive effect on the LHV of the syngas for all the samples as can be seen in Figure 4.6 (a). According to the definition of LHV adopted in the current

research and presented in Equation (4.4), CO is the main contributor to the increase in LHV of the syngas with temperature. The rate of increase in LHV with temperature was high for WT0PB1. The LHV values increased from 3.38-3.53 MJ/Nm<sup>3</sup> at 973 K to maximum and minimum values of 8.13 and 6.14 corresponding to WT1PB3 and WT3PB1, respectively, at a temperature of 1273 K. Syngas derived from both WT1PB0 and WT3PB1 showed comparable changes in LHV with temperature.

Since CGE is a function of syngas yield and its LHV as defined by Equation (4.5), the increase in the content and yield of CO and H<sub>2</sub> thus the syngas yield resulted in an increase in CGE. The increase in CGE with temperature change between 973 and 1098 K was relatively similar between the samples. However, at temperatures higher than 1123 K, CGE markedly increased for the samples with the higher content of PB (i.e. WT0PB1, WT1PB3 and WT1PB1) in comparison to other samples. Similar to the current study, Policella et al. (2019) reported the highest CGE during CO<sub>2</sub> gasification of the waste tyre at 1273 K, which was 62.30% compared to 54.91% for WT1PB0 in the current study. However, WT0PB1 showed the highest CGE among the samples studied with a value exceeding 100% at 1273 K. Mauerhofer et al. (2021) outlined an increase in CGE with temperature to a value higher than 70% at the highest examined temperature of 840 °C (1113 K) during CO<sub>2</sub> gasification of softwood pellets in pilot scale dual fluidized bed reactor. The increase in CGE to a value higher than 100% could be ascribed to the significant increase in CO fraction and yield thus the overall syngas yield.

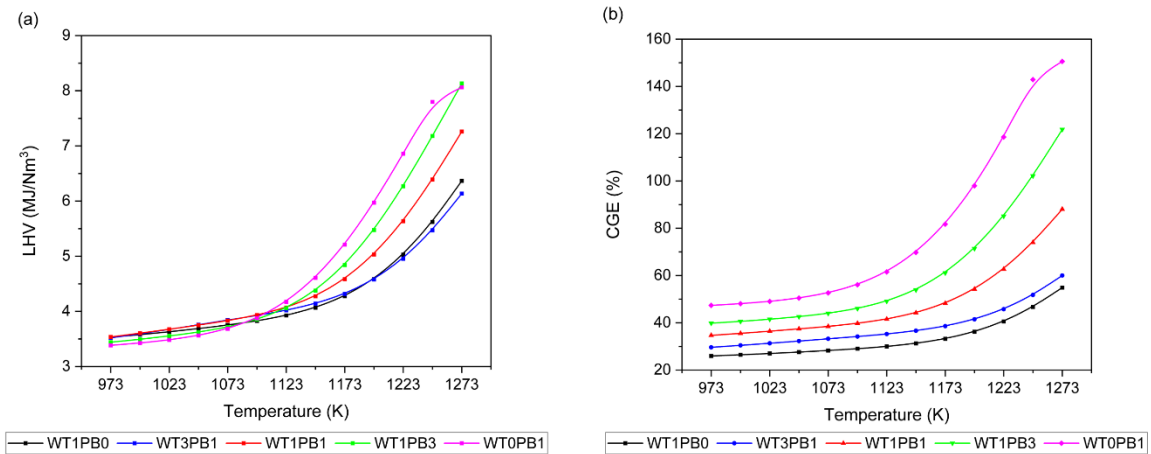


**Figure 4.6** Effect of gasification temperature on (a) LHV of the syngas and (b) CGE of the process during CO<sub>2</sub> gasification of pine bark and waste tyre at different blend ratios

#### 4.3.4 Effect of CO<sub>2</sub> flow rate (CO<sub>2</sub>-to-feed ratio)

*Justification for case study:* According to Islam (2020), the use of CO<sub>2</sub> as gasifying agent governs the production of syngas with different H<sub>2</sub>/CO ratios which in turn affect its end uses. As a result, investigating the effect of CO<sub>2</sub>-to-feed ratio on the syngas composition and yield, and process performance will provide insight into the feasibility of utilising CO<sub>2</sub> as gasifying medium for syngas production and probably offset its adverse effect on the environment.

*Setup of the case study:* Based on the total feed flow rate of 0.045 kg/hr and the examined range of CO<sub>2</sub>-to-feed ratio, the CO<sub>2</sub> flow rate is calculated. The selection of the CO<sub>2</sub>-to-feed ratio of 0.20-5.00 is based on the experimental condition used to validate the model. The operating temperature and feed flow rate were kept constant at 1173 K and 0.045 kg/hr, respectively.

*Results and discussion:* Syngas composition and yield

The effect of the CO<sub>2</sub>-to-feed ratio on syngas composition and yield is depicted in Figure 4.7. At lower values of CO<sub>2</sub>-to-feed ratio of less than 1.00, WT1PB0 resulted in a higher fraction of H<sub>2</sub> in the syngas compared to other samples. It was surprising that as the CO<sub>2</sub>-to-feed ratio increased, the difference in H<sub>2</sub> fraction between different samples was low. The H<sub>2</sub> yield

exhibited a maximum value of 0.36 mol/hr for WT0PB1 at a CO<sub>2</sub>-to-feed ratio of 1.60. At a lower CO<sub>2</sub>-to-feed ratio, the syngas was dominated by CO followed by CO<sub>2</sub> then H<sub>2</sub> for all the samples except WT1PB0. This could be contributed to the low reactivity of tyre-derived char with CO<sub>2</sub> through BD reaction (i.e. **R14**), contributing towards lower production of CO. This finding was observed in the study conducted by Lahijani *et al.* (2013), in which the reactivity of tyre-derived char with CO<sub>2</sub> was lower than the waste tyre and biomass blended samples in terms of CO<sub>2</sub> conversion. The decrease in H<sub>2</sub> yield and the increase in CO yield at CO<sub>2</sub>-to-feed ratio higher than 1.50 is contributed to the following; (1) shift of the BD reaction (i.e. **R14**) in the forward direction, and (2) enhanced RWGS reaction in the forward direction resulting in a decline in H<sub>2</sub> yield and fraction. In addition, the decrease in H<sub>2</sub> and CO content might be due to the dilution effect by the increased amount of CO<sub>2</sub> (Mauerhofer et al., 2021)

However, the increase in the CO<sub>2</sub>-to-feed ratio resulted in an increase in CO<sub>2</sub> fraction and yield. A possible explanation for this might be that the high O<sub>2</sub> content of the biomass at a lower CO<sub>2</sub>-to-feed ratio contributes to the gasification to a greater extent than CO<sub>2</sub> as a gasifying agent (Renganathan et al., 2012). This results in a higher fraction of unutilised CO<sub>2</sub> in the syngas. In addition, the deviation of the RWGS reaction from thermodynamic equilibrium moves the reaction towards the reactant resulting in a higher amount of unconverted CO<sub>2</sub> in the syngas (Mauerhofer et al., 2021).

A similar observation in terms of the change in syngas composition and yield was reported in the previous studies considering the variation in CO<sub>2</sub> flow rate as CO<sub>2</sub>-to-C ratio. Sadhwani et al. (2016) reported only an increase in the yield of CO in terms of g per kg of dry biomass in response to the change in CO<sub>2</sub> flow rate as CO<sub>2</sub>-to-C ratio with no details on the variation of CO<sub>2</sub>. Similarly, Prabowo et al. (2015), found an increase and decrease in CO<sub>2</sub> and CO content, respectively, while CO yield increased in the syngas in response to the increase in CO<sub>2</sub>/C ratio

during the auto-thermal gasification of coconut shells. The current finding is contrary to the study of Mauerhofer et al. (2021) who have outlined that the increase in CO<sub>2</sub>-to-C ratio positively affects both CO and CO<sub>2</sub> content of syngas. Moreover, Cheng et al. (2016) noticed during the numerical simulation of wood waste gasification in a fluidized bed using the Euler method that the CO<sub>2</sub> mole fraction decreased while the CO increased as the CO<sub>2</sub>-to-biomass ratio increased. Therefore, operating conditions including the temperature, type of reactor, type of feed and others play a role in how the flow rate of the gasifying agent will affect the composition of end products.

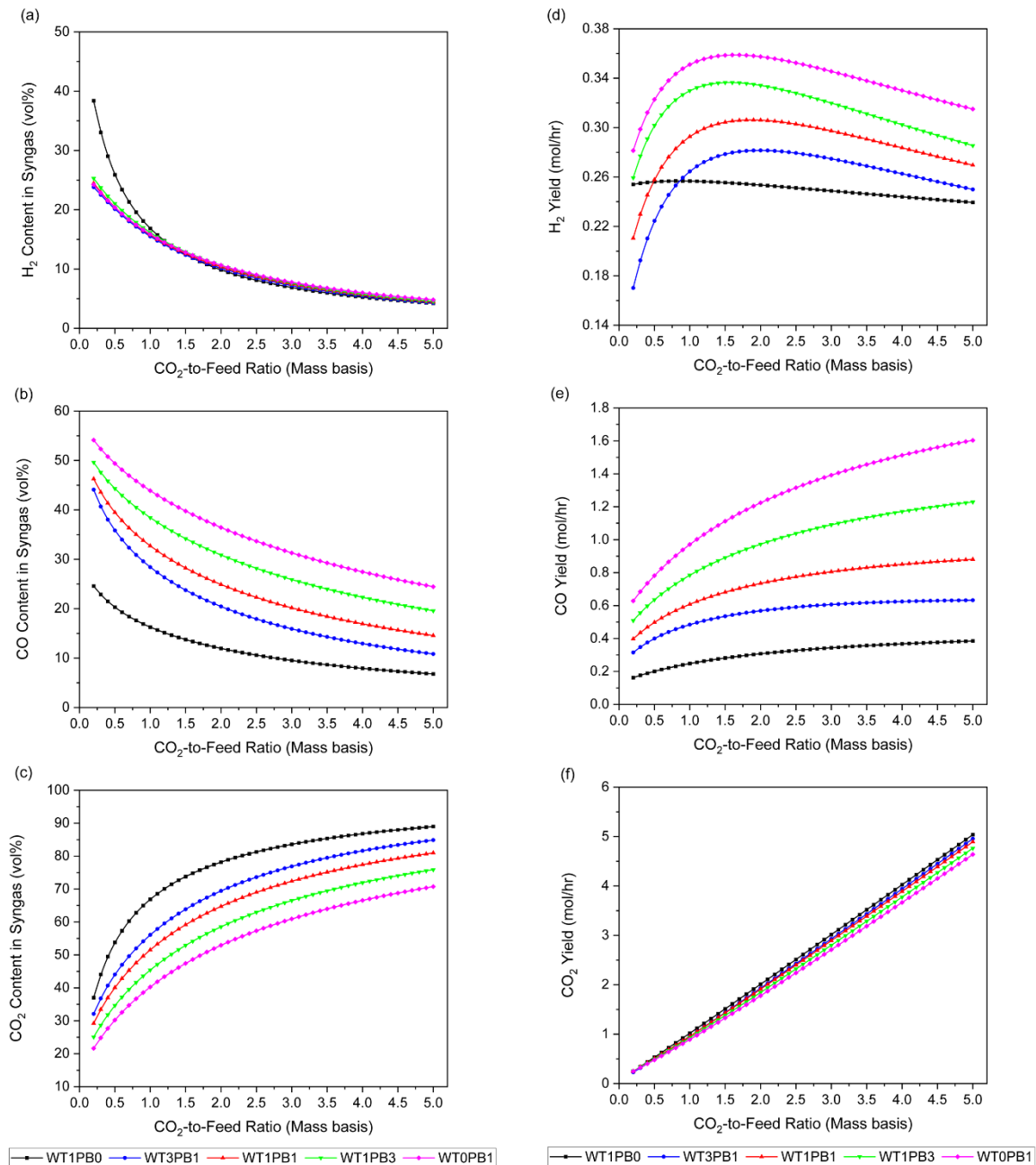


**Figure 4.7** Effect of CO<sub>2</sub>-to-feed ratio (0.2-5.0) on syngas composition (a) H<sub>2</sub>, (b) CO, (c) CO<sub>2</sub>, and yield (d) H<sub>2</sub>, (e) CO, (f) CO<sub>2</sub> during CO<sub>2</sub> gasification of pine bark and waste tyre at different blend ratios

#### Results and discussion: H<sub>2</sub>/CO and CO/CO<sub>2</sub> Ratio

As it is reported in Figure 4.8 (a), the increase in CO<sub>2</sub>-to-feed ratio caused a decrease in the H<sub>2</sub>/CO ratio of the syngas. The higher H<sub>2</sub>/CO ratio was at a lower CO<sub>2</sub>-to-feed ratio of less than 0.50 for all the samples with the WT1PB0 sample representing the higher values over the entire examined range of CO<sub>2</sub>-to-feed ratio. The highest value was 1.56 at the CO<sub>2</sub>-to-feed

ratio of 0.20. The observed decrease in  $H_2/CO$  ratio could be attributed to the higher fraction of  $CO$  in the syngas compared to  $H_2$ . The  $CO/CO_2$  ratio showed a steep decrease over the  $CO_2$ -to-feed ratio of 0.20 to 1.00 due to an increased fraction of unutilised  $CO_2$  which is directly shown in the syngas as presented in Figure 4.7 (c). Comparing the change in the  $CO/CO_2$  ratio of different samples with the increase in  $CO_2$ -to-feed ratio, the WT1PB0 showed the lowest values of  $CO/CO_2$  ratio. This observation further supports the findings of Lahijani *et al.* (2013), confirming the low reactivity of tyre-derived char in the  $CO_2$  environment which is enhanced in the presence of biomass due to the catalytic effect induced by the alkali earth metals presented in biomass-derived char. However, the rate of decrease in the  $CO/CO_2$  ratio was lower at the higher  $CO_2$ -to-feed ratio. This could be due to insignificant changes in both  $CO$  and  $CO_2$  content of the syngas at higher  $CO_2$ -to-feed ratios as illustrated in Figures 4.7 (b) and (c).

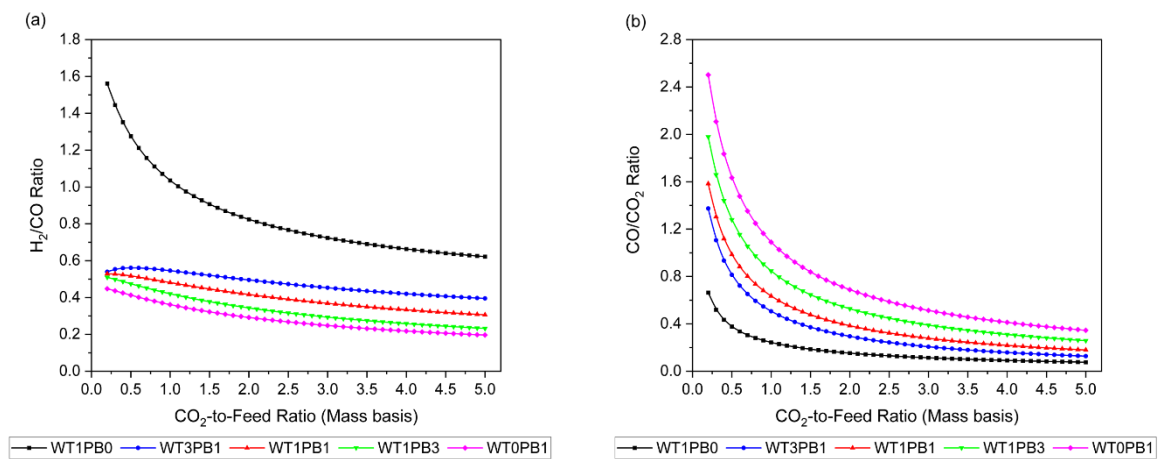


**Figure 4.8** Effect of  $CO_2$ -to-feed ratio on the syngas characteristics; (a)  $H_2/CO$  and (b)  $CO/CO_2$  ratios during  $CO_2$  gasification process of pine bark and waste tyre at different blend ratios

Mauerhofer *et al.* (2021) outlined a decrease in  $H_2/CO$  ratio from 1.49 to 0.36 when the share of  $CO_2$  as gasifying agent increased from 0 to 1 during the gasification of softwood in the pilot scale dual fluidized bed reactor.

*Results and discussion:* LHV and CGE

The LHV of the syngas is affected negatively by the increase in the CO<sub>2</sub>-to-feed ratio as shown in Figure 4.9 (a). This is because the LHV of the syngas is related to the volume fraction of the combustible constituents in the syngas. The combustible constituents represent hydrogen, CO and hydrocarbons which decreased in response to the increase in CO<sub>2</sub>-to-feed ratio. The LHV of the syngas varied in the range of 13.83-17.75 MJ/Nm<sup>3</sup> at a CO<sub>2</sub>-to-feed ratio of 0.20 to 3.48-4.47 MJ/Nm<sup>3</sup> at the ratio of 5.00. The interesting about the current results of LHV is the presence of the turning point at CO<sub>2</sub>-to-feed ratio of 1.50 at which the LHV of the syngas derived from samples with the highest fraction of pine bark (i.e. WT0PB1 and WT1PB3) is higher compared to other samples.

The increase in CO<sub>2</sub>-to-feed ratio increased the CGE, with WT0PB1 showing the highest value over the studied range as presented in Figure 4.9 (b). The change in CGE of the samples with higher waste tyre content including WT1PB0 and WT3PB1 was relatively low, in the range of 12.23-12.69%. Although CGE deals with the ratio of LHV of the syngas to the LHV of the feed, it incorporates the total syngas yield as stated earlier. Therefore, the increased content of both CO and CO<sub>2</sub> is mainly contributing to the increased syngas yield thus CGE. The highest CGE value of 85.22% was achieved with the use of WT0PB1 at a CO<sub>2</sub>-to-feed ratio of 5.00. The recent results of the effect of CO<sub>2</sub>-to-feed ratio on the CGE are consistent with those of Cheng et al. (2016) in which the increase in CO<sub>2</sub>-to-biomass ratio affected positively the CGE.

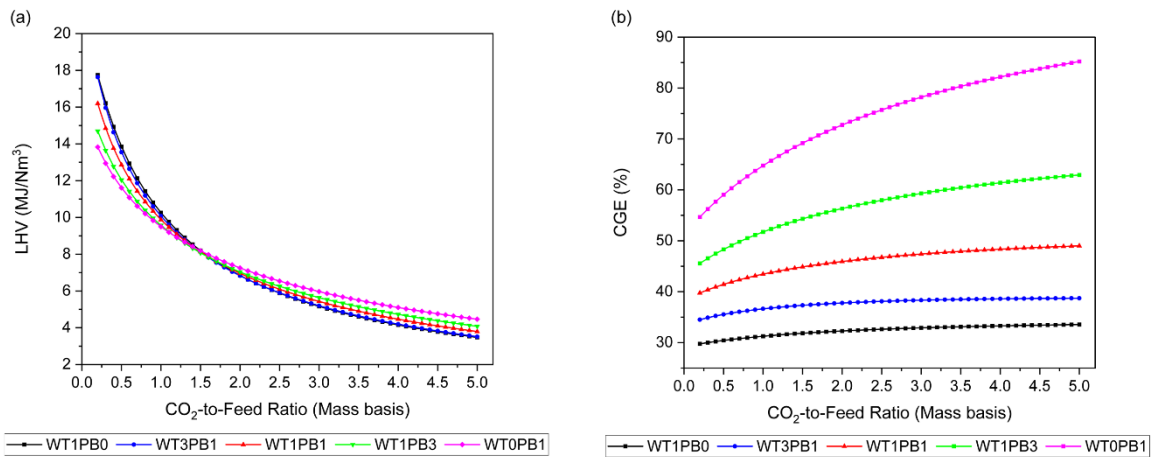


**Figure 4.9** Effect of CO<sub>2</sub>-to-feed ratio on syngas characteristic (a) LHV of the syngas and (b) CGE of the process during CO<sub>2</sub> gasification of pine bark and waste tyre at different blend ratios

#### 4.3.5 Effect of feed flow rate

*Justification for case study:* Depending on the type of gasification reactor, the increase in the feeding rate of the feedstock is beneficial in boosting the production capacity. Although an excessive feeding rate would increase the gas yield, it decreases the gas residence time which in turn leads to gas with lower quality associated with higher production of tar (Guo et al., 2014). As a result, it is necessary to investigate the influence of feed flow rate on the syngas characteristics and the process performance.

*Setup of the case study:* To implement this case, the gasification temperature and CO<sub>2</sub>-to-feed ratio of 1173 K and 3.90, respectively, was used. The feed flow rate for different blend samples varied between 0.02 and 2.00, covering the feed flow rate used in the model validation.

#### *Results and discussion:* Syngas composition and yield

As Figure 4.10 shows, the feed flow rate had a positive effect on syngas composition and yield in terms of H<sub>2</sub> and CO. The main constituents of the syngas derived from all the samples were CO<sub>2</sub> followed by CO and H<sub>2</sub>. The highest H<sub>2</sub> fraction of 17.81 vol% was achieved with the use of WT1PB0 at a feed flow rate of 0.20 kg/hr. On the other hand, the use of WT0PB1 resulted

in syngas with the highest CO fraction of 35.62 vol% at a feed flow rate of 0.20 kg/hr. The increase in H<sub>2</sub> fraction along with CO could be due to their increase in the devolatilization stage as well as the DR reaction (i.e. **R12**) and BD reaction (i.e. **R14**) in the gasification stage. The highest fraction of CO<sub>2</sub> was reported with the use of WT1PB0. This confirms the low reactivity of waste tyre char with CO<sub>2</sub>, thus resulting in lower content of CO in the syngas. The highest total H<sub>2</sub> and CO content was achieved at a higher feed flow rate. It has values of 30.47, 37.65, 41.32, 45.90 and 49.89 vol% for WT1PB0, WT3PB1, WT1PB1, WT1PB3 and WT0PB1, respectively.

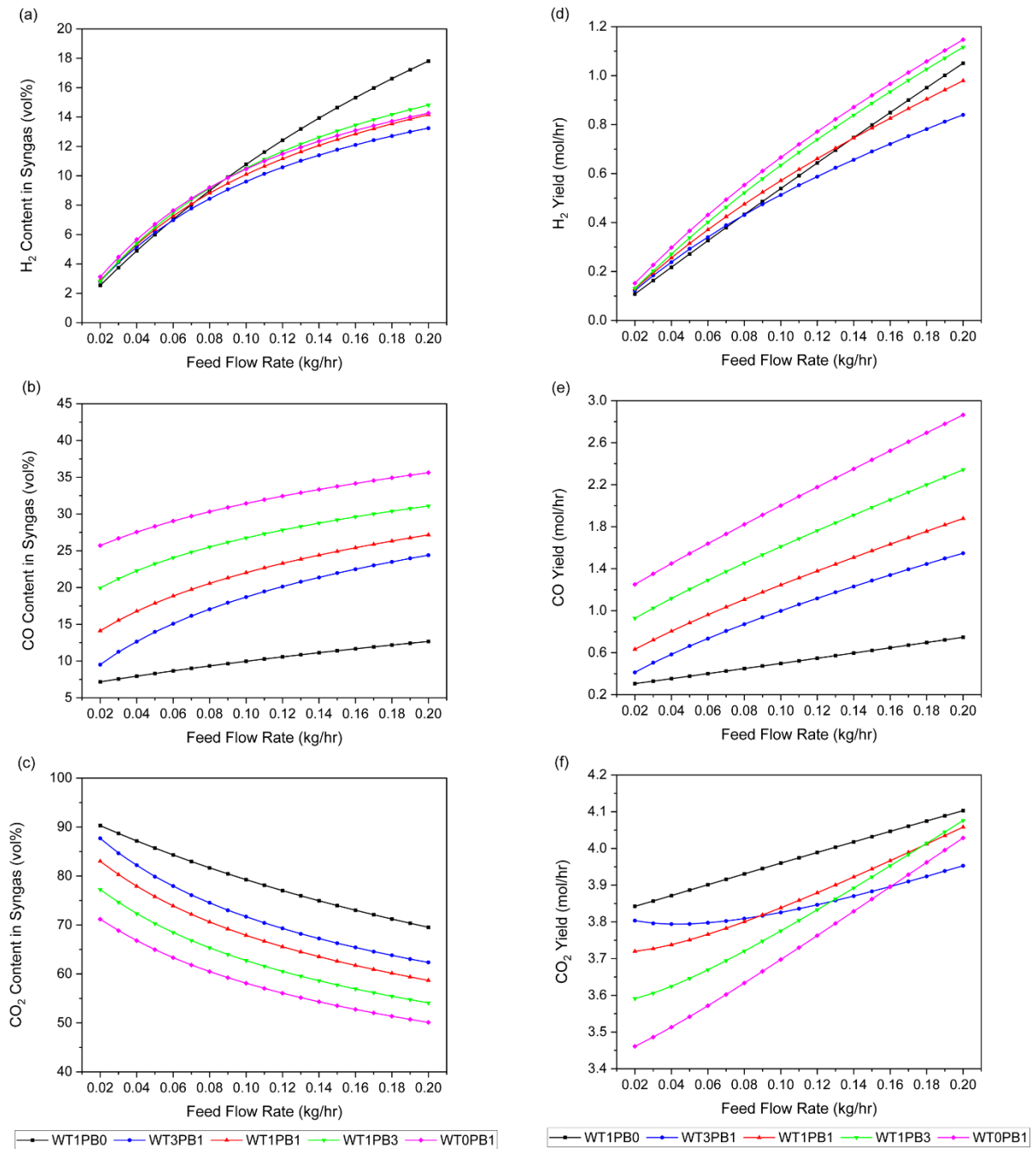


**Figure 4.10** Effect of feed flow rate (0.2-2.0 kg/hr) on syngas composition (a) H<sub>2</sub>, (b) CO, (c) CO<sub>2</sub>, and yield (d) H<sub>2</sub>, (e) CO, (f) CO<sub>2</sub> during CO<sub>2</sub> gasification process of pine bark and waste tyre at different blend ratios

*Results and discussion: H<sub>2</sub>/CO and CO/CO<sub>2</sub> Ratio*

The increase in feed flow rate affected positively both H<sub>2</sub>/CO and CO/CO<sub>2</sub> ratios of the syngas from all the samples. The H<sub>2</sub>/CO ratio of the syngas from all the samples except WT1PB0 increased continuously and then started to nearly stabilize at a minimum feed flow rate of 0.10 kg/hr. However, WT1PB0-derived syngas showed a continuous increase in H<sub>2</sub>/CO ratio

to a maximum value of 1.41 at a feed flow rate of 0.20 kg/hr. This value of the H<sub>2</sub>/CO ratio makes the syngas a possible feed for Fe and Co catalyst-based FTS. Comparing the increase in CO/CO<sub>2</sub> ratio with an increase in feed flow rate, WT0PB1 showed the highest values over the studied range of feed flow rate compared to other samples.

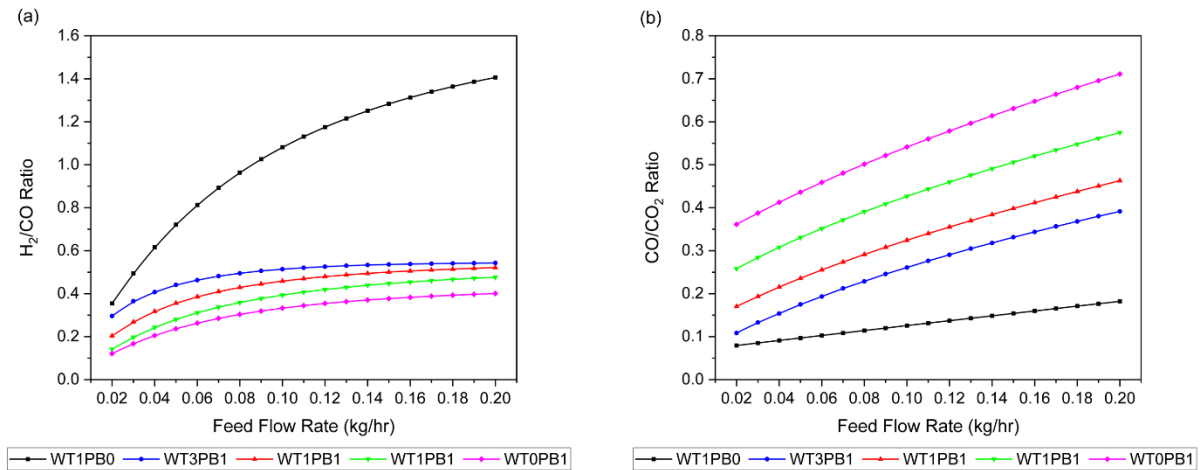


**Figure 4.11** The variation in (a) H<sub>2</sub>/CO ratio and (b) CO/CO<sub>2</sub> ratio in response to the change in feed flow rate during CO<sub>2</sub> gasification of pine bark and waste tyre at different blend ratios

*Results and discussion: LHV and CGE*

The effect of feed flow rate on the LHV of the syngas from different blended samples is reported in Figure 4.12 (a). It is noticed that the LHV of the syngas increases with the increase in feed flow rate. Despite the continual increase in the LHV of the syngas, there is a complete swap in the LHV at a feed flow rate of 0.09 kg/hr. This means that the LHV of the syngas was higher for the WT1PB0 followed by WT1PB3, WT1PB1, WT3PB1 and WT0PB1 for the feed flow rate lower than 0.09, but the order became opposite at higher feed flow rates (i.e. > 0.09 kg/hr). The increase in LHV is attributed to the increase in both H<sub>2</sub> and CO yield as provided in Figures 4.10 (a) and (b). On the other hand, the CGE decreased with an increase in feed flow rate and then started to flatten at a feed flow rate of about 0.06 kg/hr.

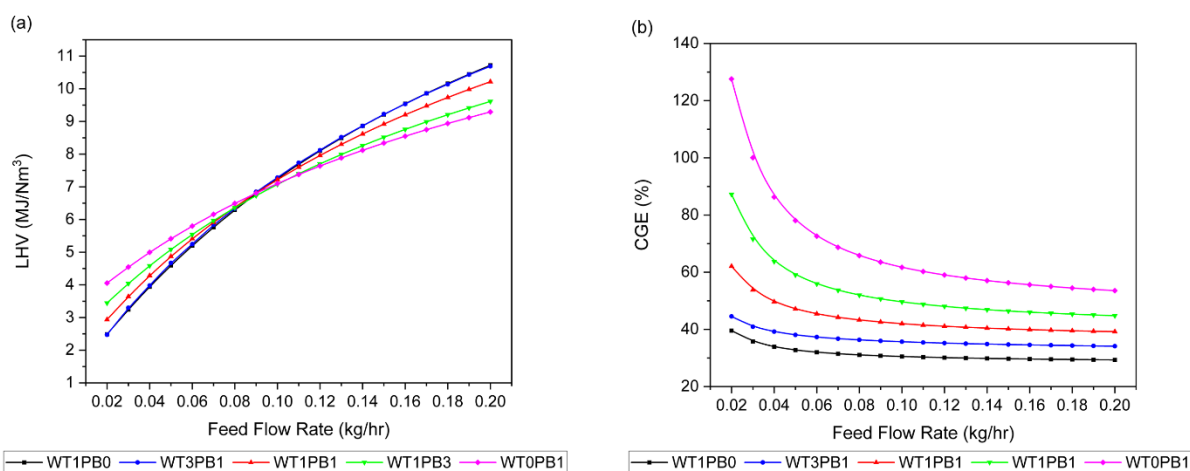


**Figure 4.12** Effect of feed flow rate on the gasification performance (a) LHV of the syngas and (b) CGE of the CO<sub>2</sub> gasification process of pine bark and waste tyre at different blend ratios

#### 4.4 Synergetic interaction between waste tyre and pine bark in CO<sub>2</sub> environment

To evaluate the existence of synergy between pine bark and waste tyre in terms of syngas composition and process performance, it can be clearly seen from the analysis results of various operating conditions that there might be no synergetic interaction between pine bark and waste tyre. This is because the syngas composition in terms of H<sub>2</sub>, CO and CO<sub>2</sub> content, and yield is sandwiched between the single samples. However, slight synergy is noticed in terms of higher H<sub>2</sub> content and yield from WT1PB3 gasification compared to single samples (i.e. WT1PB0 and WT0PB1) over the temperature range of 1023-1123 K as shown in Figure 4.4 (a) and (d).

#### 4.5 Conclusion

Co-gasification of pine bark and waste tyre using CO<sub>2</sub> through process modelling and simulation was carried out in ASPEN Plus® software. The effect of gasification temperature, CO<sub>2</sub>-to-feed ratio and feed flow rate on syngas composition and yield as well as process performance was analysed.

Gasification temperature affected positively the syngas composition and yield in terms of H<sub>2</sub> and CO content. The H<sub>2</sub> content increased to its maximum yield and content at a temperature

of around 1173 K and then decreased. However, a maximum value of H<sub>2</sub>/CO ratio was achieved with the use of a single waste tyre sample at a temperature of 1073 K. Both LHV and CGE showed positive responses to the change in the gasification temperature.

The variation in the CO<sub>2</sub>-to-feed ratio affected negatively both syngas composition and yield as well as process performance. The LHV of the syngas for all the samples as well as H<sub>2</sub>/CO and CO/CO<sub>2</sub> ratios decreased with an increase in CO<sub>2</sub>-to-feed ratio. However, The CGE of the process improved. Therefore, a lower CO<sub>2</sub>-to-feed ratio resulted in syngas with better quality.

Feed flow rate had a noticeable effect on H<sub>2</sub> as well as CO content and yield in which the maximum fraction and yield of both components were obtained at the highest feed flow rate of 2.00 kg/hr. The H<sub>2</sub>/CO ratio, CO/CO<sub>2</sub> ratio and LHV of the syngas improved with the increase in feed flow rate whereas CGE decreased up to a feed flow rate of around 0.06 kg/hr and then started to show a negligible effect.

The syngas produced using WT1PB0 with a H<sub>2</sub>/CO ratios of; (1) 1.23 at a temperature, CO<sub>2</sub>-to-feed ratio and feed flow rate of 1073 K, 3.9 and 0.045 kg/hr, respectively, and (2) 1.41 at a temperature, CO<sub>2</sub>-to-feed ratio and feed flow rate of 1173 K, 0.88 and 0.20 kg/hr, respectively, are suitable for catalyst-based FT synthesis of various hydrocarbons.

The present study provides the first comprehensive assessment of the effect of different operating parameters on the co-gasification of pine bark and waste tyre in the CO<sub>2</sub> environment.

## CHAPTER 5 Comparative evaluation of co-gasification of pine bark and waste tyre using steam and steam/CO<sub>2</sub> mixture through process modelling and simulation

In this chapter, the validated model of CO<sub>2</sub> co-gasification of biomass and waste tyre in Chapter 4 was used to investigate the role of steam and steam/CO<sub>2</sub> mixture as gasifying agents in improving syngas production and quality. In *Section 5.1*, the modifications carried out on the existing model are introduced. In *Section 5.2*, the process analysis of pine bark and waste tyre co-gasification using steam is carried out. In *Section 5.3*, the results of process analysis using steam/CO<sub>2</sub> mixture are presented. In *Section 5.4* a comparison of syngas composition and quality as well as process performance between CO<sub>2</sub>, steam and steam/CO<sub>2</sub> mixture is provided.

### 5.1 Modification in the developed model

To understand the effect of using steam and steam/CO<sub>2</sub> mixture as gasifying agents on the syngas quantity and quality as well as process performance, additional blocks and streams were introduced in the existing model. The streams **G-AGNT-2** and **H-AGNT-2** are used to represent steam flow at standard temperature and elevated temperature, respectively. The additional blocks and their purposes are provided in Table 5.1. The process flowsheet of the improved model is shown in Figure 5.1.

**Table 5.1** List of additional blocks and their application in the existing model

Name of the unit	Type of the block	Utilisation in model development
<b>HEATER-1</b>	Heater block	for heating single or mixed gasifying agent ( <b>MIX-AGNT</b> ) to the desired temperature
<b>MIXER-4</b>	A mixer block	for mixing different gasifying agents ( <b>G-AGNT-1</b> , <b>H-AGNT-2</b> )

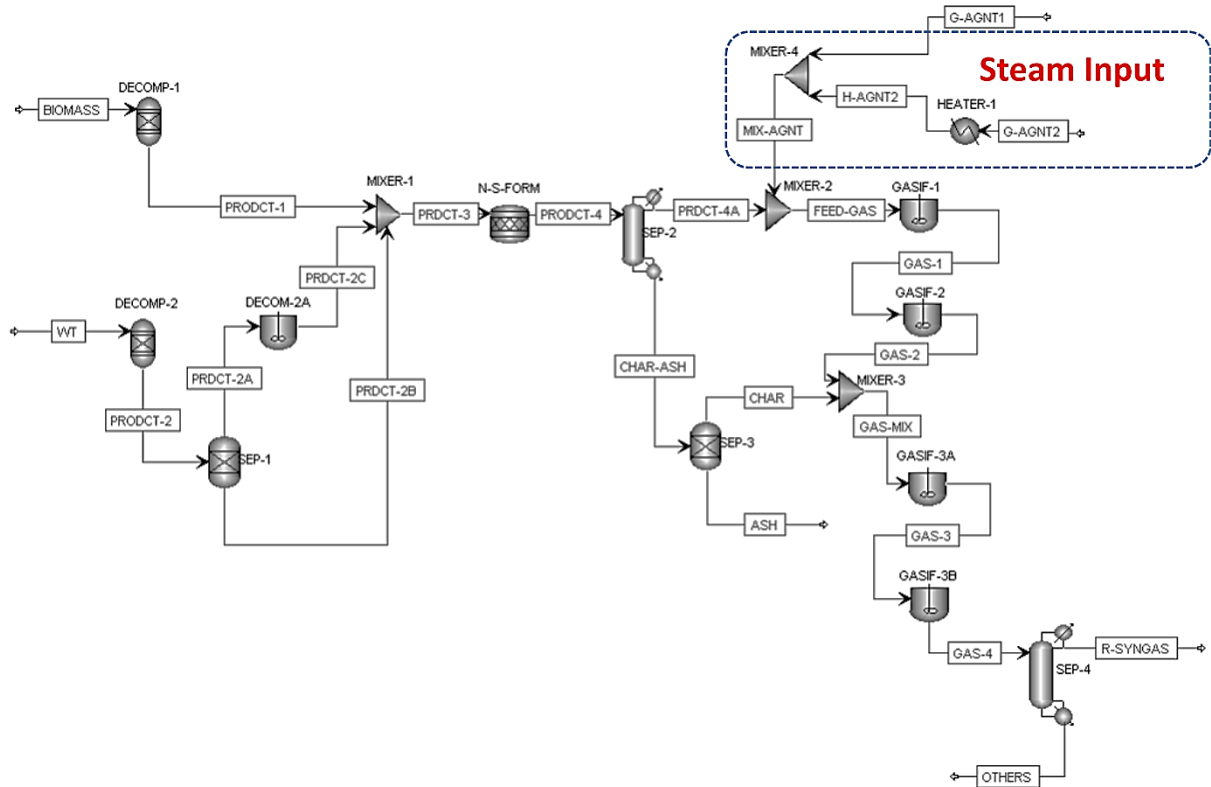


**Figure 5.1** Process flowsheet for the improved model

The performance indices introduced in Chapter 4 are used to evaluate the model prediction under different gasifying agents.

## 5.2 Process analysis of steam co-gasification of pine bark and waste tyre: Case 1

The first case of the process analysis examines the effect of steam gasification on syngas composition and yield as well as process performance at different operating conditions. Details of the process analysis are summarised in Table 5.2. The effect of gasification temperature is analysed by varying the temperature between 973 and 1273 K while keeping both steam-to-feed ratio and feed flow rate at 3.90 and 0.045 kg/hr. To study the influence of steam-to-feed ratio (i.e. SFR) and feed flow rate, they varied between 0.20-5.00 and 0.02-0.20, respectively. The other operating conditions are fixed as provided in Table 5.2.

**Table 5.2** Process analysis plan for case 1: steam co-gasification of pine bark and waste tyre

Case ID	Variables		
	Gasification Temperature (K)	Steam-to-feed ratio (Mass basis)	Feed flow rate (kg/hr)
Section 5.2.1	973-1273	3.90	0.045
Section 5.2.2	1173	0.20-5.00	0.045
Section 5.2.3	1173	3.90	0.02-0.20

### 5.2.1 Effect of temperature

#### *Syngas composition and yield*

The results for the effect of gasification temperature on syngas composition and yield for different PB and WT blended samples are displayed in Figure 5.2. From the data in Figure 5.2 (a)-(c), there is a clear trend of increasing the H<sub>2</sub> and CO<sub>2</sub> content of the syngas and decreasing the fraction of CO for all the blended samples. The increase in H<sub>2</sub> and CO<sub>2</sub> fraction and the decrease in CO at low gasification temperatures of less than 1173 K is due to the accelerated WGS, MR and WG reactions (i.e. **R10**, **R11** and **R15**) (Islam, 2020; Shahbaz et al., 2017). However, at higher temperatures, both H<sub>2</sub> and CO<sub>2</sub> content decreased while CO increased. This is because the exothermic WGS reaction favours low temperature (i.e. 973 to 1223 K in our case), so further increase in temperature shifts the reaction equilibrium backward to the reactants side according to the Le Chatelier principle, resulting in lower production of CO and H<sub>2</sub>, and hence increasing CO<sub>2</sub> concentration (Zheng et al., 2016).

Despite the decrease in H<sub>2</sub> content at higher temperatures, there is a progressive increase in its yield along with carbon monoxide. This would be an indication of the combined contribution of multiple reactions including tar and hydrocarbon cracking (i.e. **R2-R4**) and reforming reactions (i.e. **R5-R7**) in the gasification stage along with the BD reaction (i.e. **R14**) (Brachi et al., 2014; Portofino et al., 2013; Waheed et al., 2016). The highest H<sub>2</sub> content of 71.4 vol% was obtained at 1223 K for WT1PB0 which corresponds to a yield of 1.66 mol/hr.

The current results are in agreement with the previous studies. Waheed et al. (2016) reported an increase in the H<sub>2</sub> content of the syngas during the catalytic pyrolysis/reforming of rice husk in a two-stage fixed bed reactor, achieving a maximum value of 65.18 vol% at 1323 K. However, Elbaba and Williams (2012) investigated the effect of temperature on syngas composition during steam gasification of the waste tyre in a two-stage fixed bed reactor using a Ni-Alumina catalyst. They found that the maximum H<sub>2</sub> concentration was obtained at the temperature of 600° C (873 K), then it decreased with an increase in the temperature to 800 °C (1073 K) and started to increase thereafter.

Comparing the syngas composition and yield between different blended samples, WT1PB0 showed the highest content of H<sub>2</sub> over the entire examined temperature range from 973 to 1273 K with values of 35.40 and 69.55 vol%, respectively. However, WT0PB1 resulted in syngas with higher content of CO and CO<sub>2</sub> compared to other samples. These results reflect those of Galvagno et al. (2009) who investigated syngas production from steam gasification of three different feedstocks at 850 °C (1123 K). They found that the syngas derived from the waste tyre is dominated by H<sub>2</sub> and other hydrocarbons compared to CO and CO<sub>2</sub> forming the main fraction of the syngas from poplar wood sawdust. It was suggested that the high fraction of oxygen contained in the biomass, mainly in cellulose and hemicellulose, is the explanation for the difference in the H<sub>2</sub>, CO and CO<sub>2</sub> fraction of the syngas between biomass and waste tyre (Arregi et al., 2017).

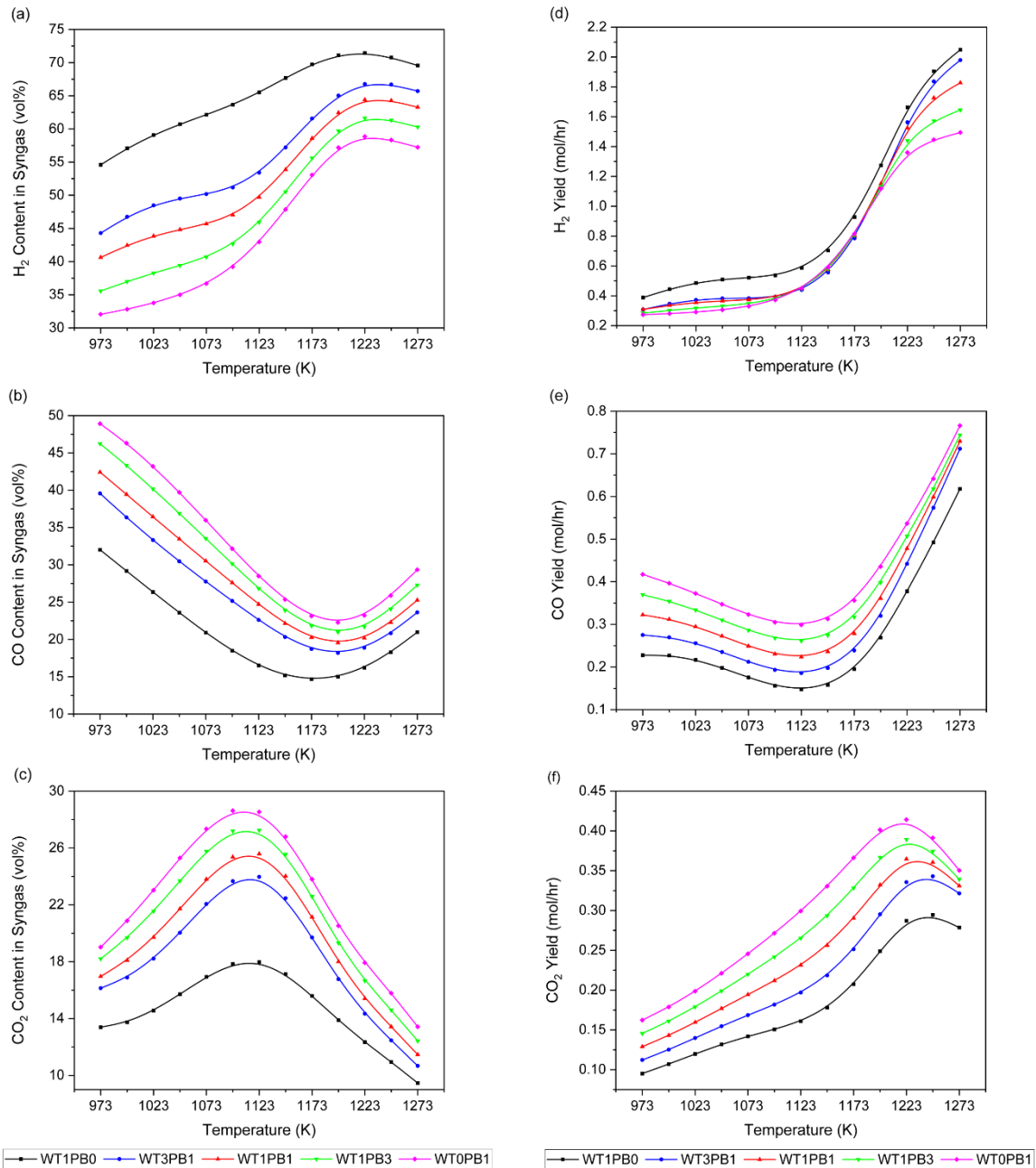


**Figure 5.2** Effect of gasification temperature on syngas composition (a) H<sub>2</sub>, (b) CO, (c) CO<sub>2</sub>, and yield (d) H<sub>2</sub>, (e) CO, (f) CO<sub>2</sub> during steam gasification of pine bark and waste tyre at different blend ratios

In agreement with the current result, the CO<sub>2</sub> fraction decreased with increase in temperature from 850 to 1050 °C (1123 to 1323 K) in the study of Waheed et al., (2016) and its been suggested to be due to enhanced endothermic DR and BD reactions at high gasification temperatures.

### H<sub>2</sub>/CO and CO/CO<sub>2</sub> Ratio

It can be seen from Figure 5.3 (a) and (b) that the trend of  $H_2/CO$  and  $CO/CO_2$  ratio in response to the change in gasification temperature is opposite to each other. The  $H_2/CO$  ratio increased and peaked at a temperature of 1198 K and then decreased. This is consistent with the maximum and minimum  $H_2$  and CO content of the syngas reported in Figures 5.2 (a) and (b) at a temperature 1198 K.

A remarkable increase in  $H_2/CO$  ratio along with a decrease in  $CO/CO_2$  ratio over the temperature from 973 to 1173 K for all the samples would be attributed to the WGS reaction which in turn enhances  $H_2$  as well as  $CO_2$  formation. However, a change in the trend of  $H_2/CO$  and  $CO/CO_2$  ratios at temperatures higher than 1173 K indicates the increased formation of CO which might be due to the enhanced endothermic reactions (i.e. BD) as mentioned earlier. The highest  $H_2/CO$  ratio was reported for WT1PB0 with a value of 4.76 at a temperature of 1173 K. The WT0PB1 sample resulted in syngas with the highest  $H_2/CO$  ratio of 2.57 at a temperature of 1198 K. The  $H_2/CO$  ratio of all the blended samples is sandwiched between the single samples. Wieckert et al. (2013) studied steam gasification of different feedstocks in a 150  $kw_{th}$  packed-bed solar reactor. They found that tyre chips produced syngas with a higher  $H_2/CO$  ratio compared to sugar cane bagasse which was 4.40 compared to 2.00. These values of  $H_2/CO$  ratios are comparable to the current results.

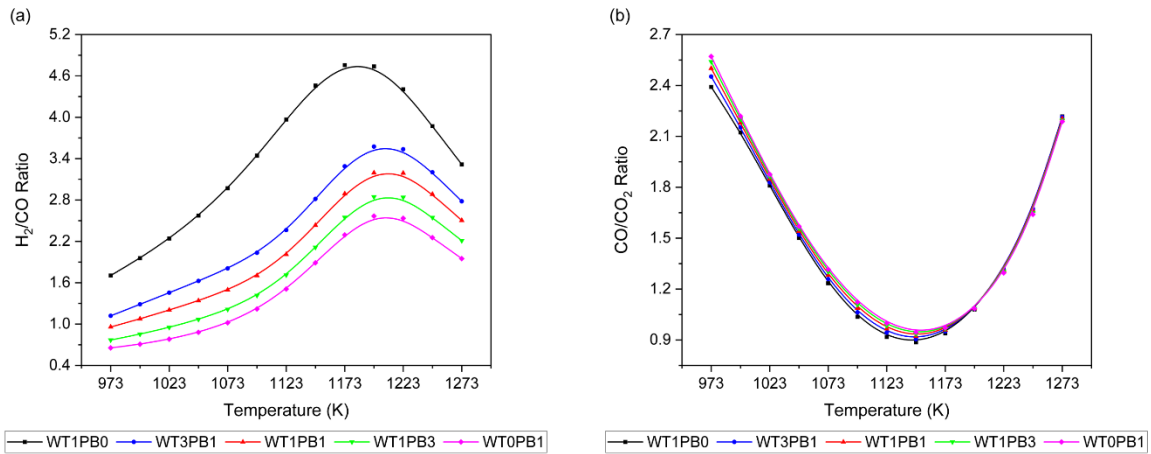


**Figure 5.3** Effect of gasification temperature on (a)  $H_2/CO$  ratio and (b)  $CO/CO_2$  ratio of the syngas during steam gasification of pine bark and waste tyre at different blend ratios

### LHV and CGE

It was observed that the LHV of the syngas derived from all the blended samples decreased gradually over the temperature from 973 to 1098 K and then there was a sharp decline as shown in Figure 5.4 (a). Interestingly, the LHV trend reversed at a temperature higher than 1223 K. The increase in LHV at temperatures higher than 1223 K could be explained by the increase in the CO content of the syngas.

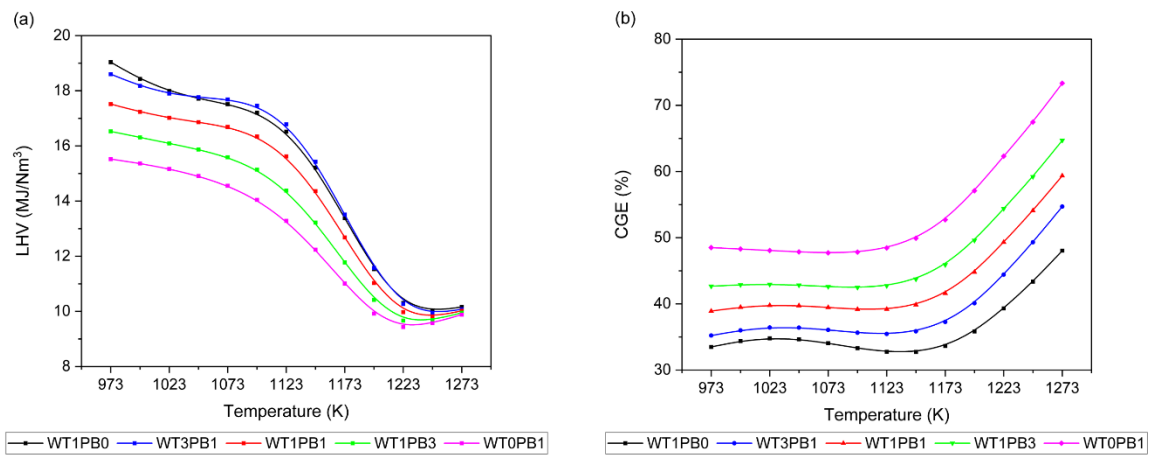


**Figure 5.4** Effect of gasification temperature on (a) LHV of the syngas and (b) CGE of the process during steam gasification of pine bark and waste tyre at different blend ratios

According to the current results, the highest LHV was achieved with the use of WT1PB0 at a temperature of 973 K and it was  $19.04 \text{ MJ/Nm}^3$  which was slightly higher than  $18.60 \text{ MJ/Nm}^3$  in the case of WT3PB1. The LHV of the syngas reported in the literature varies depending on

the operating conditions as well as the type and composition of the feedstock. According to the literature, the LHV of the syngas derived from steam gasification of biomass varied between 12.70 and 14.95 MJ/Nm<sup>3</sup> (Galvagno et al., 2009; Mauerhofer et al., 2019; Peng et al., 2012) and might be higher than that while the LHV of waste tyre-derived syngas reaches up to 25.33 MJ/Nm<sup>3</sup> (Galvagno et al., 2009). The CGE was improved at higher gasification temperatures due to the same reason as LHV along with the improved yield of H<sub>2</sub> and CO thus total syngas. The maximum CGE of 73.33% was achieved with the gasification of WT0PB1 compared to other samples. Shahbaz et al. (2017) reported a decrease in both LHV and CGE over the temperature from 650 to 750 °C (923 to 1023 K) at a steam-to-biomass ratio of 1.50 using CaO as a CO<sub>2</sub> adsorbent.

#### 5.2.2 Effect of steam-to-feed ratio (i.e. SFR)

##### *Syngas composition and yield*

The results of the variation in the syngas composition and yield with the change in SFR from 0.20 to 5.00 are presented in Figure 5.5. Looking at Figure 5.5 (a) and (d) it's worth noting that the H<sub>2</sub> content and yield for all the blended samples are affected positively with the increase in SFR. The CO content and yield decreased while those of CO<sub>2</sub> increased in response to the increase in SFR. For instance, the H<sub>2</sub> content and yield increased from 44.62 vol% and 0.37 mol/hr (i.e. SFR = 0.20) to 61.60 vol% and 0.78 mol/hr (i.e. SFR = 5.00), respectively, for WT3PB1. Similarly, CO<sub>2</sub> content and yield keep increasing from 15.99 vol% and 0.13 mol/hr (i.e. SFR = 0.20) to 19.15 vol% and 0.24 mol/hr (i.e. SFR = 5.00), respectively, as presented in Figure 5.5 (c) and (f). This positive effect of increasing SFR on H<sub>2</sub> content and yield was reported in the previous studies of steam gasification of biomass (Chai et al., 2022; Pala et al., 2017; Yusup et al., 2013) and waste tyre (Karatat et al., 2012; Lerner et al., 2012).

Since steam (i.e.  $H_2O$ ) works as a reactant in different gasification reactions including tar reforming (i.e. **R5-R7**), WGS (i.e. **R10**), MR (i.e. **R11**) and WG (i.e. **R15**), so increasing the reactant flow into the system will promote these reactions into more products formation according to the Le Chatelier principle (Chai et al., 2020; Zheng et al., 2016). Therefore, adding more steam into the system results in increased consumption of  $CO_2$  along with increased production of  $H_2$  and  $CO$ . This explains the results shown in Figure 5.5. According to the results of  $CO$  content and yield, WGS reaction is dominant compared to MR because the latter improves  $CO$  production to some extent which is not the case here.

Noticeably, the variation in the syngas composition was negligible at SFR higher than 2.90, resulting in  $H_2$  content of 69.70, 61.31, 58.37, 55.48 and 53.03 vol% for WT1PB0, WT3PB1, WT1PB1, WT1PB3 and WT0PB1, respectively. Therefore, the SFR at around 2.50-3.50 is suitable to obtain relatively a syngas with high content of  $H_2$ . Lerner et al. (2012) studied steam-plasma gasification of automobile tyre through numerical simulation. They observed that at a steam flow rate of 3.50 in mol per mol of C in the feed there was negligible change in  $H_2$  and  $CO$  concentration in mol%.

Comparing different blended samples, syngas obtained using WT1PB0 reported higher  $H_2$  content and yield which had maximum values of 69.75 vol% and 0.93 mol/hr at SFR of 3.50. Although WT1PB0 resulted in higher production of  $H_2$ , the  $CO_2$  content and yield were lower than in other samples. This could be due to the lower oxygen content of WT compared to PB which in turn results in lower production of  $CO$  and  $CO_2$  in the devolatilization stage.

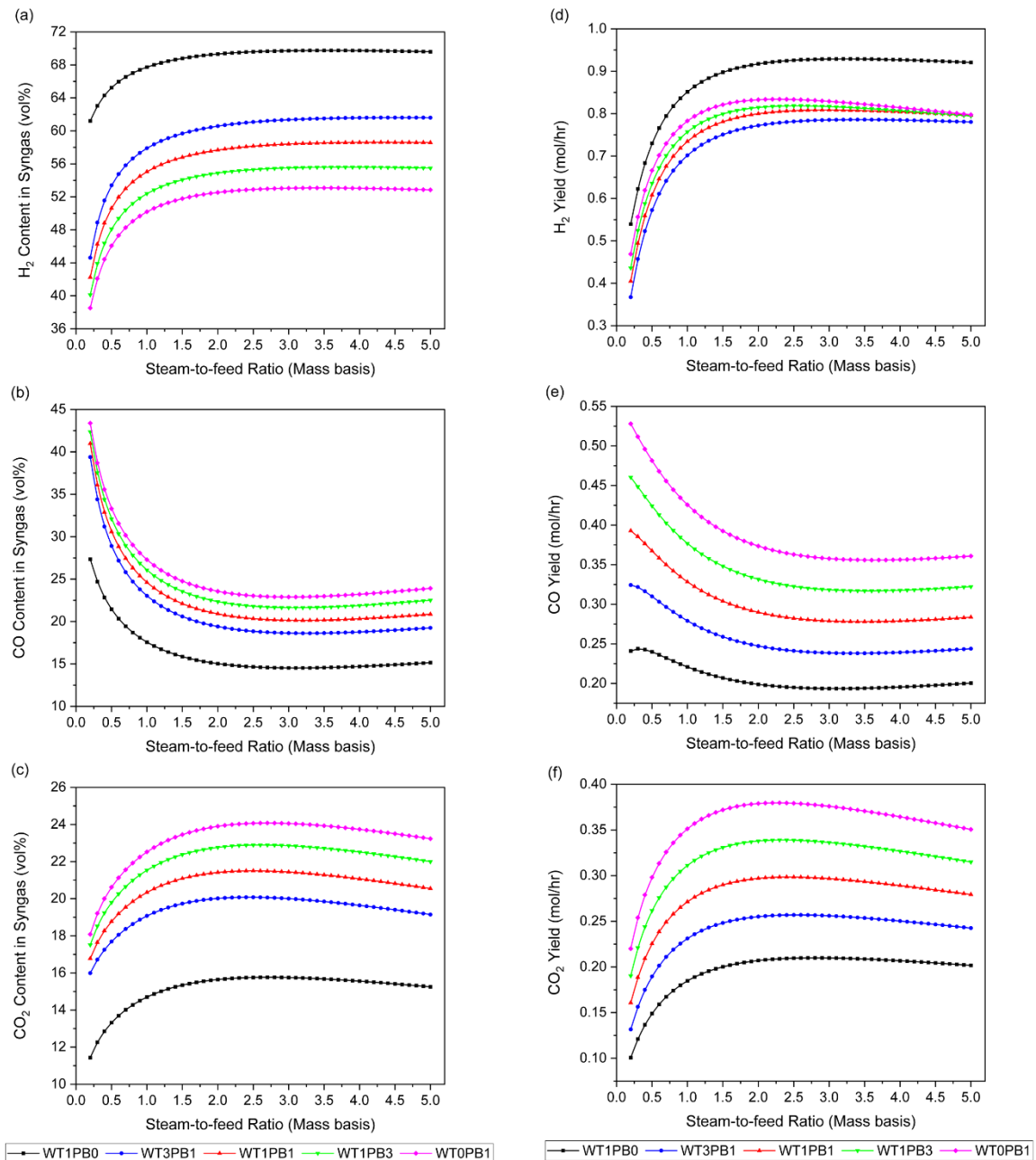


**Figure 5.5** Effect of steam to feed ratio on syngas composition (a) H<sub>2</sub>, (b) CO, (c) CO<sub>2</sub>, and yield (d) H<sub>2</sub>, (e) CO, (f) CO<sub>2</sub> during steam gasification of pine bark, waste tyre and their blends

### *H<sub>2</sub>/CO and CO/CO<sub>2</sub> Ratio*

Following the increase in H<sub>2</sub> production and CO consumption in response to the increase in SFR, H<sub>2</sub>/CO ratio increased and CO/CO<sub>2</sub> ratio decreased. This is presented in Figure 5.6 (a) and (b). The H<sub>2</sub>/CO ratio peaked at SFRs of 3.10, 3.40, 3.30, 3.20 and 3.10 for WT1PB0, WT3PB1, WT1PB1, WT1PB3 and WT0PB1, respectively. The peak H<sub>2</sub>/CO ratio was between 2.32 and

4.80 where the higher bound was achieved with the use of WT1PB0. This is consistent with the H<sub>2</sub> and CO content reported earlier. On the other hand, the CO/CO<sub>2</sub> ratio decreased to its minimum value ranging between 0.92 and 0.95 at SFR of  $\approx$  3. The reported values of the H<sub>2</sub>/CO ratio of all the blended samples make the derived syngas suitable for further processing in FTS (Ephraim et al., 2016).

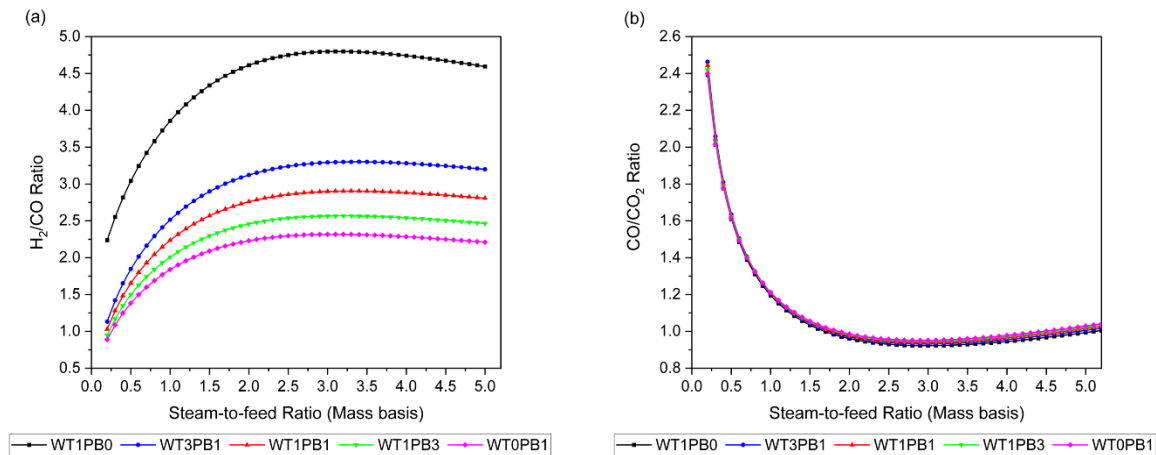


**Figure 5.6** Variation in syngas characteristics (a) H<sub>2</sub>/CO, and (b) CO/CO<sub>2</sub> ratio with the change in steam-to-feed ratio for different samples during steam gasification

### LHV and CGE

From Figure 5.7 (a), it could be found that the tendency of the change in LHV of all the blended samples with SFR resembles that of CO content in the syngas shown in Figure 5.5 (b). The LHV of the syngas from WT3PB1 was higher than other samples. The decrease in the LHV of the syngas from all the blended samples was more significant at lower SFR up to a value of around 1.50 in which the change was less noticeable at higher values. Karatas et al. (2012) reported a decrease in LHV of the syngas from 15.07 to 14.26 MJ/Nm<sup>3</sup> as the steam-to-waste tyre ratio increased from 0.273 to 0.50 during waste tyre gasification in a bubbling fluidized bed gasifier. In addition, Zheng et al. (2016) found that the LHV of syngas for polyethylene decreased from 16.11 to 10.52 MJ/Nm<sup>3</sup> as SFR increased from 0.40 to 1.00 during steam gasification in a bench-scale fixed bed reactor at 800 °C (1073 K). However, they observed insignificant

improvement in the LHV of the syngas for bamboo which increased from 5.43 to 5.84 MJ/Nm<sup>3</sup>.

The latter is in contrast to the current finding of the LHV of WT0PB1.

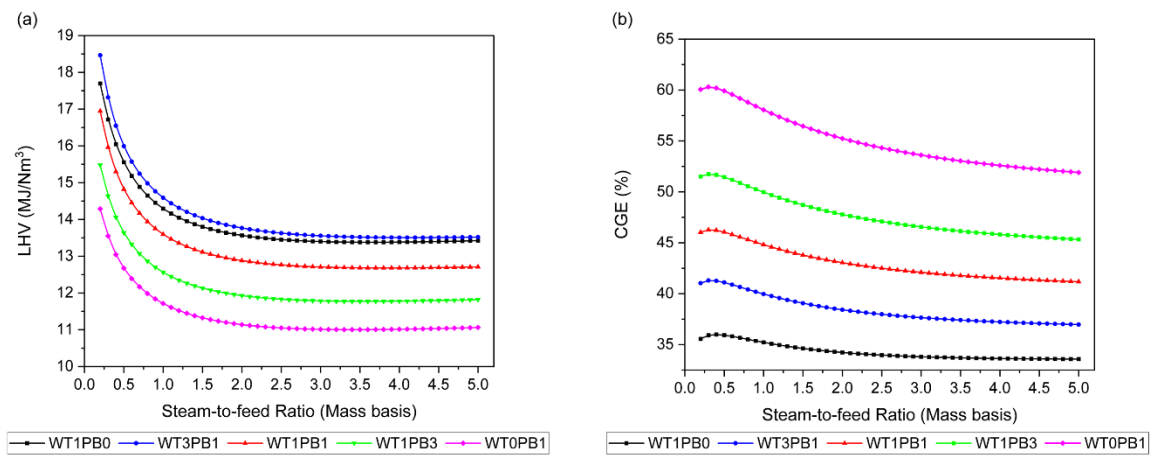


**Figure 5.7** Effect of steam-to-feed ratio on (a) LHV of the syngas, and (b) CGE of the steam gasification process of different pine bark and waste tyre blended samples

As presented in Figure 5.7 (b), the CGE of the gasification process of all the blended samples increased slightly at a lower SFR of around 0.20-0.40 then decreased from 35.99-60.31 MJ/Nm<sup>3</sup> to 33.64-50.79 MJ/Nm<sup>3</sup> at SFR of 5.00. The reduction in CGE was higher for the samples with a high content of PB. For example, the CGE of the WT0PB1 and WT1PB0 reduced by 13.48 and 6.79%, respectively, over SFR of 0.30 to 3.50. This contributed to the higher rate of reduction in CO compared to the increase in H<sub>2</sub> due to the WGS reaction.

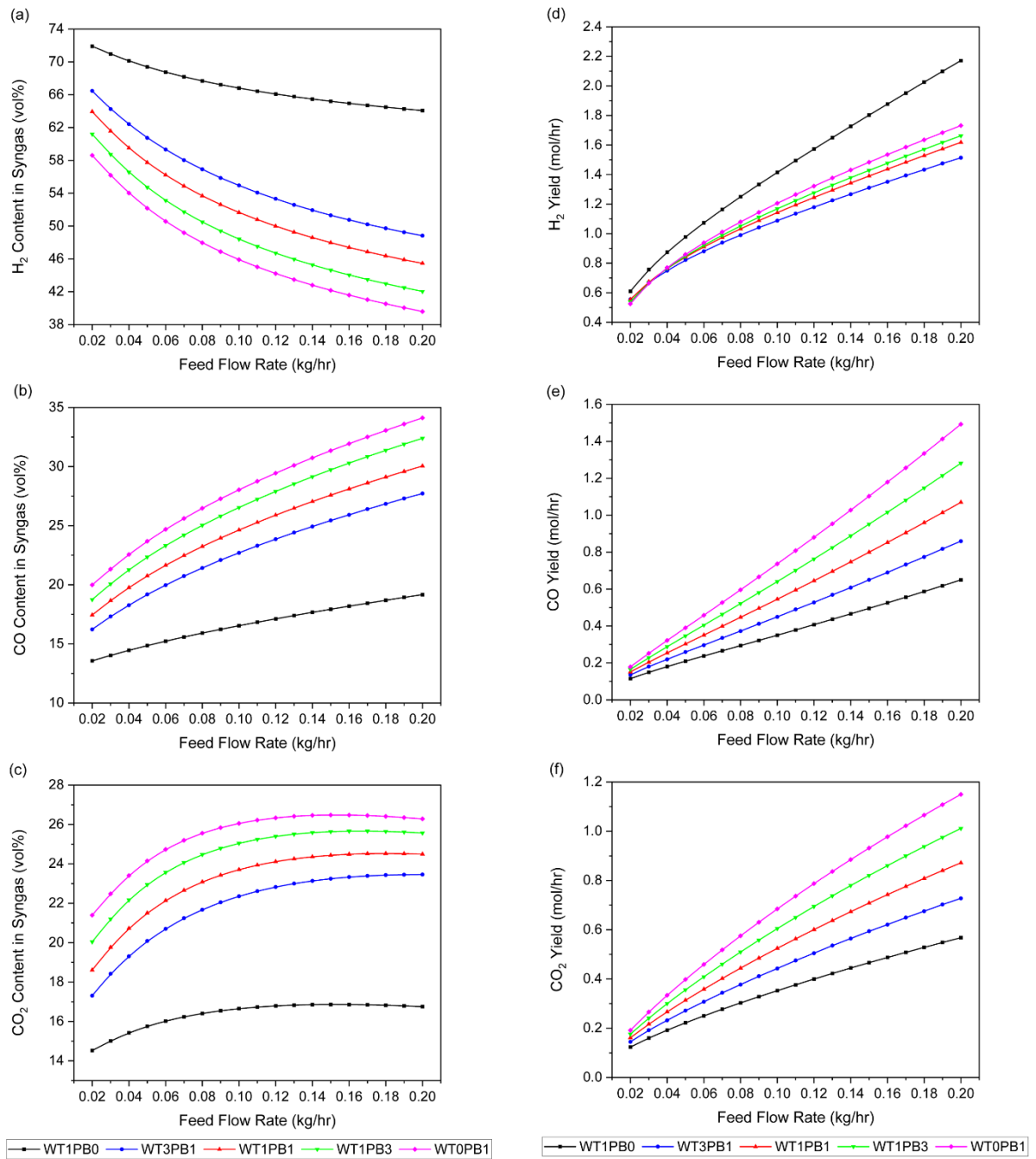
### 5.2.3 Effect of feed flow rate

#### *Syngas composition and yield*

The effect of feed flow rate on syngas composition and yield is depicted in Figure 5.8. Increasing the feed flow rate from 0.02 to 0.20 kg/hr showed a positive effect on CO and CO<sub>2</sub> content and yield. However, H<sub>2</sub> content decreased while its yield increased. The increase in CO and CO<sub>2</sub> contents and the decrease in H<sub>2</sub> is explained by Guo et al. (2014) in which the increased feed flow rate might result in low tar cracking and reforming which in turn

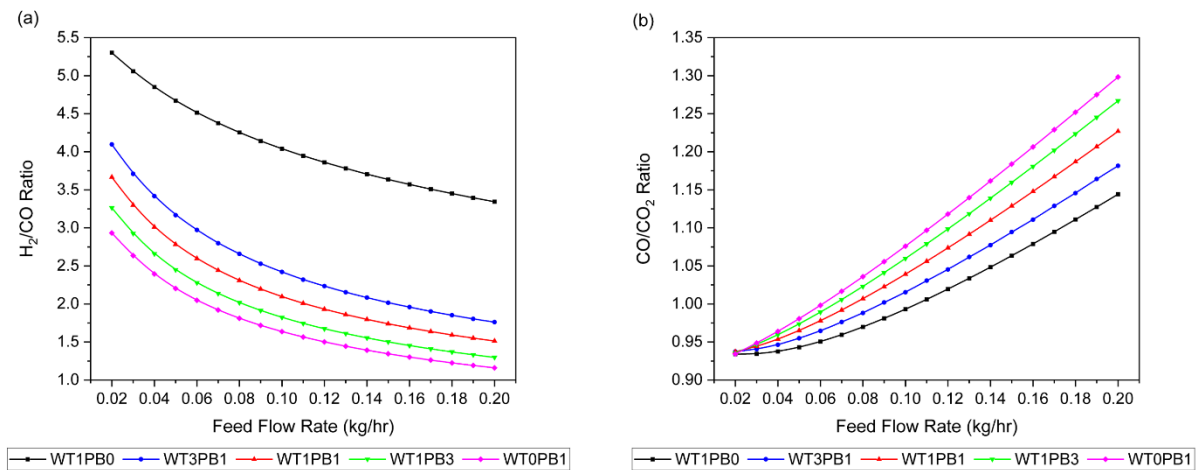
decreases the H<sub>2</sub> content. However, the H<sub>2</sub> formed the main syngas component followed by CO and CO<sub>2</sub>.

Comparing different blended samples, the rate of increase and decrease in the content and yield of different syngas components is the lowest for WT1PB0. The higher H<sub>2</sub> content and yield in the case of WT1PB0 compared to other sample could be due to the higher content of hydrogen in the WT than PB which is 6.66 compared to 4.20 wt%.



**Figure 5.8** Variation in syngas composition (a) H<sub>2</sub>, (b) CO, (c) CO<sub>2</sub>, and yield (d) H<sub>2</sub>, (e) CO, (f) CO<sub>2</sub> with the change in feed flow rate during steam gasification of pine bark and waste tyre at different blend ratios

## H<sub>2</sub>/CO and CO/CO<sub>2</sub> Ratio



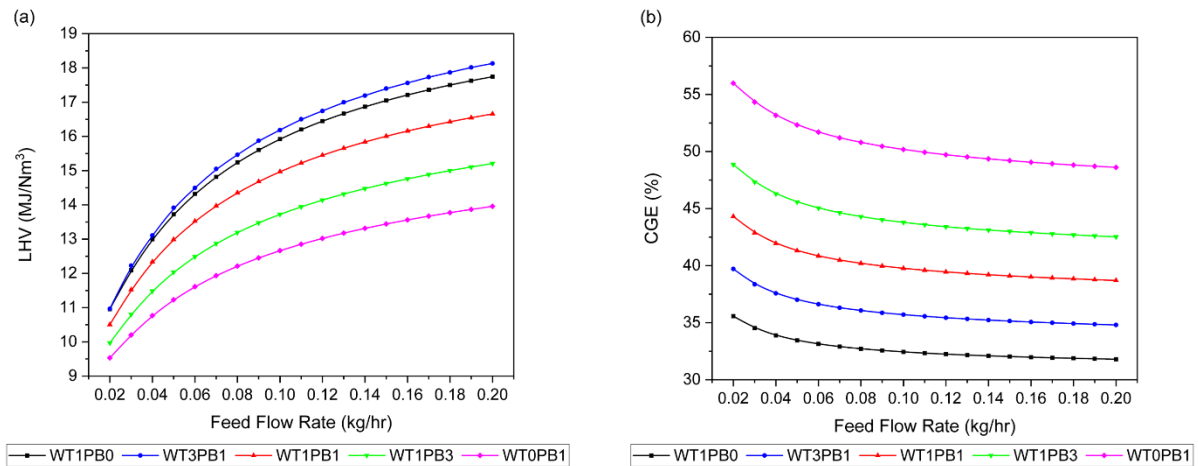
**Figure 5.9** Change in syngas characteristics (a) H<sub>2</sub>/CO, and (b) CO/CO<sub>2</sub> ratio with the change in the feed flow rate for different blend samples during steam gasification

Figure 5.9 presents the syngas characteristics in terms of the H<sub>2</sub>/CO and CO/CO<sub>2</sub> ratios of different blended samples. According to Figure 5.9 (a), the H<sub>2</sub>/CO ratio of the syngas from all the samples showed almost a similar trend. It decreased from 2.93-5.30 to 1.16-3.34 with the highest value obtained at the lowest investigated feed flow rate (i.e. 0.02 kg/hr). The lower and upper bound of the H<sub>2</sub>/CO ratio represents the syngas derived from WT0PB1 and WT1PB0, respectively. As shown earlier that the H<sub>2</sub> content of the syngas from WT1PB0 is higher and the CO content is the lowest compared to other samples, the H<sub>2</sub>/CO in the WT1PB0 case was the higher. The change in H<sub>2</sub>/CO and CO/CO<sub>2</sub> ratio is attributed to the change in the syngas composition as discussed earlier.

## LHV and CGE

Figure 5.10 (a) and (b) display the results of the effect of the change in the feed flow rate on the LHV of the syngas and CGE of the process, respectively. The LHV of the syngas improved with the increase in the feed flow rate. However, the CGE of the process gradually decreased over the examined range of the feed flow rate by 10.59, 12.34, 12.66, 12.96 and 13.17% for WT1PB0, WT3PB1, WT1PB1, WT1PB3 and WT0PB1, respectively. The highest CGE was

achieved with the use of WT0PB1, having minimum and maximum values of 55.98 and 48.61% at feed flow rates of 0.02 and 0.20 kg/hr, respectively.



**Figure 5.10** Effect of feed flow rate on the (a) LHV of the syngas, and (b) CGE of the steam gasification process of different pine bark and waste tyre blended samples

### 5.3 Process analysis of steam/CO<sub>2</sub> co-gasification of pine bark and waste tyre: Case 2

To assess the effect of using steam/CO<sub>2</sub> mixture as gasifying agents on the production of syngas with improved characteristics while utilising CO<sub>2</sub>, the process analysis was conducted. The blended samples; WT1PB0, WT3PB1 and WT0PB1 were selected. This is because the blended samples were sandwiched between the single samples of WT and PB as investigated in Chapter 4 and Case 1 of the current chapter in terms of syngas composition and characteristics as well as process performance. In addition, syngas with better quality in steam gasification, considering H<sub>2</sub>/CO ratio and syngas composition, was obtained with the use of WT1PB0 followed by WT3PB1. Therefore, the effect of operating conditions, including gasification temperature, SFR, CO<sub>2</sub>-to-steam ratio on a mass basis and feed flow rate, is analysed for WT3PB1 in comparison to the single samples; WT1PB0 and WT0PB1.

Details of the process analysis are summarised in Table 5.3. The influence of gasification temperature was investigated in the range from 973 to 1273 K whereas the feed flow rate, CO<sub>2</sub>-to-feed ratio and steam-to-feed ratio remain constant at values of 0.045 kg/hr, 1.90 and

1.90. In addition, the variation in SFR between 0.20 and 5.00 was examined while other operating conditions remain unchanged. To study the effect of varying the CO<sub>2</sub>-to-steam mass ratio between 0.1 and 0.9, the CO<sub>2</sub>-to-feed ratio and steam-to-feed ratio (i.e. SFR) are calculated accordingly, assuming a total gasifying agent flow of 0.173 kg/hr. At the gasification temperature and CO<sub>2</sub>-to-steam ratio of 1173 K and 1:1, the effect of the change in feed flow rate between 0.02 and 0.20 was analysed.

**Table 5.3** Process analysis plan for case 2: steam/CO<sub>2</sub> co-gasification of pine bark and waste tyre

Case ID	Variables			
	Gasification Temperature (K)	CO <sub>2</sub> -to-feed ratio (Mass basis)	SFR (Mass basis)	Feed flow rate (kg/hr)
Section 5.3.1	973-1273	1.90	1.90	0.045
Section 5.3.2	1173	1.90	0.20-5.00	0.045
Section 5.3.3	1173	0.39-3.47	0.39-3.47	0.045
Section 5.3.4	1173	1.90	1.90	0.02-0.20

### 5.3.1 Effect of temperature

#### *Syngas composition and yield*

The effect of the gasification temperature on the composition and yield of the syngas is investigated by setting the CO<sub>2</sub>-to-feed and SFR at 1.90 each, then varying the gasification temperature between 973 and 1273 K. It is found from Figure 5.11 (a) that the concentration of H<sub>2</sub> gradually increases from 15.93 to 19.68 vol% (for WT1PB0) and from 13.80 to 17.17 vol% (for WT3PB1) as the temperature increases from 973 to 1073 K, then nearly stabilize. However, a further increase in the temperature from 1073 to 1273 K causes a surge in the H<sub>2</sub> concentration which increased by 76.85 and 90.34% in the case of WT1PB0 and WT3PB1, respectively. Compared to WT1PB0 and WT3PB1, H<sub>2</sub> concentration in the syngas for WTOPB1 increases continuously from 11.55 to 27.29 vol% when the temperature is raised from 973 to

1273 K. The H<sub>2</sub> yield changed in a similar pattern as the H<sub>2</sub> concentration with an increase in temperature as shown in Figure 5.11 (d).

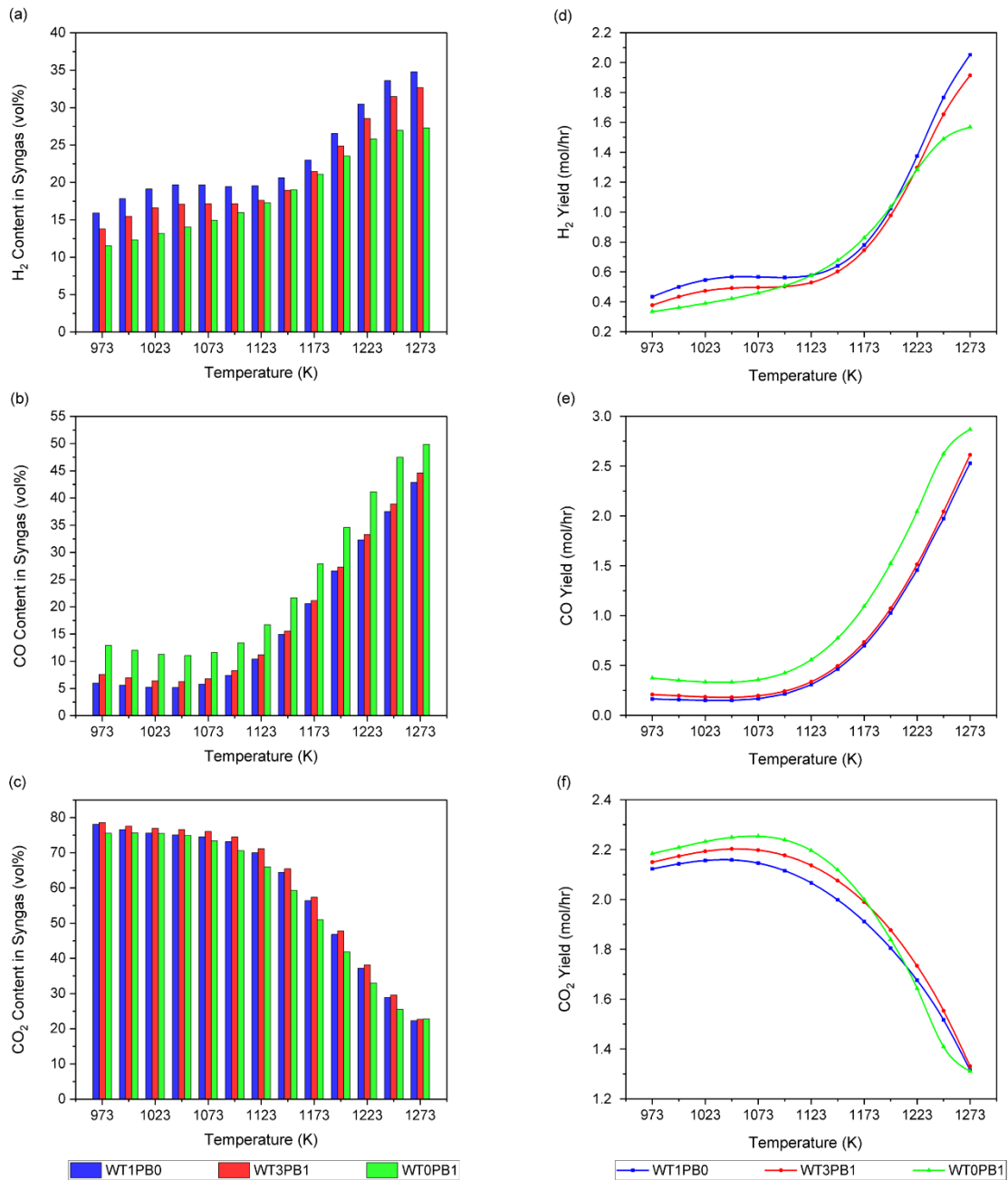
On the other hand, the CO concentration decreased from 6.00 to 5.20 vol% (in the case of WT1PB0), from 7.59 to 6.27 vol% (in the case of WT3PB1) and from 12.89 to 11.05 vol% (in the case of WT0PB1) with the rise in the temperature from 973 to 1048 K. This is presented in Figure 5.11 (b). However, a further increase in the temperature caused an increase in the CO concentration to a final value of 42.89, 44.60 and 49.90 vol% for WT1PB0, WT3PB1 and WT0PB1, respectively, at 1273 K.

Figure 5.11 (c) and (f) display the variation in the CO<sub>2</sub> concentration and yield in the syngas with the temperature change. It is observed that the CO<sub>2</sub> increases at lower temperatures whereas it decreases as the temperature increased from 1073 to 1273 K. Although a decrease in the concentration of CO<sub>2</sub> is noticed at higher temperatures, it is found to be higher than the other gas constituents until a temperature of 1223 K. This is due to the high endothermicity of CO<sub>2</sub>-induced reactions.

The variation in the syngas composition and yield could be explained by the following (i) At lower gasification temperatures (i.e. 973 to 1073 K) the domination of the exothermic WGS reaction (i.e. **R10**) and MR reaction (i.e. **R11**) causes a decrease in CO concentration and yield in favour of increasing H<sub>2</sub> concentration and yield along with CO<sub>2</sub>, (ii) At higher temperatures (i.e. 1098-1273 K), the endothermic MDR (i.e. **R12**) and BD (i.e. **R14**) reactions as well as WG reaction (i.e. **R15**) are dominant causing a steep decrease in CO<sub>2</sub> concentration and yield while CO predominantly increases as well as H<sub>2</sub> (Yusup et al., 2013). Additionally, the increase in H<sub>2</sub> concentration and yield at higher temperatures could also be contributed to the cracking reactions. A total maximum composition and yield of H<sub>2</sub> and CO with a value of 77.68 vol% and 4.58 mol/hr, respectively, was achieved for WT1PB0 at 1273 K and steam-to-CO<sub>2</sub> mass

ratio of 0.50:0.50. This is comparable to WT3PB1 and WT0PB1 with a total composition of 77.28 and 77.19 vol%, respectively, at the same conditions.

Lv et al. (2003) studied air-steam gasification of pine sawdust in a fluidized bed reactor and found that both CO and CO<sub>2</sub> fraction in the syngas given in vol% decreased whereas H<sub>2</sub> increased as the gasification temperature increased from 700 to 900 °C (973 to 1173 K). In contrast, Beheshti et al. (2015) simulated air-steam gasification of biomass in ASPEN Plus® and found that the concentration of both H<sub>2</sub> and CO increases over the temperature from 600 to 800 °C (873 to 1073 K) while that of CO<sub>2</sub> and CH<sub>4</sub> decreases. These discrepancies in the syngas composition between different studies are contributed to the type of feedstock, experimental-related differences, the assumptions made in the case of simulation works, etc.



**Figure 5.11** Variation in syngas composition; (a) H<sub>2</sub>, (b) CO and (c) CO<sub>2</sub>, and yield; (d) H<sub>2</sub>, (e) CO and (f) CO<sub>2</sub> with gasification temperature for steam/CO<sub>2</sub> gasification of WT1PB0, WT3PB1 and WT0PB1

*H<sub>2</sub>/CO and CO/CO<sub>2</sub> Ratio*

The change in H<sub>2</sub>/CO ratio with temperature during steam/CO<sub>2</sub> gasification is depicted in Figure 5.12 (a) for WT1PB0, WT3PB1 and WT0PB1. It can be clearly seen that the increase in the temperature from 973 to 1048 K caused an increase in the H<sub>2</sub>/CO ratio of the syngas. However, H<sub>2</sub>/CO ratio decreased for all the samples with a further increase in the temperature

to 1273 K. The H<sub>2</sub>/CO ratio varies in response to the change in syngas composition, namely H<sub>2</sub> and CO content as explained earlier. The maximum H<sub>2</sub>/CO ratio was achieved at 1048 K for all the samples where it was higher for WT1PB0 with a value of 3.79.

The CO/CO<sub>2</sub> ratio of the syngas for all the samples decreased slightly at lower temperatures. However, a rise in the temperature beyond 1073 K resulted in a noticeable increase in the ratio as provided in Figure 5.12 (b). The highest values of the CO/CO<sub>2</sub> ratio were achieved at the highest temperature (i.e. 1273 K) where it was higher for WT0PB1 than other samples. This could be explained by the enhanced conversion of CO<sub>2</sub> to CO mainly through the BD reaction.

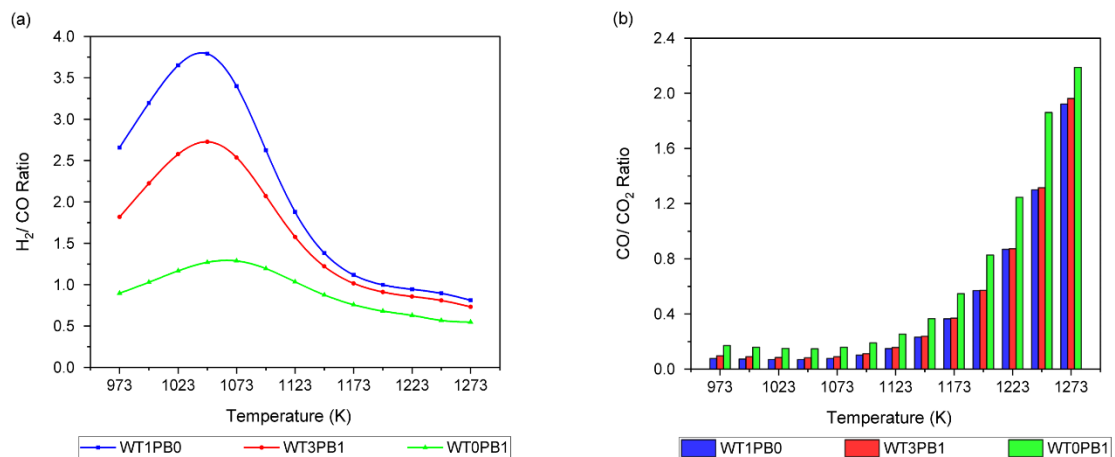


**Figure 5.12** Effect of gasification temperature on syngas characteristics; (a) H<sub>2</sub>/CO, and (b) CO/CO<sub>2</sub> ratios for steam/CO<sub>2</sub> gasification of WT1PB0, WT3PB1 and WT0PB1

### LHV and CGE

Figure 5.13 (a) shows the effect of temperature variation on the LHV of the syngas. It is observed that there is negligible variation in the LHV of the syngas for all the samples over the temperature from 973 to 1073 K where the LHVs were higher for WT1PB0 followed by WT3PB1 and WT0PB1. The increase in LHV of the syngas was more obvious at higher temperatures in which it increased from 6.76 to 9.23 MJ/Nm<sup>3</sup> (in case of WT1PB0), from 6.51 to 9.23 MJ/Nm<sup>3</sup> (in case of WT3PB1) and from 5.68 to 9.25 MJ/Nm<sup>3</sup> (in case of WT0PB1) over

a temperature from 1098 to 1273 K. The rate of increase was higher for WT0PB1 with an increase of 62.74% compared to other samples. This is ascribed to the higher content of CO for WT0PB1 than other syngas constituents compared to other samples.

Figure 5.13 (b) shows that the change in CGE of the process with temperature follows a similar pattern to LHV. It is seen from the figure that the change in CGE is visibly negligible up to a temperature of 1123 K; afterwards, it steeply increases at higher values of gasification temperature (i.e. 1123-1273 K). The CGE of WT1PB0 and WT3PB1 increased from 36.72 and 40.33% to 87.41 and 97.53%, respectively, over the temperature range 1123 to 1273 K. However, WT0PB1 gasification resulted in much higher CGE ranging between 60.55 and 151.02% over the same temperature range.

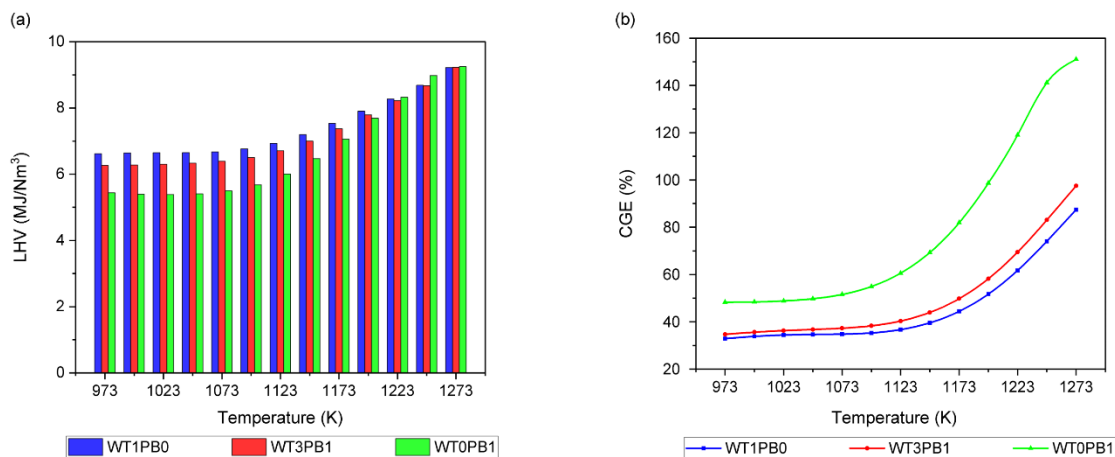


**Figure 5.13** Effect of gasification temperature on (a) LHV of syngas, and (b) CGE of the steam/CO<sub>2</sub> gasification process of WT1PB0, WT3PB1 and WT0PB1

### 5.3.2 Effect of steam-to-feed ratio (i.e. SFR)

#### *Syngas composition and yield*

The effect of the variation in SFR at a fixed CO<sub>2</sub>-to-feed ratio of 1.90 on syngas composition and yield is shown in Figure 5.14. It can be figured out that the increase in SFR had a positive effect on the H<sub>2</sub> concentration as well as yield due to enhanced WGS (Waheed et al., 2016) as well as hydrocarbons and tar reforming reactions, which in turn reduce the CO concentration

and yield while increasing the CO<sub>2</sub>. This is shown in Figure 5.14 (b), (c), (e) and (f). A similar observation was reported by Renganathan et al. (2012) and Kannan et al. (2017) in which increasing the % of steam as a gasifying agent for any fixed value of mol of CO<sub>2</sub>/C results in an increase in H<sub>2</sub> composition and a decrease in CO during steam/CO<sub>2</sub> gasification of a model biomass and waste plastics, respectively, in ASPEN Plus®.

The increase in H<sub>2</sub> content and yield in the case of WT1PB0 was higher than in other samples. The H<sub>2</sub> content and yield increased from 13.73 vol%, 0.43 mol/hr (i.e. SFR = 0.20) to 26.45 vol%, 0.91 mol/hr (i.e. SFR = 5.00). Although the CO<sub>2</sub> content and yield keep increasing, it was lower than other samples. On the other hand, the CO content and yield continue decreasing, where both WT1PB0 and WT3PB1 showed a similar pattern and slight differences at higher SFR.

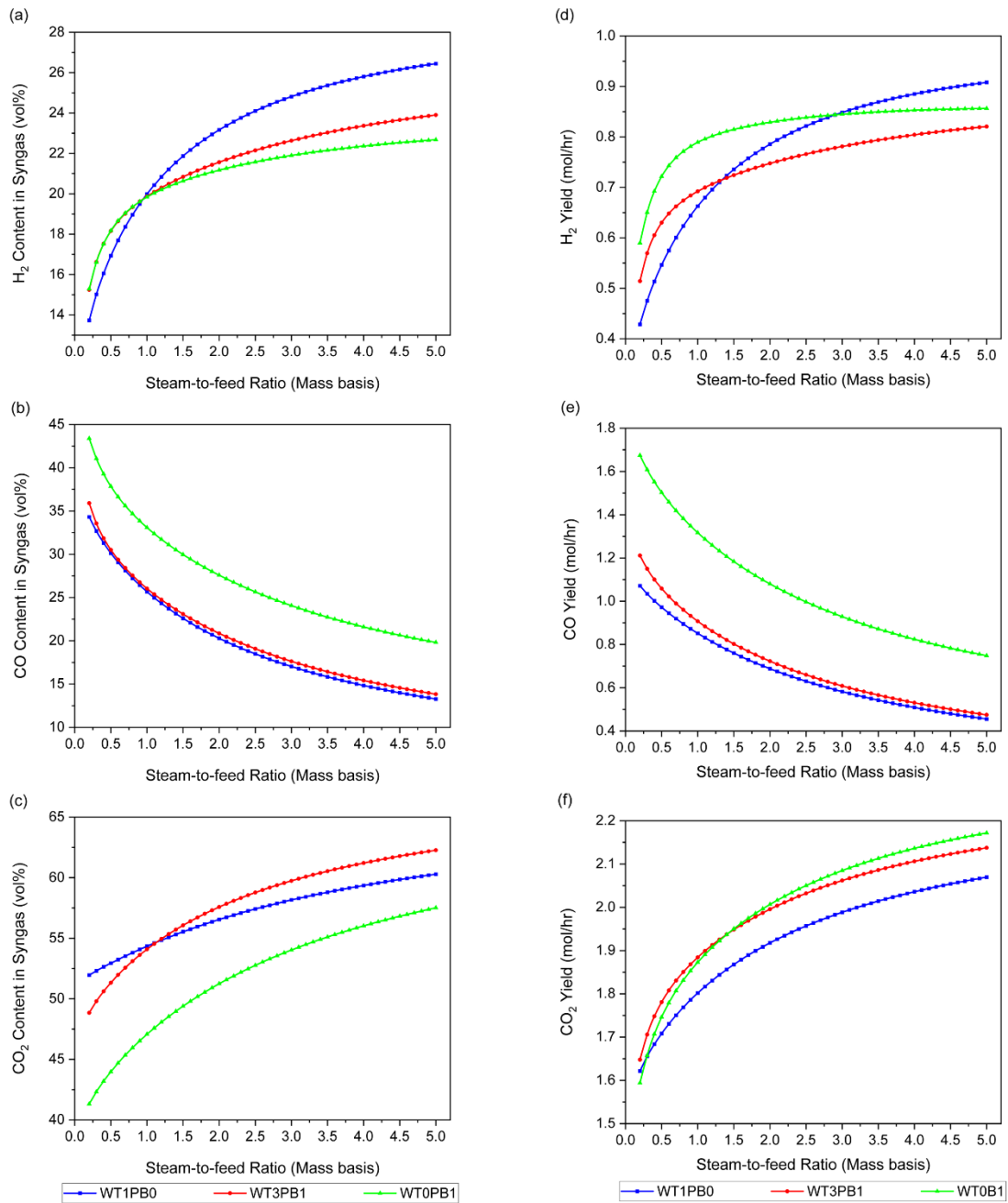


**Figure 5.14** Effect of steam-to-feed ratio on syngas composition; (a) H<sub>2</sub>, (b) CO and (c) CO<sub>2</sub>, and yield; (a) H<sub>2</sub>, (b) CO and (c) CO<sub>2</sub> during steam/CO<sub>2</sub> gasification of WT1PB0, WT3PB1 and WT0PB1

### *H<sub>2</sub>/CO and CO/CO<sub>2</sub> Ratio*

The variation in H<sub>2</sub>/CO and CO/CO<sub>2</sub> ratios in response to the change in SFR showed opposite trends to each other. The results are displayed in Figure 5.15 (a) and (b). The increase in H<sub>2</sub>/CO ratio was relatively linear and it is associated with the increase in H<sub>2</sub> content and the decrease in CO content for all the blend samples. The maximum H<sub>2</sub>/CO ratio was achieved at a SFR of

5.00, where it was the highest for WT1PB0 with a value of 1.99. Looking at Figure 5.15 (b), the CO/CO<sub>2</sub> ratio, on the other hand, decreased gradually for all the samples where WT1PB0 and WT3PB1 showed relatively similar values of CO/CO<sub>2</sub> ratio over the examined range of SFR with an average percentage difference of 1.60%. The CO/CO<sub>2</sub> ratio decreased from 1.05 to 0.34 for WT0PB1.

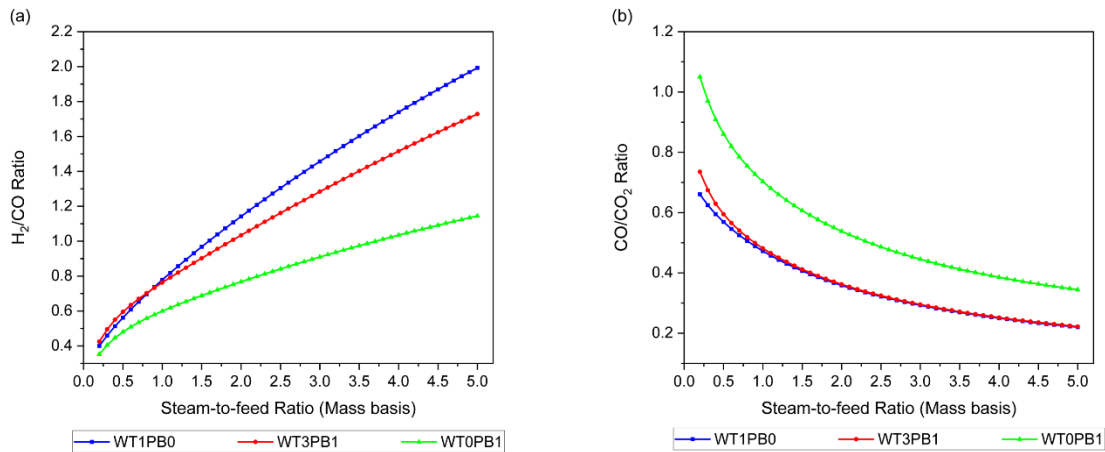


**Figure 5.15** Effect of steam-to-feed ratio on syngas characteristics; (a) H<sub>2</sub>/CO, and (b) CO/CO<sub>2</sub> ratios for WT1PB0, WT3PB1 and WT0PB1 during steam/CO<sub>2</sub> gasification

### LHV and CGE

The results of the influence of SFR on LHV of the syngas and CGE of the process are shown in Figure 5.16 (a) and (b), respectively. Both LHV of the syngas and CGE of the process decreased with the increase in the SFR. However, WT1PB0 showed higher LHV but lower CGE compared to other samples. The LHV of the syngas decreased from 8.96, 8.62 and 8.38 MJ/Nm<sup>3</sup> to 6.77, 6.62 and 6.18 MJ/Nm<sup>3</sup> for WT1PB0, WT3PB1 and WT0PB1, respectively, when the SFR increased from 0.02 to 5.00. The decrease in LHV is associated with the change in syngas composition, in which the decrease in CO is higher than the increase in H<sub>2</sub> as shown in Figure 5.14 (a) and (b). The CGE of the process, on the other hand, decreased from 50.02, 56.94 and 95.91% to 41.17, 44.02 and 68.88% for WT1PB0, WT3PB1 and WT0PB1, respectively, when the SFR increased from 0.02 to 5.00. Fajimi et al. (2021), however, found an increase in the

LHV of the syngas in response to the increase in steam-to-waste tyre ratio in air-steam gasification of the waste tyre. Karatas et al. (2012) reported syngas with LHV of 15.21 MJ/Nm<sup>3</sup> during steam gasification of the waste tyre in the bubbling fluidized bed at temperature and SFR of around 1073 K and 0.38, respectively.

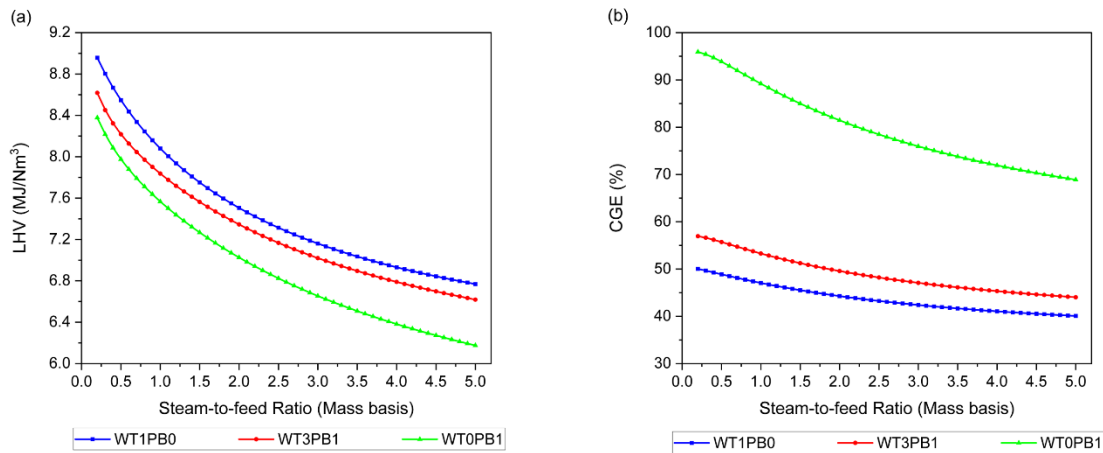


**Figure 5.16** Effect of steam-to-feed ratio on (a) LHV of syngas, and (b) CGE of the steam/CO<sub>2</sub> gasification process of WT1PB0, WT3PB1 and WT0PB1

### 5.3.3 Effect of CO<sub>2</sub>-to-steam ratio

#### *Syngas composition and yield*

The effect of CO<sub>2</sub>-to-steam ratio on syngas composition and yield was examined at a temperature of 1173 K. This is conducted by varying steam and CO<sub>2</sub> flow rate while keeping the total flow constant. The results are presented in Figure 5.17. From Figure 5.17 (a) and (d), we can see that increasing the steam fraction in the gasifying agent by replacing CO<sub>2</sub> results in an increase in both H<sub>2</sub> concentration and yield in the syngas for all the samples. However, the rate of increase is higher for WT1PB0 compared to WT3PB1 and WT0PB1. Compared to pure steam and CO<sub>2</sub> gasification, the highest H<sub>2</sub> concentration and yield was observed at CO<sub>2</sub>-to-steam mass ratio of 0.10:0.90 for all blended samples which was higher for WT1PB0 with values of 52.76 vol% and 0.93 mol/hr. In contrast, an opposite trend was observed with CO concentration and yield. It decreased from 28.48 vol%, 1.40 mol/hr to 12.27 vol%, 0.22 mol/hr

(in case of WT1PB0), from 29.27 vol%, 1.51 mol/hr to 13.76 vol%, 0.24 mol/hr (in case of WT3PB1) and from 36.68 vol%, 2.08 mol/hr to 20.50 vol%, 0.43 mol/hr (in case of WT0PB1) in response to the change in steam fraction in the gasifying agent from 0.10 to 0.90. Looking at CO<sub>2</sub> composition and yield displayed in Figure 5.17 (c) and (f), there is a slight decrease in the CO<sub>2</sub> concentration in the syngas as the CO<sub>2</sub>-to-steam ratio decreased from 0.90:0.10 to 0.60:0.40, afterwards, the decrease in CO<sub>2</sub> concentration was more obvious. The CO<sub>2</sub> concentration and yield were lower in the syngas in the case of pure steam compared to the steam/CO<sub>2</sub> mixture. For example, syngas from WT3PB1 had CO<sub>2</sub> concentration and yield of 19.70 vol% and 0.25 mol/hr, respectively, in the case of pure steam compared to 38.99 vol% and 0.69 mol/hr with steam/CO<sub>2</sub> mixture with a mass ratio of 0.90:0.10. Although the dry and steam reforming reactions along with the WGS reaction would be playing a role as indicated by the increase in H<sub>2</sub> concentration and yield, there would be a fraction of unconverted CO<sub>2</sub> in the syngas. This leads to lower CO and higher CO<sub>2</sub> concentration with the use of a steam/CO<sub>2</sub> mixture with higher steam content compared to pure steam. The selection of a proper CO<sub>2</sub>-to-steam ratio would contribute to obtaining syngas with a flexible H<sub>2</sub>/CO ratio while ensuring the proper utilisation of CO<sub>2</sub>. The total H<sub>2</sub> and CO concentration in syngas was higher than 60.00 vol% for all the samples at a CO<sub>2</sub>-to-steam mass ratio of 0.10:0.90.

Pandey et al. (2022) studied biomass gasification in an auto-thermal downdraft fixed bed gasifier using a mixture of air and CO<sub>2</sub> as a gasifying agent where CO<sub>2</sub> is used by replacing N<sub>2</sub> at a specific fraction. They found that increasing CO<sub>2</sub> content in the gasifying agent resulted in an increase in CO<sub>2</sub> as well as CO fraction in the syngas. However, the CO fraction in the produced gas was reduced when the CO<sub>2</sub> content in the gasifying agent was higher than 30.00 vol%. On the other hand, Kannan et al. (2017) reported an increase in CO mole fraction with an increase in CO<sub>2</sub>/C mol ratio and steam content to a specific value where any further

increase caused a negative effect on the CO fraction of the syngas. However, for a specific value of the CO<sub>2</sub>/C molar ratio, the higher the steam content in the gasifying agent is the lower the CO content and the higher the CO<sub>2</sub> content.

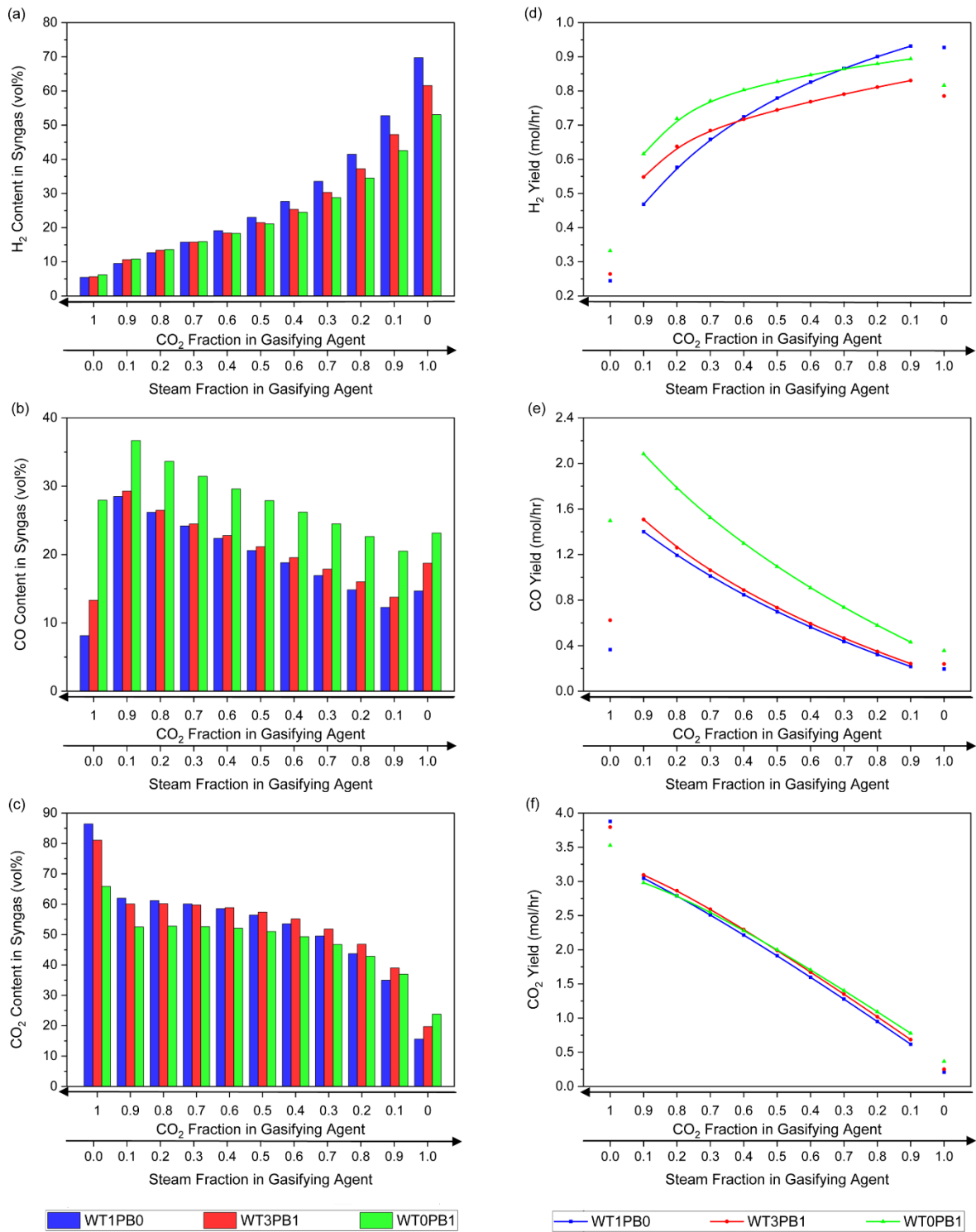


**Figure 5.17** Effect of CO<sub>2</sub>-to-steam ratio in the gasifying agent on syngas composition; (a) H<sub>2</sub>, (b) CO and (c) CO<sub>2</sub>, and yield; (a) H<sub>2</sub>, (b) CO and (c) CO<sub>2</sub> during steam/CO<sub>2</sub> gasification of WT1PB0, WT3PB1 and WT0PB1

### *H<sub>2</sub>/CO and CO/CO<sub>2</sub> Ratio*

Due to the variation in the syngas composition and yield with the change in CO<sub>2</sub>-to-steam ratio, the H<sub>2</sub>/CO and CO/CO<sub>2</sub> ratios change accordingly. The results are shown in Figure 5.18 (a) and (b).

It can be seen that the increase in steam content in the gasifying coupled with the decrease in CO<sub>2</sub> results in an increase in H<sub>2</sub>/CO ratio due to enhanced steam reforming, WGS and WG reactions as explained before. The average H<sub>2</sub>/CO ratio varied between 0.33 and 3.27 over the examined CO<sub>2</sub>-to-steam ratio, considering all the samples. Similar to the total H<sub>2</sub> and CO composition and excluding the pure steam gasification, the highest H<sub>2</sub>/CO ratio with a value of 4.30 is reported for WT1PB0 with CO<sub>2</sub>-to-steam ratio of 0.10:0.90. Due to the wide variety of the H<sub>2</sub>/CO ratio of the syngas from the use of steam/CO<sub>2</sub> mixture, it confirms the flexibility of the syngas for the various end-uses through the adjustment of CO<sub>2</sub>-to-steam ratio.

On the contrary, the CO/CO<sub>2</sub> ratio decreased with an increase in steam content in the gasifying agent. However, it was higher in the case of pure steam and lower in the case of pure CO<sub>2</sub>.

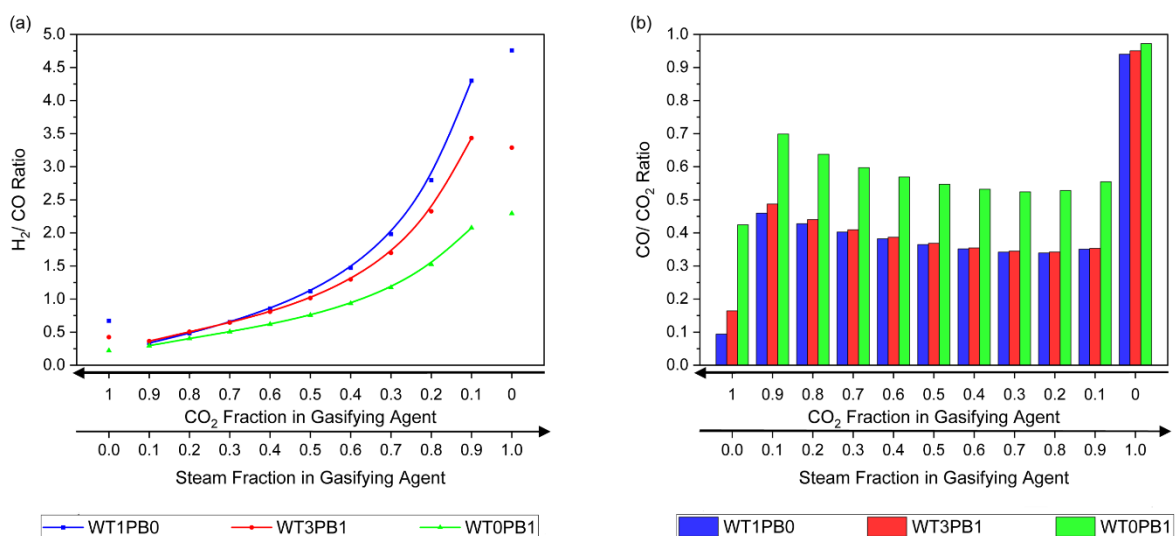


**Figure 5.18** Variation in syngas characteristics; (a) H<sub>2</sub>/CO, and (b) CO/CO<sub>2</sub> ratios for WT1PB0, WT3PB1 and WT0PB1 with the change in CO<sub>2</sub>-to-steam ratio in the gasifying agent during steam/CO<sub>2</sub> gasification

### *LHV and CGE*

The variation in the LHV of the syngas and CGE of the gasification process with the change in CO<sub>2</sub> and steam content of the gasifying agent is shown in Figure 5.19 (a) and (b). From Figure 5.19 (a), it is apparent that the increase in steam fraction in the gasifying agent while decreasing the CO<sub>2</sub> content had a positive effect on the LHV of the syngas from all the samples. At lower steam contents of 0.1 to 0.6 (on a mass basis) in the gasifying agent, the rate of increase was lower compared to higher steam content. The increase in LHV of the syngas from WT1PB0 and WT3PB1 was higher than WT0PB1. It increased by 51.44, 52.80 and 34.07% from the CO<sub>2</sub>-to-steam ratio of 0.60:0.40 to 0.10:0.90 for WT1PB0, WT3PB1 and WT0PB1, respectively. This is explained by the higher production of H<sub>2</sub> for WT1PB0 and WT3PB1 compared to WT0PB1 coupled with the decrease in CO production. During pure steam gasification, the highest LHV of a value of 13.51 MJ/Nm<sup>3</sup> was obtained from waste tyre and pine park blend with a waste tyre content of 75.00 wt%. This is in agreement with the study of Yusup et al. (2013) in which the increase in waste tyre content in the blend to 30 wt%, improved the LHV of the syngas to a value of 12.30 MJ/Nm<sup>3</sup> during steam gasification of waste tyre and palm kernel blend. Use of steam/CO<sub>2</sub> mixture produced syngas with better LHV compared to pure CO<sub>2</sub>. In the case of using steam/CO<sub>2</sub> mixture as a gasifying agent, the highest LHV with the values of 10.91, 10.75 and 9.20 MJ/Nm<sup>3</sup> was obtained at a CO<sub>2</sub>-to-steam ratio of 0.10:0.90 for WT1PB0, WT3PB1 and WT0PB1, respectively. Pandey et al. (2022) noticed an increase in the LHV of the producer gas from biomass as the fraction of CO<sub>2</sub> in the gasifying agent (i.e. a mixture of air and CO<sub>2</sub>) increased. It increased from 5.79 to 6.44 MJ/Nm<sup>3</sup> with an increase in CO<sub>2</sub> fraction in the gasifying agent from 0 to 30 vol% using 35 vol% O<sub>2</sub>-enriched air.

Figure 5.19 (b) shows that the increase in steam content in the gasifying agent coupled with the decrease in CO<sub>2</sub> content results in a decline in CGE over the examined range of CO<sub>2</sub>-to-steam mass ratio. However, the use of steam/CO<sub>2</sub> mixture resulted in higher CGE than pure CO<sub>2</sub> shown as a CO<sub>2</sub> fraction of 1 for all the samples. This would be associated with the decrease in the product of syngas yield and LHV. The maximum CGE was achieved at a CO<sub>2</sub>-to-steam ratio of 0.90:0.10 where the CGE values were 56.87, 64.21 and 111.37% for WT1PB0, WT3PB1 and WT0PB1, respectively.

In agreement with the current results, Renganathan et al. (2012) found that the CGE of the gasification of a model biomass increased with the increase in the mole of CO<sub>2</sub> as gasifying agent per mole of C in the feed, reaching a maximum value of 1.20 (120%) regardless the increase in the mol fraction of steam in the gasifying agent. However, the CGE was reported by Renganathan et al. (2012) to be higher with the higher fraction of steam in the gasifying agent at a given mol of CO<sub>2</sub> per mol of C.

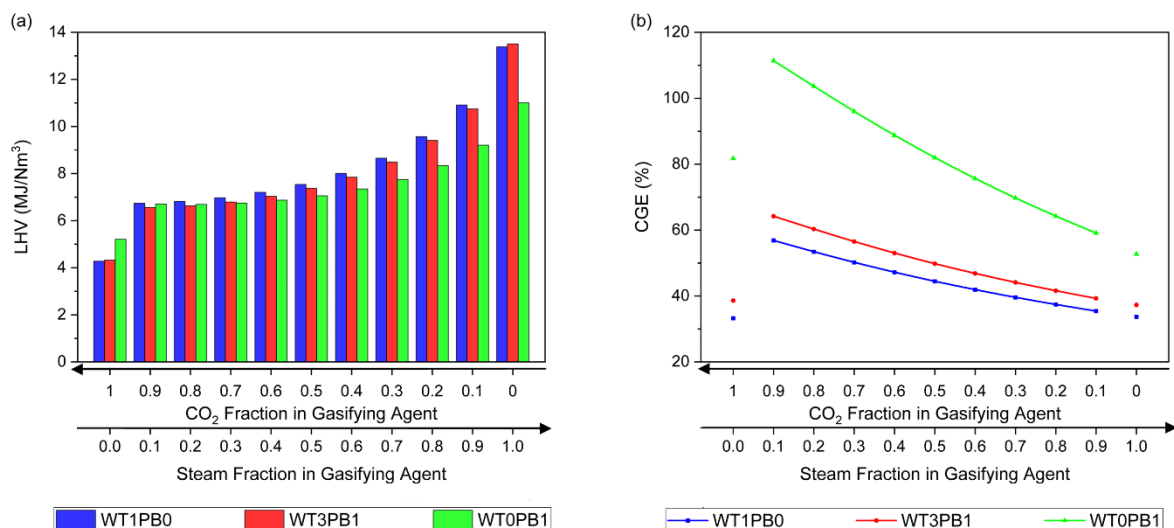


**Figure 5.19** Results of the effect of CO<sub>2</sub>-to-steam ratio in the gasifying agent on (a) LHV of syngas, and (b) CGE of the steam/CO<sub>2</sub> gasification process for WT1PB0, WT3PB1 and WT0PB1

#### 5.3.4 Effect of feed flow rate

##### *Syngas composition and yield*

The increase in feed flow rate during steam/CO<sub>2</sub> gasification of the waste tyre, pine bark and their blend showed a positive effect on H<sub>2</sub> content and yield as provided in Figure 5.20 (a) and (d). The H<sub>2</sub> content for WT1PB0 was higher than other samples. This could be due to a higher fraction of H in the composition of WT compared to PB. This will result in a higher formation of hydrocarbons and tar during devolatilization which then take part in cracking as well as steam and dry reforming reactions. The difference in the H<sub>2</sub> content for WT3PB1 and WT0PB1 was low at lower feed flow rates (i.e. 0.02-0.08 kg/hr) and then the H<sub>2</sub> content increases to maximum values of 33.12 and 30.65 vol%, respectively at a feed flow rate of 0.20 kg/hr.

However, CO and CO<sub>2</sub> content were negatively affected whereas the yield of both components increased. Looking at Figure 5.20 (b) it can be noticed that the CO content of syngas varies between the samples where it decreases for WT1PB0 from 22.82 to 15.74 vol% over the examined range of feed flow rate. However, the CO content of the syngas for WT3PB1 decreases first from 22.92 to 18.88 vol% corresponding to the decrease in feed flow rate from 0.02 to 0.16 kg/hr and then shows a negligible increase to 19.00 vol% at a feed flow rate of 0.20 kg/hr. Compared to WT1PB0 and WT3PB1, the decrease in CO content for WT0PB1 is much lower and decreases from 29.92 to 26.52 vol% over the feed flow rate 0.02-0.11 kg/hr then starts to increase to a final concentration of 27.61 vol% at feed flow rate of 0.20 kg/hr.

The CO<sub>2</sub> content of the syngas decreases with the feed flow rate as shown in Figure 5.20 (c). A higher CO<sub>2</sub> content is reported with WT3PB1 followed by WT1PB0. However, WT0PB1 shows the lowest CO<sub>2</sub> content. The higher CO<sub>2</sub> content of the syngas for the samples with

higher content of WT could be attributed to a higher fraction of unconverted CO<sub>2</sub> contributing to the composition of the final syngas product.

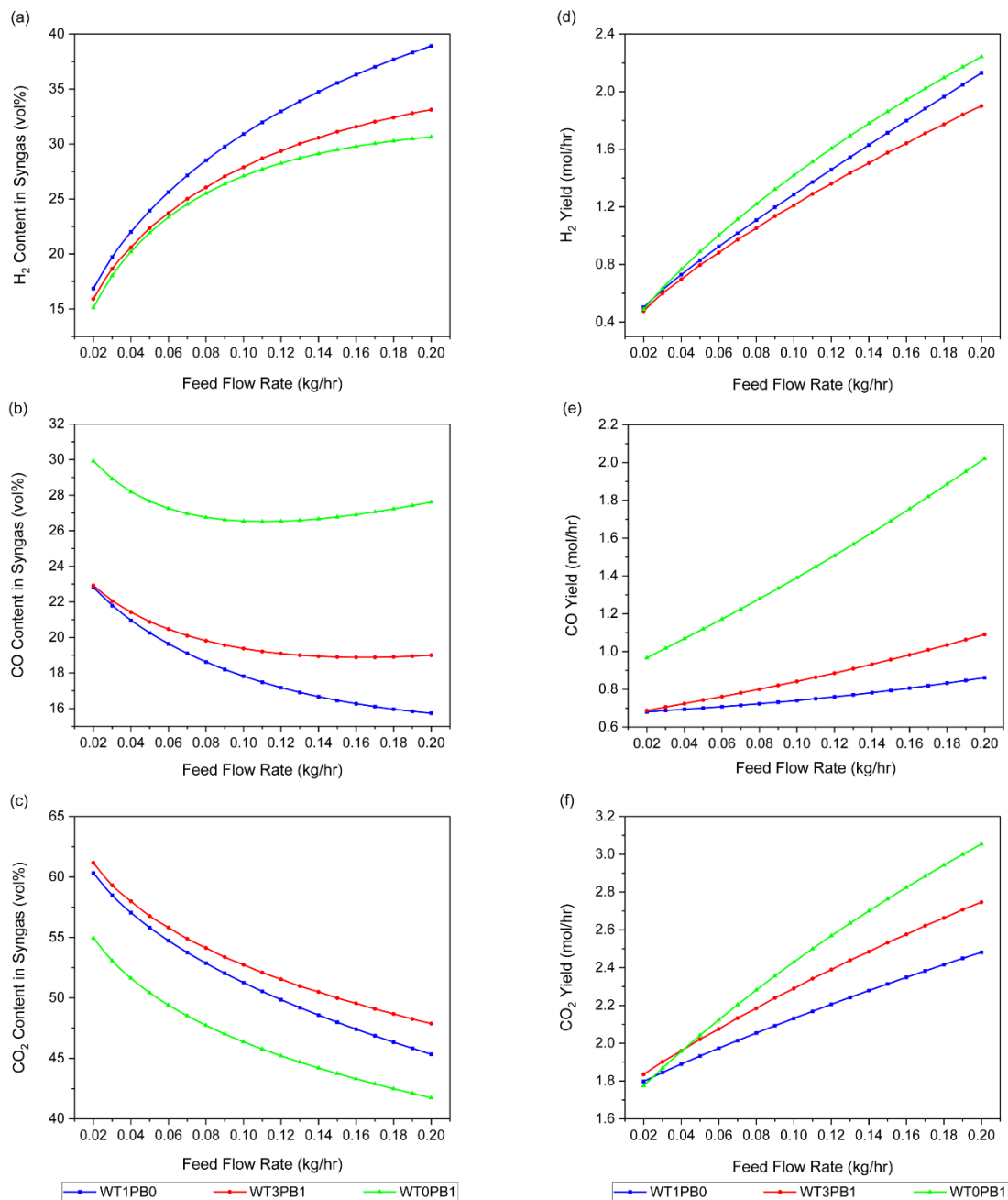


**Figure 5.20** Effect of feed flow rate on syngas composition; (a) H<sub>2</sub>, (b) CO and (c) CO<sub>2</sub>, and yield; (a) H<sub>2</sub>, (b) CO and (c) CO<sub>2</sub> during steam/CO<sub>2</sub> gasification of WT1PB0, WT3PB1 and WT0PB1

### H<sub>2</sub>/CO and CO/CO<sub>2</sub> Ratio

The effect of feed flow rate on H<sub>2</sub>/CO and CO/CO<sub>2</sub> ratios is illustrated in Figure 5.21 (a) and (b). As Figure 5.21 (a) shows, there is an increase in the H<sub>2</sub>/CO ratio of the syngas for all the

samples. However, the increase for WT1PB0 was much higher than other samples in which it increased from 0.74 to 2.74 as the waste tyre flow increases from 0.02 to 0.20 kg/hr. The H<sub>2</sub>/CO ratio for WT0PB1 increases gradually as the feed flow increases from 0.02 to 0.15 kg/hr, thereafter it relatively shows a nearly constant value of 1.11 where the increase was less than 1%. This could be associated with the lower rate of increase in the H<sub>2</sub> content along with the slight increase of CO content starting at feed flow rate of nearly 0.11 kg/hr as highlighted earlier and confirmed by the increase in CO/CO<sub>2</sub> ratio as shown in Figure 5.21 (b).

The change of CO/CO<sub>2</sub> ratio for different samples in response to the increase in feed flow rate resembles the CO content variation. It decreases for WT1PB0 and increases for WT0PB1. However, CO/CO<sub>2</sub> ratio for WT3PB1 decreases first and then increases at a feed flow rate of 0.08 kg/hr.

The highest H<sub>2</sub>/CO ratio of 2.47, 1.74 and 1.11 is reported for WT1PB0, WT3PB1 and WT0PB1, respectively, at a feed flow rate of 0.2 kg/hr whereas the highest CO/CO<sub>2</sub> ratio of 0.66 is found for WT0PB1.

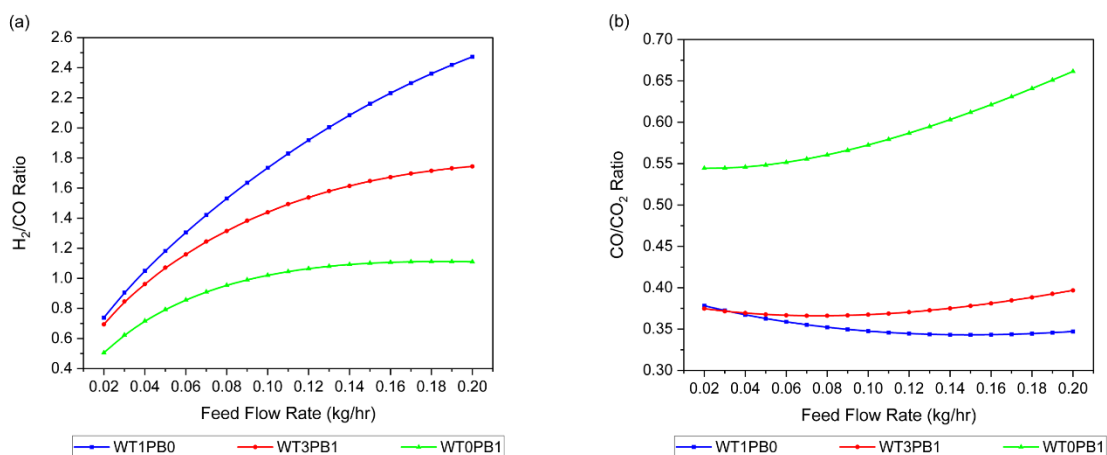


**Figure 5.21** Variation in syngas characteristics; (a) H<sub>2</sub>/CO, and (b) CO/CO<sub>2</sub> ratios for WT1PB0, WT3PB1 and WT0PB1 with the change in feed flow rate during steam/CO<sub>2</sub> gasification

## LHV and CGE

The change in LHV of the syngas and CGE of the process shows an opposite trend to each other with the change in feed flow rate. These results are presented in Figure 5.22 (a) and (b).

The LHV of the syngas increases with the increase in feed flow rate. It improved from 5.61, 5.54 and 5.85 MJ/Nm<sup>3</sup> to 13.01, 12.50 and 10.34 MJ/Nm<sup>3</sup> for WT1PB0, WT3PB1 and WT0PB1, respectively.

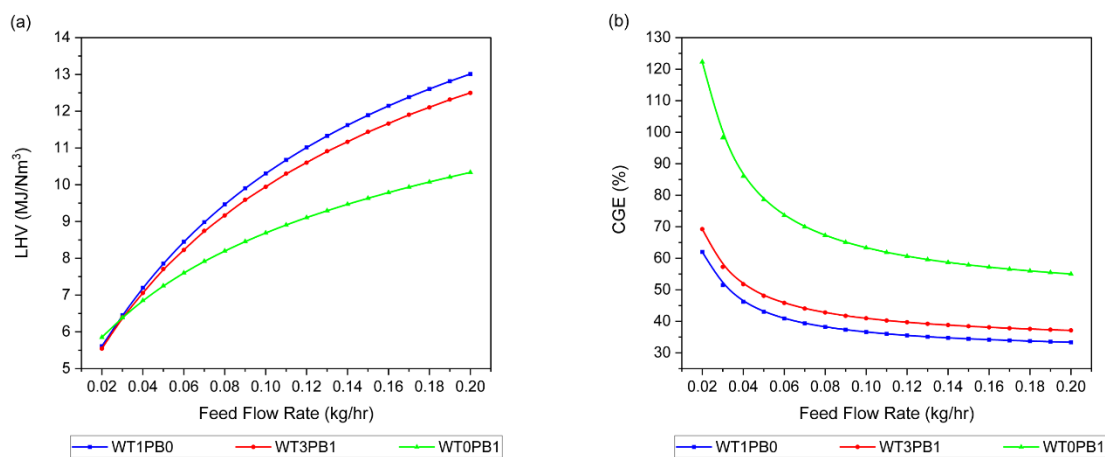


**Figure 5.22** Results of the effect of feed flow rate on (a) LHV of syngas, and (b) CGE of the steam/CO<sub>2</sub> gasification process for WT1PB0, WT3PB1 and WT0PB1

On the other hand, the CGE decreases with the feed flow rate in which the rate of decrease was high for WT0PB1 and lower for WT1PB0. It decreased by 46.20, 46.39 and 55.02% for WT1PB0, WT3PB1 and WT0PB1, respectively.

## 5.4 Comparative evaluation of syngas composition and process performance from CO<sub>2</sub>, steam and steam/CO<sub>2</sub> gasification

A comparison of gasification of WT1PB0, WT3PB1 and WT0PB1 using different gasifying agents was made. Table 5.4 summarises both the operating conditions and process analysis results of CO<sub>2</sub>, steam and steam/CO<sub>2</sub> gasification at the given conditions. Comparing the effect of different gasifying agents for a single sample at temperature and feed flow rate of 1173 K and 0.045 kg/hr, respectively, the use of a steam/CO<sub>2</sub> mixture produced syngas with

higher content and yield of H<sub>2</sub> and CO. The effect was more obvious with WT1PB0 and WT3PB1. The H<sub>2</sub> concentration improved from an average value of 5.77 vol% (in the case of CO<sub>2</sub> gasification) to 21.86 vol% (in the case of steam/CO<sub>2</sub> gasification). Although the steam participates in the WGS reaction producing H<sub>2</sub> along with CO<sub>2</sub>, replacing 50% of CO<sub>2</sub> on a mass basis by steam, reduced CO<sub>2</sub> concentration in the syngas by 34.73, 29.20 and 22.54% for WT1B0, WT3PB1 and WT0PB1, respectively. The total H<sub>2</sub> and CO concentration during steam/CO<sub>2</sub> gasification was highest for WT1PB0 and found to be 3 times higher than CO<sub>2</sub> gasification. The H<sub>2</sub>/CO ratio improved from 0.67 to 1.12 for WT1PB0, from 0.43 to 1.02 for WT3PB1 and from 0.22 to 0.76 for WT0PB1. The average LHV increased from 4.60 MJ/Nm<sup>3</sup> (in the case of CO<sub>2</sub> gasification) to 7.32 MJ/Nm<sup>3</sup> (in the case of steam/CO<sub>2</sub> gasification). A positive change in the CGE of the process is found with the use of steam/CO<sub>2</sub> compared to steam only. It increased from 33.25, 38.58 and 81.72% to 44.44, 49.79 and 81.93% for WT1PB0, WT3PB1 and WT0PB1.

Steam gasification resulted in syngas with the highest H<sub>2</sub> content and lowest CO<sub>2</sub> content in the syngas compared to CO<sub>2</sub> and steam/CO<sub>2</sub> gasification. The H<sub>2</sub>/CO ratio improved by more than 3 times compared to steam/CO<sub>2</sub> gasification and by more than 7 times compared to CO<sub>2</sub> gasification.

WT1PB0 showed the lowest H<sub>2</sub> and highest CO<sub>2</sub> content during CO<sub>2</sub> gasification compared to other samples. During steam/CO<sub>2</sub> gasification, however, WT1PB0-derived syngas had the highest H<sub>2</sub> content and the lowest CO<sub>2</sub> content.

**Table 5.4** A comparison of CO<sub>2</sub>, steam and steam/CO<sub>2</sub> gasification results of WT1PB0, WT3PB1 and WT0PB1 at a temperature of 1173 K

Sample	WT1PB0			WT3PB1			WT0PB1		
Gasification medium	CO <sub>2</sub> only	Steam/CO <sub>2</sub>	Steam only	CO <sub>2</sub> only	Steam/CO <sub>2</sub>	Steam only	CO <sub>2</sub> only	Steam/CO <sub>2</sub>	Steam only
<b>Condition</b>									
Feed flow rate (kg/hr)	0.045			0.045			0.045		
CO <sub>2</sub> -to-feed ratio	3.90	1.90	N/A	3.90	1.90	N/A	3.90	1.90	N/A
CO <sub>2</sub> flow rate (kg/hr)	0.174	0.087	N/A	0.174	0.087	N/A	0.174	0.087	N/A
SFR	N/A	1.90	3.90	N/A	1.90	3.90	N/A	1.90	3.90
Steam flow rate (kg/hr)	N/A	0.087	0.174	N/A	0.087	0.174	N/A	0.087	0.174
<b>Syngas Composition (vol%)</b>									
H <sub>2</sub>	5.45	23.00	69.74	5.65	21.47	61.57	6.20	21.11	53.06
CO	8.13	20.59	14.66	13.31	21.15	18.72	27.95	27.89	23.14
CO <sub>2</sub>	86.42	56.41	15.60	81.05	57.38	19.71	65.85	51.00	23.80
<b>Syngas Yield (mol/hr)</b>									
H <sub>2</sub>	0.25	0.78	0.93	0.26	0.74	0.79	0.33	0.82	0.82
CO	0.37	0.70	0.20	0.62	0.73	0.24	1.50	1.09	0.36
CO <sub>2</sub>	3.88	1.91	0.21	3.79	1.99	0.25	3.53	2.00	0.37
Syngas yield (Nm <sup>3</sup> /kg of feed)	2.59	1.96	0.84	2.65	2.00	0.82	2.95	2.18	0.90
H <sub>2</sub> /CO	0.67	1.12	4.76	0.43	1.02	3.29	0.22	0.76	2.29
CO/CO <sub>2</sub>	0.09	0.37	0.94	0.16	0.37	0.95	0.43	0.55	0.97
LHV (MJ/Nm <sup>3</sup> )	4.28	7.54	13.38	4.32	7.37	13.51	5.21	7.06	11.01
CGE (%)	33.25	44.44	33.65	38.58	49.79	37.28	81.72	81.93	52.71

Syngas with such a composition reported for steam/CO<sub>2</sub> gasification can be used for further processing in Fe and Co-based FTS (Ephraim et al., 2016). Therefore, gasification with steam/CO<sub>2</sub> mixture should be considered as a promising solution for the simultaneous utilisation of CO<sub>2</sub> and waste tyre streams.

## 5.5 Conclusion

In conclusion, the effect of gasification temperature, gasifying agent-to-feed ratio, feed flow rate and CO<sub>2</sub>-to-steam ratio, on syngas composition and yield as well as process performance was analysed during steam and steam/CO<sub>2</sub> gasification of the WT1PB0, WT0PB1 and WT3PB1.

Results showed that the temperature had a significant effect on H<sub>2</sub> content and yield where the highest values were obtained during steam gasification of WT1PB0 at a temperature of 1223 K. Maximum H<sub>2</sub>/CO ratio of 4.76 was obtained for WT1PB0 at a temperature of 1198 K during steam gasification compared to 3.79 at 1048 K in steam/CO<sub>2</sub> gasification. Both CO/CO<sub>2</sub> ratio and CGE increased at temperatures higher than 1123 K in steam as well as steam/CO<sub>2</sub> gasification.

The change in syngas composition was negligible at a SFR higher than 2.90 during steam gasification, resulting in H<sub>2</sub> content ranging between 53.03 and 69.70 vol% with H<sub>2</sub>/CO ratio higher than 2.00. In contrast, steam/CO<sub>2</sub> gasification resulted in the highest H<sub>2</sub> content ranging between 22.68 vol% (for WT0PB1) and 26.45 vol% (for WT1PB0) at SFR of 5. This corresponds to H<sub>2</sub>/CO ratio between 1.15 and 1.99. In both steam and steam/CO<sub>2</sub> gasification, LHV and CGE decreased with the increase in SFR.

The increase in the steam fraction of the gasifying agent by replacing CO<sub>2</sub> resulted in an increase in the fraction of H<sub>2</sub> in the syngas and a decrease in CO and CO<sub>2</sub> content. As a result, H<sub>2</sub>/CO ratio improved to values higher than 2.00. The effect of feed flow rate on syngas

composition and yield varied between the samples and with the use of different gasifying agents. The maximum H<sub>2</sub> content and H<sub>2</sub>/CO ratio was obtained at a feed flow rate of 0.20 kg/hr in steam/CO<sub>2</sub> gasification whereas it was at a feed flow rate of 0.02 kg/hr in steam gasification.

The use of a CO<sub>2</sub>-steam mixture could provide a viable route to offset CO<sub>2</sub> emissions while producing syngas with a wide range of H<sub>2</sub>/CO ratio compared to CO<sub>2</sub> gasification only.

## CHAPTER 6 Conclusions and recommendations for future work

### 6.1 Concluding remarks

#### 6.1.1 Evaluation of the existence of synergetic interaction between pine bark and waste tyre

In **Chapter 3**, the thermal decomposition behaviour of pine bark and waste tyre at different blend ratios and four heating rates was examined using TGA. The existence of synergetic interaction was evaluated through the calculation of the difference in weight loss. Results indicated that different blend samples showed different synergetic interactions in response to the change in heating rate. The highest value of the difference in weight loss was reported for the blended sample with pine bark to waste tyre mass ratio of 3:1 at heating rates of 30 and 40 K/min

#### 6.1.2 Estimation of the kinetics underlying the co-pyrolysis of waste tyre and pine bark at different blend ratios

In **Chapter 3**, the kinetics underlying the thermal decomposition of pine bark and waste tyre at different mass ratios was estimated using different methods including model fitting, iso-conversional and combined kinetics analysis. Despite the variation in the approximations used in these methods, the blended samples reported lower activation energy than the single waste tyre. The lowest activation energy was predicted for the blended sample with pine bark to waste tyre mass ratio of 1:3 and it was in the range of 225.04 to 239.68 kJ/mol for all the methods excluding Coats-Redfern.

Whilst these findings are limited to the specified type of biomass and waste tyre material, they highlight the potential of initiating the thermal decomposition of waste tyre at lower energy through the use of biomass as co-feeding material.

### 6.1.3 CO<sub>2</sub> utilisation in the co-gasification of waste tyre and pine bark for syngas production through process modelling and simulation

In **Chapter 4**, the co-gasification of pine bark and waste tyre using CO<sub>2</sub> as a gasifying agent was conducted through process modelling and simulation. The effect of operating conditions including temperature, CO<sub>2</sub>-to-feed ratio and feed flow rate on syngas production and composition is analysed. The main findings are as follows:

- ✓ Gasification temperature has a predominant effect on syngas production through the conversion of CO<sub>2</sub> to CO in particular at higher temperatures (i.e. > 1123 K). The produced syngas is CO-rich in particular at higher temperatures.
- ✓ Increasing CO<sub>2</sub>-to-feed ratio has a negative effect on H<sub>2</sub> and CO content. Therefore, a low CO<sub>2</sub>-to-feed ratio is ideal for syngas with better H<sub>2</sub> content.
- ✓ The feed flow rate improved both the H<sub>2</sub> and CO content of the syngas. Increased feed flow rate resulted in syngas with better H<sub>2</sub> and CO content and improved LHV.
- ✓ Syngas produced using pine bark showed higher H<sub>2</sub> and CO content and better conversion of CO<sub>2</sub> to CO for the investigated operating conditions compared to other samples.

### 6.1.4 Improve syngas composition while utilising CO<sub>2</sub> in the gasification process through process analysis

In **Chapter 5**, the influence of using steam as a pure gasifying agent and mixed with CO<sub>2</sub> on the syngas composition and process performance is examined. The effect of various operating conditions including gasification temperature, gasifying agent-to-feed ratio, CO<sub>2</sub>-to-steam mass ratio and feed flow rate, during steam and steam/CO<sub>2</sub> gasification, is analysed. The main findings are as follows:

- ✓ Syngas composition and yield varied positively in terms of H<sub>2</sub> at lower gasification temperatures (i.e. 973-1223 K) during steam gasification compared to higher temperatures of 1123-1273 K during steam/CO<sub>2</sub> gasification.
- ✓ Compared to CO<sub>2</sub> gasification, steam/CO<sub>2</sub> gasification improved the syngas in terms of H<sub>2</sub> composition and yield, H<sub>2</sub>/CO ratio, CGE and LHV.
- ✓ Significant increase in the total H<sub>2</sub> and CO content of the syngas with steam/CO<sub>2</sub> gasification compared to CO<sub>2</sub> gasification.
- ✓ The use of steam/CO<sub>2</sub> mixture as a gasifying agent compared to CO<sub>2</sub> only would provide a viable pyrolysis/gasification route to improve syngas composition while utilising CO<sub>2</sub> as a gasifying agent.

## 6.2 Future Recommendations

### 6.2.1 Using different type of biomass and waste tyre to evaluate the synergetic interaction and the kinetics analysis

In terms of future research work, it would be interesting to investigate the decomposition behaviour of different types of biomass materials and waste tyre to evaluate the existence of synergetic interaction. This is because both waste tyre and biomass are heterogeneous in their composition so it is not practical to generalize the behaviour of a single sample of waste tyre or biomass over others. The novelties of the future research direction are summarised as follows.

- (1) A comparative evaluation of the synergetic interaction between different types of biomass and waste tyre will be conducted. This is believed to provide insight into the potential of co-processing of these two materials through pyrolysis or gasification for fuel production. In addition, it provides a better understanding of the influence of the

feedstock composition on its thermal co-processing with other materials and addresses the issue of the limited type of biomass being used during thermal processing with the waste tyre.

- (2) From the kinetics analysis perspective, multi-step kinetics analysis will be conducted through peak deconvolution. This would be a fruitful area for further work since it provides an understanding of the decomposition behaviour of the Pseudocomponents which are making up both pine bark and waste tyre and the possible synergy in terms of activation energy. In addition, the estimation of the kinetics underlying the thermal co-processing of two different materials like biomass and waste tyre at their components level is not widely studied.
- (3) Use different kinetic models to derive the kinetics underlying the gasification of biomass and waste tyre. This includes distributed activation energy model and deactivation model which considers the variation in the rate constants as the degree of conversion changes.

#### 6.2.2 Detailed process modelling and simulation of co-gasification of biomass and waste tyre

- (1) It would be interesting to compare the CO<sub>2</sub> pyrolysis/gasification process of biomass and waste tyre and thermal processing of conventional fuels like coal gasification for syngas production from the perspectives of CO<sub>2</sub> emission, CO<sub>2</sub> utilisation and energy consumption analysis.
- (2) Since the syngas quality and quantity is affected by other operating conditions, it is important to examine the effect of pressure, residence time and feedstock moisture

content through process analysis. In addition, the effect of using catalyst and the potential of its deactivation due to tar production could be considered.

- (3) Process optimisation can be carried out to find the optimal operating conditions to achieve the highest syngas production in terms of H<sub>2</sub> and CO while maximizing CO<sub>2</sub> utilisation through the gasification process. In this case, maximizing syngas production, mainly H<sub>2</sub> and CO, thus H<sub>2</sub>/CO ratio will be the objective function. The optimum gasification temperature, CO<sub>2</sub>-to-steam ratio and pine bark to waste tyre blend ratio will be considered as decision variables.
- (4) Although the current model of biomass and waste tyre gasification is based on power law using Arrhenius rate constant, it provided reasonable results regarding syngas quality and quantity. However, developing more robust kinetic model while considering residence times and reactor hydrodynamics would be advantageous for better prediction of process performance.

## References

- Abdelouahed, L., Authier, O., Mauviel, G., Corriou, J.P., Verdier, G. and Dufour, A. (2012) 'Detailed modeling of biomass gasification in dual fluidized bed reactors under Aspen Plus', *Energy & Fuels*, 26(6), pp. 3840–3855.
- Abnisa, F. and Daud, W.M.A.W. (2014) 'A review on co-pyrolysis of biomass: An optional technique to obtain a high-grade pyrolysis oil', *Energy Conversion and Management*, 87, pp. 71–85.
- Abu El-Rub, Z., Bramer, E.A. and Brem, G. (2008) 'Experimental comparison of biomass chars with other catalysts for tar reduction', *Fuel*, 87(10–11), pp. 2243–2252.
- Aghaalikhani, A., Schmid, J.C., Borello, D., Fuchs, J., Benedikt, F., Hofbauer, H., Rispoli, F., Henriksen, U.B., Sárossy, Z. and Cedola, L. (2019) 'Detailed modelling of biomass steam gasification in a dual fluidized bed gasifier with temperature variation', *Renewable Energy*, 143, pp. 703–718.
- Ahmed, I. and Gupta, A.K. (2011) 'Characteristic of hydrogen and syngas evolution from gasification and pyrolysis of rubber', *International Journal of Hydrogen Energy*, 36(7), pp. 4340–4347.
- Akubo, K., Nahil, M.A. and Williams, P.T. (2019) 'Pyrolysis-catalytic steam reforming of agricultural biomass wastes and biomass components for production of hydrogen/syngas', *Journal of the Energy Institute*, 92(6), pp. 1987–1996.
- Al-Malah, K.I.M. (2017) *Aspen Plus : chemical engineering applications*. Hoboken, New Jersey: Wiley.
- Al-Rahbi, A.S., Onwudili, J.A. and Williams, P.T. (2016) 'Thermal decomposition and gasification of biomass pyrolysis gases using a hot bed of waste derived pyrolysis char', *Bioresource Technology*, 204, pp. 71–79.

Al-Rahbi, A.S. and Williams, P.T. (2017) 'Hydrogen-rich syngas production and tar removal from biomass gasification using sacrificial tyre pyrolysis char', *Applied Energy*, 190, pp. 501–509.

Alvarez, J., Kumagai, S., Wu, C., Yoshioka, T., Bilbao, J., Olazar, M. and Williams, P.T. (2014) 'Hydrogen production from biomass and plastic mixtures by pyrolysis-gasification', *International Journal of Hydrogen Energy*, 39(21), pp. 10883–10891.

Anca-Couce, A. (2016) 'Reaction mechanisms and multi-scale modelling of lignocellulosic biomass pyrolysis', *Progress in Energy and Combustion Science*, 53, pp. 41–79.

Antolini, D., Shivananda, A.S., Patuzzi, F., Grigiante, M. and Baratieri, M. (2019) 'Experimental and modeling analysis of Air and CO<sub>2</sub> biomass gasification in a reverse lab scale downdraft gasifier', *Energy Procedia*, 158, pp. 1182–1187.

Arias, A.M., Moreno-Piraján, J.C. and Giraldo, L. (2022) 'Kinetic study of waste tire pyrolysis using thermogravimetric analysis', *ACS Omega*, 7, pp. 19298–16305.

Arregi, A., Amutio, M., Lopez, G., Artetxe, M., Alvarez, J., Bilbao, J. and Olazar, M. (2017) 'Hydrogen-rich gas production by continuous pyrolysis and in-line catalytic reforming of pine wood waste and HDPE mixtures', *Energy Conversion and Management*, 136, pp. 192–201.

Awais, M., Omar, M.M., Munir, A., Li, W., Ajmal, M., Hussain, S., Ahmad, S.A. and Ali, A. (2022) 'Co-gasification of different biomass feedstock in a pilot-scale (24 kW<sub>e</sub>) downdraft gasifier: An experimental approach', *Energy*, 238, p. 121821.

Azizi, K., Haghghi, A.M., Keshavarz Moraveji, M., Olazar, M. and Lopez, G. (2019) 'Co-pyrolysis of binary and ternary mixtures of microalgae, wood and waste tires through TGA', *Renewable Energy*, 142, pp. 264–271.

Aznar, M.P., Caballero, M.A., Sancho, J.A. and Francés, E. (2006) 'Plastic waste elimination by co-gasification with coal and biomass in fluidized bed with air in pilot plant', *Fuel Processing*

*Technology*, 87(5), pp. 409–420.

Banerjee, S., Tiarks, J.A. and Kong, S.-C. (2015) 'Modeling biomass gasification system using multistep kinetics under various oxygen–steam conditions', *Environmental Progress & Sustainable Energy*, 34(4), pp. 1148–1155.

Begum, S., Rasul, M.G., Akbar, D. and Ramzan, N. (2013) 'Performance analysis of an integrated fixed bed gasifier model for different biomass feedstocks', *Energies*, 6(12), pp. 6508–6524.

Beheshti, S.M., Ghassemi, H. and Shahsavan-Markadeh, R. (2015) 'Process simulation of biomass gasification in a bubbling fluidized bed reactor', *Energy Conversion and Management*, 94, pp. 345–352.

Biagini, E., Barontini, F. and Tognotti, L. (2017) 'Thermal decomposition of agricultural and food residues: Comparison of kinetic models', *Canadian Journal of Chemical Engineering*, 95(5), pp. 913–921.

Blasi, C. Di (2008) 'Modeling chemical and physical processes of wood and biomass pyrolysis', *Progress in Energy and Combustion Science*, 34(1), pp. 47–90.

Blasi, C. Di and Branca, C. (2001) 'Kinetics of primary product formation from wood pyrolysis', *Industrial and Engineering Chemistry Research*, 40(23), pp. 5547–5556.

BP (2022) *BP Statistical Review of World Energy 2022, (71st edition)*.

Brachi, P., Chirone, R., Miccio, F., Miccio, M., Picarelli, A. and Ruoppolo, G. (2014) 'Fluidized bed co-gasification of biomass and polymeric wastes for a flexible end-use of the syngas: Focus on bio-methanol', *Fuel*, 128, pp. 88–98.

Burra, K.G. and Gupta, A.K. (2018) 'Kinetics of synergistic effects in co-pyrolysis of biomass with plastic wastes', *Applied Energy*, 220, pp. 408–418.

Butterman, H.C. and Castaldi, M.J. (2009) 'CO<sub>2</sub> as a Carbon Neutral Fuel Source via Enhanced

Biomass Gasification', *Environmental Science & Technology*, 43(23), pp. 9030–9037.

Cai, J. and Liu, R. (2009) 'Kinetic analysis of solid-state reactions: A general empirical kinetic model', *Industrial and Engineering Chemistry Research*, 48(6), pp. 3249–3253.

Cerone, N., Zimbardi, F., Contuzzi, L., Baleta, J., Cerinski, D. and Skvorčinskienė, R. (2020) 'Experimental investigation of syngas composition variation along updraft fixed bed gasifier', *Energy Conversion and Management*, 221, p. 113116.

Chai, Y., Gao, N., Wang, M. and Wu, C. (2020) 'H<sub>2</sub> production from co-pyrolysis/gasification of waste plastics and biomass under novel catalyst Ni-CaO-C', *Chemical Engineering Journal*, 382, p. 122947.

Chai, Y., Packham, N. and Wang, M. (2022) 'Process improvement analysis of pyrolysis/gasification of biomass and waste plastics with carbon capture and utilisation through process simulation', *Fuel*, 324, p. 124571.

Chan, Y.H., Syed Abdul Rahman, S.N.F., Lahuri, H.M. and Khalid, A. (2021) 'Recent progress on CO-rich syngas production via CO<sub>2</sub> gasification of various wastes: A critical review on efficiency, challenges and outlook', *Environmental Pollution*, 278, p. 116843.

Chandrasekaran, A., Ramachandran, S. and Subbiah, S. (2017) 'Determination of kinetic parameters in the pyrolysis operation and thermal behavior of *Prosopis juliflora* using thermogravimetric analysis', *Bioresource Technology*, 233, pp. 413–422.

Chatrattanawet, N., Authayanun, S., Saebea, D. and Patcharavorachot, Y. (2019) 'Syngas production from sugarcane leftover gasification integrated with absorption process for green liquid production', *Journal of Cleaner Production*, 235, pp. 519–534.

Chen, F., Wu, C., Dong, L., Jin, F., Williams, P.T. and Huang, J. (2015) 'Catalytic steam reforming of volatiles released via pyrolysis of wood sawdust for hydrogen-rich gas production on Fe-Zn/Al<sub>2</sub>O<sub>3</sub> nanocatalysts', *Fuel*, 158, pp. 999–1005.

Chen, F., Wu, C., Dong, L., Vassallo, A., Williams, P.T. and Huang, J. (2016) 'Characteristics and catalytic properties of Ni/CaAlO<sub>x</sub> catalyst for hydrogen-enriched syngas production from pyrolysis-steam reforming of biomass sawdust', *Applied Catalysis B: Environmental*, 183, pp. 168–175.

Chen, J., Ma, X., Yu, Z., Deng, T., Chen, X., Chen, L. and Dai, M. (2019a) 'A study on catalytic co-pyrolysis of kitchen waste with tire waste over ZSM-5 using TG-FTIR and Py-GC/MS', *Bioresource Technology journal*, 289, p. 121585.

Chen, J.H., Chen, K.S. and Tong, L.Y. (2001) 'On the pyrolysis kinetics of scrap automotive tires', *Journal of Hazardous Materials*, 84(1), pp. 43–55.

Chen, K.S., Yeh, R.Z. and Chang, Y.R. (1997) 'Kinetics of thermal decomposition of styrene-butadiene rubber at low heating rates in nitrogen and oxygen', *Combustion and Flame*, 108(4), pp. 408–418.

Chen, Q., Xu, F., Zong, P., Song, F., Wang, B., Tian, Y., Wu, F., Zhao, X. and Qiao, Y. (2022) 'Influence of CaO on the thermal kinetics and formation mechanism of high value-added products during waste tire pyrolysis', *Journal of Hazardous Materials*, 436, p. 129220.

Chen, R., Lun, L., Cong, K., Li, Q. and Zhang, Y. (2019b) 'Insights into pyrolysis and co-pyrolysis of tobacco stalk and scrap tire: Thermochemical behaviors, kinetics, and evolved gas analysis', *Energy*, 183, pp. 25–34.

Chen, R., Zhang, J., Lun, L., Li, Q. and Zhang, Y. (2019c) 'Comparative study on synergistic effects in co-pyrolysis of tobacco stalk with polymer wastes: Thermal behavior, gas formation, and kinetics', *Bioresource Technology*, 292, p. 121970.

Cheng, Y., Thow, Z. and Wang, C.H. (2016) 'Biomass gasification with CO<sub>2</sub> in a fluidized bed', *Powder Technology*, 296, pp. 87–101.

Cherop, P.T., Kiambi, S.L. and Musonge, P. (2018) 'Kinetic study of non-isothermal co-pyrolysis

of tyre crumb with eucalyptus sawdust', *International Journal of Environment and Waste Management*, 21(3), pp. 184–200.

Cherubini, F. (2010) 'The biorefinery concept: Using biomass instead of oil for producing energy and chemicals', *Energy Conversion and Management*, 51(7), pp. 1412–1421.

Chiodini, A., Bua, L., Carnelli, L., Zwart, R., Vreugdenhil, B. and Vocciante, M. (2017) 'Enhancements in Biomass-to-Liquid processes: Gasification aiming at high hydrogen/carbon monoxide ratios for direct Fischer-Tropsch synthesis applications', *Biomass and Bioenergy*, 106, pp. 104–114.

Choi, G.G., Oh, S.J. and Kim, J.S. (2016) 'Scrap tire pyrolysis using a new type two-stage pyrolyzer: Effects of dolomite and olivine on producing a low-sulfur pyrolysis oil', *Energy*, 114, pp. 457–464.

Conesa, J.A., Martín-Gullón, I., Font, R. and Jauhiainen, J. (2004) 'Complete Study of the Pyrolysis and Gasification of Scrap Tires in a Pilot Plant Reactor', *Environmental Science & Technology*, 38(11), pp. 3189–3194.

Criado, J.M., Malek, J. and Ortega, A. (1989) 'Applicability of the master plots in kinetic analysis of non-isothermal data', *Thermochimica Acta*, 147, pp. 377–385.

Czajka, K.M. (2021) 'The impact of the thermal lag on the interpretation of cellulose pyrolysis', *Energy*, 236, p. 121497.

Danon, B., Mkhize, N.M., Van Der Gryp, P. and Görgens, J.F. (2015) 'Combined model-free and model-based devolatilisation kinetics of tyre rubbers', *Thermochimica Acta*, 601, pp. 45–53.

Das, P. and Tiwari, P. (2017) 'Thermal degradation kinetics of plastics and model selection', *Thermochimica Acta*, 654(2017), pp. 191–202.

Díez, D., Urueña, A., Piñero, R., Barrio, A. and Tamminen, T. (2020) 'Determination of hemicellulose, cellulose, and lignin content in different types of biomasses by

thermogravimetric analysis and pseudocomponent kinetic model (TGA-PKM Method)', *Processes*, 8, p. 1048.

Ding, Y., Ezekoye, O.A., Lu, S. and Wang, C. (2016) 'Thermal degradation of beech wood with thermogravimetry/Fourier transform infrared analysis', *Energy Conversion and Management*, 120, pp. 370–377.

Donatelli, A., Iovane, P. and Molino, A. (2010) 'High energy syngas production by waste tyres steam gasification in a rotary kiln pilot plant. Experimental and numerical investigations', *Fuel*, 89(10), pp. 2721–2728.

Dong, L., Wu, C., Ling, H., Shi, J., Williams, P.T. and Huang, J. (2017) 'Promoting hydrogen production and minimizing catalyst deactivation from the pyrolysis-catalytic steam reforming of biomass on nanosized NiZnAlO<sub>x</sub> catalysts', *Fuel*, 188, pp. 610–620.

Duan, P., Jin, B., Xu, Y. and Wang, F. (2015) 'Co-pyrolysis of microalgae and waste rubber tire in supercritical ethanol', *Chemical Engineering Journal*, 269, pp. 262–271.

Ebrahimi-Kahrizsangi, R. and Abbasi, M.H. (2008) 'Evaluation of reliability of Coats-Redfern method for kinetic analysis of non-isothermal TGA', *Transactions of Nonferrous Metals Society of China*, 18, pp. 217–221.

EIA (2023) *Monthly Energy Review- January 2023*. Washington, DC 20585.

Elbaba, I.F. and Williams, P.T. (2014) 'Deactivation of nickel catalysts by sulfur and carbon for the pyrolysis-catalytic gasification/reforming of waste tires for hydrogen production', *Energy and Fuels*, 28(3), pp. 2104–2113.

Elbaba, I.F. and Williams, P.T. (2013) 'High yield hydrogen from the pyrolysis-catalytic gasification of waste tyres with a nickel/dolomite catalyst', *Fuel*, 106, pp. 528–536.

Elbaba, I.F. and Williams, P.T. (2012) 'Two stage pyrolysis-catalytic gasification of waste tyres: Influence of process parameters', *Applied Catalysis B: Environmental*, 125(3), pp. 136–143.

Elbaba, I.F., Wu, C. and Williams, P.T. (2011) 'Hydrogen production from the pyrolysis–gasification of waste tyres with a nickel/cerium catalyst', *International Journal of Hydrogen Energy*, 36(11), pp. 6628–6637.

Ephraim, A., Pozzobon, V., Louisnard, O., Minh, D.P., Nzihou, A., Sharrock, P., Ephraim, A., Pozzobon, V., Louisnard, O., Minh, D.P., Nzihou, A., Ephraim, A., Pozzobon, V., Louisnard, O., Minh, D.P., Nzihou, A. and Sharrock, P. (2016) 'Simulation of biomass char gasification in a downdraft reactor for syngas production', *AIChE Journal*, 62(4), pp. 1079–1091.

Fajimi, L.I., Oboirien, B.O. and Adams, T.A. (2021) 'Simulation studies on the co-production of syngas and activated carbon from waste tyre gasification using different reactor configurations', *Energy Conversion and Management: X*, 11, p. 100105.

Farooq, M.Z., Zeeshan, M., Iqbal, S., Ahmed, N. and Shah, S.A.Y. (2018) 'Influence of waste tire addition on wheat straw pyrolysis yield and oil quality', *Energy*, 144, pp. 200–206.

Farzad, S., Mandegari, M.A. and Görgens, J.F. (2016) 'A critical review on biomass gasification, co-gasification, and their environmental assessments', *Biofuel Research Journal*, 3(4), pp. 483–495.

Ferreiro, A.I., Rabaçal, M. and Costa, M. (2016) 'A combined genetic algorithm and least squares fitting procedure for the estimation of the kinetic parameters of the pyrolysis of agricultural residues', *Energy Conversion and Management*, 125, pp. 290–300.

Font, R., Conesa, J.A., Moltó, J. and Muñoz, M. (2009) 'Kinetics of pyrolysis and combustion of pine needles and cones', *Journal of Analytical and Applied Pyrolysis*, 85(1–2), pp. 276–286.

Fu, W., Zhang, Y., Cui, L., Liu, H. and Maqsood, T. (2023) 'Experimental microwave-assisted air gasification of biomass in fluidized bed reactor', *Bioresource Technology*, 369, p. 128378.

Gagliano, A., Nocera, F., Bruno, M. and Cardillo, G. (2017) 'Development of an Equilibrium-based Model of Gasification of Biomass by Aspen Plus', *Energy Procedia*, 111, pp. 1010–1019.

Galvagno, S., Casciaro, G., Casu, S., Martino, M., Mingazzini, C., Russo, A. and Portofino, S. (2009) 'Steam gasification of tyre waste, poplar, and refuse-derived fuel: A comparative analysis', *Waste Management*, 29(2), pp. 678–689.

Ganeshan, G., Shadangi, K.P. and Mohanty, K. (2018) 'Degradation kinetic study of pyrolysis and co-pyrolysis of biomass with polyethylene terephthalate (PET) using Coats–Redfern method', *Journal of Thermal Analysis and Calorimetry*, 131(2), pp. 1803–1816.

Gao, N., Kamran, K., Ma, Z. and Quan, C. (2021) 'Investigation of product distribution from co-pyrolysis of side wall waste tire and off-shore oil sludge', *Fuel*, 285, p. 119036.

Gašparovič, L., Šugár, L., Jelemenský L., L. and Markoš, J. (2013) 'Catalytic gasification of pyrolytic oil from tire pyrolysis process', *Chemical Papers*, 67(12), pp. 1504–1513.

Gerun, L., Paraschiv, M., Vîjeu, R., Bellettre, J., Tazerout, M., Gøbel, B. and Henriksen, U. (2008) 'Numerical investigation of the partial oxidation in a two-stage downdraft gasifier', *Fuel*, 87(7), pp. 1383–1393.

Giudicianni, P., Cardone, G. and Ragucci, R. (2013) 'Cellulose, hemicellulose and lignin slow steam pyrolysis: Thermal decomposition of biomass components mixtures', *Journal of Analytical and Applied Pyrolysis*, 100, pp. 213–222.

González, J.F., Encinar, J.M., Canito, J.L. and Rodríguez, J.J. (2001) 'Pyrolysis of automobile tyre waste. Influence of operating variables and kinetics study', *Journal of Analytical and Applied Pyrolysis*, 58–59, pp. 667–683.

Guo, F., Dong, Y., Dong, L. and Guo, C. (2014) 'Effect of design and operating parameters on the gasification process of biomass in a downdraft fixed bed: An experimental study', *International Journal of Hydrogen Energy*, 39(11), pp. 5625–5633.

Han, J., Li, W., Liu, D., Qin, L., Chen, W. and Xing, F. (2018) 'Pyrolysis characteristic and mechanism of waste tyre: A thermogravimetry-mass spectrometry analysis', *Journal of*

*Analytical and Applied Pyrolysis*, 129, pp. 1–5.

Hassan, H., Lim, J.K. and Hameed, B.H. (2016) 'Recent progress on biomass co-pyrolysis conversion into high-quality bio-oil', *Bioresource Technology*, 221, pp. 645–655.

Haydary, J. (2018) 'Aspen simulation of two-stage pyrolysis/gasification of carbon based solid waste', *Chemical Engineering Transactions*, 70, pp. 1033–1038.

Hejazi, B., Grace, J.R., Bi, X. and Mahecha-Botero, A. (2017) 'Kinetic Model of Steam Gasification of Biomass in a Bubbling Fluidized Bed Reactor', *Energy and Fuels*, 31(2), pp. 1702–1711.

Hidayat, S., Bakar, M.S.A., Ahmed, A., Iryani, D.A., Hussain, M., Jamil, F. and Park, Y.-K. (2021) 'Comprehensive kinetic study of Imperata Cylindrica pyrolysis via Asym2sig deconvolution and combined kinetics', *Journal of Analytical and Applied Pyrolysis*, 156, p. 105133.

Hita, I., Arabiourrutia, M., Olazar, M., Bilbao, J., Arandes, J.M. and Castaño Sánchez, P. (2016) 'Opportunities and barriers for producing high quality fuels from the pyrolysis of scrap tires', *Renewable and Sustainable Energy Reviews*, 56, pp. 745–759.

Hu, Q., Tang, Z., Yao, D., Yang, H., Shao, J. and Chen, H. (2020) 'Thermal behavior, kinetics and gas evolution characteristics for the co-pyrolysis of real-world plastic and tyre wastes', *Journal of Cleaner Production*, 260, p. 121102.

Huang, F. and Jin, S. (2019) 'Investigation of biomass (pine wood) gasification: Experiments and Aspen Plus simulation', *Energy Science & Engineering*, 7(4), pp. 1178–1187.

IEA (2022) *Global Energy Review : CO2 Emissions in 2021*. Paris.

IEA Bioenergy (n.d.) *Global database of biomass conversion facilities, including advanced biofuels, combustion, gasification and pyrolysis plants*.

Inayat, M., Sulaiman, S.A., Kurnia, J.C. and Shahbaz, M. (2019) 'Effect of various blended fuels on syngas quality and performance in catalytic co-gasification: A review', *Renewable and*

*Sustainable Energy Reviews*, 105, pp. 252–267.

IPCC (2014) *Climate Change 2014: Mitigation of Climate Change. Contribution of Working Group III to the Fifth Assessment Report of the Intergovernmental Panel on Climate Change*. Cambridge, UK.

Islam, M.W. (2020) 'Effect of different gasifying agents (steam, H<sub>2</sub>O<sub>2</sub>, oxygen, CO<sub>2</sub>, and air) on gasification parameters', *International Journal of Hydrogen Energy*, 45(56), pp. 31760–31774.

Ismail, H.Y., Abbas, A., Azizi, F. and Zeaiter, J. (2017) 'Pyrolysis of waste tires: A modeling and parameter estimation study using Aspen Plus<sup>®</sup>', *Waste Management*, 60, pp. 482–493.

Janajreh, I. and Raza, S.S. (2015) 'Numerical simulation of waste tyres gasification', *Waste Management & Research*, 33(5), pp. 460–468.

Janajreh, I., Raza, S.S. and Valmundsson, A.S. (2013) 'Plasma gasification process: Modeling, simulation and comparison with conventional air gasification', *Energy Conversion and Management*, 65, pp. 801–809.

Jess, A. (1996) 'Mechanisms and kinetics of thermal reactions of aromatic hydrocarbons from pyrolysis of solid fuels', *Fuel*, 25(12), pp. 1441–1448.

Kaewluan, S. and Pipatmanomai, S. (2011) 'Gasification of high moisture rubber woodchip with rubber waste in a bubbling fluidized bed', *Fuel Processing Technology*, 92(3), pp. 671–677.

Kan, T., Strezov, V. and Evans, T. (2017) 'Fuel production from pyrolysis of natural and synthetic rubbers', *Fuel*, 191, pp. 403–410.

Kandasamy, J. and Gökalp, I. (2014) 'Pyrolysis, combustion, and steam gasification of various types of scrap tires for energy recovery', *Energy and Fuels*, 29(1), pp. 346–354.

Kannan, P., Lakshmanan, G., Al Shoaibi, A. and Srinivasakannan, C. (2017) 'Equilibrium model

analysis of waste plastics gasification using CO<sub>2</sub> and steam', *Waste Management and Research*, 35(12), pp. 1247–1253.

Karatas, H., Olgun, H. and Akgun, F. (2012) 'Experimental results of gasification of waste tire with air&CO<sub>2</sub>, air&steam and steam in a bubbling fluidized bed gasifier', *Fuel Processing Technology*, 102, pp. 166–174.

Karatas, H., Olgun, H., Engin, B. and Akgun, F. (2013) 'Experimental results of gasification of waste tire with air in a bubbling fluidized bed gasifier', *Fuel*, 105, pp. 566–571.

Kartal, F. and Özveren, U. (2023) 'Energy and exergy analysis of entrained bed gasifier/GT/Kalina cycle model for CO<sub>2</sub> co-gasification of waste tyre and biochar', *Fuel*, 331, p. 125943.

Kaushal, P. and Tyagi, R. (2017) 'Advanced simulation of biomass gasification in a fluidized bed reactor using ASPEN PLUS', *Renewable Energy*, 101, pp. 629–636.

Kaza, S., Yao, L.C., Bhada-Tata, P. and Van Woerden, F. (2018) *What a Waste 2.0: A Global Snapshot of Solid Waste Management to 2050*. Washington.

Kihedu, J.H., Yoshiie, R. and Naruse, I. (2016) 'Performance indicators for air and air–steam auto-thermal updraft gasification of biomass in packed bed reactor', *Fuel Processing Technology*, 141, pp. 93–98.

Kordoghli, S., Khiari, B., Paraschiv, M., Zagrouba, F. and Tazerout, M. (2017) 'Impact of different catalysis supported by oyster shells on the pyrolysis of tyre wastes in a single and a double fixed bed reactor', *Waste Management*, 67, pp. 288–297.

Kordoghli, S., Khiari, B., Paraschiv, M., Zagrouba, F. and Tazerout, M. (2019) 'Production of hydrogen and hydrogen-rich syngas during thermal catalytic supported cracking of waste tyres in a bench-scale fixed bed reactor', *International Journal of Hydrogen Energy*, 44(22), pp. 11289–11302.

- Kumabe, K., Hanaoka, T., Fujimoto, S., Minowa, T. and Sakanishi, K. (2007) 'Co-gasification of woody biomass and coal with air and steam', *Fuel*, 86(5–6), pp. 684–689.
- Labaki, M. and Jeguirim, M. (2017) 'Thermochemical conversion of waste tyres—a review', *Environmental Science and Pollution Research*, 24(11), pp. 9962–9992.
- Lah, B., Klinar, D. and Likozar, B. (2013) 'Pyrolysis of natural, butadiene, styrene–butadiene rubber and tyre components: Modelling kinetics and transport phenomena at different heating rates and formulations', *Chemical Engineering Science*, 87, pp. 1–13.
- Lahijani, P., Mohammadi, M. and Mohamed, A.R. (2019) 'Investigation of synergism and kinetic analysis during CO<sub>2</sub> co-gasification of scrap tire char and agro-wastes', *Renewable Energy*, 142, pp. 147–157.
- Lahijani, P., Zainal, Z.A., Mohamed, A.R. and Mohammadi, M. (2013) 'Co-gasification of tire and biomass for enhancement of tire-char reactivity in CO<sub>2</sub> gasification process', *Bioresource Technology*, 138, pp. 124–130.
- Lahijani, P., Zainal, Z.A., Mohammadi, M. and Mohamed, A.R. (2015) 'Conversion of the greenhouse gas CO<sub>2</sub> to the fuel gas CO via the Boudouard reaction: A review', *Renewable and Sustainable Energy Reviews*, 41, pp. 615–632.
- Lee, R.A. and Lavoie, J.-M. (2013) 'From first- to third-generation biofuels: Challenges of producing a commodity from a biomass of increasing complexity', *Animal Frontiers*, 3(2), pp. 6–11.
- Lee, U., Chung, J.N. and Ingley, H.A. (2014) 'High-temperature steam gasification of municipal solid waste, rubber, plastic and wood', *Energy and Fuels*, 28(7), pp. 4573–4587.
- Lerner, A.S., Bratsev, A.N., Popov, V.E., Kuznetsov, V.A., Ufimtsev, A.A., Shengel', S. V. and Subbotin, D.I. (2012) 'Production of hydrogen-containing gas using the process of steam-plasma gasification of used tires', *Glass Physics and Chemistry*, 38(6), pp. 511–516.

Leung, D.Y.C. and Wang, C.L. (1999) 'Kinetic Modeling of Scrap Tire Pyrolysis', *Energy & Fuels*, 13(2), pp. 421–427.

Li, K., Zhang, R. and Bi, J. (2010) 'Experimental study on syngas production by co-gasification of coal and biomass in a fluidized bed', *International Journal of Hydrogen Energy*, 35(7), pp. 2722–2726.

Likun, P.K.W. and Zhang, H. (2020) 'Insights into pyrolysis of torrefied-biomass, plastics/tire and blends: Thermochemical behaviors, kinetics and evolved gas analyses', *Biomass and Bioenergy*, 143, p. 105852.

Liu, L., Huang, Y., Cao, J., Liu, C., Dong, L., Xu, L. and Zha, J. (2018a) 'Experimental study of biomass gasification with oxygen-enriched air in fluidized bed gasifier', *Science of The Total Environment*, 626, pp. 423–433.

Liu, X., Burra, K.G., Wang, Z., Li, J., Che, D. and Gupta, A.K. (2020) 'On deconvolution for understanding synergistic effects in co-pyrolysis of pinewood and polypropylene', *Applied Energy*, 279, p. 115811.

Liu, Z., Zhang, F., Liu, H., Ba, F., Yan, S. and Hu, J. (2018b) 'Pyrolysis/gasification of pine sawdust biomass briquettes under carbon dioxide atmosphere: Study on carbon dioxide reduction (utilization) and biochar briquettes physicochemical properties', *Bioresource Technology*, 249, pp. 983–991.

Lv, P., Chang, J., Xiong, Z., Huang, H., Wu, C., Chen, Y. and Zhu, J. (2003) 'Biomass air–steam gasification in a fluidized bed to produce hydrogen-rich gas', *Energy Fuels*, 17(3), pp. 677–682.

Machin, E.B., Pedroso, D.T. and de Carvalho, J.A. (2017) 'Energetic valorization of waste tires', *Renewable and Sustainable Energy Reviews*, 68, pp. 306–315.

Martínez, J.D., Murillo, R., García, T. and Arauzo, I. (2014) 'Thermodynamic analysis for syngas production from volatiles released in waste tire pyrolysis', *Energy Conversion and*

*Management*, 81, pp. 338–353.

Martínez, J.D., Puy, N., Murillo, R., García, T., Navarro, M.V. and Mastral, A.M. (2013) 'Waste tyre pyrolysis – A review', *Renewable and Sustainable Energy Reviews*, 23, pp. 179–213.

Mastellone, M.L., Zaccariello, L. and Arena, U. (2010) 'Co-gasification of coal, plastic waste and wood in a bubbling fluidized bed reactor', *Fuel*, 89(10), pp. 2991–3000.

Mauerhofer, A.M., Fuchs, J., Müller, S., Benedikt, F., Schmid, J.C. and Hofbauer, H. (2019) 'CO<sub>2</sub> gasification in a dual fluidized bed reactor system: Impact on the product gas composition', *Fuel*, 253, pp. 1605–1616.

Mauerhofer, A.M., Müller, S., Bartik, A., Benedikt, F., Fuchs, J., Hammerschmid, M. and Hofbauer, H. (2021) 'Conversion of CO<sub>2</sub> during the DFB biomass gasification process', *Biomass Conversion and Biorefinery*, 11(1), pp. 15–27.

Menares, T., Herrera, J., Romero, R., Osorio, P. and Arteaga-Pérez, L.E. (2020) 'Waste tires pyrolysis kinetics and reaction mechanisms explained by TGA and Py-GC/MS under kinetically-controlled regime', *Waste Management*, 102, pp. 21–29.

Miranda, M., Pinto, F., Gulyurtlu, I. and Cabrita, I. (2013) 'Pyrolysis of rubber tyre wastes: A kinetic study', *Fuel*, 103, pp. 542–552.

Mishra, G., Kumar, J. and Bhaskar, T. (2015) 'Kinetic studies on the pyrolysis of pinewood', *Bioresource Technology*, 182, pp. 282–288.

Mishra, R.K. and Mohanty, K. (2018) 'Pyrolysis kinetics and thermal behavior of waste sawdust biomass using thermogravimetric analysis', *Bioresource Technology*, 251, pp. 63–74.

Mitta, N.R., Ferrer-Nadal, S., Lazovic, A.M., Parales, J.F., Velo, E. and Puigjaner, L. (2006) 'Modelling and simulation of a tyre gasification plant for synthesis gas production', *Computer Aided Chemical Engineering*, 21, pp. 1771–1776.

Molino, A., Chianese, S. and Musmarra, D. (2016) 'Biomass gasification technology: The state

of the art overview', *Journal of Energy Chemistry*, 25(1), pp. 10–25.

Mondal, P., Dang, G.S. and Garg, M.O. (2011) 'Syngas production through gasification and cleanup for downstream applications - Recent developments', *Fuel Processing Technology*, 92(8), pp. 1395–1410.

Mozafari, A., Farshchi Tabrizi, F., Farsi, M. and Seyed Mousavi, S.A.H. (2017) 'Thermodynamic modeling and optimization of thermolysis and air gasification of waste tire', *Journal of Analytical and Applied Pyrolysis*, 126, pp. 415–422.

Mui, E.L.K., Cheung, W.H., Lee, V.K.C. and McKay, G. (2010) 'Compensation effect during the pyrolysis of tyres and bamboo', *Waste Management*, 30(5), pp. 821–830.

Muzenda, E. (2014) 'A comparative review of waste tyre pyrolysis, gasification and liquefaction (PGL) processes', *International Conference on Chemical Engineering Advanced Computational Technologies*. Pretoria, South Africa, pp. 24–25.

Neves, D., Thunman, H., Matos, A., Tarelho, L. and Gómez-Barea, A. (2011) 'Characterization and prediction of biomass pyrolysis products', *Progress in Energy and Combustion Science*, 37(5), pp. 611–630.

Nie, S.Q., Chen, M.Q. and Li, Q.H. (2022) 'Investigation of the depolymerization process of hydrothermal gasification natural rubber with ReaxFF-MD simulation and DFT computation', *Journal of Thermal Analysis and Calorimetry*, 147, pp. 9999–10011.

Nikoo, M.B. and Mahinpey, N. (2008) 'Simulation of biomass gasification in fluidized bed reactor using ASPEN PLUS', *Biomass and Bioenergy*, 32(12), pp. 1245–1254.

Oboirien, B.O. and North, B.C. (2017) 'A review of waste tyre gasification', *Journal of Environmental Chemical Engineering*, 5(5), pp. 5169–5178.

Pala, L.P.R., Wang, Q., Kolb, G. and Hessel, V. (2017) 'Steam gasification of biomass with subsequent syngas adjustment using shift reaction for syngas production: An Aspen Plus

model', *Renewable Energy*, 101, pp. 484–492.

Pandey, B., Sheth, P.N. and Prajapati, Y.K. (2022) 'Air-CO<sub>2</sub> and oxygen-enriched air-CO<sub>2</sub> biomass gasification in an autothermal downdraft gasifier: Experimental studies', *Energy Conversion and Management*, 270, p. 116216.

Park, J.H., Park, H.W., Choi, S. and Park, D.W. (2016) 'Effects of blend ratio between high density polyethylene and biomass on co-gasification behavior in a two-stage gasification system', *International Journal of Hydrogen Energy*, 41(38), pp. 16813–16822.

Pauls, J.H., Mahinpey, N. and Mostafavi, E. (2016) 'Simulation of air-steam gasification of woody biomass in a bubbling fluidized bed using Aspen Plus: A comprehensive model including pyrolysis, hydrodynamics and tar production', *Biomass and Bioenergy*, 95, pp. 157–166.

Peng, L., Wang, Y., Lei, Z. and Cheng, G. (2012) 'Co-gasification of wet sewage sludge and forestry waste in situ steam agent', *Bioresource Technology*, 114, pp. 698–702.

Perejón, A., Sánchez-Jiménez, P.E., García-Garrido, C. and Pérez-Maqueda, L.A. (2021) 'Kinetic study of complex processes composed of non-independent stages: pyrolysis of natural rubber', *Polymer Degradation and Stability*, 188, p. 109590.

Phyllis2 (2023) *Database for (treated) biomass, algae, feedstocks for biogas production and biochar.*, TNO Biobased and Circular Technologies Available at: <https://phyllis.nl/> (Accessed: 22 March 2022).

Pinto, F., Franco, C., Andre, R.N., Miranda, M., Gulyurtlu, I. and Cabrita, I. (2002) 'Co-gasification study of biomass mixed with plastic wastes', *Fuel*, 81, pp. 291–297.

Poletto, M., Zattera, A.J. and Santana, R.M.C. (2012) 'Thermal decomposition of wood: Kinetics and degradation mechanisms', *Bioresource Technology*, 126, pp. 7–12.

Policella, M., Wang, Z., Burra, K.G. and Gupta, A.K. (2019) 'Characteristics of syngas from

pyrolysis and CO<sub>2</sub>-assisted gasification of waste tires', *Applied Energy*, 254, p. 113678.

Portofino, S., Casu, S., Iovane, P., Russo, A., Martino, M., Donatelli, A. and Galvagno, S. (2011) 'Optimizing H<sub>2</sub> production from waste tires via combined steam gasification and catalytic reforming', *Energy and Fuels*, 25(5), pp. 2232–2241.

Portofino, S., Donatelli, A., Iovane, P., Innella, C., Civita, R., Martino, M., Matera, D.A., Russo, A., Cornacchia, G. and Galvagno, S. (2013) 'Steam gasification of waste tyre: Influence of process temperature on yield and product composition', *Waste Management*, 33(3), pp. 672–678.

Prabowo, B., Susanto, H., Umeki, K., Yan, M. and Yoshikawa, K. (2015) 'Pilot scale autothermal gasification of coconut shell with CO<sub>2</sub>-O<sub>2</sub> mixture', *Frontiers in Energy*, 9(3), pp. 362–370.

Puig-Gamero, M., Argudo-Santamaria, J., Valverde, J.L., Sánchez, P. and Sanchez-Silva, L. (2018) 'Three integrated process simulation using aspen plus®: Pine gasification, syngas cleaning and methanol synthesis', *Energy Conversion and Management*, 177, pp. 416–427.

Rafati, M., Hashemisohe, A., Wang, L. and Shahbazi, A. (2015) 'Sequential modular simulation of hydrodynamics and reaction kinetics in a biomass bubbling fluidized-bed gasifier using Aspen Plus', *Energy and Fuels*, 29(12), pp. 8261–8272.

Raman, P.K., Walawender, W.P. and Fan, L.T. (1981) 'Gasification of waste tires in a fluid bed reactor', *Conservation & Recycling*, 4(2), pp. 79–88.

Ramos, A., Monteiro, E., Silva, V. and Rouboa, A. (2018) 'Co-gasification and recent developments on waste-to-energy conversion: A review', *Renewable and Sustainable Energy Reviews*, 81, pp. 380–398.

Renganathan, T., Yadav, M.V., Pushpavanam, S., Voolapalli, R.K. and Cho, Y.S. (2012) 'CO<sub>2</sub> utilization for gasification of carbonaceous feedstocks: A thermodynamic analysis', *Chemical Engineering Science*, 83, pp. 159–170.

Research and Markets (2021) *Syngas Market by Gasifier, Technology, Feedstock, and Application: Global Opportunity Analysis and Industry Forecast, 2020-2027*.

Saddawi, A., Jones, J.M., Williams, † A and Ojtowicz, M.A.W. (2010) 'Kinetics of the Thermal Decomposition of Biomass', *Energy & Fuels*, 24, pp. 1274–1282.

Sadhwani, N., Adhikari, S. and Eden, M.R. (2016) 'Biomass gasification using carbon dioxide\_ Effect of temperature, CO<sub>2</sub>-C Ratio and the study of reactions influencing the process', *Industrial and Engineering Chemistry Research*, 55, pp. 2883–2891.

Saito, I., Sakae, K., Ogiri, T. and Ueda, Y. (1987) 'Effective use of waste tyres by gasification in cement plant.', *World Cement*, 18(7), pp. 264 – 266, 268.

Sánchez-Jiménez, P.E., Pérez-Maqueda, L.A., Perejón, A. and Criado, J.M. (2013) 'Generalized master plots as a straightforward approach for determining the kinetic model: The case of cellulose pyrolysis', *Thermochimica Acta*, 552, pp. 54–59.

Sánchez, D., Paez, M., Sierra, R. and Gordillo, G. (2013) 'Waste tire rubber gasification using air steam for partial oxidation and N<sub>2</sub> as carrier gas', *Proceedings of the ASME Turbo Expo 2013: Turbine Technical Conference and Exposition*. Texas, USA, Vol.2, pp. 1–10.

Sansaniwal, S.K., Pal, K., Rosen, M.A. and Tyagi, S.K. (2017) 'Recent advances in the development of biomass gasification technology: A comprehensive review', *Renewable and Sustainable Energy Reviews*, 72, pp. 363–384.

Serrano, D., Horvat, A., Batuecas, E. and Abelha, P. (2022) 'Waste tyres valorisation through gasification in a bubbling fluidised bed: An exhaustive gas composition analysis', *Renewable Energy*, 200, pp. 1438–1446.

Shahbaz, M., Yusup, S., Inayat, A., Ammar, M., Patrick, D.O., Pratama, A. and Naqvi, S.R. (2017) 'Syngas production from steam gasification of palm kernel shell with subsequent CO<sub>2</sub> capture using CaO sorbent: An Aspen Plus modeling', *Energy and Fuels*, 31(11), pp. 12350–12357.

- Sharma, S. and Sheth, P.N. (2016) 'Air–steam biomass gasification: Experiments, modeling and simulation', *Energy Conversion and Management*, 110, pp. 307–318.
- Shen, Y., Li, X., Yao, Z., Cui, X. and Wang, C.-H. (2019) 'CO<sub>2</sub> gasification of woody biomass: Experimental study from a lab-scale reactor to a small-scale autothermal gasifier', *Energy*, 170, pp. 497–506.
- Sieradzka, M., Mlonka-Mędrala, A. and Magdziarz, A. (2022) 'Comprehensive investigation of the CO<sub>2</sub> gasification process of biomass wastes using TG-MS and lab-scale experimental research', *Fuel*, 330, p. 125566.
- Singh, S., Wu, C. and Williams, P.T. (2012) 'Pyrolysis of waste materials using TGA-MS and TGA-FTIR as complementary characterisation techniques', *Journal of Analytical and Applied Pyrolysis*, 94, pp. 99–107.
- Škrbić, B.D., Đurišić-Mladenović, N. and Cvejanov, J. (2018) 'Differentiation of syngases produced by steam gasification of mono- and mixed sources feedstock: A chemometric approach', *Energy Conversion and Management*, 171, pp. 1193–1201.
- Slopiecka, K., Bartocci, P. and Fantozzi, F. (2012) 'Thermogravimetric analysis and kinetic study of poplar wood pyrolysis', *Applied Energy*, 97, pp. 491–497.
- Straka, P. and Bučko, Z. (2009) 'Co-gasification of a lignite/waste-tyre mixture in a moving bed', *Fuel Processing Technology*, 90(10), pp. 1202–1206.
- Tang, X., Chen, Z., Liu, J., Chen, Z., Xie, W., Evrendilek, F. and Buyukada, M. (2021) 'Dynamic pyrolysis behaviors, products, and mechanisms of waste rubber and polyurethane bicycle tires', *Journal of Hazardous Materials*, 402, p. 123516.
- Tezer, Ö., Karabağ, N., Öngen, A., Çolpan, C.Ö. and Ayol, A. (2022) 'Biomass gasification for sustainable energy production: A review', *International Journal of Hydrogen Energy*, 47(34), pp. 15419–15433.

Umeki, K., Yamamoto, K., Namioka, T. and Yoshikawa, K. (2010) 'High temperature steam-only gasification of woody biomass', *Applied Energy*, 87(3), pp. 791–798.

Uzun, B. and Yaman, E. (2014) 'Thermogravimetric characteristics and kinetics of scrap tyre and Juglans regia shell co-pyrolysis', *Waste Management & Research*, 32(10), pp. 961–970.

Vyazovkin, S., Burnham, A.K., Criado, J.M., Pérez-Maqueda, L.A., Popescu, C. and Sbirrazzuoli, N. (2011) 'ICTAC Kinetics Committee recommendations for performing kinetic computations on thermal analysis data', *Thermochimica Acta*, 520, pp. 1–19.

Waheed, Q.M.K., Wu, C. and Williams, P.T. (2016) 'Pyrolysis/reforming of rice husks with a Ni–dolomite catalyst: Influence of process conditions on syngas and hydrogen yield', *Journal of the Energy Institute*, 89(4), pp. 657–667.

Wang, J., Yellezuome, D., Zhang, Z., Liu, S., Lu, J., Zhang, P., Zhang, S., Wen, P., Rahman, M.M., Li, C. and Cai, J. (2022) 'Understanding pyrolysis mechanisms of pinewood sawdust and sugarcane bagasse from kinetics and thermodynamics', *Industrial Crops and Products*, 177, p. 114378.

Wang, J., Zhong, Z., Ding, K., Li, M., Hao, N., Meng, X., Ruan, R. and Ragauskas, A.J. (2019a) 'Catalytic fast co-pyrolysis of bamboo sawdust and waste tire using a tandem reactor with cascade bubbling fluidized bed and fixed bed system', *Energy Conversion and Management*, 180, pp. 60–71.

Wang, L., Chai, M., Liu, R. and Cai, J. (2018) 'Synergetic effects during co-pyrolysis of biomass and waste tire: A study on product distribution and reaction kinetics', *Bioresource Technology*, 268, pp. 363–370.

Wang, X., Hu, M., Hu, W., Chen, Z., Liu, S., Hu, Z. and Xiao, B. (2016) 'Thermogravimetric kinetic study of agricultural residue biomass pyrolysis based on combined kinetics', *Bioresource Technology*, 219, pp. 510–520.

Wang, Y., Dai, L., Fan, L., Duan, D., Liu, Y., Ruan, R., Yu, Z., Liu, Y. and Jiang, L. (2017) 'Microwave-assisted catalytic fast co-pyrolysis of bamboo sawdust and waste tire for bio-oil production', *Journal of Analytical and Applied Pyrolysis*, 123, pp. 224–228.

Wang, Z., Burra, K.G., Lei, T. and Gupta, A.K. (2019b) 'Co-gasification characteristics of waste tire and pine bark mixtures in CO<sub>2</sub> atmosphere', *Fuel*, 257, p. 116025.

Wang, Z., Burra, K.G., Zhang, M., Li, X., He, X., Lei, T. and Gupta, A.K. (2020a) 'Syngas evolution and energy efficiency in CO<sub>2</sub>-assisted gasification of pine bark', *Applied Energy*, 269, p. 114996.

Wang, Z., Burra, K.G., Zhang, M., Li, X., Policella, M., Lei, T. and Gupta, A.K. (2020b) 'Co-pyrolysis of waste tire and pine bark for syngas and char production', *Fuel*, 274, p. 117878.

Wang, Z., He, T., Qin, J., Wu, J., Li, J., Zi, Z., Liu, G., Wu, J. and Sun, L. (2015) 'Gasification of biomass with oxygen-enriched air in a pilot scale two-stage gasifier', *Fuel*, 150, pp. 386–393.

White, J.E., Catallo, W.J. and Legendre, B.L. (2011) 'Biomass pyrolysis kinetics: A comparative critical review with relevant agricultural residue case studies', *Journal of Analytical and Applied Pyrolysis*, 91(1), pp. 1–33.

Wieckert, C., Obrist, A., von Zedtwitz, P., Maag, G. and Steinfeld, A. (2013) 'Syngas production by thermochemical gasification of carbonaceous waste materials in a 150 kWth packed-bed solar reactor', *Energy Fuels*, 27(8), pp. 4770–4776.

Williams, P.T. (2013) 'Pyrolysis of waste tyres: A review', *Waste Management*, 33(8), pp. 1714–1728.

Williams, P.T. (2005) *Waste Treatment and Disposal*. 2nd edn. Chichester, West Sussex, England ; Hoboken, NJ, USA: Wiley.

Williams, P.T. and Besler, S. (1995) 'Pyrolysis-thermogravimetric analysis of tyres and tyre components', *Fuel*, 74(9), pp. 1277–1283.

Woolcock, P.J. and Brown, R.C. (2013) 'A review of cleaning technologies for biomass-derived syngas', *Biomass and Bioenergy*, 52, pp. 54–84.

Wu, K., Ren, T., Chen, H. and Zhu, Y. (2017) 'Experimental investigation of whole tires and biomass mixed firing in reverse burning fixed-bed gasifier', *Energy Procedia*. Beijing, China, Vol.105, pp. 583–589.

Xie, Q., Kong, S., Liu, Y. and Zeng, H. (2012) 'Syngas production by two-stage method of biomass catalytic pyrolysis and gasification', *Bioresource Technology*, 110, pp. 603–609.

Xu, C., Hu, S., Xiang, J., Zhang, L., Sun, L., Shuai, C., Chen, Q., He, L. and Edreis, E.M.A. (2014) 'Interaction and kinetic analysis for coal and biomass co-gasification by TG-FTIR', *Bioresource Technology*, 154, pp. 313–321.

Yang, Y., Zhu, J., Yang, L. and Zhu, Y. (2019) 'Co-gasification characteristics of scrap tyre with pine sawdust using thermogravimetric and a whole-tyre gasifier reactor', *Energy Procedia*, 158, pp. 37–42.

Ye, M., Tao, Y., Jin, F., Ling, H., Wu, C., Williams, P.T. and Huang, J. (2018) 'Enhancing hydrogen production from the pyrolysis-gasification of biomass by size-confined Ni catalysts on acidic MCM-41 supports', *Catalysis Today*, 307, pp. 154–161.

Yeo, J.Y., Chin, B.L.F., Tan, J.K. and Loh, Y.S. (2019) 'Comparative studies on the pyrolysis of cellulose, hemicellulose, and lignin based on combined kinetics', *Journal of the Energy Institute*, 92(1), pp. 27–37.

Yu, H., Li, Z., Yang, X., Jiang, L., Zhang, Z. and Chen, D. (2013) 'Experimental research on oxygen-enriched gasification of straw in an entrained-flow gasifier', *Journal of Renewable and Sustainable Energy*, 5(5), p. 053127.

Yusup, S., Moghadam, R.A., Al Shoaibi, A., Melati, M., Khan, Z., Tzeng, L.M. and GH, W.A.A.K. (2013) 'Hydrogen production from catalytic steam co-gasification of waste tyre and palm

kernel shell in pilot scale fluidized bed gasifier', in *Biomass processing, conversion and biorefinery*. Nova Science Publishers, Inc., pp. 181–192.

Zang, G., Jia, J., Shi, Y., Sharma, T. and Ratner, A. (2019) 'Modeling and economic analysis of waste tire gasification in fluidized and fixed bed gasifiers', *Waste Management*, 89, pp. 201–211.

Zhang, X., Lei, H., Chen, S. and Wu, J. (2016a) 'Catalytic co-pyrolysis of lignocellulosic biomass with polymers: a critical review', *Green Chemistry*, 18(15), pp. 4145–4169.

Zhang, Y., Fu, W., Cui, L., Maqsood, T. and Li, B. (2023) 'Experimental microwave-assisted air gasification of biomass for syngas production', *Fuel*, 339, p. 126954.

Zhang, Y., Tao, Y., Huang, J. and Williams, P. (2017) 'Influence of silica–alumina support ratio on H<sub>2</sub> production and catalyst carbon deposition from the Ni-catalytic pyrolysis/reforming of waste tyres', *Waste Management and Research*, 35(10), pp. 1045–1054.

Zhang, Y. and Williams, P.T. (2016) 'Carbon nanotubes and hydrogen production from the pyrolysis catalysis or catalytic-steam reforming of waste tyres', *Journal of Analytical and Applied Pyrolysis*, 122, pp. 490–501.

Zhang, Y., Wu, C., Nahil, M.A. and Williams, P. (2015) 'Pyrolysis-catalytic reforming/gasification of waste tires for production of carbon nanotubes and hydrogen', *Energy and Fuels*, 29(5), pp. 3328–3334.

Zhang, Y., Wu, C., Nahil, M.A. and Williams, P. (2016b) 'High-value resource recovery products from waste tyres', *Proceedings of the Institution of Civil Engineers - Waste and Resource Management.*, Vol.169, pp. 137–145.

Zheng, J.L., Zhu, Y.H., Zhu, M.Q., Wu, H.T. and Sun, R.C. (2018) 'Bio-oil gasification using air - Steam as gasifying agents in an entrained flow gasifier', *Energy*, 142, pp. 426–435.

Zheng, X., Chen, C., Ying, Z. and Wang, B. (2016) 'Experimental study on gasification

performance of bamboo and PE from municipal solid waste in a bench-scale fixed bed reactor', *Energy Conversion and Management*, 117, pp. 393–399.

## Appendix A

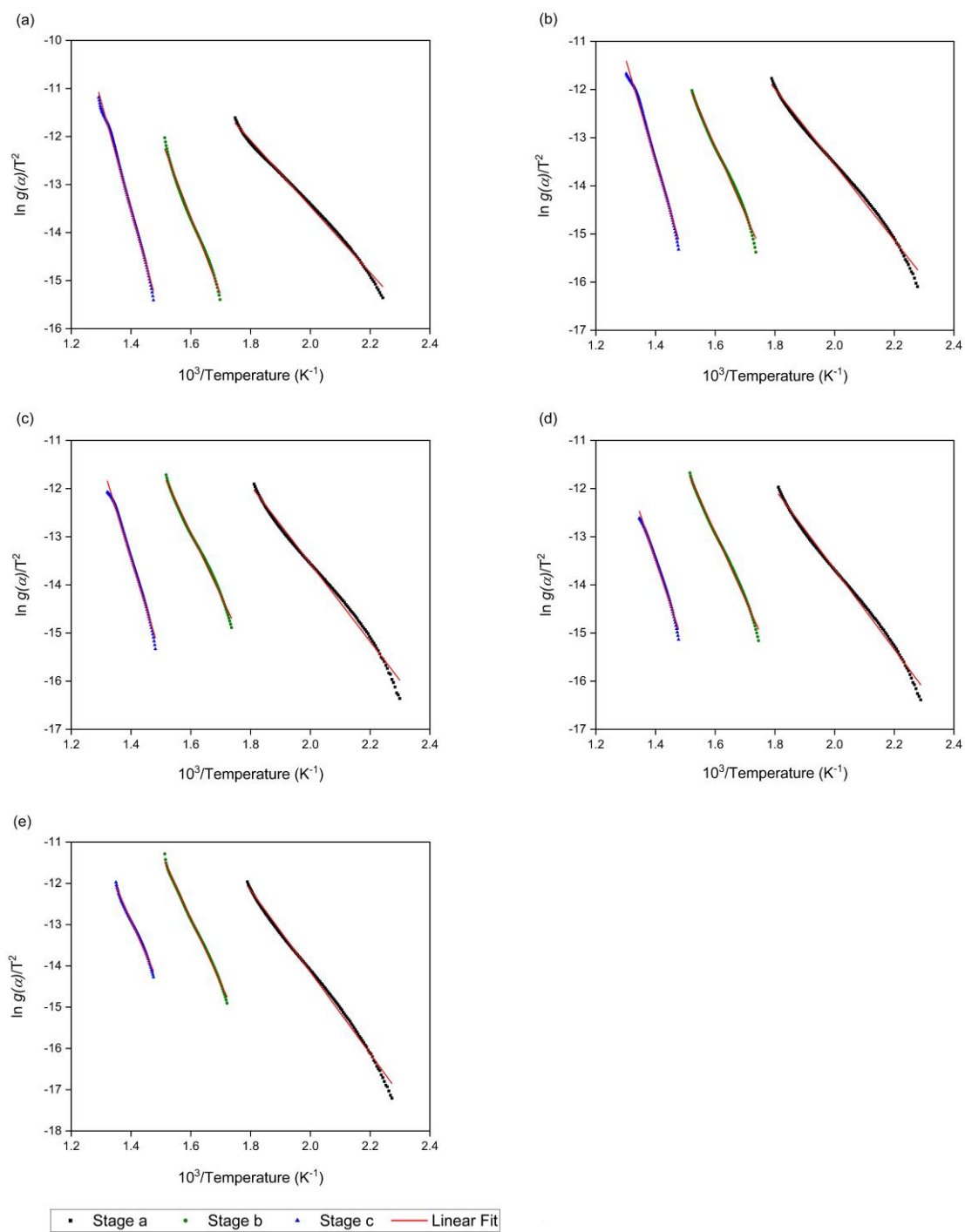


**Figure A.1** Kinetics analysis curves of  $\ln g(\alpha)/T^2$  versus  $1/T$  of different blend samples; (a) WT1PB0, (b) WT3PB1, (c) WT1PB1, (d) WT1PB3 and (e) WTOPB1 at 10 K/min

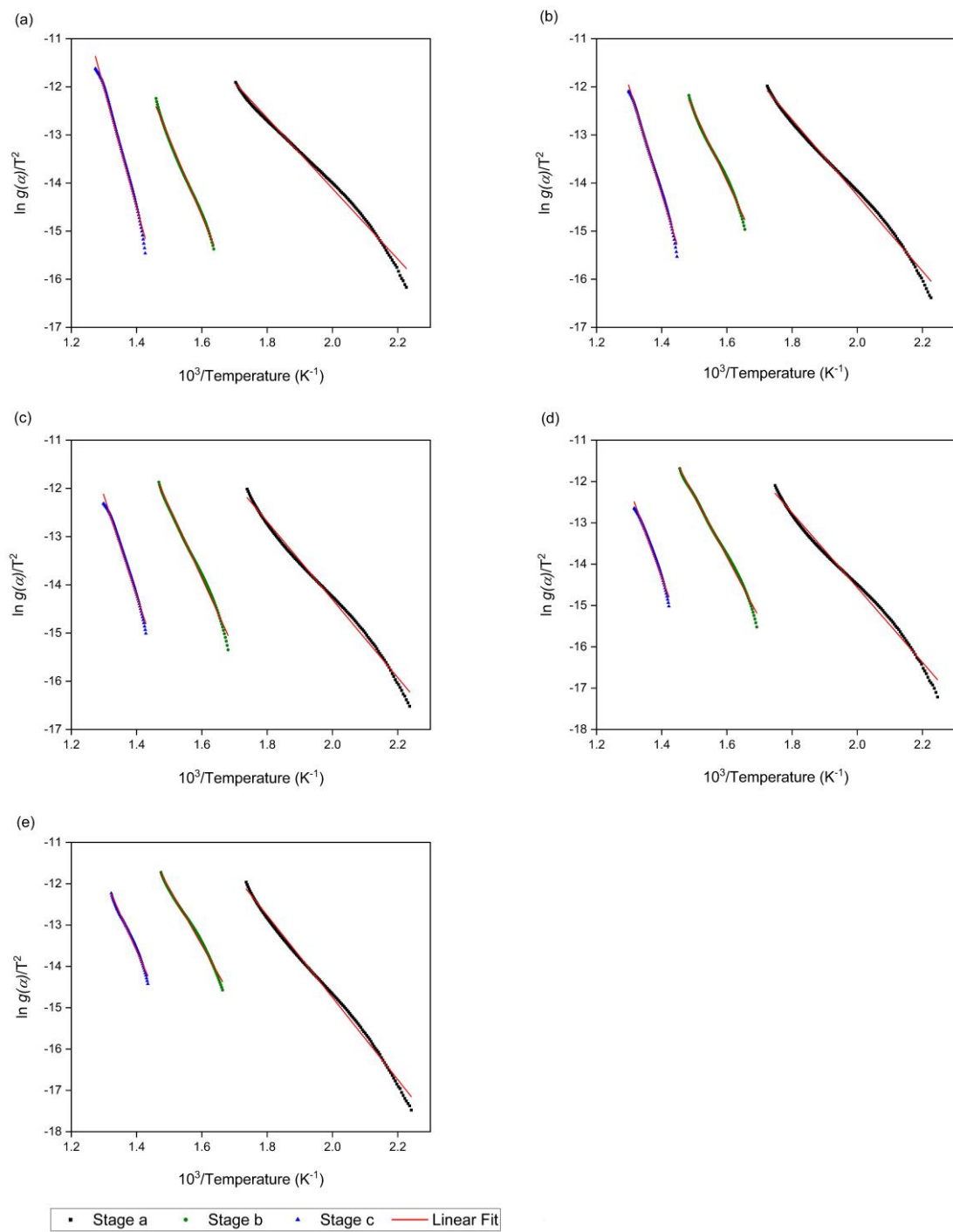


**Figure A.2** Kinetics analysis curves of  $\ln g(\alpha)/T^2$  versus  $1/T$  of different blend samples; (a) WT1PB0, (b) WT3PB1, (c) WT1PB1, (d) WT1PB3 and (e) WT0PB1 at 30 K/min

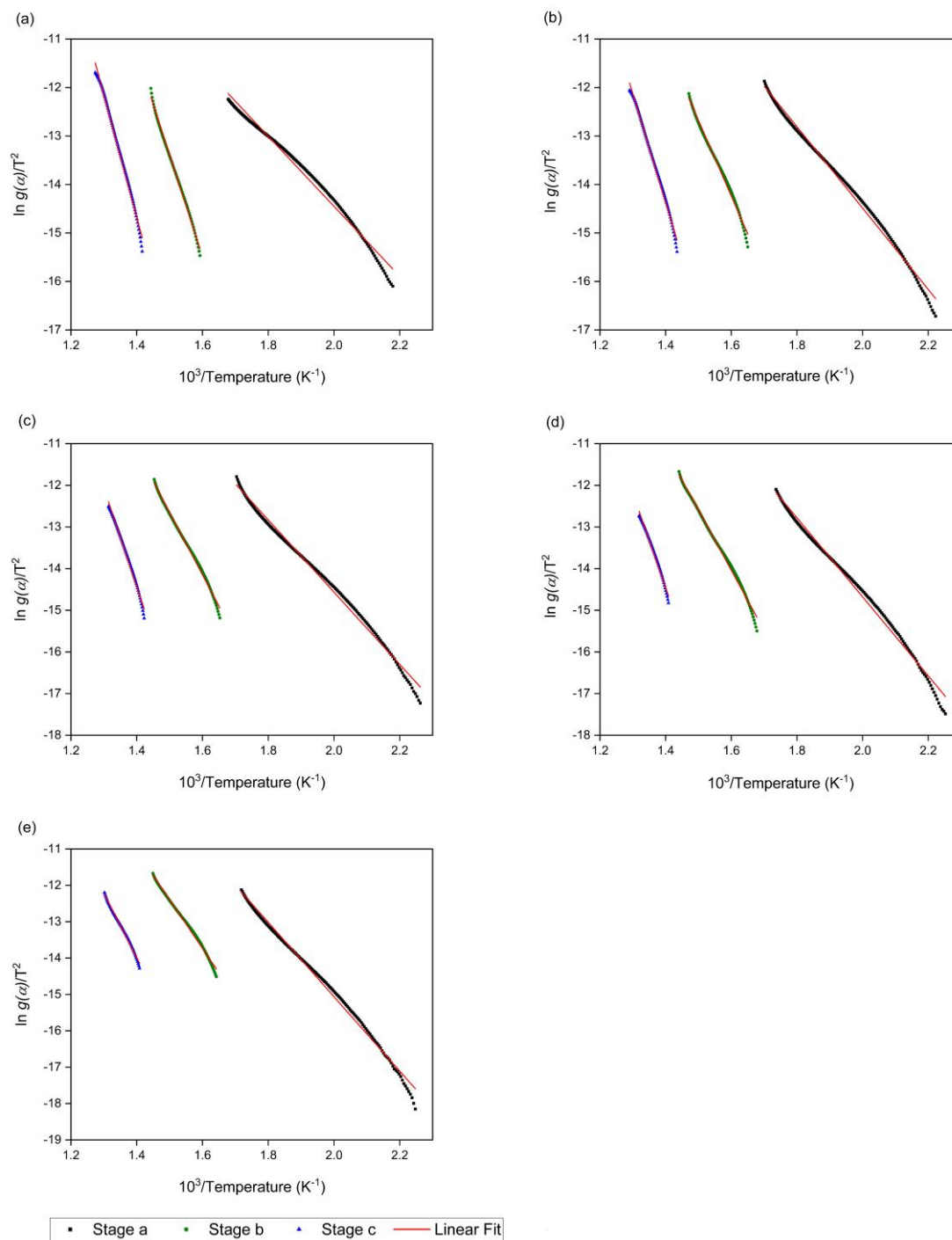


**Figure A.3** Kinetics analysis curves of  $\ln g(\alpha)/T^2$  versus  $1/T$  of different blend samples; (a) WT1PB0, (b) WT3PB1, (c) WT1PB1, (d) WT1PB3 and (e) WT0PB1 at 40 K/min

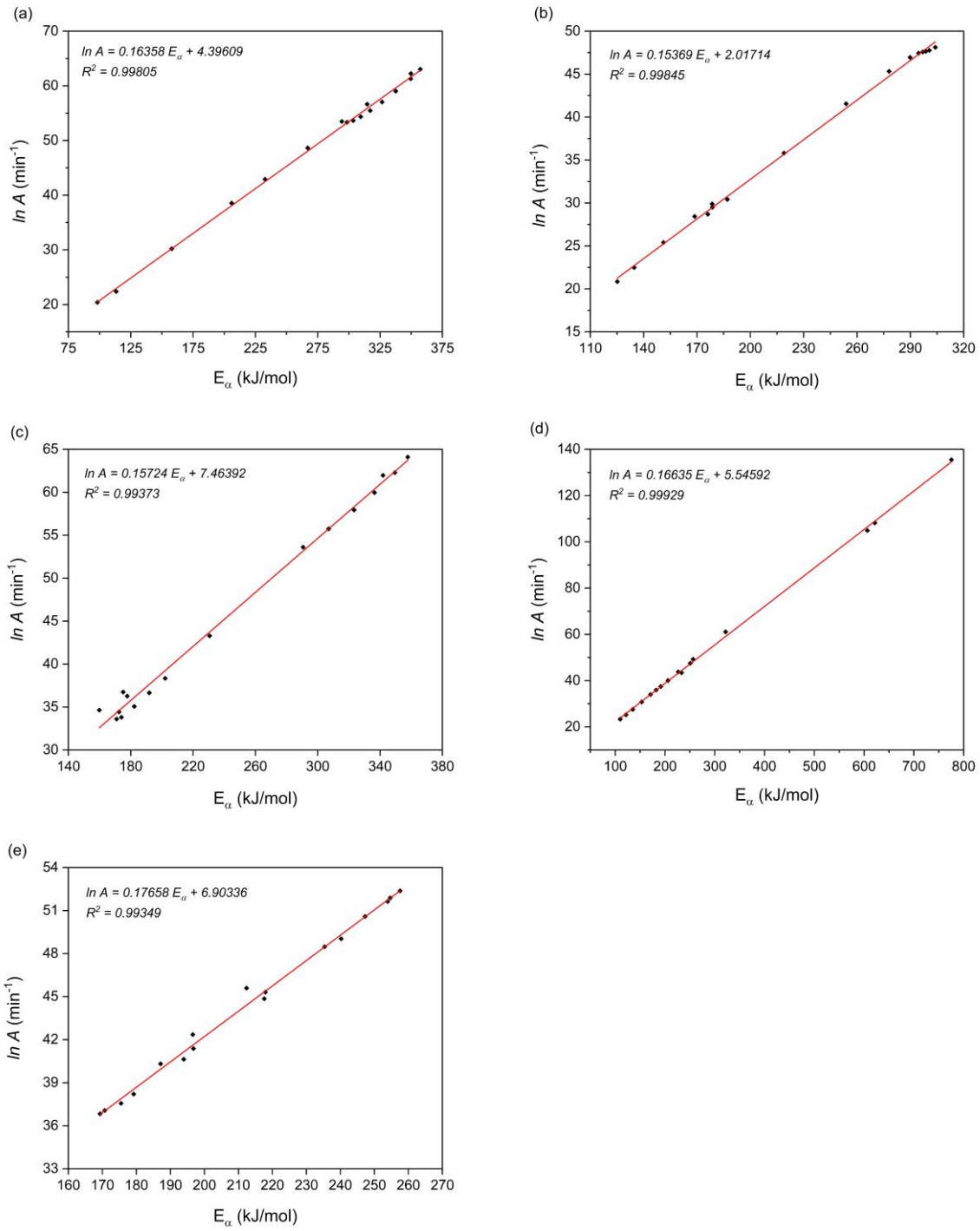


**Figure A.4** Linear relationship of compensation effect between  $\ln A$  and  $E_{\alpha}$  of different blend samples; (a) WT1PB0, (b) WT3PB1, (c) WT1PB1, (d) WT1PB3 and (e) WTOPB1 using kinetics obtained through KAS method

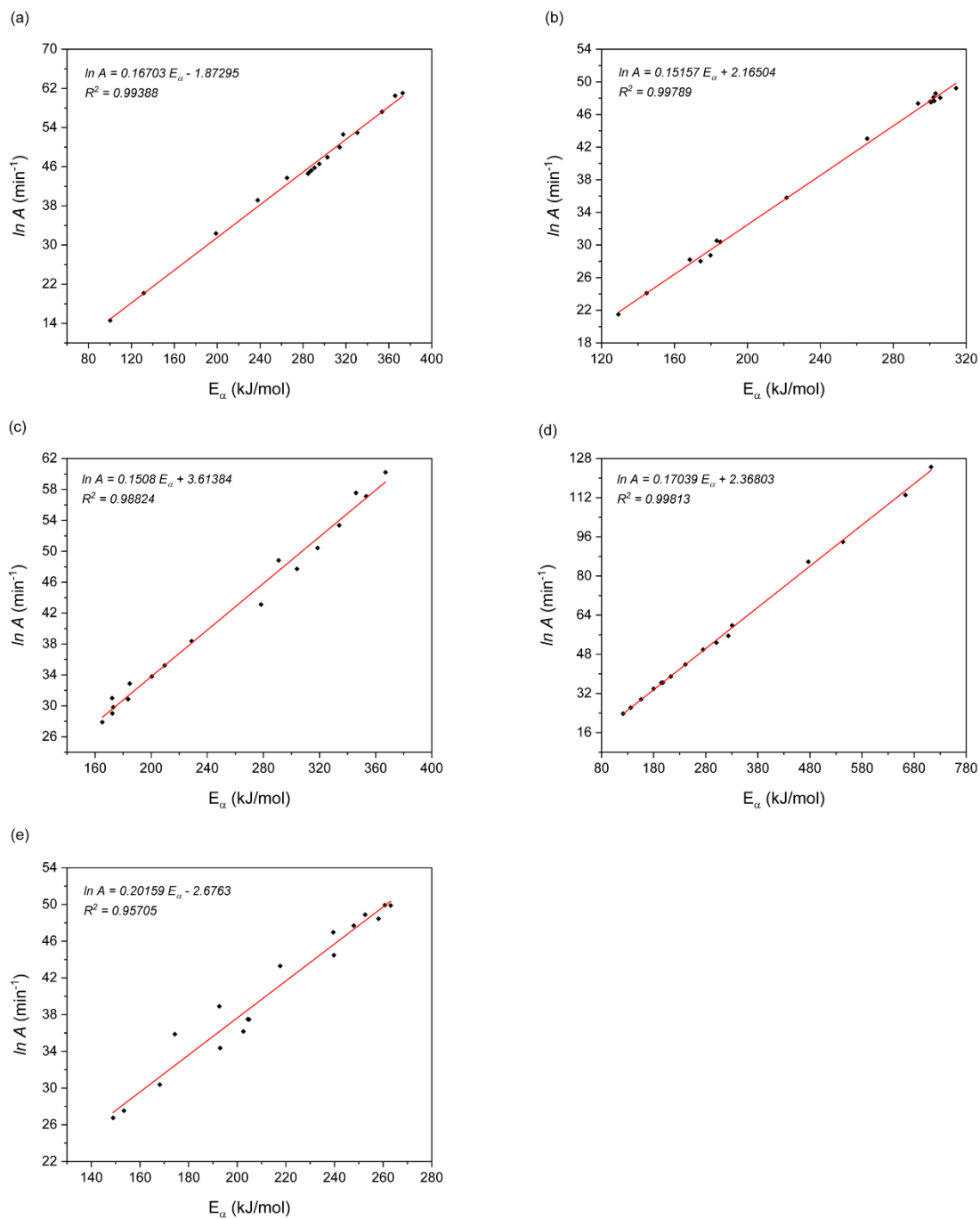


**Figure A.5** Linear relationship of compensation effect between  $\ln A$  and  $E_{\alpha}$  of different blend samples; (a) WT1PB0, (b) WT3PB1, (c) WT1PB1, (d) WT1PB3 and (e) WTOPB1 using kinetics obtained through FR method